Study of a urea-based phase change material for thermal energy storage

DOCTORAL THESIS

LAURA MARCELA QUANT COLÓN

2020

Under the supervision of:
Dr. Ane Miren García Romero
Prof. Jean Pierre Bédécarrats

This thesis is an original work entirely developed by the author under the supervision of Dr Ane Miren García Romero and Professor Jean Pierre Bédécarrats, in cotutelle between the University of the Basque Country (UPV/EHU), and the University of Pau et des Pays de l'Adour (UPPA).

The thesis is adscribed to the doctorate programs of Energy Efficiency and Sustainability in Engineering and Architecture of the University of the Basque Country and Fluid Mechanics (mention in Energy) of the University of Pau et des Pays de l'Adour.

The thesis has been carried out in the Department of Mining Engineering, Metallurgy and Materials Science, in the School of Engineering of Bilbao (UPV/EHU), and in the Laboratoire de Thermique, Energétique et Procédés in Pau (LaTEP) in Pau (UPPA).

Dissertation at the premises of the University of the Basque Country (UPV/EHU) in fulfillment of the requirements for the degree on Doctor of Philosophy.

Acknowledgments / Remerciements/ Agradecimientos

Estas líneas van dedicadas a todas las personas que han contribuido de una u otra manera a que este trabajo haya salido adelante.

En primer lugar, quiero agradecer a mis directores de tesis quienes me han apoyado de forma incondicional durante los últimos años, Ana García Romero y Jean-Pierre Bedecarrats.

A Ana, por ser mi mentora, mi guía en este camino, por dejar que siga mis inquietudes, por confiar en mí y enseñarme aspectos de la investigación que van más allá del contenido. Por ser una persona comprometida con su trabajo y con su equipo. Gracias.

A Álvaro y Gonzalo, que han colaborado en gran medida en la realización de mi trabajo de investigación. Especialmente a Gonzalo, quien me enseñó absolutamente todo lo que sé de técnicas experimentales y caracterización de materiales desde mi inicio en el laboratorio. Por ofrecerme siempre una opinión. Gracias por dedicarme parte de su valioso tiempo. A mis compañeros Lourdes y Pello. A las personas que han pasado por el laboratorio en estos años: Miriam, Cristina y Ander.

À Jean Pierre, qui, malgré sa position à la tête de Latep et son engagement professionnel à toute épreuve, a toujours trouvé du temps pour mes recherches. Pour être une personne aussi agréable et facile à vivre.

Á mes collègues du LaTEP, pour une bonne année dans un environnement différent de celui de d'habitude et en m'incluant comme personne à part entière du groupe dès le premier jour, pour une expérience française complète. Á Didier Haillot pour avoir fait le lien entre les universités.

A los técnicos que me han ayudado en la construcción, mantenimiento y uso de los montajes experimentales. Daniel de Miguel, Iker Bustinza y Marc Bagole. A los servicios de SGiker, en especial a Mamen Sampedro, Aitor Larrañaga, Sergio Fernández y Alfredo Sarmiento.

Por otra parte, quiero dar gracias a mis padres y a toda mi familia por estar a mi lado, desde muy lejos y muy cerca. Por ser ejemplos de vida excepcionales. Quiero agradecer especialmente a mi madre que no ha dudado ni un momento de mis decisiones y ha apoyado todos mis proyectos personales y profesionales. Mamá, una de las motivaciones de mi vida es que estés orgullosa de tu única hija, de la que llamas el motor de tu vida ¡Este logro va para ti!

A todas las personas que hacen parte de mi vida y me han acompañado en lo personal. A mis amigas que me han ayudado a mantener la cordura, o locura según se mire. A Iñigo, por ir de la mano y hacer que todo parezca más fácil.

A mí misma. Por no tirar la toalla y disfrutar del camino.

A todos Gracias.

"Preguntó qué ciudad era aquella, y le contestaron con un nombre que nunca había oído, que no tenía significado alguno, pero que tuvo en el sueño una resonancia sobrenatural: Macondo"

Gabriel García Márquez

Summary - Study of a urea-based phase change material for thermal energy storage

This work presents a contribution to the latent heat thermal energy storage LHTES technology by working on both phase change materials PCM and storage systems that are technically and economically viable for their integration in buildings.

The study comprises an in-depth analysis of the thermal behavior that the urea and Sodium nitrate eutectic mixture would provide for its use as latent heat thermal storage material for the Domestic Heating Water (DHW) and heating applications. According to former studies, the mixture had been considered an excellent candidate material for this purpose, but the behavior under the operation conditions, including the long-term use had not been studied before. One of the main objectives of the Ph. D. thesis was the characterization of these aspects to evaluate the feasibility to use the urea and Sodium nitrate eutectic mixture as a PCM in the application. Accordingly, the following aspects have been assessed in this work: hygroscopicity, thermal degradation, phase segregation, and supercooling. Several testing methodologies have been developed in order to attain results representative of the operation in the final application. This aim arises from the need to get knowledge about how the materials will behave in the real application, which can greatly differ from laboratory scale, also taking into account the potential long-term use of the materials.

The characterization of the hygroscopicity, or water uptake, of the urea and Sodium nitrate eutectic mixture was evaluated under different conditions. Phase identification and thermal properties characterization were carried out on hydrated and dry samples to study the influence of the water intake on the materials behavior and to find solutions suitable for its use as a PCM. A method for sample preparation and handling of the mixture to avoid water uptake has been developed.

The thermal degradation of the urea and Sodium nitrate eutectic mixture was studied by determining the thermophysical properties when the mixture was exposed at different temperatures for prolonged periods. DSC (Differential Scanning Calorimetry) was used to determine the changes on the melting enthalpy, melting onset temperature and melting peak temperature, which are directly related to the PCM thermal energy storage properties. In addition, the degradation products and their influence on the system thermal properties were assessed by means of different analytical techniques, including HPLC (liquid chromatography), XRD (X-ray diffraction and FTIR (Fourier transformed infrared spectroscopy).

The eutectic mixture showed an unforeseen segregation phenomenon when it was exposed to repeated melting-solidification cycles. As a result, the phenomenon was researched and the causes that produce it were determined. A test campaign consisting on thermal cycling of samples using different cooling rates was carried out, and subsequently the segregated materials were analyzed by different techniques, including XRD, DSC and microscopy (PLM and SEM). The results established a relationship between the operation conditions, more specifically

the cooling rates, with the resulting crystal structures, which explain the phase segregation in the eutectic mixture. A mitigation measure was determined.

The mixture-supercooling was studied from a different approach to the usual approaches employed in the PCM research community. The aim was to further improve the knowledge about the supercooling relationship to the system parameters, to efficiently design LHTES systems to be used with materials that exhibit supercooling. Experiments were designed to determine the relationship of the supercooling degree with parameters associated with the system, like the sample volume, the cooling media properties, and finally the PCM properties. To do it, several sample containers with different geometries and volumes, several cooling rates, two heat transfer fluids (HTF) and two PCM were used (urea and Sodium nitrate eutectic mixture and polyethylene glycol 10000).

Finally, regarding the storage system a shell and tubes heat exchanger was studied in order to evaluate the use of devices which are commercially available (i.e. potentially more economical and readily feasible) for the use as latent heat energy storage LHTES devices. The first objective was to attain a deeper understanding of the device thermal behavior. The characterization was performed using RT60 paraffin as PCM inside the shell, a well known commercial material, to assure the reproducibility of the results, and water as heat transfer fluid HTF in the tubes. Several flow rates and temperature ranges were used to obtain a greater scope of the operation of the device as LHTES. The work included the determination of the thermal losses, and the study of charging and discharging cycles with different HTF, initial and final temperatures, and flow rates. The temperatures of both, the HTF and in the PCM, were monitored during the tests in several different locations. Then, the charging and discharging times and parameters related to the stored and released energy were determined.

The memory has been written in 8 chapters. Each chapter, except chapter 1 (Introduction), chapter 7 (conclusions) and chapter 8 (references), has its own initial introduction where the main scientific and technical aspects required to approach the chapter have been added, as well a brief analysis of the bibliography pertaining to the subject dealt with in the chapter. As a result, the chapter 1 includes a brief presentation about the technical and scientific aspects relevant to the develoment of the latent heat thermal storage and the phase change materials, and the presentation of the objectives and structure of the thesis.

Résumé - Étude d'un matériau à changement de phase à base d'urée pour le stockage de l'énergie thermique

La technologie de stockage de l'énergie thermique par chaleur latente (Latent Heat Thermal Energy Storage – LHTES) est abordée en travaillant à la fois sur les matériaux à changement de phase MCP utilisés et sur les systèmes de stockage techniquement et économiquement viables pour leur intégration dans les bâtiments.

En ce qui concerne le matériau MCP, un mélange eutectique d'urée et de nitrate de Sodium a été précédemment identifié comme un bon candidat pour les applications Eau Chaude Sanitaire (ECS) et chauffage. Cependant, le mélange présente plusieurs caractéristiques qui pourraient compromettre son utilisation à long terme et qui n'ont pas été encore suffisamment étudiées, telles que l'hygroscopicité, la dégradation thermique, la ségrégation de phase et la surfusion. Pour cette raison, l'un des principaux objectifs de la thèse de doctorat était la caractérisation de ces aspects pour évaluer l'utilisation du mélange eutectique d'urée et de nitrate de Sodium comme MCP. L'étude du matériau comprend le développement de méthodologies qui sont plus représentatives de son utilisation dans l'application finale que celles traditionnellement rencontrées pour la caractérisation des MCP. Cet objectif découle de la nécessité d'acquérir des connaissances sur le comportement des matériaux en conditions réelles de fonctionnement, qui peuvent être très différentes de l'échelle du laboratoire, en tenant compte également de l'utilisation potentielle à long terme des matériaux.

La caractérisation de l'hygroscopicité ou de l'absorption d'eau du mélange eutectique d'urée et de nitrate de Sodium a été réalisée dans différentes conditions. L'identification des phases et l'évaluation des propriétés thermiques ont été effectuées sur des échantillons hydratés et secs afin d'évaluer la nécessité éventuelle de sécher les matériaux en vue de leur utilisation finale. Une méthode de préparation des échantillons et des conditions de manipulation sont proposées pour éviter l'absorption d'eau du mélange.

La dégradation thermique du mélange eutectique d'urée et de nitrate de Sodium a été évaluée en étudiant le comportement thermo-physique après un temps d'exposition à différentes températures. Des mesures DSC (Differential Scanning Calorimetry) ont été effectuées pour déterminer la variation d'enthalpie lors de la fusion, la température de début de fusion et celle du pic de fusion, qui sont des propriétés directement liées au stockage de l'énergie thermique du MCP et à sa stabilité à long terme. En outre, les produits obtenus lors de la dégradation et leur influence sur la variation des propriétés du MCP ont été étudiés.

Le mélange eutectique a montré une ségrégation imprévue à des températures supérieures au point de fusion lors des cycles de fusion et de solidification. Plusieurs tests ont été effectués, notamment le cyclage thermique sur des échantillons de 4 à 5 g en utilisant différentes vitesses de refroidissement, la diffraction par rayons X des phases due à la ségrégation, la calorimétrie différentielle après la redissolution de ces phases dans le matériau liquide et la microscopie (PLM et MEB) d'échantillons refroidis dans différentes conditions. Les expériences ont permis d'établir une relation entre les conditions de fonctionnement, plus précisément les vitesses de

refroidissement, et les structures cristallines résultantes qui expliquent la ségrégation de phase dans le mélange eutectique, et la manière de la réduire et d'inverser le processus.

L'étude de la surfusion comprenait l'utilisation de deux MCPs : l'eutectique urée - nitrate de Sodium et le polyéthylène glycol 10000. Les expériences ont été réalisées dans différentes conditions : des récipients de géométrie et de volume différents, diverses vitesses de refroidissement et divers fluides de transfert thermique. Enfin, les résultats ont servi à évaluer la relation entre le degré de surfusion et les paramètres associés au volume de l'échantillon, au milieu de refroidissement et aux caractéristiques du MCP. Après la détermination des paramètres les plus pertinents, des modèles de régression linéaire ont été définis pour chaque matériau puis pour les deux matériaux. L'objectif spécifique de ce chapitre est de faire un pas de plus dans la compréhension et la prédiction de la surfusion, afin de concevoir efficacement des systèmes LHTES utilisant des matériaux qui peuvent présenter une surfusion.

Enfin, en ce qui concerne le système de stockage, un échangeur de chaleur à tubes-calandre est étudié afin d'évaluer l'utilisation de ce type de dispositifs déjà commercialisés (potentiellement plus économiques et facilement réalisables) comme dispositifs de stockage de l'énergie thermique latente (LHTES). Le premier objectif était de mieux comprendre le comportement thermique de l'échangeur. L'étude a été réalisée en utilisant, dans la calandre, de la paraffine RT60 comme MCP, un matériau commercial bien connu assurant ainsi la reproductibilité des résultats, et de l'eau comme fluide de transfert de chaleur (Heat Transfer Fluid HTF) dans les tubes. Plusieurs débits et plages de température ont été envisagés pour réaliser l'étude complète du fonctionnement de l'échangeur. Le travail a inclus la détermination des pertes thermiques et l'étude des cycles de charge et de décharge avec différentes températures initiales et finales et différents débits du HTF. Les températures du HTF et celles du MCP (mesurées à 15 endroits différents à l'intérieur de la calandre) ont été relevées pendant les essais. Ensuite, les temps de charge et de décharge et les paramètres liés à la puissance stockée et libérée ont été déterminés.

La mémoire a été écrite en 8 chapitres. Chaque chapitre, à l'exception du chapitre 1 (Introduction), du chapitre 7 (conclusions) et du chapitre 8 (références), a sa propre introduction initiale dans laquelle les principaux aspects scientifiques et techniques nécessaires pour traiter le chapitre ont été inclus, ainsi qu'un bref analyse de la bibliographie sur le sujet traité dans le chapitre. En conséquence, le chapitre 1 comprend une brève présentation sur les aspects techniques et scientifiques pertinents pour le développement des matériaux de stockage de chaleur latente et à changement de phase, ainsi que la présentation des objectifs et de la structure de la thèse.

Resumen - Estudio de un material de cambio de fase basado en la urea para el almacenamiento de energía térmica

Este trabajo presenta una contribución a la tecnología de almacenamiento de energía térmica latente LHTES. Incluye el estudio de materiales de cambio de fase PCM y de sistemas de almacenamiento que son técnica y económicamente viables para su integración en edificios.

El estudio comprende un análisis en profundidad del comportamiento térmico que la mezcla eutéctica de urea y nitrato de sodio proporcionaría para su uso como material de almacenamiento térmico de calor latente, destinada a un uso de agua caliente doméstica y calefacción (ACS). Según estudios anteriores, la mezcla había sido considerada un excelente material candidato para este propósito, pero el comportamiento bajo las condiciones de operación, incluido el uso a largo plazo, no se había estudiado antes. Uno de los objetivos principales de la tesis de doctorado fue la caracterización de estos aspectos para evaluar la viabilidad de utilizar la mezcla eutéctica de urea y nitrato de sodio como PCM en la citada aplicación. En consecuencia, los siguientes aspectos se han evaluado en este trabajo: higroscopicidad, degradación térmica, segregación de fase y sobreenfriamiento. Se han desarrollado varias metodologías de ensayo para lograr resultados que puedan ser representativos del comportamiento en la aplicación final. Este objetivo surge de la necesidad de conocer cómo se comportarán los materiales en la aplicación real, que puede diferir enormemente de la escala del laboratorio, también teniendo en cuenta el uso potencial a largo plazo de los materiales.

La caracterización de la higroscopicidad, o absorción de agua, de la mezcla eutéctica de urea y nitrato de sodio se evaluó en diferentes condiciones. La identificación de fases y la caracterización de propiedades térmicas se llevaron a cabo en muestras hidratadas y secas para estudiar la influencia de la ingesta de agua en el comportamiento de los materiales y para encontrar soluciones adecuadas para su uso como PCM. Se ha desarrollado un método para la preparación de muestras y el manejo de la mezcla que permitan evitar la absorción de agua.

La degradación térmica de la mezcla eutéctica de urea y nitrato de sodio se estudió determinando las propiedades termofísicas tras la exposición de la mezcla a diferentes temperaturas durante períodos prolongados. Se usó DSC (calorimetría diferencial de barrido) para determinar los cambios en la entalpía de fusión, la temperatura de inicio de fusión y la temperatura máxima de fusión, que están directamente relacionadas con las propiedades de almacenamiento de energía térmica del PCM. Además, se evaluaron los productos de degradación y su influencia en las propiedades térmicas del sistema, mediante HPLC (cromatografía líquida), XRD (difracción de rayos X), y FTIR (espectrometría de infrarrojos por transformada de Fourier).

La mezcla eutéctica mostró un fenómeno imprevisto de segregación de fases cuando se expuso a ciclos repetidos de fusión-solidificación. Como resultado de ello, se investigó el fenómeno y se determinaron las causas que lo producen. Se realizó una campaña de ensayos que consistió en someter a las muestras a un número dado de ciclos térmicos utilizando diferentes velocidades

de enfriamiento. Posteriormente los materiales segregados se analizaron mediante diferentes técnicas, incluyendo XRD, DSC y microscopía (PLM y SEM). Los resultados establecieron una relación entre las condiciones de operación, más específicamente las velocidades de enfriamiento, con las estructuras cristalinas resultantes, que explican la segregación de fase en la mezcla eutéctica. Se determinaron posibles medidas de mitigación.

El estudio del sobrenfriamiento se realizó desde un enfoque diferente a los enfoques habitualmente empleados en la comunidad de investigación de PCM. El objetivo era mejorar el conocimiento sobre la relación del sobrenfriamiento con los parámetros del sistema, para diseñar de manera eficiente los sistemas LHTES, permitiendo el uso de materiales que exhiben sobrenfriamiento. Los experimentos se diseñaron para determinar la relación del grado de sobrenfriamiento con los principales parámetros del sistema, como son el volumen de la muestra, las propiedades de los fluidos caloportadores (HTF), las condiciones de enfriamiento y, finalmente, las propiedades del PCM. En el estudio se usaron varios contenedores con diferentes geometrías y volúmenes, varias velocidades de enfriamiento, dos fluidos de transferencia de calor (HTF) y dos PCM (mezcla eutéctica de urea y nitrato de sodio y polietilenglicol 10000).

Por último, en lo que respecta al sistema de almacenamiento, se estudió un intercambiador de calor de carcasa y tubos para evaluar el uso de dispositivos disponibles en el mercado (potencialmente más económicos y viables desde un punto de vista comercial) para su utilización como dispositivos de almacenamiento de energía térmica latente LHTES. El primer objetivo era conocer en profundidad el comportamiento térmico y operatividad del dispositivo. Para ello se llevó a cabo un estudio paramétrico de caracterización, utilizando parafina RT60 como PCM en el interior de la carcasa, un material comercial conocido para asegurar la reproducibilidad de los resultados y descartar efectos asociados al material PCM, y agua como fluido caloportador (HTF) en los tubos. Se utilizaron varios caudales y rangos de temperatura para obtener un mayor conocimiento del funcionamiento del dispositivo como LHTES. El trabajo incluyó la determinación de las pérdidas térmicas y el estudio de los ciclos de carga y descarga con diferentes caudales, y temperaturas iniciales y finales. Durante los ensayos se monitorearon las temperaturas de ambos materiales, el HTF y el PCM, en varios lugares diferentes. Tras ello, se determinaron los tiempos de carga y descarga y los parámetros relacionados con la energía almacenada y liberada.

La memoria ha sido escrita en 8 capítulos. Cada capítulo, excepto el capítulo 1 (Introducción), el capítulo 7 (conclusiones) y el capítulo 8 (referencias), tiene su propia introducción inicial donde se han incluido los principales aspectos científicos y técnicos necesarios para abordar el capítulo, así como un breve análisis de la bibliografía sobre el tema tratado en el capítulo. Como resultado, el capítulo 1 incluye una breve presentación sobre los aspectos técnicos y científicos relevantes para el desarrollo del almacenamiento térmico latente y los materiales de cambio de fase, así como la presentación de los objetivos y la estructura de la tesis.

Index of Contents

Index of Figures

Index of Tables

Nomenclature and symbols

Abbreviations

DSC - Differential scanning calorimetry

FT-IR - Fourier transform infrared

HPLC - High performance liquid chromatography

HTF - Heat transfer fluid

LHTES - Latent heat thermal storage

PCM - Phase change material

PEG - Poly ethylene glycol

PLM - Polarized light microscopy

RH - Relative humidity

SEM - Scanning electron microscopy

TES - Thermal storage

U-SN - Urea and Sodium nitrate

XRD - X-ray diffraction

Dimensionless numbers

Bi - Biot number

Nu - Nusselt number

Pr - Prandt number

Re - Reynolds number

Greek letters

λ - latent heat of phase transformation

ϒ - Surface tension

α - Thermal diffusivity

ν - kinematic viscosity

ξ - Surface roughness

Nomenclature

a - Chemical activity

a_r - Degree of conversion of a reaction

ΔH - Reaction heat per unit mass

Δh - Enthalpy change

ΔG - Gibbs free energy

ΔG_v - Volumetric Gibbs free energy

ΔS_f - Entropy of fusion

C_p - Specific heat

D - Diameter

f - Friction factor

h - Heat transfer coefficient

K - Equilibrium constant

k - Thermal conductivity

L - Length

L_c - Characteristic length

m - Mass

$\dot{m}$ - Mass flow rate

P - Pressure

Q - Heat

r - Radius

T_m - Melting temperature

T_c - Crystallization temperature

T - Temperature

$\overline{U}$ - Overall heat transfer coefficient

v - Heating or cooling rate

wt - Weight

Chapter 1 : Introduction and objectives

1.1 INTRODUCTION

Energy is an essential need in modern society. From keeping our homes warm and being part of our day-to-day chores to fueling industry and transport. The great advances in technology and health during the last century resulted in disproportionate population growth. Therefore, the demand for resources increased at a high speed, as well as the associated demand for energy. The world energy production mainly depends on non-renewable resources. This fact inevitably entails a series of environmental, economic, and political problems. At a first instance, the non-responsible consumption of fossil fuels has increased the atmospheric greenhouse-effect-emissions and, leading to a severe global warming in a few decades. Furthermore, the centralized nature of the energy production makes many countries to be dependent on imports while the supply to consumers reaches increasingly unattainable prices, and also put pressure on the energy resources.

To stop the current energy situation, some countries reached a series of agreements dealing with greenhouse-gas-emissions mitigation, adaptation, and finance (Kyoto protocol, Paris agreement). At the European Union level, this is reflected in the implementation of an ambitious energy policy, which promotes all energy sources to be sustainable and aims to achieve a safe, competitive, and sustainable energy economy. To do it, the research policies target to introduce new technologies to achieve these objectives, based both on the use of renewable energy sources and on the development of improvements in energy efficiency.

Figure 1. 1 shows the evolution of the energy consumption by different sectors in Europe from 1990 to 2017 [1]. The residential sector and the commercial and public services sector account for 40% of the energy demand in Europe. Both sectors share many similar features in relation to the energy consumption, mostly related to the building operation, as well as to its construction.

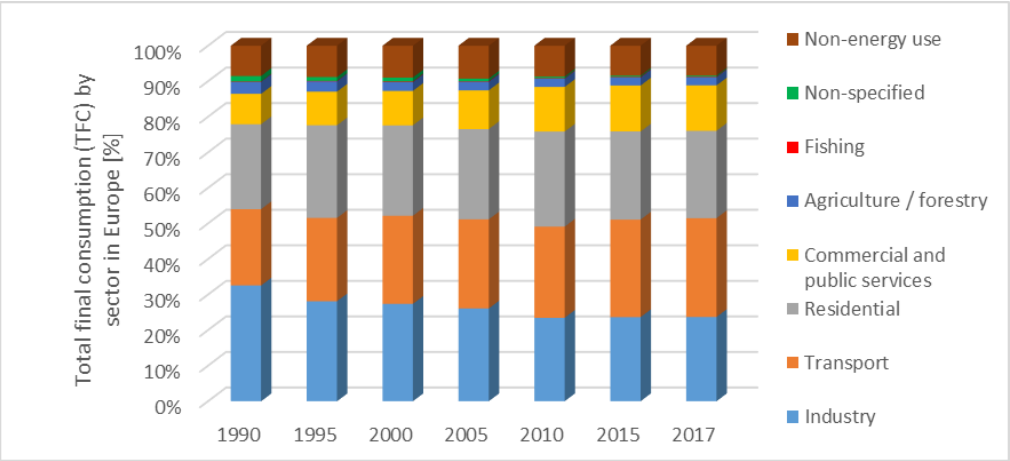

Figure 1. 1 Evolution of energy consumption in Europe by sectors/final use

In fact, a large part of this consumption is devoted to space heating and domestic hot water (DHW). The energy for DHW and space heating can be attained in-situ or can be produced in

other places and, in that case it needs to be transported. This entails great losses (such as electricity for heating production). Hence, it is necessary to encourage the development of technologies that allow the generation and use of thermal energy in situ to higher energy efficiency rates. Solar thermal and micro-cogeneration technologies stand out for this purpose in buildings, given the 100% renewable nature of the former and the high energy efficiency of the latter. However, these technologies have as a disadvantage the mismatch between the time when the energy is available and the time when it is needed, i.e. generation and consumption are produced in a deferred manner. This requires to implement a correct storage system where the heat (produced when the energy is available) is stored until it is required. This type of storage is known as thermal energy storage, TES [2], [3]. TES provides a high degree of flexibility and can integrate a variety of energy harvesting technologies, like for example solar collectors, biofuel combustors, heat pumps, and off-peak electricity generators.

There is a certain number of TES technologies, which are based either in chemical methods (use of the heat generated in chemical reactions) or in physical methods (use of sensible heat, latent heat and sorption). This thesis focuses the research on the use of latent heat for thermal energy storage, LHTES. Latent heat is the thermal energy exchanged when a phase change takes place. It is the (thermal) energy needed for a determined mass of a material to completely change its state of aggregation (from solid to liquid, from liquid to gas, from solid to gas, and viceversa in all the three cases[1]) , which occurs at a constant temperature or in a small range of temperature. The heat is then released in the reverse phase transformation.

The high storage density of the latent heat storage systems makes them suitable for integration in buildings, where there are generally space problems [4]. One of the main limitations for the development of thermal energy storage systems is the storage material itself. These materials are called phase change materials, PCM. They should meet a long list of physical, chemical, thermodynamic, kinetic and technical parameters, which make the search for a suitable PCM a very difficult duty. In addition to that, for the technology to be implemented it is necessary to develop materials that are economically feasible and have high energy density [5].

For the specific application of water and space heating for buildings, PCM with a melting temperature between 60 and 90 °C are necessary. The material should have the largest possible melting enthalpy, which provides the latent storage capacity. To draw a broad picture, the lowest acceptable melting enthalpy is generally drawn at a phase change enthalpy of 120 kJ/kg, while the maximum acceptable cost is generally defined at 3 €/kg, although these values are provided only to give an idea of the numbers behind the technology and are not true-limit numbers.

The herein presented work studies the development of a PCM based on the urea and Sodium nitrate eutectic mixture for the following reasons: No pure material was identified for thermal storage at the required temperature interval, 60-90°C. As a result, the search for adequate mixtures was carried out. The proposed mixture is formed by urea and Sodium nitrate. Urea is

[1] There are also phase changes from a crystalline phase to a different crystalline phase, but they have not been included for not being useful in the purpose of the thermal energy storage

a very cheap compound (1 €/kg), the melting point is 133 °C with a high storage density. However, it has degradation problems. Sodium nitrate also has good thermal characteristics for energy storage. It is currently being studied as PCM in concentrated solar power (CSP) because of its high melting point (308 °C). Previous research shows that the two compounds form a eutectic point with the following composition: 78.25 wt% urea and 21.75 wt% Sodium nitrate. The mixture melting point is 85 °C, lower than the original components melting temperature and within the application temperature range (between 60 °C and 90 °C).

1.2 THERMAL ENERGY STORAGE, TES

Thermal energy refers to the energy related to the movement of the particles that compose matter. The transfer of thermal energy from one body to another by means of a temperature difference is called heat. This transfer is carried out in such a way that if two bodies come into contact at different temperatures, the higher temperature body transfers part of its energy to the lower temperature body until the thermal equilibrium is reached, that is until the temperatures of both bodies are equal.

Heat is a very important resource for industrial, and building applications. In buildings, it is needed in domestic and tertiary sectors for space heating and hot water, among others. There is a need to store the heat when it is available, in order to use it when it is demanded and to be able to assure a continuous supply of heat. Storage can increase energy efficiency because it allows the use of surplus energy or waste-heat, which would be irremediably lost by dissipation into the ambient if they are not stored.

There are different ways in which heat can be stored: sensible heat, latent heat, and thermochemical heat.

Sensible TES

Sensible heat is the most common method of thermal storage. It consists of the transfer of heat to a body or storage material, which will consequently increase its temperature according to one intrinsic characteristic, the specific heat. Specific heat corresponds to the amount of heat required by one unit of mass of a thermodynamic substance to raise its temperature in one unit. It is expressed by equation 1.1.

$$Q = m \cdot C_p \cdot \Delta T \qquad (1.1)$$

Where:
Q: stored heat
m: mass of material
C_p: specific heat
ΔT: temperature increase

Sensible heat storage is widely used due to its simple engineering and low cost. The solid materials used for sensible heat storage are rocks, concrete, bricks and other ceramics for a wide variety of uses, including the use of the solar heat. Water, some organic oils and molten salts are used as liquid storage materials, especially in industrial heat exchange operations. Gaseous

substances have very low volumetric calorific capacity and, therefore they are not used in sensible thermal storage.

Latent TES

Latent heat is the heat associated with phase transformations. It is the heat that must be provided for materials to change from one phase to another, or from one state of aggregation to another. Heat is stored when the material changes from the most ordered phase (low entropy) to the less ordered one (high entropy) and is released by the material when it reverses back to the previous state. It is given by the equation 1.2.

$$Q = m \cdot \lambda \tag{1.2}$$

Where:
Q: stored heat
m: mass of material
λ: latent heat of phase transformation

The latent heat is measured in terms of energy per material mass [J/kg]. Storage can occur through four types of phase transformations, these being the following: solid ↔ liquid, liquid ↔ gas, solid ↔ gas, solid ↔ solid.

During the phase transformations, the temperature remains constant. Phase changes of pure materials are isothermal processes. The temperature where the phase change takes place is called transition temperature or phase change temperature. It is a material´s characteristic which depends on the pressure. Mixtures formed by several compounds present a, so called, semisolid range, instead of an isothermal melting. They start melting at a given temperatureand do not complete the melting until they reach another temperature. The semisolid range is a material´s characteristic. It depends on the mixture composition and the pressure. For a given composition, at atmospheric pressure, the semisolid interval of the mixture is a constant material characteristic that can be determined.

Thermochemical TES

Thermochemical TES refers to the energy stored as heat of a chemical reaction in reversible chemical processes. Endothermic reactions store heat, recovered back by the reverse reaction, which will be exothermic. This is depicted in the generic equation 1.3. As equation 1.4 shows, the heat amount stored in a chemical reaction depends on the mass employed, the heat of reaction and on the degree of conversion achieved in the reaction. They are generally very energetic processes, where a great energy quantity can be stored in a small volume. In addition, they have the advantage that no thermal insulation is needed to store the reaction products.

$$A + B \leftrightarrow C + D + \Delta H \tag{1.3}$$

$$Q = a_r \cdot m \cdot \Delta H \tag{1.4}$$

Where:
Q: stored heat
a_r: degree of conversion achieved
m: mass of material
ΔH: reaction heat per unit mass

Most chemical reactions are irreversible when they take place under simple operating conditions because they evolve by producing volatile products. Therefore, for thermochemical storage, generally the reactor design is very important. Some examples of chemical reactions presently under research for thermal storage are the decomposition of metal hydrides, peroxides, ammonia salts, carbonates, etc.

A specific form of thermochemical energy is the heat of adsorption/desorption of water molecules or a gas in a material. At present time, this is the simplest form of thermochemical storage. It is carried out using materials with very high microporosity; through which, they allow a high exchange of water absorption/desorption.

The different thermal storage types 8sensible, latent, thermochemical) are suitable for different applications. The main factors affecting the suitability are the storage time (daily, long term, seasonal), the economic viability and the operating conditions. Table 1. 1 shows the advantages and disadvantages of different thermal storage systems.

In order, to select a TES system for a determined application several criteria have to be taken into account, such as technical, economic and environmental criteria [5], [6]. The technical criteria include the storage capacity, the lifespan, the size, the resources used, the efficiency, the safety, etc. The economic requirements are mainly the system cost and the commercial availability. And finally, the environmental criteria require that the used materials are non-toxic or hazardous and must not cause adverse effects on the environment during the production, the distribution, the installation or the operation.

Table 1. 1 Advantages and disadvantages of the different types of thermal energy storage TES: sensible, latent and thermochemical

	ADVANTAGES	DISADVANTAGES
Sensible TES	• Inexpensive • Simple engineering	• Low energy density • Insulation required
Latent TES	• Medium to high energy density • Compact devices • Absorption and release of energy at constant temperature	• Insulation required • Complex at technical level
Thermochemical TES	• Very high energy density, higher than sensible and latent heat • Insulation not required	• Research phase • High price • Limited reversibility • Complex engineering

Currently, regarding the state of development, storage capability, commercial availability and durability, the developmental degree of the three TES types is visually depicted in Figure 1. 2 *[7]*.

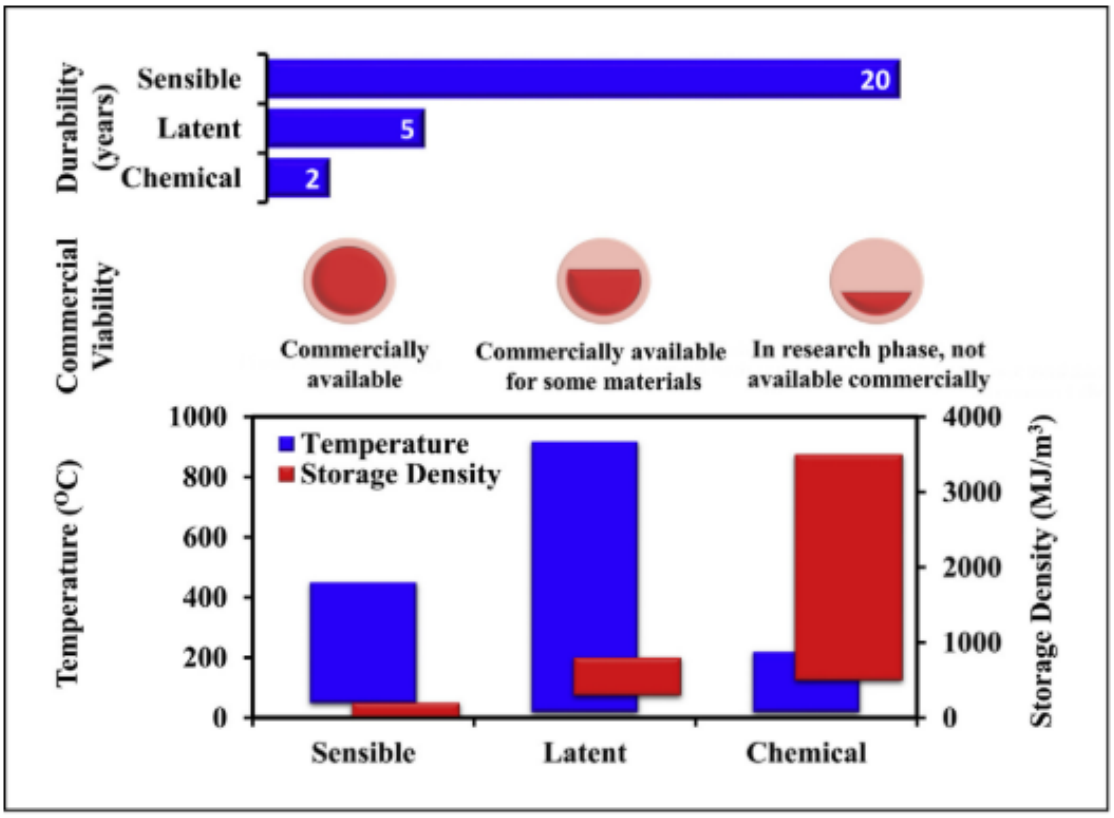

Figure 1. 2 Storage capabilities, commercial viabilities and durability aspects of PCM for thermal energy storage [7]

The sensible TES has been traditionally used even the storage density is not optimal due to the simplicity of its use and plenty availability in nature, it poses the longer durability and is fully commercially available.

Latent heat TES can be used at very different temperatures, depending on the selected PCM, and it provides the largest temperature operational range of the three types. It has a good storage density compared to sensible TES. Even though it has been studied during the last decades, the developmental degree do not yet fulfill the market needs. One of the main reasons for this situation is the lack of PCM materials to satisfy all the requisites needed, and other important one are the high prices that the storage device can reach for commercialization [8].

The thermochemical TES pose the higher storage densities, however pose very short durability and is not commercially available because it is still a developing technology, but very promising for the future [9]–[14].

Figure 1. 3 shows the classification of materials used for thermal energy storage [15]. The complexity of the TES technologies makes them more suitable for seasonal storage, while the latent heat thermal energy storage LHTES is more interesting for short term storage.

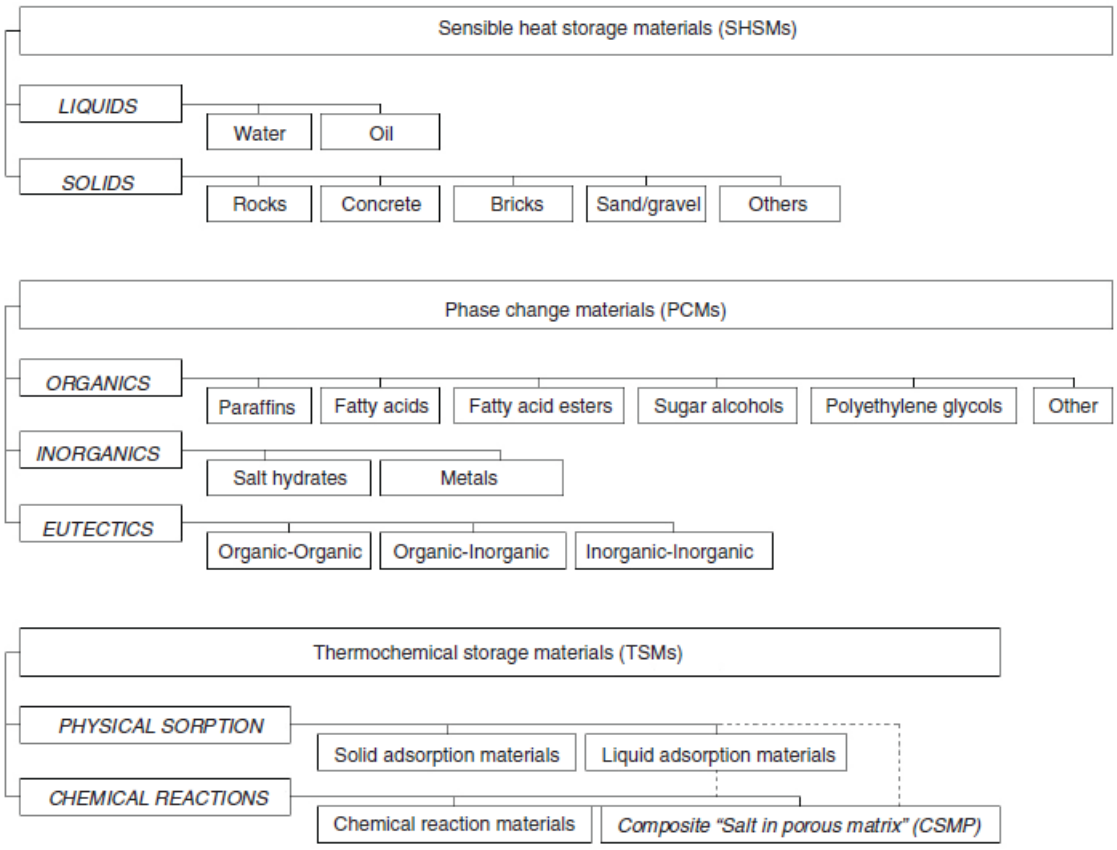

Figure 1. 3 Classification of thermal energy storage materials [15]

1.3 LATENT HEAT THERMAL ENERGY STORAGE LHTES

Latent heat thermal energy storage, LHTES, uses as a storage medium the latent heat of materials when they undergo a phase transformation or phase change. When heat is supplied to a material, it increases its temperature according to its specific heat storing sensible heat. Once the phase change temperature is reached, the heat supplied is used to break the existing bonds by disrupting the internal structure of the material, without modifying the temperature until the transformation has finished. The energy absorbed during the phase transformation is stored in the form of latent enthalpy. Figure 1. 4 shows the temperature evolution versus the stored/released energy (at constant pressure). As the energy input increases, the temperature increases while storing the energy as sensible heat, until the phase-change temperature is reached. Then, the isothermal transformations (solid-liquid and liquid-gas) occur, according to the material´s latent heat.

The largest latent heat transformations are those that end-up in a gas phase, the liquid-gas or solid-gas transitions. However, the engineering of gas containing processes are costly. As a result, the most suitable and efficient phase transformations for the thermal storage in buildings and the tertiary sector are the solid-liquid transitions. They require of a much simpler and lower cost engineering. Solid-solid transitions may also be used, but presently there has not been

determined any option, attractive enough in terms of phase change enthalpy, for the temperature range 60-90°C.

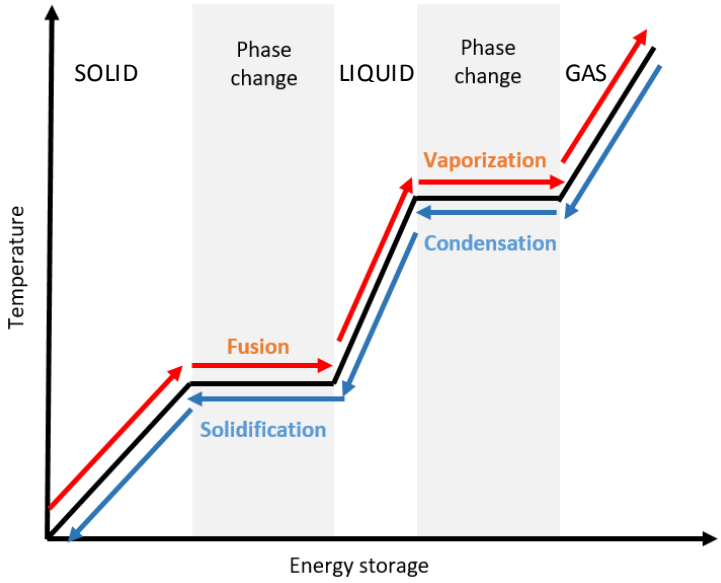

Figure 1. 4 Generic phase change scheme of materials

The LHTES technology needs systems research and improvement to tune-up the design to the requirements of each process/application. Different applications require different output characteristics: charging and discharging time, power, total energy, operation temperature, etc. Much research has been devoted to the improvement of the efficiency of such systems by working on different geometrical configurations, improvement of the thermal conductivity, etc. [16]–[18]. The published research works mostly deal with tailored systems designed and produced purposefully to carry out the research work [19]–[25]. Few commercial devices for very specific applications are available [26]–[30]. This makes LHTES an expensive technology, difficult to afford for the domestic/tertiary sector. Therefore, there is a need to lower LHTES systems costs in order to successfully introduce the technology in the market. Commercially available industrial heat exchangers may be modified to serve as a solution, to lower the system price. Research is required in order to characterize and propose convenient modifications. Within this work, an industrial shell and tubes heat exchanger was characterized as LHTES using Rubitherm RT60™[2] as PCM. This is a commercial paraffin, fully characterized, which provides a large stability on thermal cycling behavior.

1.4 PHASE CHANGE MATERIALS PCM

The materials used as a mean for storing heat in LHTES applications, are known as phase change materials, PCM. These materials may be pure substances or mixtures. The number of pure compounds is limited and, as a result, there are not as enough compounds to match any melting temperature that could be defined. Indeed, it is difficult to find pure compound that melt in

[2] https://www.rubitherm.eu/en/index.php/productcategory/organische-pcm-rt

some temperature ranges. This is the case for the storage temperature range required for the sanitary water and space heating of buildings, 60-90 °C. Few pure compounds present a melting temperature range in that interval, and a smaller number of them are indeed suitable for their use as PCM [31].

It is necessary to take into account some characteristics that a phase change material must meet in order to be considered competitive and suitable for its function. These are physical, chemical, thermodynamic, kinetic and technical characteristics [5]:

- Phase change temperature suitable for the process or application.
- Phase change taking place at a unique temperature, or in a very small phase change interval.
- High phase-change enthalpy to provide a high energy storage density.
- Low price, to be competitive with other thermal storage options (heat or cold).

When the previously mentioned requirements are met, other characteristics must be fulfilled, to a larger or shorter extent:

- Stability: no degradation and reproducible phase change properties with thermal cycling for the intended application
- Small volume change on the phase change
- Low vapor pressure
- Small or no supercooling
- Large thermal conductivity
- Compatibility with container materials, and other materials in contact with PCM (to avoid corrosion)
- High crystal growth rate (fast energy recovery).
- Environmental or other safety requirements: Low toxicity, biocompatibility, non-allergenic, non-flammable, self-extinguishing, non-explosive, etc.
- Sustainability: Renewable sustainable sources preferred, good recyclability, for environmental and economic reasons.

Mixtures are an alternative option for producing PCM with the required characteristics. Mixtures are formed by two or more pure compounds and, when solid, the material is generally formed by two or more phases (in the case of PCM, it generally consists of two phases), which are intricately and intimately attached and interpenetrated to each other on a micro-nanoscale. The mixture of the two solid phases do not generally presents a melting point. Instead, it melts (and solidifies) following a temperature interval, called the semisolid interval. Given the large number of possible combinations, there is a great potential number of candidate PCM formed by mixtures. However, the fact that they pose a semisolid interval is not suitable for most applications unless this interval is very small. Mixtures, in addition, might pose some problems specific to themselves, such as the instability to thermal cycling or the phase segregation. Some mixtures, corresponding to specific compositions, melt and solidify at one defined melting temperature, like pure compounds (although they are formed by two solid phases). Eutectic

mixtures correspond to this feature. Due to this characteristic, eutectic mixtures are a very interesting option for producing PCM.

Currently, several PCM classifications are proposed by different authors. The one by Sharma and Sagara [32] is interesting for the purpose of this work. PCM are classified as organic, inorganic, eutectic and mixed PCM:

Organic PCM include paraffin waxes, fatty acids, sugar alcohols, some polymers and their mixtures. Most organic PCM stand out for being chemically stable, for having congruent fusions and negligible supercooling, however they have lower volume melting enthalpies than inorganic PCM, that is to say, lower volume storage capacity. Paraffin waxes are mostly used due to their high stability, practically negligible supercooling and easy engineering to be produced with the desired melting point. The use of the non paraffinic organic compounds, such as fatty acids, sugars, or their mixtures is not as common as paraffins and few of these materials are commercialized as PCM[3].

Fatty acids have a large possibility of use at comfort temperatures in buildings. They have a high latent heat of fusion, reproducible fusion and crystallization behavior without supercooling. They can be made from common oils of vegetable and animal origin, which present a large potential for a sustainable use and development in comparison to paraffins. Their main disadvantages are a price 2 to 2.5 times higher than that of paraffins and its moderately corrosive nature [15], [33]–[35].

Sugar alcohols have a great number of advantages, such as high melting points (between 90-200 °C). They can be suitable for thermal storage in auxiliary energy systems (heating and water tanks). Their characteristics gather high energy storage density, non-toxicity, and good biocompatibility. Their main disadvantages are that, unlike other organic compounds, they have a high degree of supercooling, and also very slow crystallization rates and important oxidation problems [36]–[40].

Inorganic PCM researched until now include a large number of compounds. For storage temperatures below 100°C, hydrated salts have been widely researched. They present higher latent heat values than organic PCM, are non-flammable and readily available. Most of them are very stable chemically, are very cheap compared to organic PCM (1-3 euros/kg), have very interesting melting points for the building sector and the volumetric melting enthalpy is very high, much higher than organic products [6], [41], [42]. On the disadvantages, they can segregate in different phases during the repeated melting-solidification cycles because most of them present incongruent melting; they present important supercooling; the volumetric change during the phase change is around 10% and some of them are corrosive for most metals (the chlorides) while others are corrosive specifically for the aluminum (carbonates) [43]–[45]. Since they are ionic compounds, they are miscible with each other and it is possible to produce stable mixtures of hydrated salts between them, or between them and anhydrous salts. An interesting case is forming mixtures of anhydrous salts with hydrated salts, which in addition to modifying

[3] The companies Puretemp in USA, https://www.puretemp.com/ and Shangay tempered entropy in China www.pcmgel.com provide PCM products based on fatty acids

the melting points, reduces the supercooling and avoids the incongruent melting of the hydrated salts.

Eutectic PCM are mixtures of two or more components with a composition that pose a unique melting temperature, like a pure compound. The melting temperature of a eutectic mixture is smaller than the melting temperature of the pure compounds forming the mixture. In fact, the eutectic composition corresponds to the lowest melting temperature in the compositional pool. Each component melts and freezes together, at the same time, congruently. Eutectic mixtures, according to the formerly named classification, are classified by the nature of their constituents: organic-organic, organic-inorganic, and inorganic-inorganic. Their properties use to resemble their pure component properties. Several eutectic mixtures have been identified and studied [46].

Figure 1. 5 summarizes the PCM families as a function of temperature and melting enthalpy.

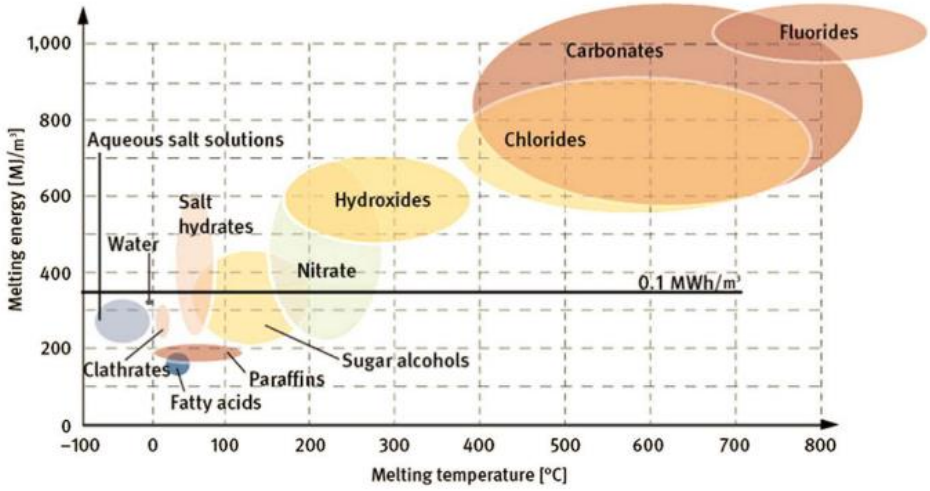

Figure 1. 5 PCM groups in function of their melting temperatures and melting energy [47]

The materials available in the range 60 to 95 °C, for the application of DHW and space heating, is small because both, few materials meet all the requisites for the implementation in a real application, and because of the high cost of those that are ready in the market [25], [48], [49]. To provide an indication of the present state of industrial development of PCM-related technologies, in 2019 around 38 companies were identified worldwide with the business focused on the commercialization of PCM, or products made with PCM [50].

In the evaluation and selection of a PCM, the most problematic aspects are generally the stability to thermal cycling, phase separation, large supercooling and poor thermal conductivity. These aspects are materials-type related characteristics, and as a general rule the organic PCM have poor thermal conductivity, while hydrated salts have poor stability.

Thermal stability

The PCM stability can be determinant in the material long-term behavior. PCM should be stable chemically and physically, in order to retain the initial thermophysical properties along their

functional life-span. Usually, however, degradation can occur over time due to oxidative, corrosive, or other processes.

Reliability

The PCM is required to reproduce exactly the same behavior for many cycles and for many years. Its thermal properties must remain unchanged during many cycles. However, in many cases this idea behavior is not met, and there are thermal properties variation. The conditions that can lead to it include the possible degradative processes, but also the polymorphism exhibited by many materials, which is especially the case of many organic compounds [36], [51]–[55]. Polymorphism is a property where one material can crystallize in different solid phases. The different possible crystallization phases are called polymorphs. Each polymorph properties are different from other polymorphs properties. Thus, if the material crystallizes into an undesired polymorph, the melting temperature, the melting enthalpy and all other properties will not be those sought for.

Phase segregation

In the case of PCM made of mixtures, phase segregation may occur in the solidification process due to the incongruent melting of the constituents. It generally happens in non-eutectic mixtures, because of the semisolid solidification interval. Phase segregation results in a decrease in the stored energy.

Supercooling

Supercooling, also called undercooling, can become a great problem for the PCM correct functioning. Supercooling is a phenomenon that occurs in all type of materials and consists in a temperature difference between the material phase change on melting and the start of solidification on cooling, which takes place at a lower temperature. It is a well known phenomenon, explained with detail in materials science and engineering books [51], [56], [57] . Supercooling affects the material capacity to deliver the stored heat since the latent heat is released at a lower temperature than the intended one, and part of this heat is used to increase the temperature of the material to the melting temperature, where final crystallization occurs. Figure 1. 6. shows this effect.

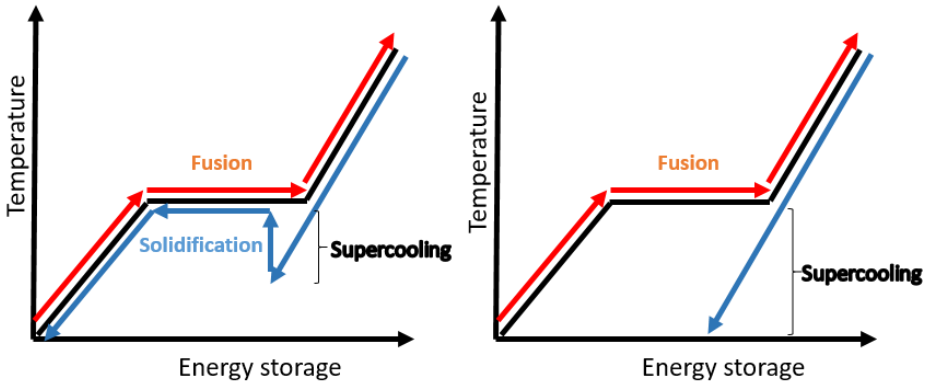

Figure 1. 6 Effect of the supercooling on thermal storage. Left represents slight supercooling and heat recovery after nucleation and right represents the case of severe supercooling when the material do not crystallize

Thermal conductivity

Thermal conductivity is defined as the heat flow per unit of area and per unit time, when the temperature decreases one degree in the unit of distance. It is a measure of the materials suitability to conduct heat. It is a very important characteristic to take into account for thermal storage because, in order to have effective heat transfer it is required to charge and discharge the heat in a specific time, depending on the process or application. Even in the cases where slow charging/discharging kinetics are acceptable, the higher the thermal conductivity of the material, the greater the chance and probability that it will be used in its entirety. In the cases where quick kinetics are required, the thermal conductivity of the PCM is usually the limiting factor for the efficiency of the systems [5], [58]. As a broad generalization, all non-metallic PCM at typical useful temperatures in buildings or in industry (-20 °C- +250 °C) have a thermal conductivity lower than desired, lower than required. Along the last decade, much research has been carried out devoted to increase the effective thermal conductivity by means of different solutions, which include the production of composites with high thermal conductivity material, the addition of nanoparticles, the addition of macrostructures and the design of high specific surface heat-exchanging devices [16]–[18], [59]–[61]].

1.5 STATE OF THE ART ON THE UREA AND SODIUM NITRATE EUTECTIC MIXTURE

The Enedi research team on latent heat thermal energy storage, where this thesis project has been carried out, investigated several mixtures composed of urea and different compounds [40], [62]–[64]. Among them, Diarce et al. [62] determined the phase diagram by means of differential scanning calorimetry DSC, the synthetic visual method and X-ray diffraction XRD. The urea and Sodium nitrate formed a eutectic system, with an interesting eutectic temperature for its use as PCM for DHW and space heating purposes, 85°C, with a supercooling degree of ~15°C. The characteristics determined in the above mentioned studies were suitable for the material use as a PCM. The eutectic mixture was thoroughly studied. The determined main characteristics are the following ones, also gathered in Table 1. 2 .

- The eutectic composition is 71.25 wt% urea and 28.75 wt% Sodium nitrate
- The results showed a melting onset temperature of 85.0 °C and a latent melting enthalpy of 172.0 J/g.
- Upon solidification, the material showed supercooling: For the experimental conditions applied, the onset crystallization temperature attained was 70.1 °C, and the crystallization enthalpy was 163.3 J/g.
- The material density is 1.48 g/cm^3 at 25 °C (solid) and of 1.423 g/cm^3 at 89 °C (liquid).
- The energy storage density on the phase change process is 245 MJ/m^3.
- The market price of the proposed eutectic material is below 1 €/kg, which is a very competitive price.
- The mixture presents a hygroscopic behavior

Table 1. 2 Main characteristics of the urea and Sodium nitrate eutectic mixture

Urea and Sodium nitrate eutectic mixture characteristics	Values
Composition	71.25 wt% urea 28.75 wt% Sodium nitrate
Temperature phase change range	85 °C
Latent heat	172 kJ/kg
Density (solid at 25 °C)	1480 kg/m^3
Density (liquid at 89 °C)	1419 kg/m^3
Volumetric energy density	425 MJ/m^3
Price	<1 €/kg

Previous works also carried out a preliminarily study related to the potential use of the material as PCM [63]. The materials involved in the system are hygroscopic, and this property could affect the thermal behavior of the mixture. In this regard, the water uptake by the eutectic mixture was studied to gain knowledge of its hygroscopic behavior. The hydrated samples, prepared under a 55% RH, presented a thermal behaviour different from that of dry samples, prepared under an atmosphere of 4% RH. The melting temperature and the latent enthalpy of the hydrated samples were lower than those of the dry material. The XRD results suggested that a new, unidentified, crystalline phase had formed in the hydrated samples, which coexisted with the urea and Sodium nitrate phases to form a ternary mixture.

On the above mentioned studies, preliminary thermal degradation studies were carried out. The thermal degradation of the eutectic mixture in the liquid state is an important parameter for the long-term use of the PCM. Pure urea is known to undergo significant thermal degradation in the liquid state above 133 °C [65], [66]. As a result, an accelerated preliminary thermal cycling study was performed to determine the mixture thermal reliability and to compare it with that of pure urea. Under the employed experimental conditions, the mixture melting enthalpy underwent a minor reduction of 1.2% after 210 cycles, and the crystallization enthalpy remained stable. Pure urea lost 79% of the thermal storage capacity in only 100 cycles[4]. These encouraging results were complemented by chromatographic analysis to determine any degradation by-product in the mixture after the cycling process. The results showed the formation of 0.4 wt% biuret after 210 thermal cycles. This amount is not relevant, although it could denote the start of a potential degradation process.

This thesis includes the continuation of the incipient research presented in the previous paragraph. The objective was to acquire valuable knowledge about the stability, long-term behavior and degradation mechanisms of this material; which could compromise its use as a PCM.

[4] The thermal cycling behavior of the eutectic material was carried out at a maximum temperature 10° above the melting point (95°C = 85+10°C), and the corresponding study with pure urea was carried out at a maximum temperature 10° above its melting point (143C = 133+10°C).

1.6 THE LATENT HEAT THERMAL ENERGY STORAGE SYSTEMS

The design of the storage systems and their operative strategy are crucial for an efficient LHTES use. Heat transfer to/from the process needs to be effective and efficient. The process has to be designed for each application, which includes many features such as thermal power, charging/discharging time, temperature range needed, etc.

The present stage of the latent heat storage systems for heating and hot water is underdeveloped. There are very few existing commercial systems [27], [28]. Hence, there is a need to develop new systems of this type.

The aspects required to take into account include the scale (prototype, pilot unit), HTF, geometry, construction materials, operational temperature range, thermal power, energy source, application, heat or cold storage, and used PCM.

Most researchers centered their studies to determine the adequacy of different geometries, and to include and/or improve the thermal exchange [40], [67], [68]. In order to analyze the influence of the device geometry in the heat transfer, several types of heat exchanger geometries have been studied, such as shell and tubes, packed bed, plate type, and others. Despite the availability of several geometry types, shell and tube geometry has been the most commonly tested due to its simplicity and compatibility with piping systems [69], [70]. Thermal power is in many cases one of the limiting operating conditions. With the aim of determining the most suitable method to increase the systems thermal power, several authors study the influence of the flow arrangements (parallel flow or counter-flow with a single pass or multi-pass) and the increase of the heat-transfer surface by including fins or matrixes [17], [71].

Most of the published research focus on design and operative aspects. Articles rarely supplies with information about the costs and feasibility of the devices commercialization. Nevertheless, recently the international research community on this field started research activities in methodologies to evaluate the systems potential commercialization [8]. The aim is to develop standardized methodologies to determine the devices levelized. Instead of developing new devices, the modification of commercially available heat exchangers is a potential economic solution. Heat exchangers are available in the market, they are already competitive for different applications. Some research works carried out experiments by adapting existing heat exchanger technologies to LHTES systems. The outcomes reported not being satisfactory [72], [73]. The need of a tailored design for each application makes it unfeasible that simple modifications to the commercially available HEX be sufficient for a good result. However, understanding the HEX pitfalls when it is used as LHTES, provides the basis for proposing sound modifications capable of guaranteeing an efficient use.

The present thesis has carried out a parametric study to acquire the above mentioned knowledge regarding a HEX which had been previously modified and preliminarily tested in previous works [74]. The PCM employed in those works was stearic acid, concerning a different temperature and application to the intended in this thesis. Some few experimental runs were carried out and the results concerning the device thermal behavior were not sufficient to

understand its performance. The present thesis performs a complete parametric analysis in order to fully characterize a commercial HEX of the shell and tubes type, for its use as latent heat thermal storage device and to analyze the feasibility of this kind of devices for thermal energy storage.

1.7 MAIN OBJECTIVES AND STRUCTURE OF THE PH. D. THESIS

This Ph. D. project seeks the goal of contributing to the knowledge above the presently existing state of the art regarding LHTES technology. The global objective of the thesis was to determine the suitability of one defined PCM, the urea-Sodium nitrate eutectic mixture, and one defined LHTS device, a shell and tubes heat exchanger, for their implementation as a latent heat thermal energy storage technology, technically and economically viable for their integration in buildings. Both, the material and the LHTS device provided encouraging results in previous works, and the target vision was that they could integrate to conform a future thermal storage technology suitable for hot water and space heating application in building. As a result, the objective of the present thesis was to perform an in-depth study of the urea-Sodium nitrate eutectic mixture, and to acquire the expertise to define the modifications required on a commercial shell and tube HEX for its use as LHTES.

Several different specific objectives have been targeted in this project. Regarding the materials characterization:

To study the long term stability of the PCM, the urea and Sodium nitrate eutectic mixture, and specifically the thermal degradation.

To determine and analyze several specific characteristics of the mixture that might jeopardize the long-term use of the PCM and were unknown or insufficiently researched, such as the hygroscopicity, the phase segregation and the supercooling.

A secondary objective of the materials characterization is to develop testing methodologies representative of the functional and operational conditions that the material would encounter in use. The testing approaches reported until present time involve laboratory scale conditions and accelerated testing, which in most cases are not suitable to resemble the real behavior of the material in use. Therefore, this objective arises from the need to know how the materials will behave in the real application, which can greatly differ from the laboratory scale.

Regarding the storage system, a shell and tubes heat exchanger has been studied in order to evaluate the use of commercial devices (i.e. potentially more economically feasible) as latent heat energy storage LHTES devices. Three objectives were initially set out, the first one to experimentally characterize a modified commercial industrial shell and tubes heat exchanger to acquire a deep understanding of the device thermal behavior when used a LHTES. The second objective was to model the heat exchanger using a CFD software and to validate it with the experimental campaign results. The third objective was to use the characterization and modelling activities is to be able to define and quantify the modifications required for its use as an LHTES system. An extense parametric study was carried out and the first objective was fully

accomplished. Unfortunately, due to time restrictions the modelling task could not be concluded and, as a result the expertise for the modifications was not reached.

Bearing this into mind, this thesis is composed of five different studies, four of them regarding the long term behavior of a PCM formed by a urea – Sodium nitrate eutectic mixture and a last one regarding the characterization of a commercial HEX employed as a LHTES device. Chapters 2, 3, 4 and 5 are devoted to the material characterization and Chapter 6 is devoted to the LHTES characterization. It has to be highlighted that the introduction and state of the art regarding each topic is included at the beginning of each chapter. Finally, Chapters 7 and 8 are devoted to the conclusions of the Ph. D. work and the references, respectively.

Chapter 2 is devoted to the study of the water uptake by the urea and Sodium nitrate eutectic mixture under different conditions. Phase identification and thermal properties evaluation (XRD and DSC) were carried out in hydrated and dry samples to assess the need for drying the materials in order to be used. Sample preparation methodology and handling conditions sere developed for avoiding the water uptake in the mixture.

Chapter 3 is devoted to the thermal degradation of the urea and Sodium nitrate eutectic mixture. It is sought to determine if it is possible to use the material as a PCM for medium or long term life-spans. Generally, the published literature report thermal cycling to evaluate the thermal stability of the PCM. However, accelerated thermal cycling does not differentiate different phenomena occurring in the material: thermal degradation due to instability at high temperature, phase segregation, etc. For this reason, a different experimental approach was used in the thesis, based on measuring the thermo-physical behavior after the material had been exposed at high temperatures for long times. The materials characteristics were determined after exposure (DSC measurements), specifically the melting latent enthalpy, melting onset temperature and melting peak temperature. These parameters stability is directly related to the PCM thermal energy storage and its long-term stability. In addition, the degradation products and their influence on the variation of the system properties were assessed.

Chapter 4 describes the study of an important aspect regarding the long-term use of the urea and Sodium nitrate eutectic mixture, the phase segregation. The eutectic mixture showed unforeseen segregation at temperatures above the melting point. This aspect has not been identified in previous testing because it is not noticeable on the DSC scale, and no tests had been done with samples larger than 10-15 mg until the Ph. D. work started. Indeed, this type of phenomenon is rarely discussed in other articles, with other PCMs, because most research works are carried out with small samples (DSC mostly) under accelerated testing. Several tests were done including thermal cycling, XRD, DSC and microscopy (PLM and SEM). The results established a relationship between the operation conditions, more specifically the cooling rates, with the resulting crystal structures, which explains the phase segregation occurred in the eutectic mixture. A mitigation measure how to reduce it and how to reverse the process was proposed.

Chapter 5 is devoted to the study of the supercooling. An approach different to the usual approaches employed in the PCM research community. The aim was to further improve the

knowledge about the supercooling relationship to the system parameters, to efficiently design LHTES systems to be used with materials that exhibit supercooling. Experiments were designed to determine the relationship of the supercooling degree with parameters associated with the system, like the sample volume, the cooling media properties, and finally the PCM properties. To do it, several sample containers with different geometries and volumes, several cooling rates, two heat transfer fluids (HTF) and two PCM were used (urea and Sodium nitrate eutectic mixture and polyethylene glycol 10000).

Chapter 6 is devoted to the characterization of the modified industrial heat exchanger. A complete parametric campaign was carried out. Even though the herein studied PCM, the urea and Sodium nitrate eutectic mixture, would have been ideally suited for the coherence of the thesis, there were many uncertainties related to the PCM behavior which could have jeopardize the proposed approach. Therefore, the characterization was performed using RT60 paraffin as PCM inside the shell, a well known commercial material, to assure the reproducibility of the results, and water as heat transfer fluid HTF in the tubes. Several flow rates and temperature ranges were used to obtain a greater scope of the operation of the device as LHTES. The work included the determination of the thermal losses, and the study of charging and discharging cycles with different HTF, initial and final temperatures, and flow rates. The temperatures of both, the HTF and in the PCM, were monitored during the tests in several different locations. Then, the charging and discharging times and parameters related to the stored and released energy were determined.

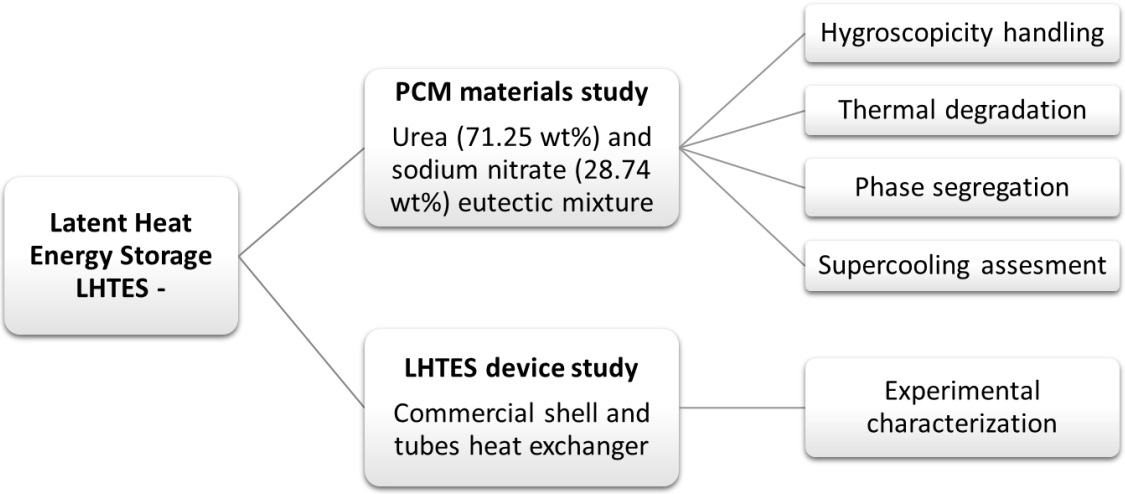

Figure 1. 7 Scheme of the thesis organization.

Chapter 2 : Urea and Sodium nitrate eutectic mixture handling and sample preparation. Hygroscopicity behavior

2.1 INTRODUCTION

The urea and Sodium nitrate eutectic mixture has been studied to evaluate its feasibility as phase change material for the DHW and space heating application. However, the mixture presents some problems that hinders its use, among them the hygroscopicity.

The pure constituents of the mixture, urea and Sodium nitrate, are hygroscopic materials [75]–[79]. Previous research show that the water uptake affects the mixture thermal properties because new phases formed [63]. The scientific literature reports that the Sodium nitrate hygroscopicity does not result in the formation of new phases [77], but urea does. The information regarding the urea-water binary system phase diagram and the urea-biuret-water ternary system phase diagram (biuret is a by-product from urea degradation) [80] correspond to eutectic systems. As a result, they include some compositions with melting temperatures lower than the pure urea melting point. Thus, in the case of the urea and Sodium nitrate eutectic mixture, the reported new phase formed due to the mixture hygroscopic behavior points towards a ternary eutectic system formed by urea, Sodium nitrate and water, although the published literature does not provide evidence to back this up. However, additional hints that point towards this possibility include the reduction of the melting point when the mixture entraps water. When a ternary eutectic forms, the melting temperature is lower than the melting temperature of the binary eutectic compositions.

To carry out any characterization study with this PCM, humid atmosphere should be avoided in order to properly discriminate the obtained values. In addition to forming new phases, water reacts with urea promoting its degradation: Water combines with urea to form carbon dioxide and ammonia [81], [82].

From the previous considerations, it can be foreseen that humid atmospheres affect the urea and Sodium nitrate eutectic mixture by interacting to cause new phases, which decrease the melting temperature, and to promote higher degradation rates.

This chapter aims to determine how the water absorption affects the mixture thermal behavior and potential degradation and to establish sample preparation procedures, and storage and handling methodologies, to obtain nearly dry urea and Sodium nitrate eutectic mixture samples without the need of complicated processing routes or facilities (i.e. the use of a glove box and controlled atmospheres).

2.2 EXPERIMENTAL DESCRIPTION

A research approach was prepared to study the moisture content of the urea and Sodium nitrate eutectic mixture, now on called U-SN eutectic, by means of the Karl Fischer reaction. The variation of the thermal characteristics when the material contained different

moisture contents were determined by means of DSC. Finally, XRD measurements were used for the phase identification, to verify that undesirable phases did not form after drying.

2.2.1. EUTECTIC MIXTURE PREPARATION

The preparation of the eutectic material was carried out according to the following procedure:

- Pure urea and pure Sodium nitrate (see Table 2. 1) were weighed using a 0.1 mg resolution precision scale (Ohaus Discovery 114C) in a glass beaker to attain the eutectic proportion (71.25 wt% urea-28.75 wt% Sodium nitrate).
- A magnetic stirrer was introduced into the beaker, which was closed using a silicone or rubber plug, and immersed in a glycerin bath at 90°C. The glycerin bath with magnetic stirring was used as a means to ensure the homogeneity of the temperature around the sample.
- The glycerin bath was heated by means of a hot plate (MR Hei End by Heidolf), controlled by a PT1000 external temperature sensor (±1°C) introduced into the glycerin to get a stable temperature. Magnetic stirring inside the sample allows the pure urea and Sodium nitrate to get into intimate contact at a temperature higher than the eutectic melting temperature (85 °C), to produce the melting of both materials and form a liquid new phase. The stirring speed used was 300 rpm. Figure 2. 1 shows the glycerin bath and the obtained molten sample.

Once the sample was melted, different paths were followed for the sample crystallization:

- Powdered sample: Pouring the liquid sample onto a large flat surface to obtain a relatively thin plate, easy to break for subsequent grinding in a ball mill;
- Plaque sample: Leaving approximately ≈1 ml height of liquid sample, to solidify inside the closed beaker to form a thin plaque (stirrer extracted).

Figure 2. 1 Eutectic preparation procedure: melting pure urea and Sodium nitrate. In the left the glycerin bath assembly and in the right the molten sample

Afterwards, samples were submitted to different storing conditions to evaluate their water uptake behavior. In addition, powdered and plaque samples were introduced in a desiccator with phosphorus pentoxide to evaluate the sample drying potential. Phosphorus pentoxide was

used for this aim because it is able to reach a very low relative humidity. In this case 6-7% HR was achieved. Table 2. 1 summarizes the raw materials used for sample preparation.

Table 2. 1 Raw materials employed for the sample preparation

Material	Supplier	Purity	Quality
Urea	Panreac Química S.L.U.	99%	Laboratory grade
Sodium Nitrate	Panreac Química S.L.U.	99%	
Phosphorus Pentoxide	Panreac Química S.L.U.	98%	

The samples humidity was determined according to the procedure explained in 2.2.2 Determination of the sample moisture content by means of Karl Fischer coulometric titration.

After determining the humidity percentage, the thermal properties of the samples was determined, as explained in 2.2.3 Evaluation of the thermal behavior by means of differential scanning calorimetry DSC.

The samples were finally analyzed by X-ray diffraction, as explained in 2.2.4 Phase identification by means of X-ray diffraction XRD.

2.2.2. Determination of the sample moisture content by means of Karl Fischer coulometric titration

Karl Fischer titration was used to determine the materials water content. A KF-31 coulometric titration system from Mitsubishi Chemical was used, using Aquamicron AX and CXU as reagents. The estimated accuracy of the device (for the experimental conditions underwent in this work) was 70.01 wt% of the total water content determined for each sample because of the small quantity that could be measured. The methodology employed for the measurements is fully described in [83]. Due to the expected moisture content, the evaluated samples consisted of 100 - 300 mg (for the reactive not to saturate).

The sample is introduced in the titration vessel, which contains the reactive. It should dissolve completely to have a reliable measurement. Therefore, all samples were grinded before the measurement in order to guarantee the adequate reaction kinetics for the measurement.

The study was carried out following a systematic procedure, carrying out measurements of humidity in several conditions:

a) 15 minutes after the material solidified in contact with the air;
b) after a certain time stored in contact with open air;
c) after a certain time stored in the refrigerator;
d) after a certain time stored in a desiccator with phosphorus pentoxide;
e) stored in powder or in a plaque without grinding.

The obtained results have a qualitative character because some variables, like the humidity and ambient temperature, were not registered throughout the entire process, only at the moment of the measurement. The procedure does not provide the required traceability in

terms of the ambient temperature and humidity evolution for the samples that underwent long storage period, so as to determine quantitative reliable values.

The measured relative air humidity values in the whole set of experiments ranged from 33 to 47 HR %, and the room temperature oscillated between 17 and 23 °C.

The moisture content of the pure urea and Sodium nitrate were also measured before the sample preparation.

2.2.3. Evaluation of the thermal behavior by means of differential scanning calorimetry DSC

Differential scanning calorimetry, DSC, measurements were made on samples of U-SN eutectic with different humidity percentage, to evaluate the influence of the sample moisture content on the thermal behavior of PCM.

Three samples were prepared:

- A dried sample, with a moisture content of 0.08%;
- A fresh sample after grinding, with 0.17% moisture content
- A sample with 10% moisture content reached after 10 days in contact with air.

Approximately 10 mg of each sample were placed in a aluminum 25 µl DSC crucible, and sealed with a lid using by means of a press. The methodology employed for the DSC measurements is fully described in [62]. The apparatus used was a Mettler Toledo DSC 1.

The samples were submitted to a heating ramp from 25°C to 200°C at 5 K/min. Generally, when DSC measurements are carried out, a first heating segment is performed to condition the samples and get better contact with the crucible, followed by a cooling ramp, and finally a second heating cycle serves to take the measurement. But in this case the procedure required to be modified. To assess the phase transitions of the resulting on samples with water content, this initial conditioning cycle had to be removed because the absorbed water can be released during the first heating cycle, thus modifying the sample composition and rendering different results in different consecutive cycles.

2.2.4. Phase identification by means of X-ray diffraction XRD

X-ray diffraction, XRD, measurements were made on dried U-SN eutectic samples to verify if there are new phases derived from the mixture reactions due to the high temperature during the preparation of the mixture (degradation), or due to water uptake or, also from potential contamination with the desiccant agents.

The diffraction patterns were obtained using a Philips X'pert Pro automatic diffractometer. The methodology employed for the XRD measurements is fully described in [62]. The Powder Diffraction File (PDF) database was consulted for phase identification.

The analyzed samples included pure urea and pure Sodium nitrate, two samples of powdered dry eutectic mixture (one sample was dried using phosphorus pentoxide and the other one using silica gel).

2.3 RESULTS

Determination of the sample moisture content by means of Karl Fischer coulometric titration

The purchased pure raw materials present a very small water content: 0.1-0,2 wt% in urea and 0.03-0.06 wt% in Sodium nitrate.

15 minutes after sample preparation: After the eutectic mixture preparation, the grinded samples exhibited values between 0.1 and 0.17 wt% moisture, measured 15 minutes after the sample preparation, where the samples solidification has taken part in contact with the air, and inside a closed beaker. The moisture content in both samples was similar, displaying values from 0.1 to 0.17 wt%. So it was determined, that the solidification of the sample in contact with air does not report a great water absorption.

1 day in contact with the humid environmental atmosphere versus in closed beaker: The behavior of the powdered samples after 1 day in contact with the humid environmental air increases to more than 3 times higher humidity content than the samples in the closed beaker surrounded by humid environmental air, and 2 times higher than samples in the closed beaker in the refrigerator as shown in Figure 2. 2 upper image.

Closed container in lab atmosphere	Closed container in refrigerator	Opened container in lab atmosphere
Water uptake A	Water uptake B = 1,5 A	Water uptake C = 3 A

The evolution of the moisture content in the powdered samples exposed to environmental air increases significantly in 10 days, reaching a moisture content of 10 wt% after only 7 days. After 22 days, small water drops could be observed on top of the samples. No measurement was feasible in these samples.

The samples in the refrigerator show a milder water trap increase, to a final value of 3.3 wt% after 22 days. The lower water trap inside the refrigerator is due to the influence of the lower temperature, which admits lesser relative humidity.

The desiccator, fitted with the Phosphorus pentoxide, provided an atmosphere with a relative humidity between 4-7%. After a time of 1 day all the samples in the desiccator contained lower moisture than the materials originally introduced in them. The humidity percentage remained unchanged in time to a value around 0.08 wt%, regardless if the samples were in plaques or in powder.

It was therefore concluded that it is possible to dry the grinded material by a method as simple as storing the material in a dry environment (relative humidity within the container ≤ 7%). The minimum values reached by this method range between 0.001 and 0.08% humidity. The time required to reduce the moisture depends on the material mass to be dried and the

relative humidity of desiccator. For sample masses between 20 and 100 grams, no more than 2 days are required when the relative humidity inside the desiccator is lower than 7%.

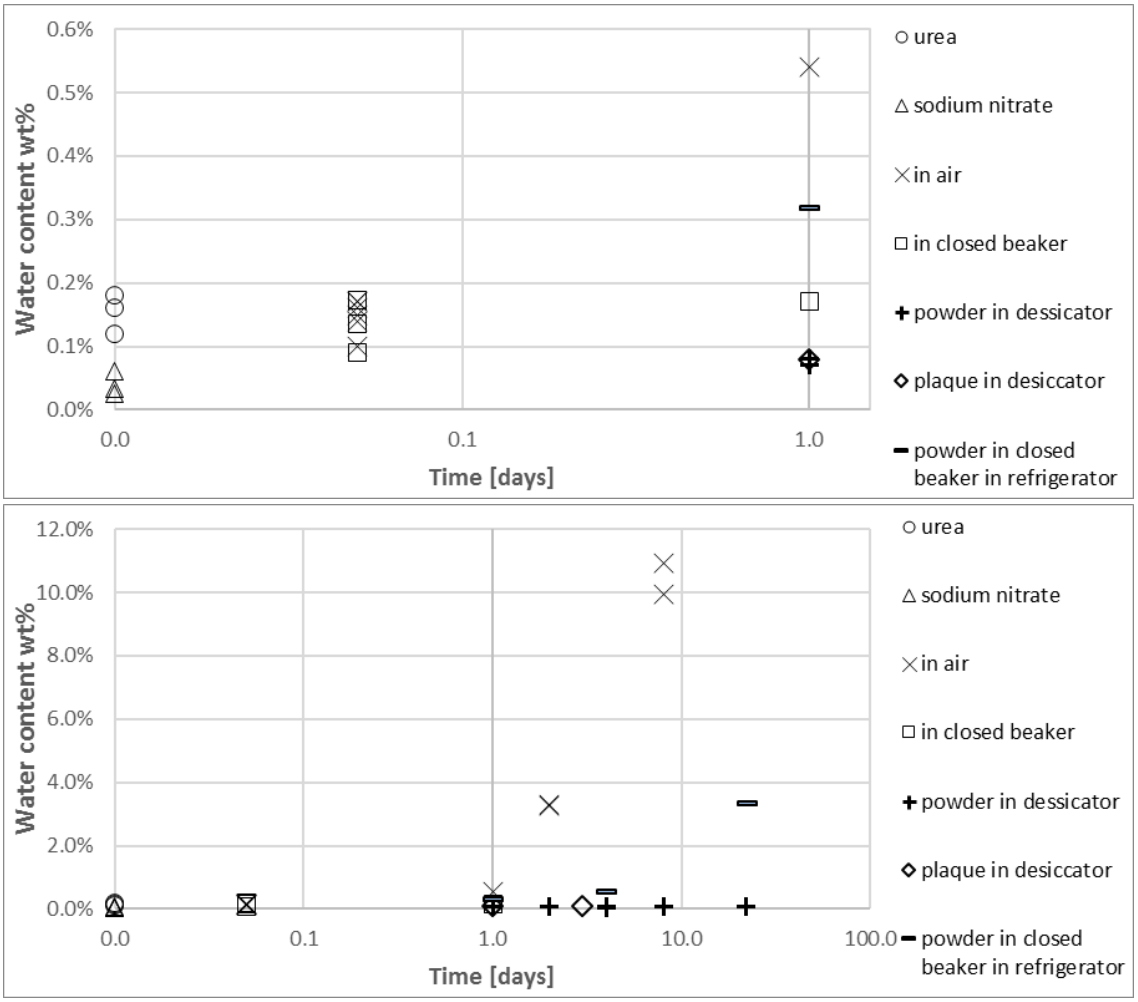

Figure 2. 2 Water content evolution in 1.4 g of urea and Sodium nitrate samples are stored in different conditions. The figure on the top show samples up to 22 days. The figure on the bottom represent samples up to 1 day after preparation.

The powdered samples were easier (quicker) to dry than the plaques, but they also absorbed water more readily. This is due to the larger powder specific surface in contact with the humid air. From this fact, if the material were to be commercially deployed, bulk material with lower surface area can be used in purpose for storing and handling to avoid greater water uptake.

Evaluation of the thermal behavior regarding the moisture content by means of differential scanning calorimetry DSC

Three samples were evaluated: a) a dried sample with a moisture content of 0.08%; b) a fresh sample after grinding, with 0.17% moisture content; and c) a sample with 10% moisture content reached after 10 days in contact with air. Figure 2. 3 shows the thermograms of the samples *a* and *b*. They exhibit the same geometry and relatively similar thermal characteristics. However, sample *b* has a slightly lower melting temperature and fusion enthalpy. The thermogram of sample *c* shows a geometry very different from that of samples *a* and *b*. Two or more thermal

events can be seen, which do not correspond to the melting temperature of the mixture. This may indicate that the material becomes a ternary mixture with a eutectic point at a lower temperature (46 °C).

These data confirmed that the U-SN eutectic mixture requires to be dried in order to achieve the desired thermal behavior. However, the samples with 0.17 wt% moisture content do not show significant thermal properties change, thus being possible to use them if a closed container is used.

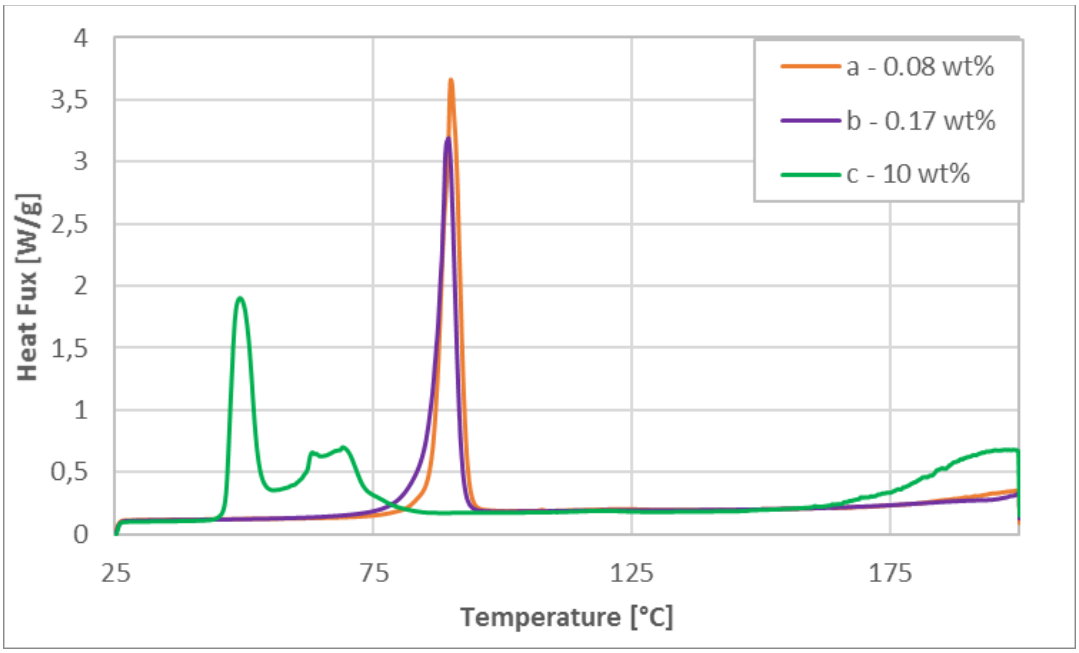

Figure 2. 3 Thermograms of samples a, b and c. Moisture content of 0.08 wt%, 0.17 wt% and 10 wt% respectively.

Phase identification by means of X-ray diffraction XRD

Figure 2. 4 shows the diffractograms of the measured samples. Pure urea and pure Sodium nitrate showed no contamination of other phases.

The diffractograms of the dry U-SN eutectic samples 1 and 2 show the same peaks, meaning no new phase has formed due to the use of phosphorus pentoxide or silica gel as desiccant agents.

The sample 1 was afterwards exposed 30 minutes in contact with air at 20 °C and 46% relative humidity, and a new diffraction measurement was carried out in order to verify the results obtained in [63] and to verify that the unidentified diffraction peaks are due to the water uptake. The diffractogram shows that some peaks emerged in positions different from those from urea and Sodium nitrate, and are enclosed in black boxes. These peaks indicate the presence of a new phase in the sample. This phase could not be identified in the available data bank for XRD compound-identification, due to the fact that there were no coincidences sufficiently adjusted with the existing phases in the database. The hypothesis is this phase to be a hydrated phase formed in the PCM. It is confirmed that humidity alters the crystalline phases in the U-SN

eutectic, causing the change of the thermal properties, threatening the potential use of U-SN as a PCM.

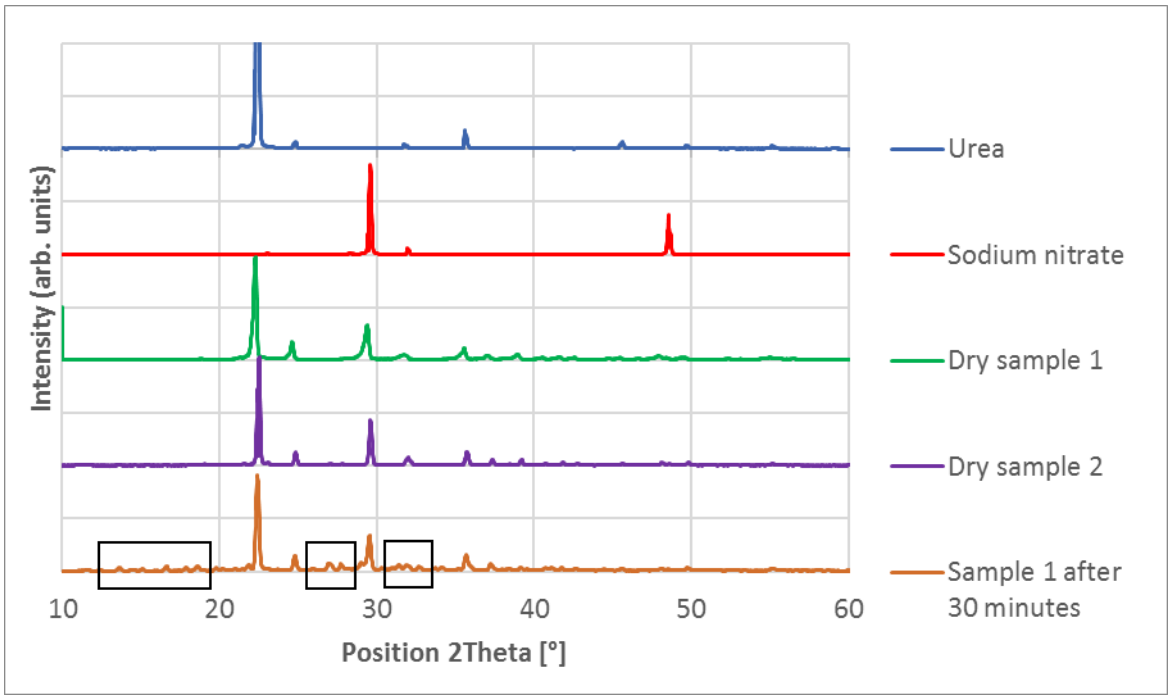

Figure 2. 4 Diffractogram of pure urea and Sodium nitrate, U-SN eutectic dry samples 1 and 2 (desiccating agent phosphorous pentoxide and silica gel respectively), and sample 1 after 30 minutes in contact with humid air (20 °C, 46% RH)

2.4 CONCLUSIONS AND REMARKS

The samples moisture content was determined from the sample preparation stage to 22 days under various storage conditions. The results concluded that the samples prepared in a closed container, with ambient conditions in the range of 33-47 HR % and 17-23 °C, have a low initial moisture content of 0.17 wt%.

The lowest water content obtained was 0.08 wt%. This was obtained by storing the material in a closed container with a humidity level of 4-7% by means of a desiccating agent. The thermal properties determined in this samples (melting temperature and latent enthalpy) were considered as the reference for the rest of the samples with larger humidity levels.

The samples with up to 0.17 wt% water content show negligible decrease on the properties in comparison to the dried mixture (0.08 wt%).

When samples are exposed to the humid air (normal environmental conditions), they absorb water and changes on the original crystalline structure. New phase(s) form, which do not correspond to any identified phase in the Powder Diffraction File (PDF) database. The introduction of this phase (in small quantity) results in a decrease in the melting temperature, the melting starts at 45 °C. Two phase transition peak signals are observed in the hydrated samples indicating that it may be a hypo or hypereutectic composition of a possible ternary

system composed of urea, Sodium nitrate and water. Therefore, it is concluded that the samples must be dry to be used as PCM.

The methodology followed allows us to know that the humid samples can be dried using desiccating agents, more readily if they are ground, but it is also possible to dry the samples in thin plaques obtaining a humidity of the same order (≈0.08 wt%). However, the handling of powders is more complicated if the samples are in contact with air, so it is recommended to store the U-SN eutectic material in form of bulk plates and/or to use dry atmospheres.

Chapter 3 : Thermal degradation study of the urea and Sodium nitrate eutectic mixture

3.1 INTRODUCTION

The eutectic mixture formed by 71.25 wt% of urea ($CO(NH_2)_2$) and 28.75 wt% of Sodium nitrate ($NaNO_3$) has a melting point of 85°C, in the range of the DHW and space heating application. It poses several interesting features, including high melting enthalpy, non-expensive price, large availability and is biodegradable (its main use is for fertilizing soils)[62], [63]. The use of pure Urea as PCM for thermal energy storage at a temperature of 132°C (Urea melting point) was researched several decades ago [4], [15], [65], [84]–[87] being discarded due to its poor thermal stability: Liquid urea quickly degrades forming different compounds. In this context, no other studies have been performed up to date that seek to prevent or eliminate the degradation or the improvement of the thermal stability.

However, since the urea and Sodium nitrate eutectic mixture presents a melting point significantly lower than pure urea, 85°C, the degradation rate could be significantly slower and, as a result, the thermal degradation in this case could become an inconvenience instead of being a limiting factor for its use as PCM. Consequently, Diarce et al. (in collaboration with the author)thoroughly studied the urea-Sodium nitrate system. Its phase diagram and main thermophysical properties were reported in [62], [63], together with a preliminary accelerated thermal cycling test. It was concluded that the mixture can be considered a good PCM candidate, although further studies on its long-term stability and degradation were required.

The degradation behavior of pure urea and pure Sodium nitrate has thoroughly been studied and reported in the literature. Pure urea is used as a precursor of ammonia in automobile Selective Catalytic Reduction SRC, for elimination of NOx in exhaust gases [81], [82], [88]–[93]; and also studied as a degradation product of urea nitrate ($CH_5N_3O_4$) thermolysis [94], [95].

The reported urea main degradation path is shown in Figure 3. 1. When submitted to high temperatures, in a first stage urea decomposes into ammonia and isocyanic acid. Then, isocyanic acid reacts with the unreacted urea to produce biuret. Afterwards, cyanuric acid may form due to the reaction of biuret with isocyanic acid. This decomposition path takes place in the absence of water. In humid atmosphere, the isocyanic acid reacts with the water causing more ammonia and carbon dioxide. Evidence points out that the presence of water promotes higher degradation rates [82]. For this reason, the present study was carried out in an atmosphere with controlled humidity.

In addition to the already mentioned decomposition products, other degradation compounds are mentioned in the literature when urea is heated up to very high temperatures under different conditions, like ammelide, ammeline, and melamine, which are formed by polymerization; and/or anions such as cyanurates, isocyanates, acetates, formates, nitrates and nitrites[92]. Indeed, most published works dealing with urea thermolysis analyze the process at temperatures higher than the operating temperature range herein sought for the urea and

Sodium nitrate eutectic mixture (<100°C). Only some few works (Désilets et al. [94]; Bernhard et al. [81]) reported urea degradation at temperatures as low as 100°C (below pure urea melting point). Besides, the degradation was generally studied on conditions different from those designed for themal energy storage (open container, catalysts, solid urea/dissolved in water, etc) and cannot be considered as a reference for the potential behavior of the mixture under the PCM working conditions. Actually, most quantitative research regarding urea thermolysis has been approached with the final objective of attaining the maximum potential conversion of urea into ammonia, for the development of system suitable for NOx elimination. As a result, they pursue to identify the operating conditions that will promote maximum urea degradation, which is the opposite objective to the aim of the present study.

For the herein studied application, however, urea decomposition is aimed to be reduced or eliminated if possible. An important parameter in the attempt to reduce the degradation of urea is the use of tightly closed containers that will lead to an equilibrium pressure of the gaseous byproducts, thus limiting the degradation of the original material.

The literature regarding the degradation of Sodium nitrate [77], [96], [97] indicates that the thermal decomposition of $NaNO_3$ depends on the temperature: at very high temperature, above 700 °C, nitrate decomposes and releases nitrogen oxides; at intermediate temperatures, from 450 °C to 700 °C, part of the Nitrate decomposes forming Nitrites, reaching an equilibrium; at low temperatures, from 308 to 450 °C ($NaNO_3$ melting temperature is, 308 °C) a small percentage of nitrite forms. Bauer et al. [77] exposed Sodium nitrate to 350°C at atmospheric pressure. The results showed that about 0.1 wt% nitrites (NO_2^-) formed within a few hours, but the decomposition progressed slowly, with a nitrite content of 0.2 to 0.25 wt% after a period longer than 100 days at 350 °C. Overall, it can be concluded that $NaNO_3$ is thermally stable at 350 °C since decomposition is limited to the formation of a very small amount of nitrite. Consequently, the decomposition of Sodium nitrate below 100°C is foreseen to be negligible. As a result, only urea decomposition in the urea-Sodium nitrate mixture requires consideration.

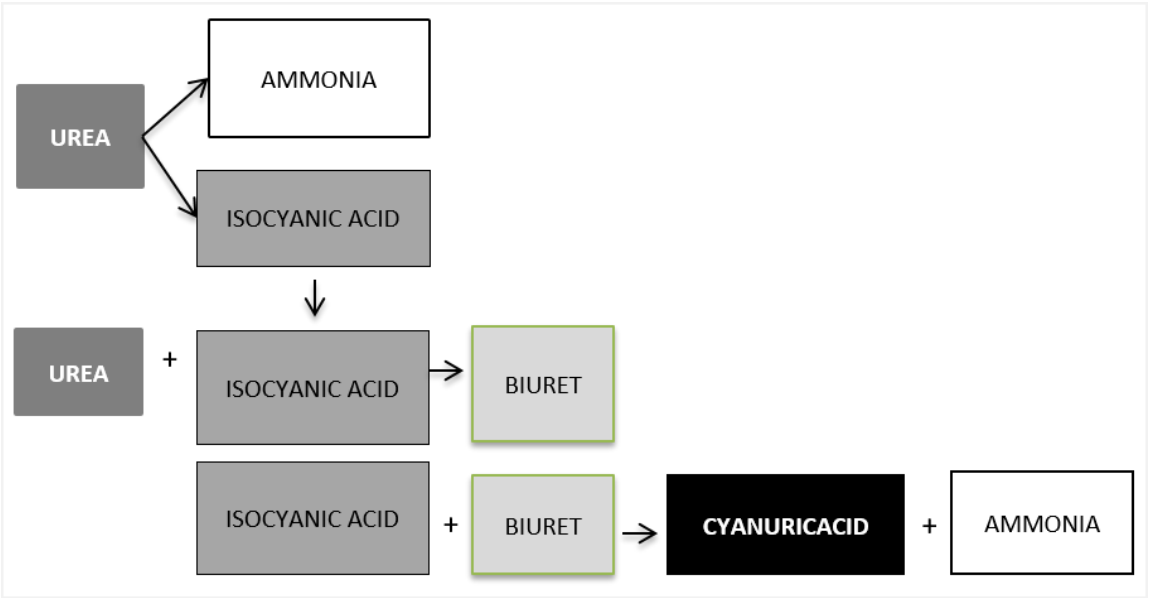

Figure 3. 1 Urea main degradation path

During the last decade, the identification of new potential phase change materials (PCM) had been a main research objective among the latent heat thermal energy storage (LHTES) research groups. As a result, it has been common practice to employ a quick method to discard materials with poor thermal stability and verify potential candidates. Most reported works determine the potential PCM thermal stability by means of accelerated melting-solidification thermal cycling tests carried out in a DSC, measuring the variation of thermal characteristics along these tests [98]. However, this type of tests may not describe the real stability/degradation behavior of PCM. Actually, the thermal cycling tests do not isolate the thermal degradation problem, but include other potential degradation features that could act together, like for instance the phase segregation, crystallization problems, supercooling, etc. Accelerated thermal cycling tests are not suitable to determine the thermal degradation due to instability of the material at high temperature. Hence, the development of reliable methods to test the degradation of PCM is one of the working focus of the international research community in this field. In this sense, the Solar Heating & Cooling Programme, Task 58 from the International Energy Agency IEA [99], is an international working group with the aim to develop and study thermal energy storage materials, where the authors collaborate. One of the objectives aimed by the group shared working programme is the development of measurement procedures for relevant material properties, including realistic thermal degradation testing.

Accordingly, the present chapter presents the study for the determination of the thermal stability of the urea and Sodium nitrate eutectic mixture, from a perspective different to the most widely employed accelerated thermal cycling, to assess the reliability of the urea and Sodium nitrate eutectic mixture as a PCM. The study includes the thermal degradation of molten samples at a temperature slightly higher to the maximum operation temperature, and the subsequent thermal and compositional analysis by means of different analytical techniques after different degradation times up to one year.

3.2 EXPERIMENTAL DESCRIPTION

Samples of the urea and Sodium nitrate eutectic mixture were introduced in DSC closed crucibles. The crucibles were kept inside a heating cabinet at 100°C for times ranging from 1 day to 1 year. Afterwards, their main thermal properties were determined by DSC (Differential Scanning Calorimetry). Selected samples were also analyzed by different techniques in order to determine the compounds present in the degraded samples. The techniques used were: for that purpose were: HPLC (High Performance Liquid Chromatography), XRD (X-ray Diffraction) and FTIR (Fourier-Transform Infrared Spectroscopy). The detailed procedure is subsequently described.

3.2.1. SAMPLE PREPARATION

Dry samples, with a composition of 71.25 wt% urea and 28.75 wt% Sodium nitrate (from now on called the U-SN eutectic mixture), were produced in glass vials and introduced in DSC closed crucibles. Table 3. 1 gathers the details of the relevant instruments used for sample preparation, while Table 3. 2 includes the main features of the employed raw materials. Special efforts were

taken to prevent any moisture uptake by the samples, due to its potential influence on the urea degradation results.

Pure reactants were first introduced into glass vials in powder; 2.85 grams of urea and 1.15 grams of Sodium nitrate were used, amounting to 4 grams of the eutectic mixture. A magnetic stirrer was introduced and the vial was tightly closed with a threaded cap. The closed vials were immersed into a glycerin bath with magnetic stirring at 90°C for 30 minutes.

By means of a micropipette, 20 µl of the molten material were poured into DSC stainless steel crucibles. The crucibles with the PCM (still without the closure-lids) were placed in a desiccator containing phosphorus pentoxide as desiccating agent. The samples remained for 3 days inside the desiccator at room temperature, under 7% relative humidity atmosphere. The water content of selected samples was measured after this process by Karl Fisher titration [83]. All the samples showed a water content below 0.1%.

The desiccator was then introduced inside a glove-box with dry air (16% relative humidity), where the DSC crucibles were closed. Medium-pressure crucibles with a sealing gasket were used to ensure tightness. PCTFE O-rings were employed since they are not permeable to ammonia gas. The closed crucibles were finally weighed in a 0.1 mg resolution scale.

Table 3. 1 Equipment used for the sample preparation

Equipment	Brand	Model
Precision balance	Ohaus	Discovery 114C
Gas-tight crucibles	Mettler Toledo	Medium pressure stainless steel crucibles with PCTFE O-rings
Micropipete	Rainin by Mettler Toledo	Pipet-Lite XLS monocanal
Glove box	Plas-Labs, Inc.	330 ABB
Karl Fischer coulometric Tritration	Mitsubishi Chemical	KF-31

Table 3. 2 Raw materials employed for the sample preparation

Material	Supplier	Purity	Quality
Urea	Panreac Química S.L.U.	99%	Laboratory grade
Sodium Nitrate	Panreac Química S.L.U.	99%	
Phosphorus Pentoxide	Panreac Química S.L.U.	98%	

3.2.2. DEGRADATION PROCEDURE

The sealed crucibles were introduced into an oven at 100 °C (± 5 °C) for a predefined soaking time. The crucibles were placed onto an aluminum sheet with a grid to keep control of each sample and to provide a homogeneous temperature to all the crucibles (see Figure 3. 2). Three samples (3 DSC crucibles) were prepared and introduced in the furnace for each degradation time.

When the predefined time elapsed, the corresponding crucibles were removed from the oven and placed in a desiccator for 30 minutes. Afterwards, they were weighted to record any sample mass variation.

Figure 3. 2 The sample rack with some of the samples in it inside the heating cabinet

3.2.3. Analytical procedure and techniques

The degraded samples were analyzed by different techniques. DSC was used to determine the evolution of melting temperature and melting enthalpy over increasing degradation time. Besides, HPLC, XRD and FTIR were used for a further understanding of the thermal degradation. Table 3. 3 gathers the equipment employed. The methodology employed for the DSC, XRD and HPLC measurements are fully described in [62]. A summary of their most important details is described onwards.

Table 3. 3 Analytical techniques used for the characterization of degraded samples

Analytical technique	Brand	Model
Differential Scanning Calorimetry (DSC)	Mettler Toledo	DSC1
High Performance Liquid Chromatography-Mass Spectrometry (HPLC-MS)	Agilent Technologies	1200 Series
X Ray Diffraction (XRD)	Philips	X'pert Pro
Powder Diffraction File (PDF) database	-	-
Fourier-Transform Infrared Spectroscopy (FTIR)	Jasco	4200

Differential scanning calorimetry DSC

The used temperature program is shown in Figure 3. 3. It consisted on two heating ramps and one cooling ramp. The first heating segment intended to settle the sample on the bottom of the crucible to achieve a good contact. The thermal properties were evaluated from the cooling and second heating ramp. Both heating and cooling rates were of 1 °C/min, and isothermal segments of 10 minutes on either side of the dynamic segments.

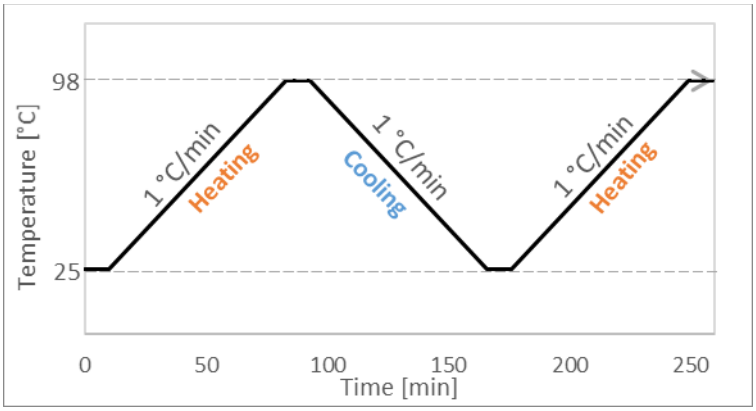

Figure 3. 3 DSC temperature program

Highly degraded samples showed crystallization problems, and did not always crystallize completely during the cooling ramp due to the high cooling rate. In some cases, the end of the crystallization was determined during the heating. In these cases DSC tests were repeated using heating and cooling rates of 0.5 K/min.

The onset and peak temperatures, the latent heat and the total enthalpy exchange on the temperature range from 60 to 95°C, were determined on the cooling segment and on the second heating segment. The total enthalpy exchange was determined (see Figure 3. 4) by measuring the area *(a)* that corresponds to latent enthalpy and the addition of area *(b)*, which corresponds to sensible and latent heat between 60 and 95°C. In the samples where any new peaks or artifacts different from the eutectic melting features occurred, they were recorded for further analysis.

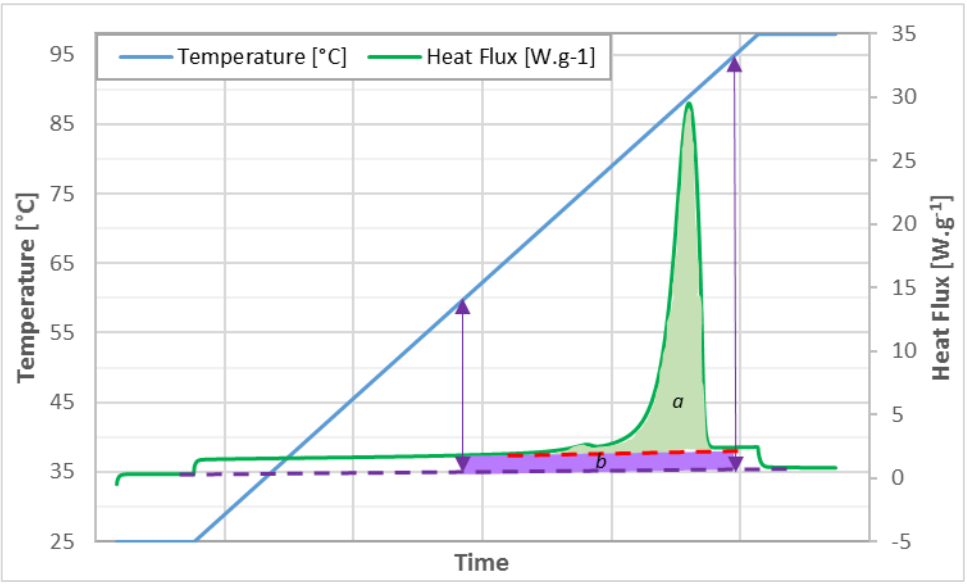

Figure 3. 4 Determination of the total enthalpy exchange. Area "a" corresponds to the melting enthalpy, and area "b" corresponds to the sensible enthalpy in the 60 to 95°C temperature range

High performance liquid chromatography HPLC

The HPLC technique was employed to determine the urea content on the degraded samples, as well as to identify and determine the content of the non-gaseous byproducts of urea on those samples. A working methodology was developed to determine the concentration of urea, biuret and cyanuric acid since these are the foreseen decomposition products. For it, only the evaluation of their specific spectra range was evaluated. In addition, samples degraded for 180 days were submitted to a procedure which covered the evaluation of a wider range of the spectra in order to determine whether other degradation compounds were present.

Calibration curves were prepared using different concentration solutions, fitted by the least squares method (linear estimation) with a correlation coefficient greater than 0.996 in all cases.

In addition, an analytical validation using pure urea, biuret and cyanuric acid samples to obtain the method precision and accuracy. Table 3. 1 summarizes the results. Urea measurements do not provide a good accuracy. Intraday precision values are not good as well. For that reason, the results from this methodology were not used to attain a proper degradation kinetics of the material, nor mass balance of the reactants and products. However, they were meant to evaluate the global evolution trends of urea and its decomposition products.

Table 3. 4 HPLC intraday and interday precision (measured within a day and on different days), and accuracy

	Precision		Accuracy %
	RSD% intraday	RSD% interday	
Urea	0.6	11.9	88.4
Biuret	0.9	6.9	97.2
Cyanuric acid	0.8	15.9	97.3

The samples were prepared for analysis by dissolving approximately 10 mg of each degraded sample in 25 ml of distilled water. For the chromatographic analysis, this solution was further diluted with distilled water to 1/100 and 1/50 ml/ml respectively. 5 µL of the diluted samples were injected into the HPLC-MS for analysis. Two samples from the dilutions 1/100 and one sample from the dilution 1/50 were measured for each of the degraded samples.

X-ray diffraction XRD

X ray diffraction was used to determine the crystalline materials in the degraded samples, and determine potential formation of glassy material. It has to be reminded that the function of a PCM is to store and exchange the latent heat of melting/crystallization. As a result, determination of the crystalline species and the potential glass formation are important aspects to analyze the validity of the material as a PCM. The samples with different degradation times were analyzed, and the evolution of the diffraction patterns were analyzed. The technique allows to determine the composition and crystallographic nature of the crystalline materials, but it does not allow to determine the composition of the amorphous compounds that could have formed.

In a previous article of the authors [62], it was determined that the U-SN eutectic mixture presents a metastable phase different from urea and from Sodium nitrate, whose diffraction patterns are unknown, or have not been included on the XRD pattern(s) database available for the analysis (see table 3). This phase is different form the one attained in samples exposed to humid air. Due to this fact, all the samples were annealed to obtain the equilibrium phases and make it possible to identify the potential byproducts appearing in the degraded samples with time. The annealing thermal treatment consisted in holding each selected sample into the DSC, at 80°C for 10 hours.

After annealing, all the material contained in the DSC crucible (around 20 mg) was removed, hand-grinded on an agate mortar to obtain a fine powder, and placed in sample holders for XRD analysis.

Fourier transform infrared spectroscopy FT-IR

Fourier-transform Infrared spectroscopy, FTIR, was used as a complementary technique to determine the composition of the samples by the determination of their infrared spectra. The technique is capable of providing additional information to ascertain the composition of the samples, including new compounds that could have formed in the degraded samples, which may be non-crystalline. The KBr tablet technique was employed, being the most usual methodology for the analysis of powdered samples. It was in transmittance mode, using a disc or tablet of potassium bromide (KBr, spectroscopic purity).

The tablets were prepared by mixing the solid samples (previously grounded) with KBr powder (approximately 300 mg), and then the mixture was ground again to obtain a good dispersion of the sample. This mixture was transferred to an IR tablet mold and placed in a hydraulic press. The pressure was increased to 10 tons and held for 3 minutes to obtain a KBr disc in which the sample was homogeneously distributed. Afterwards, the infrared spectra was obtained in the 400 to 4000 cm^{-1} region following the standard procedure, with a spectral resolution of 4 cm^{-1} and accumulating 40 scans to obtain a good signal-to-noise ratio.

Pure urea and Sodium nitrate samples were first analyzed in order to obtain the spectra of the pure components used for the sample preparation. Then 3 U-SN eutectic mixture samples were analyzed, corresponding to three different degradation times: non-degraded, 40 days and 120 days.

3.2.4. Determination of the equilibrium pressure

The objective is to determine the potential gas evolution of the U-SN eutectic mixture when submitted to 100 °C in a tightly closed container. Urea thermal decomposition reaction is heterogeneous and some of the products are gases. As a result, if the material is tightly closed, and assuming that it is a reversible reaction, when the equilibrium is reached the pressure will reach a certain value. The degradation stops when the equilibrium is reached.

To determine the pressure evolution and the equilibrium pressure of the U-SN eutectic mixture at 100°C, a simple experimental device was developed. Figure 3. 5 depicts the experimental set-up. A gas-tight container filled in with the PCM is placed inside the heating cabinet at 100°C. A

thin tube connects the container interior to a manometer placed outside the oven. As urea degrades, the ammonia production increases the pressure until the equilibrium is reached. When this occurs, the pressure stabilizes. Several different devices and test-attempts were carried out (copper tubes with regular gas fittings, Ace pressure tubes with PTFE plugs and o-rings) and demonstrated poor tightness in the working conditions. Finally, a device with all the fixtures and components made of 316 stainless steel was produced (Figure 3. 6). The PCM-container consisted on a tube (10 mm inner diameter, 200 mm length and, 15.7 cm^3 useful volume) sealed by means of a plug on the bottom and by a number of fittings on the top. The upper fittings serve to enable connection to the manometer, placed outside the oven. The plug and upper fittings (Gyrolok series from Hoke®) have a double ferrule system to provide a mechanical tight-seal (Figure 3. 6). The upper fitting connects the interior of the tube with a thin tube (2 mm inner diameter) to the manometer placed outside the oven, through an aperture available in the oven wall. To make the effective connection to the manometer an easy plug adapter and a 4mm diameter silicone tube were used. The digital manometer used had a resolution of 1mbar, a measuring pressure range of ±2000 mbar, and an accuracy of ±2%.

The PCM container was filled in with previously prepared U-SN eutectic mixture. Approximately 14 cm^3 of liquid material (20 grams) were directly poured in, filling-up the available volume almost entirely. In this way, the gas-volume available in the tube was relatively small in order to minimize the experimental time required to reach equilibrium. The gas-volume available in the connection tubes between the container and the manometer amounted to only 2.7 cm^3.

The oven temperature was monitored by a T-type thermocouple. The temperature and pressure signals were continuously recorded. The experiment lasted 120 h, from which 117 h correspond to a stable pressure.

Due to the fact that the system in the initial conditions contains air, and it should also contribute to the pressure raise with temperature, a test was done with the container filled with an inert material (sand). For the analysis of the results, the internal pressure of the air entrapped in the device when heated up at 100°C should be subtracted from the total pressure for determining the ammonia partial pressure.

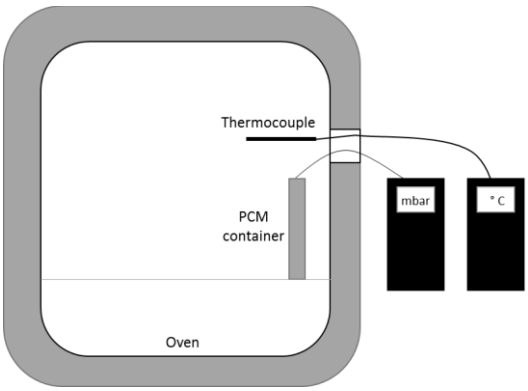

Figure 3. 5 Scheme of the experimental set-up for the determination of the equilibrium at 100°C

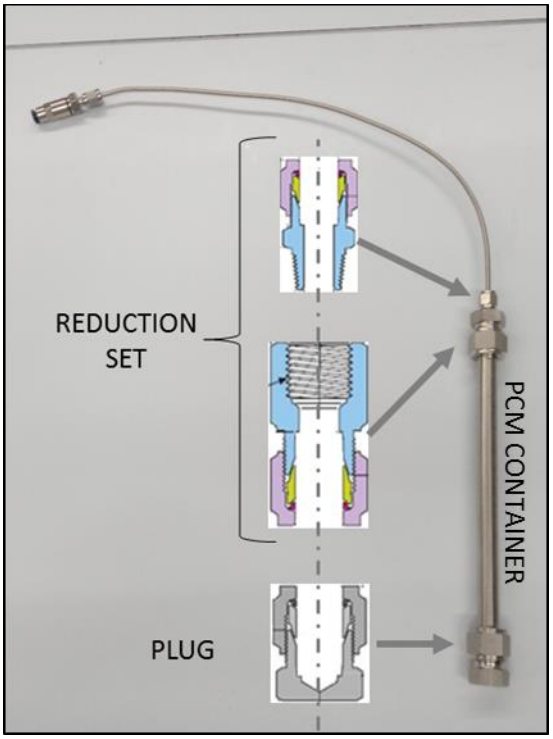

Figure 3. 6 Photograph of the actual device employed for the determination of the equilibrium pressure, with the sketches of the fittings interior design to ensure gas-tightness taken from the Hoke Gyrolok fittings catalog [100].

3.3 RESULTS

This section is devoted to present the main results experimentally attained for the thermal stability and degradation study of the U-SN eutectic mixture after controlled degradation was performed in closed containers. Besides, the results obtained in the study for the determination of the urea decomposition equilibrium pressure at ≈100 °C are also presented. The discussion of the analysis of results is presented in the next section.

3.3.1. MASS LOSS

The Urea decomposition path evolves with gas production. As a result, the degradation equilibrium and kinetics depend on these products partial pressure. If the material is contained into a gas-tightened enclosure, with no leakage, the degradation rate will be different than if the container leaks. The gas-tightness is, therefore, an important parameter for the U-SN eutectic mixture thermal stability. The leakage of gas products (gaseous mass loss) makes the reaction displace towards the formation of more products, promoting the degradation of the reactant, i.e. urea. The crucibles employed in this degradation study were selected for their gas-tightness according to the supplier´s specifications, which indicated a maximum allowed pressure of 2MPa (20 bars) and maximum working temperature <220°C, both well below the operational conditions in this study. However, the measurements carried out show that the DSC crucibles exposed at 100°C for a certain time, reported small mass variations.

All samples were weighted before and after the corresponding test at high temperature, summing up 42 samples in total (3 samples per each degradation time). Thee of the samples had

to be discarded for a poor crucible tightness. The average mass loss evolution and the standard deviation are plotted in Figure 3. 7. After 370 days the crucibles show an average mass loss of 2.2%. The mass loss trend increases with time, however the mass loss during the initial stages does not follow a linear tendency. Discussion about the samples mass loss is approached in the following sections.

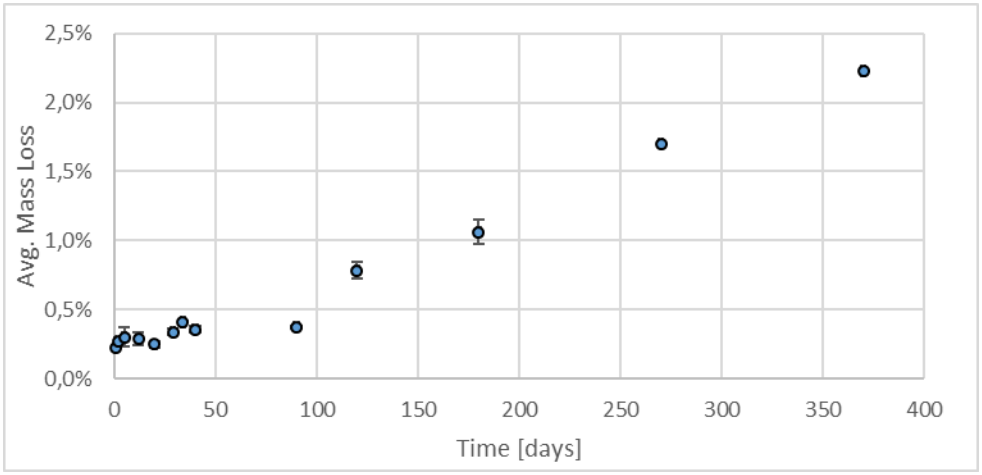

Figure 3. 7 Evolution of average mass loss with time; the bars represent the standard deviation

3.3.2. DIFFERENTIAL SCANNING CALORIMETRY DSC

The samples thermal properties were measured by means of DSC. Figure 3. 8 gathers some thermographs of selected samples, each one degraded for a different period of time. All the thermographs have been analyzed, taking into account the evolution of the graphs geometry: the melting and solidification peaks and any unexpected peak or artifacts.

The enthalpy loss, the latent heat loss and the melting temperature change are gathered in Table 3. 5, which shows the original mixture values (average of three samples) and those after 370 days at 100±5 °C. The melting enthalpy loss is smaller than 25%, and reduced to 20% in the case of the total enthalpy exchange in the 60-95°C temperature range.

Table 3. 5 Main thermal characteristics of the U-SN eutectic mixture: non-degraded and after 370 days at 100°C (average values of three samples each)

	non-degraded reference	after 360 days at 100 °C	% loss
avg. onset temperature [°C]	84.63	75.91	10%
avg. peak temperature [°C]	87.97	82.22	7%
avg. Latent heat [kJ/kg]	168.94	128.82	24%
avg. l+s heat (60-95°C) [kJ/kg]	238.18	189.74	20%

The general evolution of the melting signal with increasing degradation time shows a tendency for the endothermic peak to displace towards lower onset and lower peak temperatures. In

addition, peaks widen in detriment of sharpness and there is a reduction of the melting enthalpy and total enthalpy change in the 60-95°C temperature range. Figure 3. 9 and Figure 3. 10 show the evolution of the average onset temperatures, peak temperatures, and enthalpies, as well as their standard deviation.

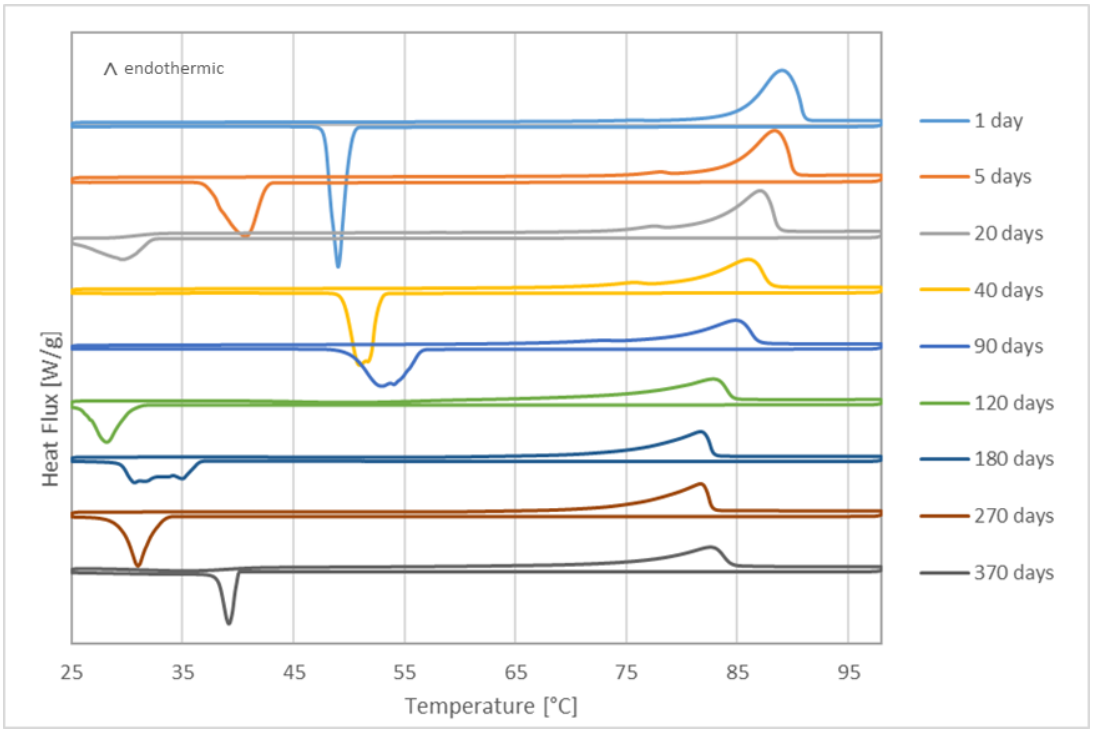

Figure 3. 8 Evolution of the thermograms with increasing degradation time (some selected samples)

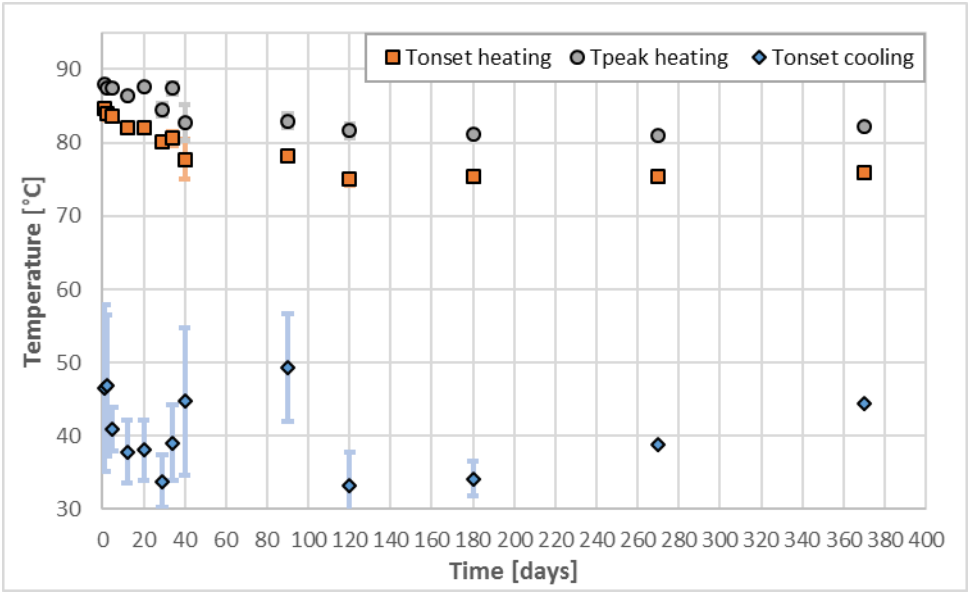

Figure 3. 9 Evolution of onset and peak temperatures in heating, and the onset temperature in cooling. The standard deviation is included as well.

Some of the degraded samples showed a small new peak on heating, around 74°C, prior to the melting signal. This new peak was determined in some samples during the first 90 days at 100°C. After long degradation times the melting peak becomes wider and the onset temperature descend from the initial 85°C to temperatures as low as 75°C. This suggests that the new peak which formed in some samples at 75°C, while the original peak at 85 °C was also present, indicating two phases to be present or that the samples do not show any more a unique melting point but show a semisolid interval. These two signals have overlapped, thus forming a unique wide peak in the samples exposed to long degradation time.

Some of the degraded samples showed a small new peak on heating, around 74°C, prior to the melting signal. This new peak was determined in some samples during the first 90 days at 100°C. After long degradation times the melting peak becomes wider and the onset temperature descend from the initial 85°C to temperatures as low as 75°C. This suggests that the new peak which formed in some samples at 75°C, while the original peak at 85 °C was also present, indicating two phases to be present or that the samples do not show any more a unique melting point but show a semisolid interval. These two signals have overlapped, thus forming a unique wide peak in the samples exposed to long degradation time.

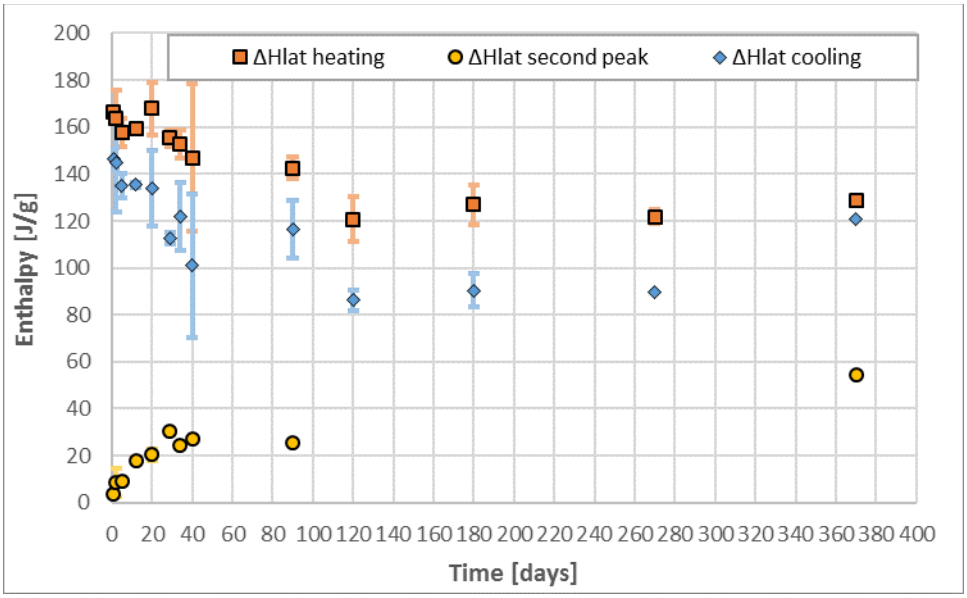

Figure 3. 10 Evolution of the average enthalpy measured on melting and on crystallization (main peaks), and the average enthalpy measured on the secondary peak on melting. The secondary peak forms in thermograms of some degraded samples, prior to the main peak. Each spot corresponds to the average of three samples. The bars represent the standard deviation.

Large supercooling occurs on crystallization, showing the large scattering typical of its stochastic nature when small samples are used. However, the scattering is almost negligible on the samples tested for a time longer than 120 days, as Figure 3. 9 shows. In all cases the enthalpy of crystallization is lower than the melting enthalpy. This phenomenon is well known, due to the recalescence that occurs after the supercooling, meaning that part of the latent heat is used for heating the sample.

To summarize, the thermal storage capacity (melting enthalpy) and the melting temperature of the samples submitted to 100±5 °C for different times decrease within the first 40 days, and remained stable at ≈125 J/g and ≈75°C respectively until 370 days elapsed, being this period the maximum degradation time tested in this study. If this trend is stable, these final values are adequate for the use of the U-SN eutectic mixture as a PCM for the intended application (DHW and heating) since the melting temperature is in the range (60-95°C) and the melting enthalpy is similar to commercial PCM (for example, Rubitherm RT60 paraffin has a melting point around 60°C and melting enthalpy 120 J/g), while its price and sustainability are more very good. If the energy storage density (enthalpy per unit volume) of the U-SN eutectic mixture and that of a typical paraffin are compared, the herein studied eutectic mixture after 370 days at 100°C presents a value of 177.5 KJ/dm^3 (initially 245 KJ/dm^3), almost double of the value offered by paraffins (94. KJ/dm^3).

The 370 days testing period (at 100°C) analyzed in the present study would be equivalent to different periods of use, depending on the design and operational use of the thermal storage system. In any case, it resembles an in-use period longer than 1 year. Nevertheless, stability conditions for longer periods should be assessed to confirm the use of the material as a PCM.

3.3.3. HIGH PERFORMANCE LIQUID CHROMATOGRAPHY HPLC

HPLC was used to identify and quantify the urea and potential urea degradation products present in the samples. Figure 3. 11 and Figure 3. 12 show the compounds evolution detected by means of HPLC-MS. The values shown in the plot were calculated as a percentage of the theoretical urea that should be present in the samples if they were not degraded (eutectic composition, where urea corresponds to 71.25% of the total mass). Each value corresponds to one sample (not the average of several samples).

All analyzed samples presented urea. Biuret and cyanuric acid were only detected in the samples dilutions 1/50 because of the low concentration of these compounds on the degraded samples. Indeed, the chromatographic signals corresponding to these two compounds were lower than those corresponding to the lowest concentrations prepared for the calibration. Therefore, extrapolation from the calibration curves was required to determine the biuret and cyanuric acid concentration in the samples.

Additionally, the scan performed to determine other compounds in a sample degraded for 180 days at 100°C did not detect any other compound different from urea, biuret and cyanuric acid. However, this method only serves to confirm the presence of compounds when they are detected, but it does not serve to discard their presence when they are not detected.

Urea content decreased with increasing degradation time. However, a steeper slope can be appreciated from the original sample to the sample tested for 40 days. Afterwards, the urea percentage does not significantly vary with time. The presence of Biuret was determined in all samples since day one of thermal treatment. The quantity, however, is very small and does not significantly increase with testing time. On the opposite, the Biuret percentage decreases after one year. Cyanuric acid was present in the samples tested for periods longer than 40 days. Again, in very low quantity like in the case of Biuret. However, the percentage of the Cyanuric acid

slightly increases after 1 year, which matches with the biuret decrease. Henceforth, this agrees with the degradation path exposed in the theoretical background of this article, and is better explained in the discussion, which propose that the cyanuric acid forms from the previously existing biuret.

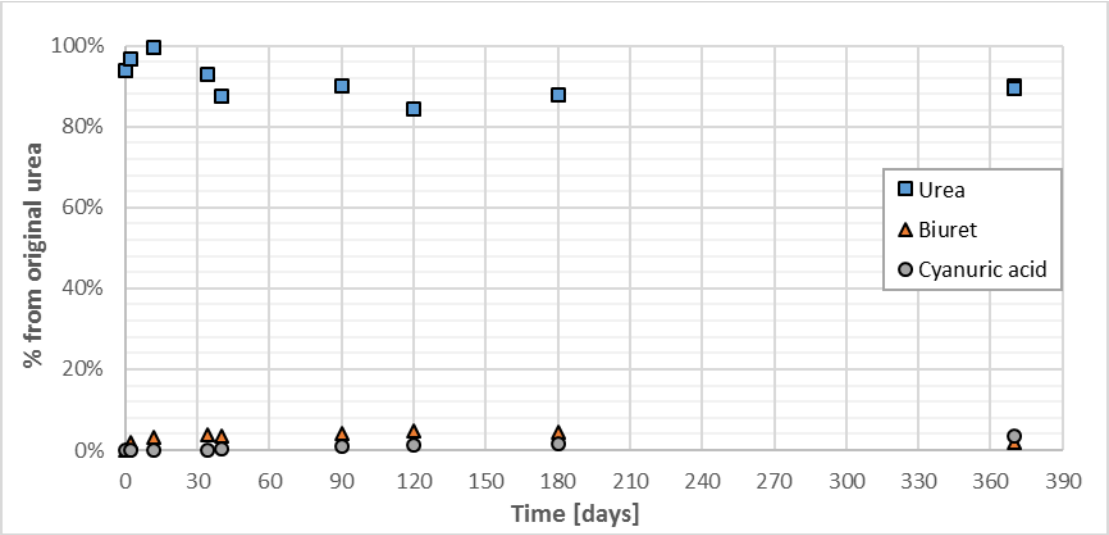

Figure 3. 11 Evolution of the Urea, Biuret and Cyanuric Acid content in the selected samples.

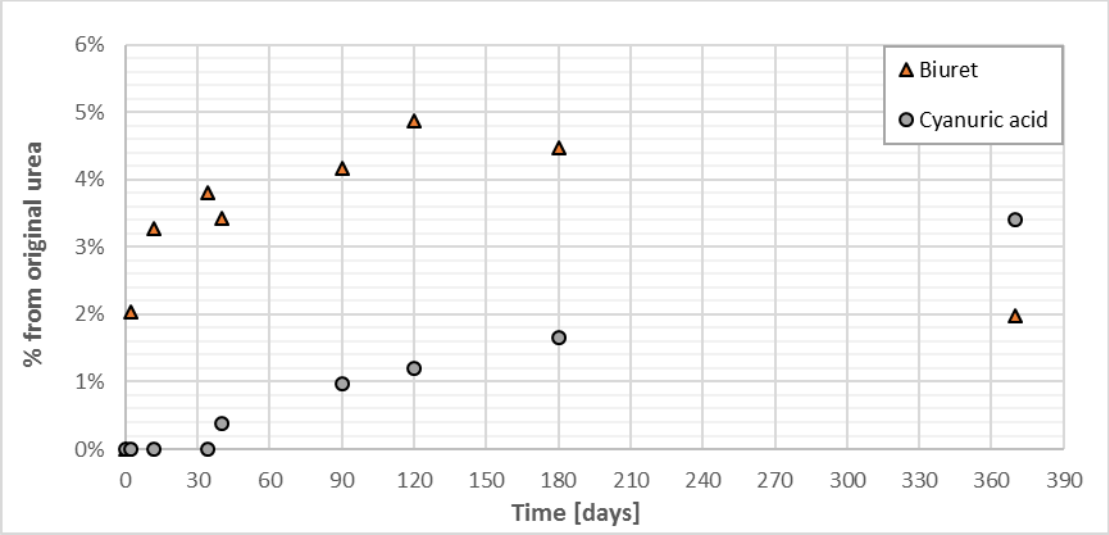

Figure 3. 12 Evolution of the Biuret and Cyanuric Acid content in the selected samples

3.3.4. X-RAY DIFFRACTION XRD

Samples from selected degradation times were analyzed by XRD in order to identify the crystalline phases present. Figure 3. 13 shows the X-ray diffraction pattern of a non-degraded sample, containing 71.25 wt% of urea and 28.75 wt% of Sodium nitrate, and illustrates the peaks identification. The peaks on the diffraction patterns identified in red correspond to pure urea

and those identified in blue correspond to Sodium nitrate. The diffraction patterns include four peaks that correspond neither to urea nor to Sodium nitrate (nor to sample holder and k-beta reflections). They are very low intensity peaks and do not match the peaks corresponding to any foreseen degradation compound: biuret, cyanuric acid, ammelide, melamine, etc. Because of the poor intensity of the few non-identified peaks, the determination of any additional compound by the XRD technique is not feasible. The quantitative analysis performed does not allow a good accuracy (10%), but it is a useful tool to determine gross changes in the crystallographic nature of compounds. The analysis of the diffraction patterns indicated that the urea/Sodium nitrate proportion in all samples remained in an approximate proportion of 70-80% urea and 20-30% Sodium nitrate, close to the original eutectic composition: 71.25 wt% of urea and 28.75 wt% of Sodium nitrate.

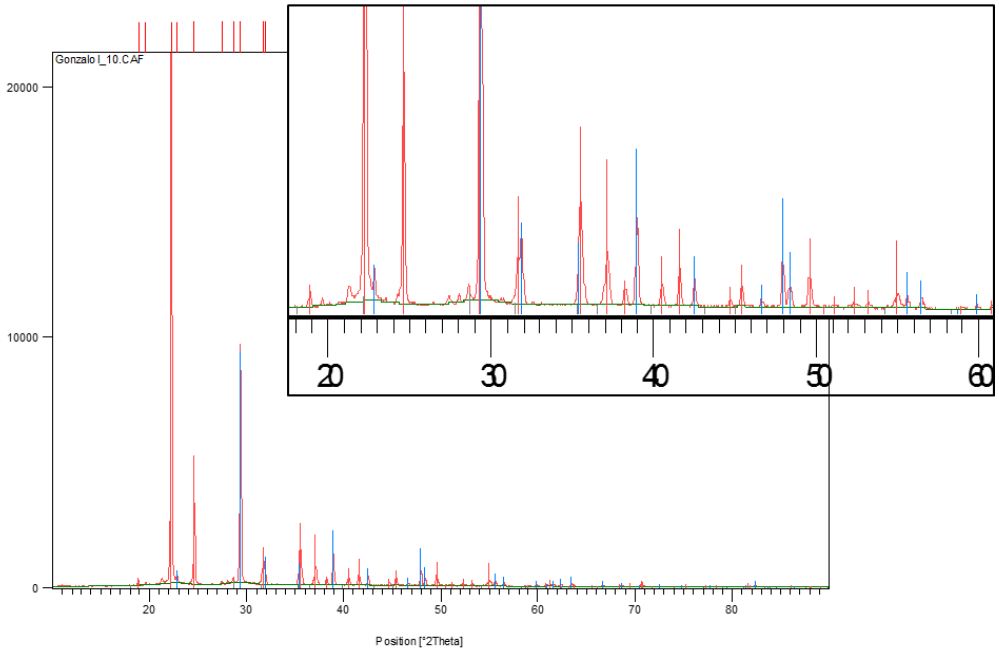

Figure 3. 13 Diffraction pattern and peak identification of a non-degraded sample (blue lines correspond to Sodium nitrate and red to urea peak positions).

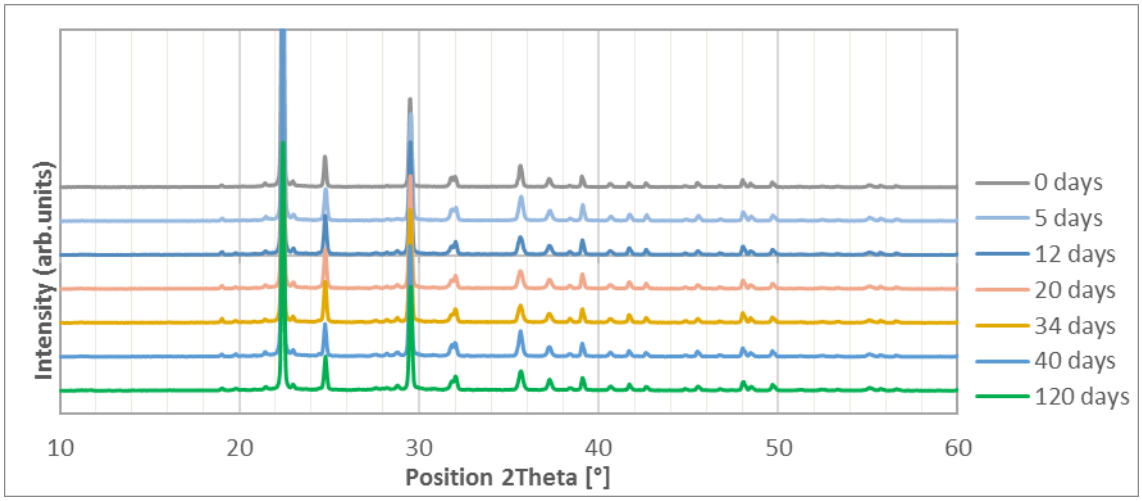

Figure 3. 14 Evolution of the diffraction patterns of samples tested for different times at 100°C.

Figure 3. 14 depicts the evolution of the diffraction patterns with testing time. The diffraction patterns of all degraded samples show the highest intensity peaks in the same 2Theta positions. However, along testing time, there are intensity proportionality changes between the urea and Sodium nitrate peaks. These variations are not large, but point towards a certain decrease in the urea content. Again, it must be reminded that the XRD methodology used is not well suited for accurate determination of compositional changes. Figure 3. 15 (a) shows the diffraction patterns in the 2Theta positions from 31 to 33 degrees showing two peaks, one corresponding to urea and the other one corresponding to Sodium nitrate. Figure 3. 15 (b) plots the evolution of the relative intensity ratio of these two peaks along testing time. It can be seen that the ratio gradually reduces from 0 days to 20 days, while after that period the ratio reaches a stable intensity proportion. Even though a quantitative conclusion cannot be de rived from this analysis, it does points towards a major urea degradation in the first 20 days, reaching equilibrium around that period (in the herein employed testing conditions).

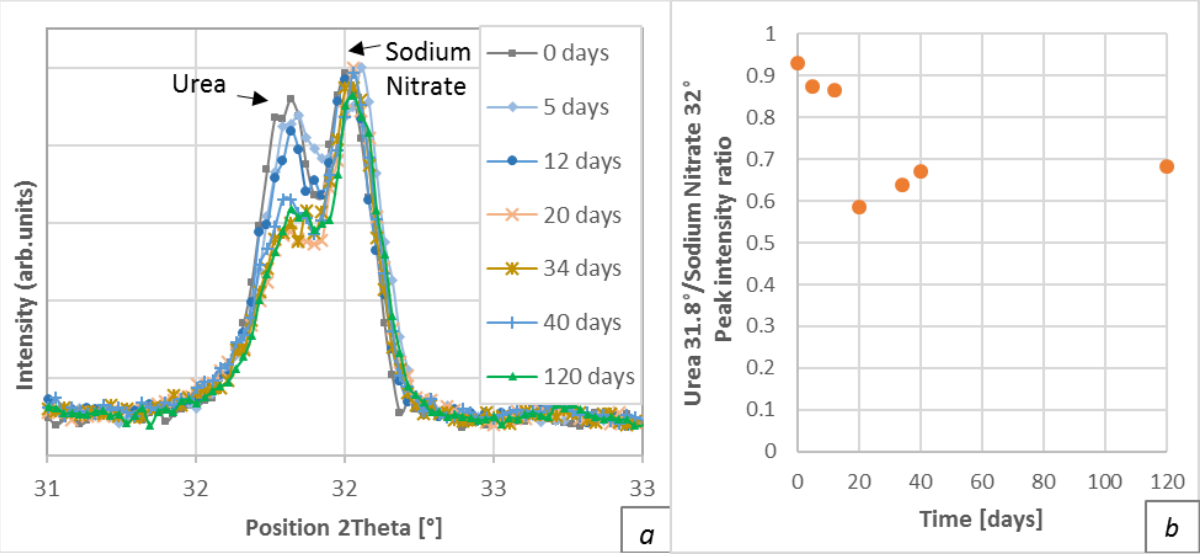

Figure 3. 15(a) Evolution of two characteristic peaks for Urea (left peak) and Sodium Nitrate (right peak). (b) Ratio of the intensity reached by the urea peak versus the nitrate peak of the tested samples

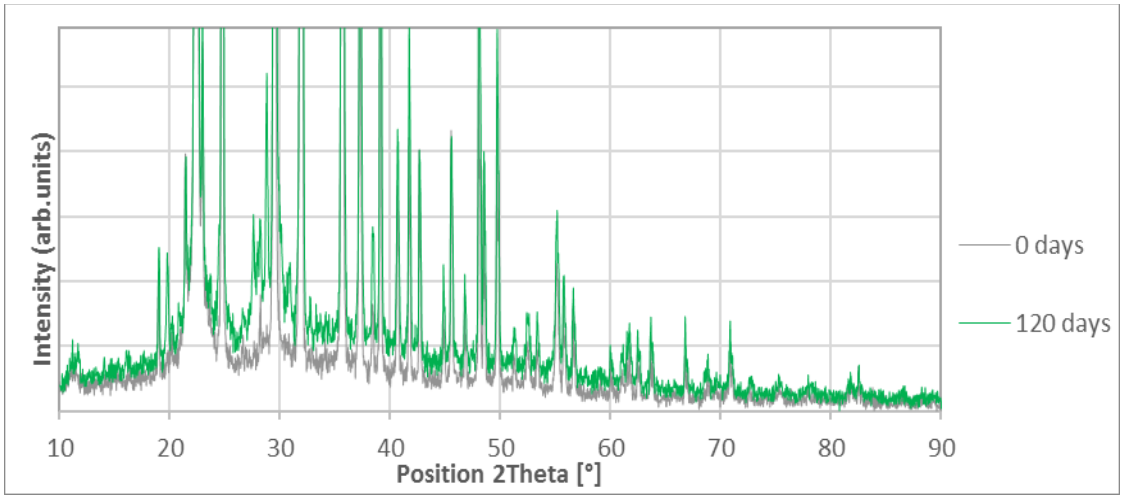

Figure 3. 16 Diffraction pattern baselines for a non-degraded sample and a sample tested for 120 days at 100 °C.

The diffraction-patterns shape provides also other noteworthy observations. The geometry of the baseline of most degraded samples diverts to some extent from the pattern obtained in non-degraded samples. This can be seen in Figure 3. 16, where the degraded samples signal-baseline is slightly "bell-shaped". From this change, it can be derived that the samples submitted to longer degradation times decrease in crystallinity and therefore, part of the degradation products might be amorphous (no information can be extracted from the amorphous part of the sample using XRD).

3.3.5. FOURIER TRANSFORM INFRARED SPECTROSCOPY FT-IR

The FTIR analysis was used for compounds identification in the samples. Measurements were carried out in a non-degraded sample, and in two samples degraded for 40 days and 120 days respectively. The results, depicted in Figure 3. 17, show that all the samples have the mixed spectrum of the urea and Sodium nitrate compounds, being the geometry of the spectrum a superposition of both pure materials. None of the spectra presented bands matched any of the foreseen degradation products.

Compared to the non-degraded sample, the degraded samples show a widening of the peaks corresponding to a wavelength between 3000 and 3800 cm^{-1} with higher degradation times. This is thought to be caused by the potential presence of moisture in the samples due to the uncontrolled ambient humidity at the time of preparing the FT-IR samples and producing the measurement, which were produced and measured one by one, while the first sample was measured the other were already introduced in the equipment with no humidity control. Oliver et al. studied the evolution of the urea spectra with hydration and dehydration processes with a similar result [101].

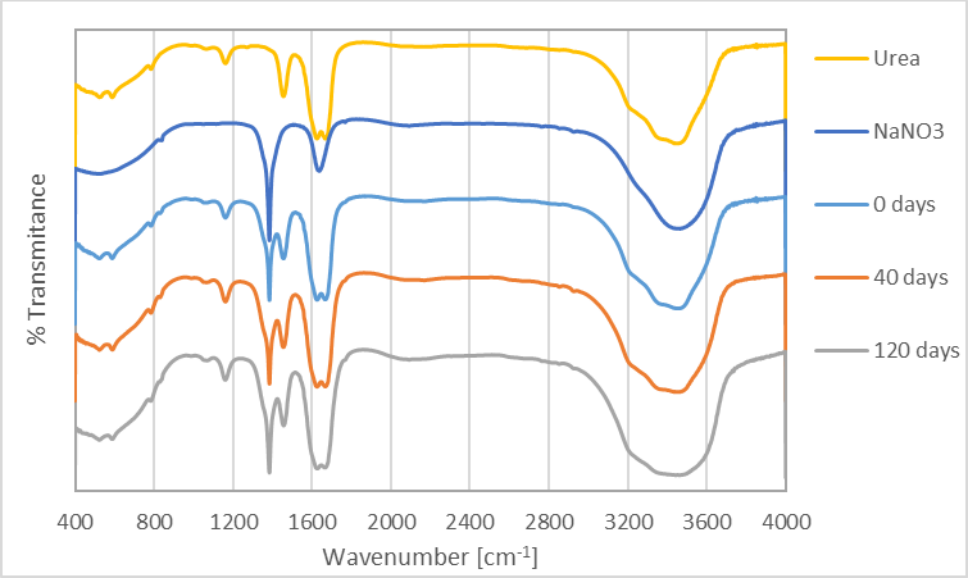

Figure 3. 17 FTIR spectra corresponding to pure Urea, pure Sodium Nitrate and the samples tested for 0, 40 and 120 days at 100°C.

3.3.6. DETERMINATION OF THE EQUILIBRIUM PRESSURE

The pressure evolution on the experimental set-up was very fast. Even though the experiment lasted for 5 days, a stable pressure was reached within 7 hours from the introduction of the container with the PCM in the oven. Figure 3. 18 depicts the evolution of the relative pressure inside the device when containing the PCM mixture, and the evolution of the relative pressure when the container is filled in with a reference blank. The pressure measured in the PCM-container represents the relative pressure of the gaseous products evolved from the mixture degradation plus the air initially present in the container. The reference blank consists of the same air-gap as in the PCM experiment. The figure only shows the evolution of the first 15 hours (900 minutes) of the main experiment, where the relative pressure stabilizes. The variation up to 5 days was negligible.

It has to be reminded that the experimental set-up was purposefully prepared for the degradation reaction to reach the equilibrium in a short time, by including a large PCM mass while leaving a tiny volume available for gas evolution, and being the system totally gas-tight.

The determined pressure values do not correspond to the gas at 100°C, even if the connections between the PCM container and the manometer were insulated. Because the available manometer maximum temperature is 50°C, it cannot be introduced in the heating cabinet. So, the experiment may not serve to establish the precise value of the gas equilibrium-pressure at 100°C, but to confirm that the equilibrium of the reaction can be reached when a completely gas-tight container is used.

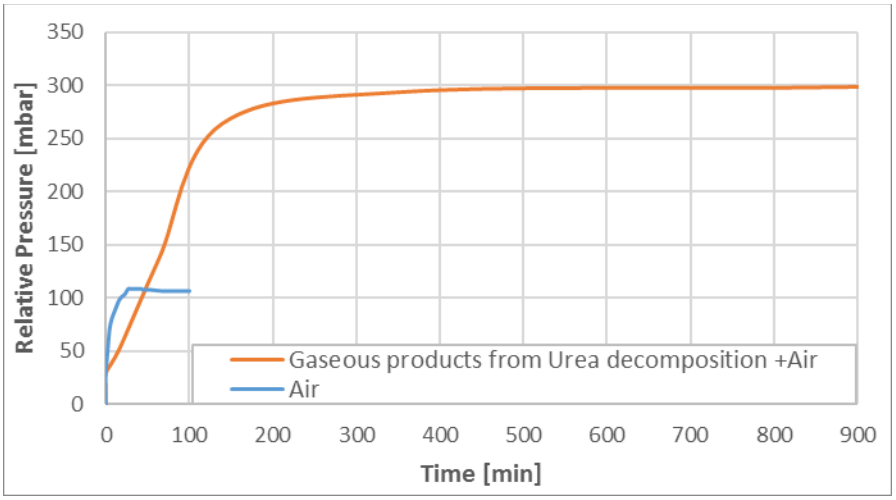

Figure 3. 18 Evolution of the relative pressure with time at 100°C

3.4 OVERALL DISCUSSION OF THE RESULTS

The objective of the experimental work was to gather knowledge about the U-SN eutectic mixture thermal degradation under the highest operation temperature of the application (≈100°C). The main results attained by each technique have been presented in the previous sections. The aim of the present section is to holistically combine the information and results obtained from all the techniques to acquire a better understanding of the process taking place.

The results from XRD and FTIR rendered substantial qualitative and compositional information about the evolution of the samples, confirming that urea and Sodium nitrate were the major constituents of all the samples. The qualitative analysis does not exclude the presence of other compounds different from the original in a very low proportion. However, these results do not render a quantitative scale that can be directly related to quantitative results determined by other techniques for the joint analysis of the samples degradation.

DSC and HPLC experimental data supply quantitative data about the PCM degradation. The melting-enthalpy (DSC) and the urea-percentage (HPLC) variation show the same evolution along degradation time, initially decreasing and afterwards presenting a stable value. The HPLC results point out that the decomposition of urea leads to the formation of biuret and cyanuric acid. The formation of these compounds results in modification of the PCM composition. Solution of biuret (and possibly cyanuric acid as well) in the urea-Sodium nitrate molten mixture leads to a change of the thermal characteristics, such as onset temperature and storage capacity.

Figure 3. 19 plots the melting enthalpy values (DSC) versus the urea loss (HPLC). It shows that there is a linear relationship. Then, it can be concluded that melting enthalpy is clearly influenced by the measured urea loss. Figure 3. 20 shows the urea loss (HPLC) versus the mass loss of the samples. In these figures, it can be observed that surprisingly, the urea mass-loss does not necessarily increase with increasing time. This finding is apparently incongruent. However, the mass loss determined after the degradation process showed that the containers tightness was not as good as it was foreseen according to the supplier specifications (they were selected specifically for their gas-tightness). Therefore, due to the gas-leaks the equilibrium is not reached and urea decomposition proceeds.

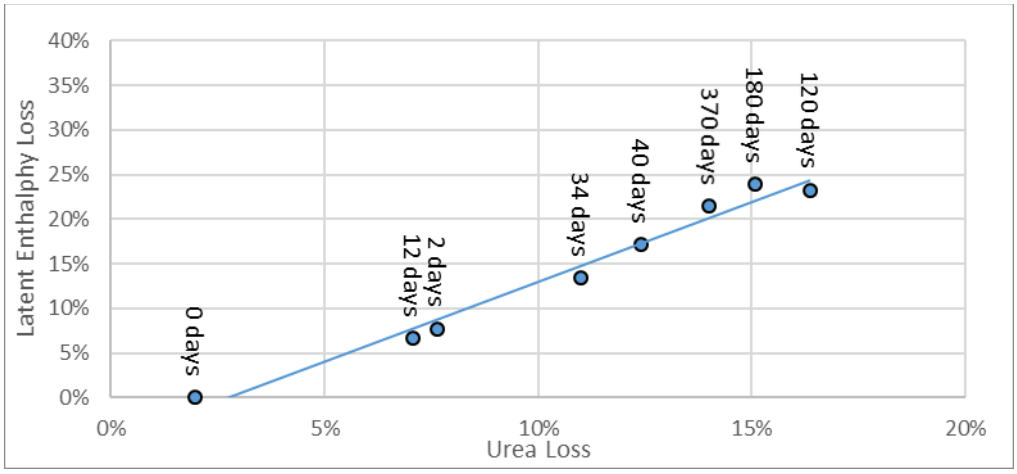

Figure 3. 19 Melting enthalpy loss measured by DSC vs. Urea loss measured by HPLC

It is important to highlight the importance of parameters that are not generally taken into account, but can have great influence in the degradation and thermal behavior of systems. In this regard, the mass loss is analyzed in following paragraphs, because it has been proved to condition the system the degradation process and consequently the degraded sample thermal behavior.

The most widely accepted urea thermal decomposition process takes place according to the following steps [16-24]:

$$NH_2 - CO - NH_2 \xrightarrow{\Delta} NH_3 + HNCO \quad (3.1)$$

Urea — Ammonia — Isocyanic acid

$$NH_2 - CO - NH_2 + HNCO \rightarrow NH_2 - CO - NH - CO - NH_2 \quad (3.2)$$

Urea — Isocyanic acid — Biuret

$$NH_2 - CO - NH - CO - NH_2 + HNCO \rightarrow NH_3 + [C(O)NH]_3 \quad (3.3)$$

Biuret — Isocyanic acid — Ammonia — Cyanuric acid

Figure 3. 20 shows the urea loss, the increment of biuret and cyanuric acid (calculated as percent of the original urea present in the sample) versus mass loss in selected crucibles analyzed by means of HPLC and DSC. It can be derived that, in the conditions employed in the experiments, the urea decreases linearly with the mass loss, and then, remain nearly constant regardless the mass loss. Indeed, two stages can be distinguished.

In the first stage, biuret percentage increases as urea decreases, both of them linearly with crucible mass loss. As depicted by equation 1, urea decomposes into gaseous ammonia and isocyanic acid, which a is very reactive compound which immediately reacts with urea to form biuret (equation 2). It can be assumed that the mass loss in stage 1 corresponds to volatile ammonia and possibly isocyanic acid as well. This will promote further urea degradation to displace the reaction for the production of the gases.

In stage 2, the crucible mass loss is nearly independent of the urea loss, while as the crucible mass loss increases the biuret proportion reduces and the Cyanuric acid proportion increases. A plausible hypothesis is that, when the biuret proportion reaches a certain value, the reaction depicted in equation 3 takes place, competing with the reaction in equation 2. Therefore, Isocyanic acid combines with biuret to produce cyanuric acid and more ammonia gas. In this situation, even though the mass loss corresponds to gaseous ammonia, it does correspond to a different reaction, where a solid product (cyanuric acid) must form together with the ammonia gas. Usually, heterogeneous reactions where solid products form have significantly slower kinetics than the reactions evolving into gas products. The reaction rate of any process conformed by sequential reactions is determined by the slowest step in the process, which therefore controls the process. As a result, once the biuret proportion in the mixture is high enough, the urea degradation rate drastically slows down. This would be in agreement with Bernhard et al. [81] conclusion for the order of reaction rates at 100 °C: the rate for biuret formation reaction (equation 2) is larger than the rate for cyanuric acid reaction (equation 3).

The urea loss and the formation of other products affects the behavior of the material, since it changes the phase diagram. A first modification, the urea loss makes the mixture to deviate from the eutectic composition, becoming a mixture with a semisolid melting range (not unique phase transition temperature), where the eutectic melting temperature will remain the same.

However, the experimental results obtained in the study show a decrease of the melting temperatures (both, onset and peak temperatures), which evidences the incorporation of the newly formed compounds into the system, further modifying the eutectic temperature. The formation of compounds other than urea and Sodium nitrate change the thermophysical properties of the initial thermodynamic system.

There is a remarkable variation of the thermograms geometry with increasing degradation times. Figure 3. 21 plots the thermograms (2nd heating section) of the samples analyzed by HPLC. Each thermogram has been labelled with the biuret and the cyanuric acid percentage (related to the original urea in the samples). The onset (melting) temperature decreases as the biuret percentage increases, and slightly increases when the cyanuric acid percentage surpasses the biuret percentage.

These experimental results showed that, increasing degradation time reduced the supercooling degree and the scattering of the crystallization temperature (Figure 3. 9). A plausible explanation for this behavior could be the introduction of new compounds into the system.

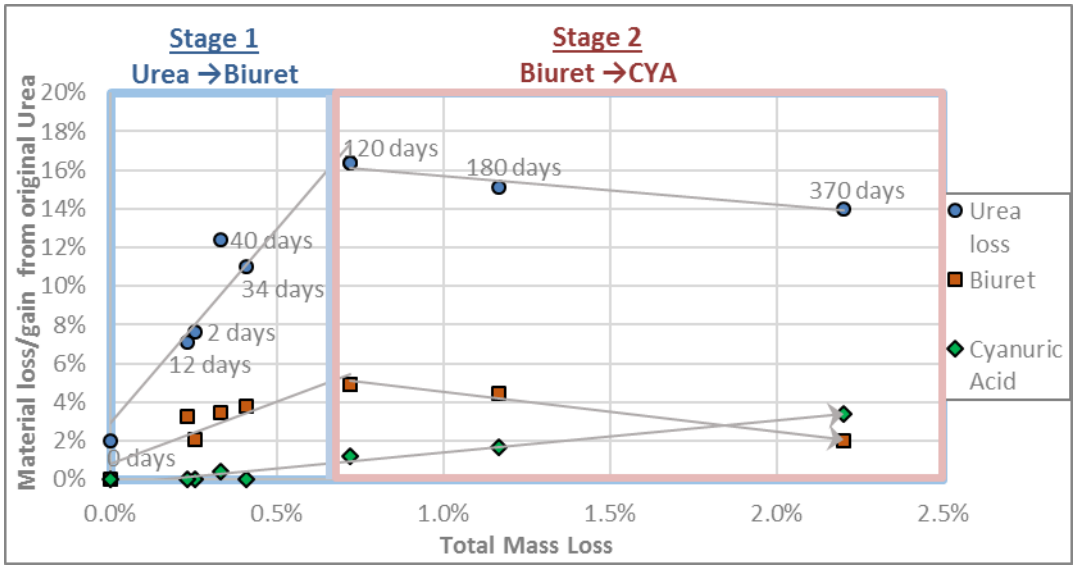

Figure 3. 20 Evolution of the composition (HPLC) and latent enthalpy (DSC) versus the total mass loss determined in the crucibles employed to carry out the tests. Urea Mass loss, biuret mass gain and cyanuric acid mass gain have been calculated as mass percentage with respect to the urea mass contained in the original, non degraded sample.

The results point towards the hypothesis that a ternary system could form (urea-biuret-Sodium nitrate) as biuret percentage increases. It is thought that it might be a ternary eutectic system with a eutectic melting temperature around 75°C. In order to have a better understanding on the influence of biuret in the studied system, samples with different proportions of urea and biuret were prepared and analyzed by DSC (28.75 wt% Sodium nitrate percentage in all cases). The analyzed compositions were: 3 wt% biuret - 68.25 wt% urea; 5 wt% biuret - 66.25 wt% urea; 7 wt% biuret - 64.25 wt% urea and 10 wt% biuret, 61.25 wt% urea.

Figure 3. 22 shows the thermograms of the biuret, urea and Sodium nitrate studied compositions, and the urea and Sodium nitrate eutectic composition. The thermograms of most of the samples that contained biuret show 2 peaks: the first peak had an onset temperature of

75°C, and the second peak had different intensities and endset temperatures. It is thought that the first peak corresponds to the eutectic signal and the second peak corresponds to the semi-solid range transition signal. The sample containing 10% of biuret show one peak, but due to the irregular geometry with a posterior bump, it is not considered the eutectic composition (but very close) with the bump corresponding to the semi-solid range transition.

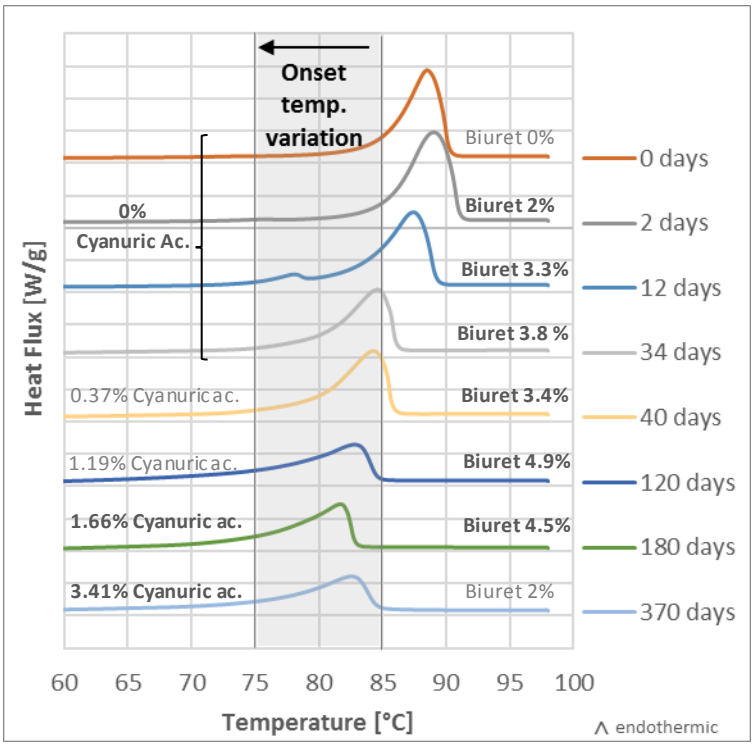

Figure 3. 21 Evolution of the DSC thermograms of selected samples, including the percentage of biuret and cyanuric acid in those samples (measured by HPLC)

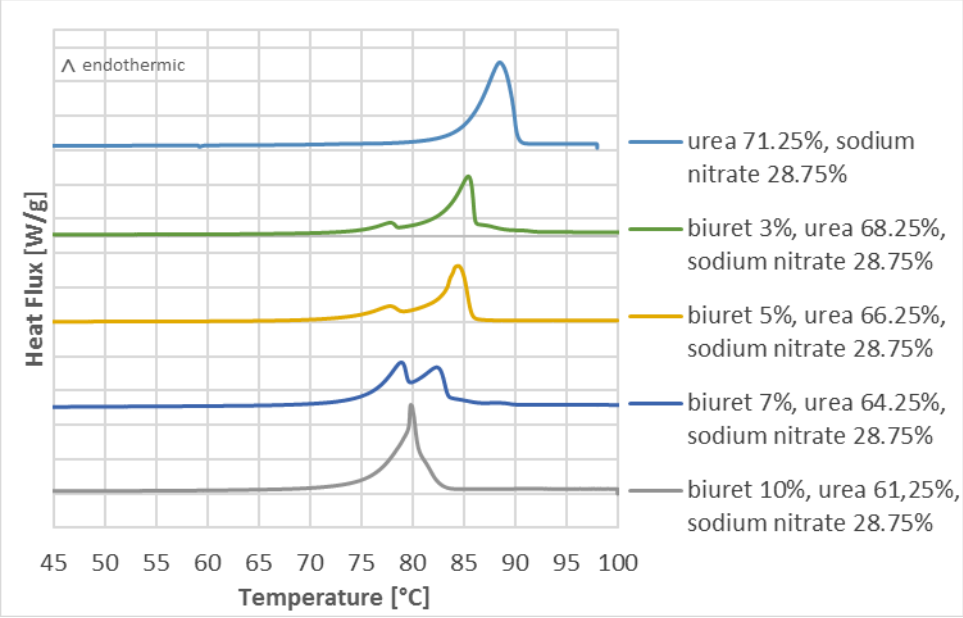

Figure 3. 22Thermograms of urea, biuret and Sodium nitrite samples with different urea and biuret composition, prepared from pure components to evaluate the phase transitions occurring with different compositions and the temperatures at which the phase transition occurs

Going back to the U-SN degradation study, the samples degraded for 90 days presented two peaks in the DSC measurements. The secondary peak onset temperature matches with the onset temperature of the hypothesized ternary eutectic biuret-urea-Sodium nitrate. The samples degraded for longer time show one broad peak, considered to be a superposition of two peaks, with the same onset temperature. A full study of the ternary system formed by urea, biuret and Sodium nitrate would help in determining the characteristics of the potential mixture formed by the system degradation.

The degraded mixtures also contain cyanuric acid, which may also influence the mixture thermal properties. Presently no study about the potential ternary or quaternary systems has been found in the scientific literature.

Theoretical considerations regarding the equilibrium of the system

The chemical reactions taking place in the urea-Sodium nitrate system at a temperature around 100°C follow a degradation path with heterogeneous reactions, where gases, liquid and solids products form and interact. If the material is placed in a tightly closed container, the degradation process continues until the equilibrium is reached because there is no mass loss, and the reactants and products are in intimate contact.

The concentration of the reactant and products (or their partial pressure in the case of gaseous compounds) are related with each other by means of the equilibrium constant, K_{eq}, which varies with temperature and pressure. If the global degradation reaction is taken into account (equation 8), the equilibrium constant corresponds to the ratio of ammonia, biuret and cyanuric acid and the reactant, i.e. urea, activities as shown in equation 9. The activity of urea, biuret and cyanuric acid can be estimated as 1 because solids and liquids effective concentration is considered constant, while the activity of gaseous ammonia is equal to its partial pressure (if considered as an ideal gas). As a result, the equilibrium constant will be a function of the ammonia partial pressure.

$$NH_2 - CO - NH_2\ (l) \xrightarrow{\Delta} 4\ NH_3\ (g) + NH_2 - CO - NH - CO - NH_2\ (l,s) + [C(O)NH]_3\ (s)$$

Urea Ammonia Biuret Cyanuric acid

$$K_{eq.p} = \frac{a^4_{Ammonia} \cdot a^1_{Biuret} \cdot a^1_{CYA}}{a^1_{Urea}} = P^4_{Ammonia}$$

Consequently, under this assumption the lifespan of the U-SN eutectic as a PCM can be greatly controlled by the use of a gas tight system where the evolution stops when the ammonia equilibrium pressure is reached. Experimentally, it was determined that the U-SN eutectic mixture can rapidly reach the equilibrium at 100°C if gas-tightened container is used. Even though the equilibrium pressure was not effectively determined in the experiments, the results of the pressure measurements are in agreement with the theoretical basis presented.

The DSC crucibles tested reported small mass variations with time, which do not exceed 2.2% of the initial mass after one year at high temperature. The mass loss corresponds to a disturbance of the equilibrium conditions, which lead to further degradation of urea. In this case, even though the mass variation is small the degradation produced has a great influence in the storage capacity of the system. To produce fully gas-tightened thermal storage devices will pose a large difference on the PCM behavior and lifetime under operational conditions. In addition, the potential use of ammonia atmospheres inside the container could prevent urea degradation by reaching the thermolysis process equilibrium pressure from the beginning, and potentially maintaining the initial urea mass, i.e. initial thermal storage capacity. As a result, a proper design of an LHTES device to operate with the U-SN PCM should be gas-tightened, made of a material which does not reacts with ammonia (Copper alloys discarded), and designed to withstand an internal pressure larger than the ammonia equilibrium pressure (of the Urea degradation process) without deformation or fracture. Determining the ammonia equilibrium pressure is one of the mandatory steps for a proper design of such LHTES device.

3.5 CONCLUSIONS

The present work presents a study for the determination of the thermal stability and reliability of a PCM consisting in the urea and Sodium nitrate eutectic mixture, composed of 71.25 wt% of urea and 28.75 wt% of Sodium nitrate, and identified with the acronym U-SN eutectic mixture in the text. The study has been carried out from a perspective different to the most widely employed accelerated thermal cycling. The proposed methodology consisted on holding molten samples inside a heating cabinet at 100 °C for different time periods, up to one year. Afterwards, thermal and compositional analysis were performed by means of different analytical techniques.

The analysis showed that after one year the melting temperature decreased in 10%, from 85 °C to final values of 75 °C, while the latent enthalpy decreased 24%, from 165 J/g to a final value of 125 J/g. The energy storage density after 1 year at 100°C is 177.5 KJ/dm^3. However, the values decreased in the first 40 days and tend to remain stable until one year. If the trend would remain stable in longer time-periods than those assessed in this study, these values could be considered the operational values for long term use. More research is required to confirm this hypothesis. In this case, the U-SN eutectic mixture would be an adequate PCM for the intended application (DHW and heating) since the melting temperature is in the required range (60-95°C), the melting enthalpy is similar to that o paraffin commercial PCM with similar melting temperature, while it would offer a significantly larger energy storage density.

The study showed that the cause for the thermal properties variations was the urea thermal decomposition to produce other compounds. Biuret and cyanuric acid were identified in the degraded samples, which is in agreement with urea thermal decomposition mechanisms proposed in the literature. The presence of this compounds modifies the initial U-SN eutectic composition with the result of diminishing its thermal properties (melting enthalpy and melting temperature). Furthermore, the formation of these products was related to the mass loss, which had a huge relevance in the material degradation. Despite that the maximum mass loss after

one year at 100 °C was only of 2.2% of the initial mass, it accounts for nearly 25% of its thermal storage capacity.

It was experimentally determined that if a gas-tight device is employed, the urea and Sodium nitrate eutectic mixture can reach the equilibrium and, consequently stop the degradation process. Hence, the degradation process can be very limited when there is no mass loss. Then, it is concluded that the lifespan of the urea and Sodium nitrate eutectic mixture as a PCM can be greatly controlled by the use of a gas tight system where the product evolution stops when the ammonia equilibrium pressure is reached. Further studies should determine effectively the system equilibrium pressure, evaluate the feasibility of obtaining an effective closed system and compatibility of the PCM and ammonia with the potential containers.

Finally, it is important to highlight the importance of having a strict control of the handling and experimental parameters. Parameters such as mass loss and water-uptake are not generally taken into account, but can have great influence in the degradation and thermal behavior of systems.

Chapter 4 : Phase segregation study of the urea and Sodium nitrate eutectic mixture

4.1 INTRODUCTION

When mixtures are to be used as PCM, several additional concerns must be taken into consideration, which do not exist in pure materials. The phase segregation is one of these issues. A material undergoes phase segregation when it does not melt / solidify congruently. This is, it melts into two different phases, usually a solid phase and a liquid phase, with composition different from each other (and different from the stoichiometric one), as well as with different specific-weight. This is the case of most mixtures, they present a semisolid melting interval instead of a melting point. Due to the solid-liquid specific-weight mismatch, the solid segregates from the liquid, generally falling down to the bottom of the container. When the material solidifies again, the contact between the two phases is not good and as a result, it can occur that the original composition cannot regenerate. Thus, the phase segregation can severely reduce the storage density because the latent heat on solidification can not be released completely, sometimes only to a small fraction. To retrieve the latent heat stored in the initial material, the correct composition of the mixture constituents is required throughout the whole sample [5].

For a long time, PCM based in eutectic mixtures have been considered a good option. Eutectic mixtures are made up of two or more components, in a specific composition that exhibit a unique melting point instead of a semisolid interval with a melting temperature range [15], [50], [54], [102]. As a result, it has traditionally been considered that eutectic mixtures melt and solidify congruently like pure materials, preventing the phase segregation. Even though this is true, the solidification of an eutectic composition proceeds differently from that of pure materials, by transformation of the liquid into a two-phases solid, each of them exhibiting a different composition.

The urea and Sodium nitrate eutectic mixture had been previously studied by the author and coworkers, who determined the phase diagram and the main thermal properties [62], [63]. The urea and Sodium nitrate eutectic mixture has a melting point of 85°C, a melting enthalpy of 172 J/g and a price below 1 euro/kg, which makes the mixture a good PCM candidate for the application under study, a TES for domestic hot water (DHW) and space heating. Nevertheless, during the recent research studies devoted to determine the stability and long-term crystallization behavior, reversible phase segregation was observed. It takes place during thermal cycling in samples with a significant mass. The thermal cycling tests performed in the small DSC crucibles did not lead to phase segregation. The fact that the segregation can be reversed implies that it is not caused by material thermal-degradation.

Phase segregation has rarely been reported, or even mentioned, in eutectic mixtures used as PCM. Congruent melting and solidification is always assumed in those cases [5], [15], [102]. However, some few authors claim that the eutectics behavior may not always be ideal. Rathod and Banerjee [54] stated that the use of these (eutectic) materials is very new to thermal storage

application and only limited data are available on thermo-physical properties. Therefore, the stability of the new eutectics has not been sufficiently researched to ensure their long-term performance.

Regarding the phase segregation phenomenon, few authors report about the possibility or the phenomenon to occur in PCM eutectics. Lane [6] states that when one of the components in an eutectic mixture presents supercooling while the other one solidifies on the melting temperature, segregation can occur although it does not usually happen. On the other hand, Gunasekara et al. [46] claimed that eutectic compositions are almost ideal as PCM if supercooling is absent. They state that, although it is not well known why an eutectic may supercool, upon supercooling phase segregation occurs due to the mixture compositional changes that take place and, the consequent phase separation is understood using the lever rule on the supercooled phases in the phase diagram.

In addition to being an uncommon phenomenon, the reasons why so few articles report phase segregation when studying eutectic mixtures as PCM, also include the fact that the published research has generally been carried out in small containers, most of them consisting in DSC measurements. The calorimeter dimensions are important in observing phase segregation. Materials segregate because of their specific-weight difference, and the DSC crucible height is too small for preventing the good contact between the segregated components. When larger containers are used, effective phase segregation can occur, preventing the segregated components to have a good contact during the thermal cycling process. Therefore, it is possible that using the same mixture, phase segregation could be observed in a T-history experiment while not in a DSC, as it is the case of the semicongruent melting of $CaCl_2 \cdot 6H_2O$ [103].

Metallurgists have gathered a deep scientific knowledge concerning very elementary aspects of metallic alloys crystallization. They include several classifications of eutectic typology according to different aspects, like the crystal growth mechanism or the microstructure morphology, and also the mechanisms that drive the eutectics to segregate and to report macro-segregation in eutectic alloys [104]–[106].

According to the crystal-growth mechanism, eutectics can be classified in two different types. One is defined as cooperative (or coupled) growth and the other one is divorced growth. Cooperative growth consists in the two eutectic phases growing together, as a diffusion couple: when a first solid crystal is formed the compositional change in the surroundings induces the crystallization of the other compound. Divorced growth occurs when the two eutectic phases grow separately. This case occurs when there is no direct exchange of solute between the two solid phases.

A second classification identifies different types of eutectic microstructures according to the interface morphology. The crystal growth kinetics of each phase cause different interface morphologies. The phases with high growth-anisotropy tend to grow fast in the preferred directions and slowly in other directions, forming facets. Isotropic phases, or those with low anisotropy, can grow at similar rates in many directions. Depending on the isotropy-anisotropy

combination of the mixture phases, the following eutectic classification is proposed: non-faceted/non-faceted (nf/nf), non-faceted/faceted (nf/f), and faceted/faceted(f/f).

The nf/nf eutectics form when both solid phases have isotropic growth-rate. They form regular microstructures, typically lamellar or rod-like. The nf/f eutectics form when one of the phases present isotropic growth-rate while the other one is anisotropic. The microstructure is formed by irregular or complex-regular morphologies. The f/f eutectics form when both solid phases have anisotropic growth-rate. The obtained microstructure is formed by irregular morphologies [107]–[109]. Examples of these regular, complex regular and irregular microstructures are shown in Figure 4. 1.

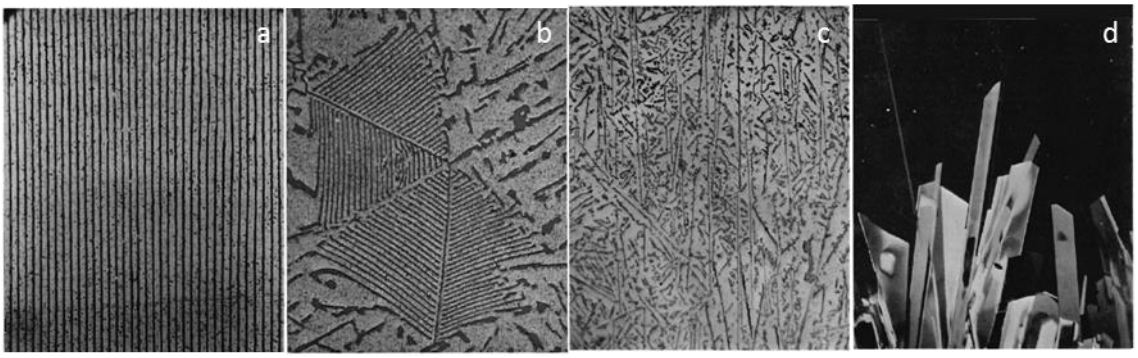

Figure 4. 1 Micrographs of materials displaying different microstructures. a) nf/nf regular (lamellar) Sn-Cd eutectic, b) nf/f complex regular Al-Si eutectic, c) nf/f irregular Al-Si eutectic, d) f/f irregular (divorced growth) Azobenzene-benzil eutectic [107]

Several authors suggest that the non-dimensional entropy of fusion, $\Delta S_f/R$, where ΔS_f is the entropy change on melting and R is the gas constant, can be used to distinguish between faceted and non- faceted interface morphologies [107], [108], [110], [111]. The materials with high $\Delta S_f/R$ have high crystal growth anisotropy. If $\Delta S_f/R < 2$ for both phases, then the eutectic is nf /nf. If the $\Delta S_f/R$ of one phase is >2 and the other one is <2 the eutectic crystallization is nf/f. If $\Delta S_f/R > 2$ in both phases, the eutectic morphology is f/f. The nf/nf and nf/f types show coupled growth and the f/f show divorced crystal growth [112]. Crocker et al. [110] propose an more extensive assessment of the resulting geometrical configurations with entropy of solution ($\Delta_{s\alpha}$) and the volume fraction (V_f) parameters indicated as in Figure 4. 2.

Many nonmetallic materials present f-f typology because they commonly have high entropy of fusion. The microstructures are mostly irregular and they grow near each other, but the crystallization of the first phase does not necessarily promote the crystallization of the second phase, following irregular structures in coupled growth or divorced growth [107]. This type of eutectic morphology has not been thoroughly studied because it not common in metallurgy. Irregular eutectics are prone to compositional heterogeneities, such as zones with higher spacing between the mixture constituents, zones which are richer in one of the compounds, etc. This could explain the phenomenon of segregation. Thus, a relationship between the eutectic type and the segregation may exist, but the fact that certain typologies produce segregation is not clearly specified in the literature.

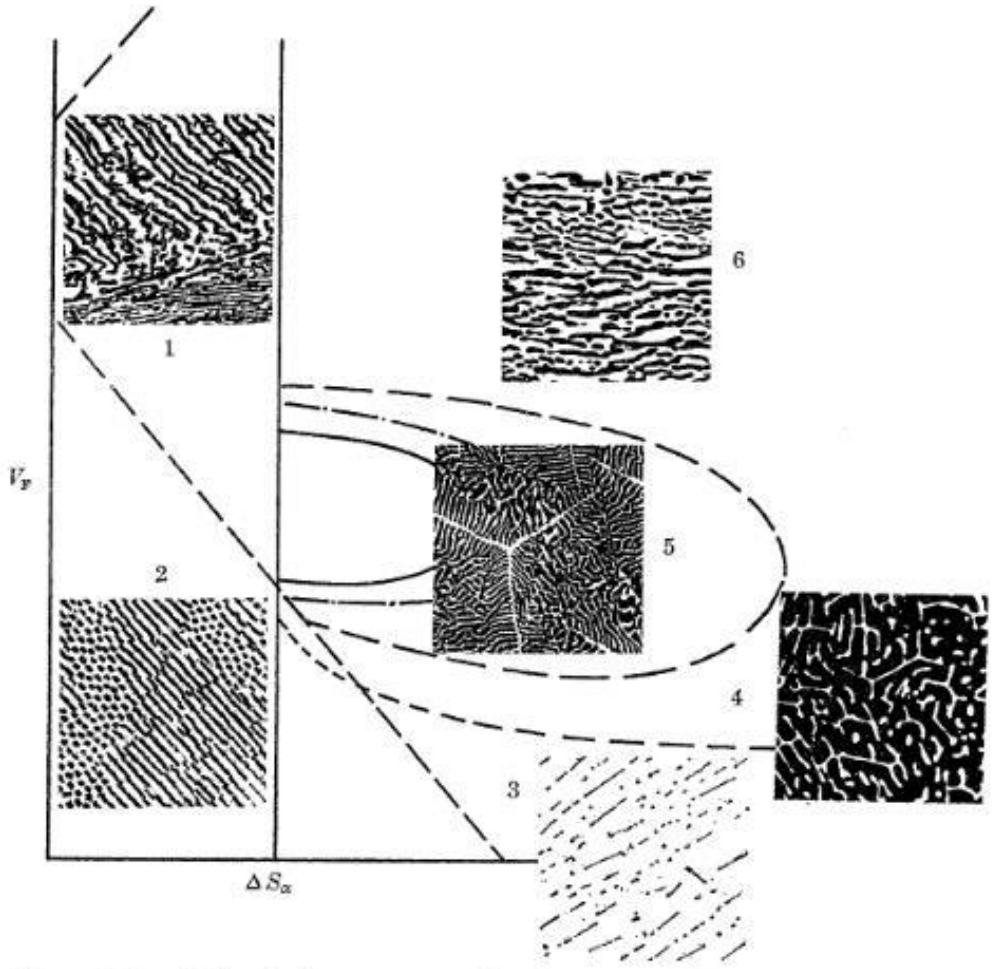

Figure 4. 2 Correlation of eutectic structures with entropy of solution ($\Delta_{s\alpha}$) and the volume fraction (V_f) parameters in a specific growth rate. 1 regular lame structures (nf/nf). 2 regular rod morphologies (nf/nf). 3 broken-lamellar structure s (nf/f). 4 irregular morphologies(f/f). 5 complex regular morphologies and regular structure in different proportions (nf/f). 6 quasi regular systems that show high degrees of ordered structures but can not be called regular (nf/f).[110]

On the other hand, the scientific literature reports two main theories about the causes of macro-segregation: natural convection within solidification (most accepted) [104], [109], [113], and the material bulk supercooling (more recent approach) [114], [115].

Boettinger and Banerjee[109], state that convection can cause long-range transport of individual species causing macro-segregation in metallic alloys. The solidification process is fundamentally driven by the heat transfer from the material, which pose a higher temperature because of the initial temperature condition and because of the latent heat after the phase change, to the cooler surroundings. It involves the consideration of important temperature and compositional gradients taking place in the liquid and in the solid phases, leading to density variations in the liquid that result in buoyancy-driven convection. The container contraction due to the cooling, and the volume change in the solidifying material also contribute to liquid movement. Therefore, solidification includes energy (heat transfer), species (solute), and momentum transport (motion of liquid and solid material). Khadivinassab et al. [104] points out that macrosegregation occurs when the alloying elements are transported over lengths larger than

the grain size causing depletion or enrichment in solute levels within the sample. Allen et al. [116] claim that if segregation occurs and the phases involved have very different densities, the effect is amplified by repeated melting/solidification cycles.

An example of eutectic composition that poses macrosegregation is the Sn-Cu_6Sn_5 eutectic mixture. Drevet et al. studied this system regarding natural convection [105]. It was determined that along the sample there were zones with compositional differences. Indeed, the segregation appeared in the hypoeutectic zones, not appearing in zones where the composition was purely eutectic. The microstructure of the segregated region was very disordered, with a high dispersion in terms of eutectic spacing when compared to the homogeneous zones, which showed a regular morphology.

Flemings [113]and Heinrich [117] report that, under convection, the cause of segregation can be related to the interdendritic flow phenomenon (flow of enriched melt exuded near the dendrite arms solidification-surface). Besides, dendritic microstructures are the consequence of a solid growth in an unstable liquid medium. This phenomenon, known as "Mullins-Sekerka instability", may happen when a solid grows into a supercooled liquid, following a process of dendritic formation [118]. However, this only happens in low melting entropy materials [107], i.e. those with isotropic growth rate.

Several authors report that there is a strong relationship between the obtained eutectic structures, the crystallization conditions (specially the cooling rate), the supercooling and the macro-segregation. The dynamics of the eutectic nucleation is a complex process involving many different parameters, and as a result leading to different microstructures [119], [120]. Experimental testing evidences that coarser crystals (generally dendrites) form in undercooled samples at slow cooling rates. In those samples, higher amounts of segregation were always found. In counterpart, quenched samples showed less amount of segregation [114], [115]. It was also observed that the eutectic morphology substantially changes with the supercooling degree: lower supercooling results in more regular structures and higher supercooling produces more irregular (anomalous) structures, which tend to have greater eutectic spacing [110], [115]. However, it must be taken into account that the supercooling degree in most cases is also a function of the cooling rate.

Galenko et al [121], determined that rapid solidification of eutectic systems can suppress the eutectic formation and, instead produce a homogeneous metastable phase formed by the initial chemical composition (the liquid phase composition).

When the supercooling phenomenon is taken into account to understand the segregation phenomenon in eutectic mixtures, authors point out that the instability introduced by supercooling causes the change the eutectic composition. Bevan Ott et al. [122] stated that supercooling is a frequent cause for the formation of metastable solids. Figure 4. 3 represents a phase diagram of an eutectic system, where the Solidus and Liquidus lines corresponding to the equilibrium conditions are the continuous lines. The dashed lines represent the freezing lines for the metastable forms when supercooling occurs. The metastability can be the cause of the phase segregation since the eutectic melting point and composition are modified. Indeed, this

agrees with the remark made by Gunasekera et al.[46] about eutectic PCM showing phase segregation when they had supercooling.

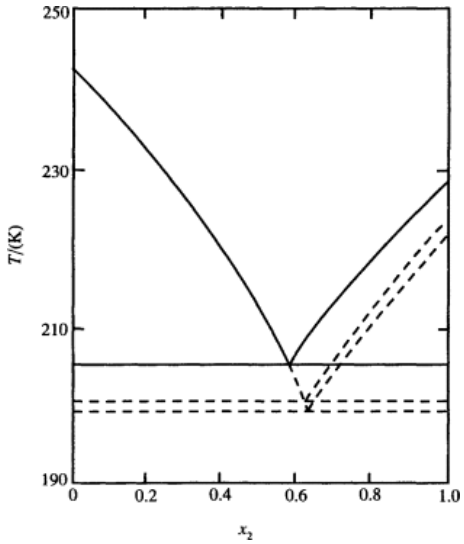

Figure 4. 3(Solid + liquid) phase equilibrium for {x1C6H5Br + x21,3,5 C6H3(CH3)3}. Continuous lines represent liquidus and solidus equilibrium temperatures, and the dashed lines represent metastable equilibrium between the liquid solution and unstable forms of 1,3,5-C6H3(CH3)3 [122]

The ease of a material to nucleate and the influence of one phase in the nucleation of the other one is also of great importance in the eutectic segregation, as shown by Kobayashi et al. in the Al-Si alloys [123]. Chiba and Spittler [124] showed in various eutectic compositions of different metallic systems that nonreciprocal nucleation have great effect on the castings microstructure-morphology. Non-reciprocal nucleation refers to the inability of one phase to act as an effective heterogeneous nucleation site for the other phase. De Groh [114] highlights the influence that a significant difference in the nucleation barriers for each phase can have in the segregation of undercooled eutectics, and is likely to result in non-reciprocal nucleation behavior. Benicio et al. [115] studied the Pb-Sn eutectic system, which corresponds to a non-reciprocal nucleation system. It was observed that solidification of the eutectic composition formed microstructures similar to those of hypoeutectic compositions, exhibiting two nucleation temperatures: one for the primary phase crystals, and one for the eutectic crystallization.

Summarizing, the scientific literature indicates that several parameters may influence the phase segregation in eutectic mixtures. In a first place, depending on the materials characteristics (morphology of the crystal interface, density of each mixture-component, their ease of crystallization, etc.), the testing conditions (specially the cooling rate), and the supercooling degree different crystalline microstructures will form. These parameters determine the formation of different phases (stable or metastable) which, in turn, can produce compositional changes and thereby phase segregation. In addition, it is well known that the compositional distribution can vary by convection during the solidification process; and mixtures of materials with high density difference tend to enhance the segregation when the separation of the segregated solids is pronounced, thus the segregation during the cycling process becomes non reversible.

4.2 EXPERIMENTAL WORK APPROACH

The present study aims to analyze the phase segregation phenomenon of the urea and Sodium nitrate eutectic mixture (onwards identified by the acronym U-SN eutectic) in order to evaluate its suitability to be used as a PCM. Phase segregation can be a problem for a reproducible and reliable use of the mixture as a phase change material for latent heat thermal energy storage [5]. The research analyzes the phase segregation phenomenon occurred in the mixture under various cooling rates and different container configurations. The objective is to understand the mechanisms and the experimental factors that cause phase segregation, and to be able to propose preventive measures to avoid it, or to reverse it. The produced eutectic microstructures have been analyzed to see whether they have influence on the phase segregation of the U-SN eutectic.

Preliminary thermal cycling tests carried out in containers with 4-5 grams of the U-SN eutectic mixture indicated that the mixture segregated solid material on the bottom of the tubes upon repeated melting-solidification cycles. This phenomenon did not occur when the material was molten for a long time, without thermal cycling. The observed segregation depended on the experimental conditions, but the reason was not assessed. The present work aims at determining the reasons and mechanisms behind the observed phase segregation, as well as its relationship with the main experimental working conditions.

The experimental work was scheduled to determine the influence of different parameters on the phase segregation observed. Thermal cycling experiments were carried out under different cooling rates and with two different container geometries. The cooling rate influences many aspects of the materials crystallization, including the formation of metastable phases, and phase segregation.

The container geometry is important in the convection processes, and convection may play a significant role in phase segregation. Taking a defined container volume as a reference, a vertical arrangement of the volume promotes high natural convection when a temperature change occurs. When density changes take place in addition to the temperature change, fluid movement pulls down the denser portions, aided by gravity. This motion, by definition, occurs mainly in the vertical direction, the direction of gravity. If the same container volume is placed in a horizontal arrangement, convection forces will be lower than in the vertical case. As a result, segregation might be affected by the container design. In order to assess whether the vertical or horizontal disposition of the tubes influences the phase segregation, two tube configurations with the same volume and aspect ratio (diameter & length) were used in the study.

The segregated phases were analyzed by means of X-ray diffraction (XRD) to determine the composition of the segregated solids. Differential scanning calorimetry (DSC) was employed to determine the materials thermal behavior after segregation occurred, and after the segregated mixture was recombined and molten again.

The microstructure and the morphological features of the microconstituents were observed under polarized light microscopy PLM, and scanning electron microscopy SEM aided with X-ray

EDS microanalysis. The feasibility of using the material as a PCM after the mixture segregated was assessed. Table 1. 1 summarizes the tests performed.

Table 4. 1 Summary of the tests performed

Testing	Testing details		Analytic technique
Thermal Cycling	0.3 °C/min	35 cycles, 4 vertical tubes - mixing and dissolution of segregates (after cycling)	Visual inspection
			PCM temperature monitorization
			XRD (segregated and mixed samples)
			DSC (mixed samples)
		16 cycles, one vertical and one horizontal tube	Visual inspection
	2 °C/min	80 cycles, 4 vertical tubes	Visual inspection
			PCM temperature monitorization
Nucleation and crystal growth assessment	One hour at isothermal conditions: 85°C, 84°C, 83°C and 82°C	one vertical and one horizontal tube	Visual inspection
Microstructure and morphological determination	Quenching 95 to 20 °C	Sample covered (glass coverslip)	PLM / SEM
	Quenching 95 to 20 °C	Crystallization promoted by spreading, not covered	
	Slow cooling at 80 °C	Sample covered (glass coverslip)	

4.2.1. SAMPLE PREPARATION

The U-SN eutectic was prepared made of the pure components (99.9 purity), purchased from Sigma-Aldrich. A sample containing 50 grams of mixture was prepared. A precision balance with 0.1 mg accuracy was used to weight the pure urea and pure Sodium nitrate to produce the eutectic composition: 71.25 wt% of urea and 28.75 wt% of Sodium nitrate. The sample was introduced in a glass flask, closed with a rubber plug and introduced into a glycerine bath at 95 °C until it was fully molten. Two magnetic stirrers, one inside the sample and one inside the glycerine bath, were used in order to provide a good temperature homogeneity.

When the mixture was molten, the test-tubes for thermal cycling were filled in with 4-5 g of the liquid material and, to prevent water absorption due to the hygroscopic nature of the material, the tubes were introduced in a desiccator with phosphorus pentoxide as desiccating agent, for the solidification to take place.

4.2.2. THERMAL CYCLING TESTS

Two different test-tube types were used in order to evaluate the potential influence of the vertical and horizontal arrangement on the phase segregation. Both tube types were made of glass, 0.002 m inner radius and 0.001 thickness. One type had a vertical arrangement, consisted in a regular tube of 0.1 m height filled up to 0.08 m. The other tube type had a horizontal arrangement, an inverted "T" shape, with the horizontal section being 0.08 m long, and the vertical section of 0.02 m height. The vertical tubes were Ace pressure tubes purchased from Sigma Aldrich, while the horizontal tubes were tailored made on purpose to resemble the Ace tubes placed on the horizontal position, like is shown in Figure 4. 4.

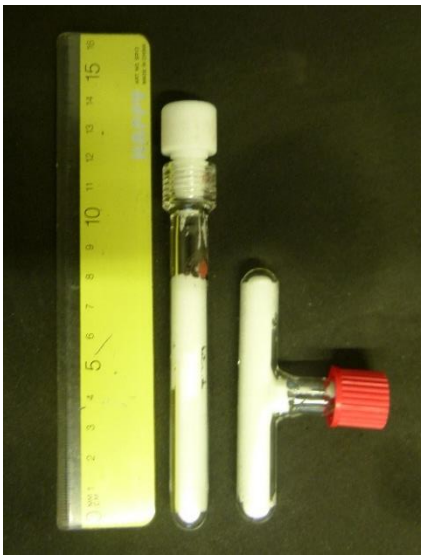

Figure 4. 4 Tube types used to achieve vertical and horizontal arrangement of the sample, containing the same sample mass

The eutectic mixture was introduced in the test-tubes, which were immersed in a programmable thermostatic bath, Lauda RP845 thermostatic bath using Bluesil 47V20 silicone thermal oil as heat transfer fluid (heating and cooling media).

Tests were carried out under two cooling rates: a fast cooling rate of 2 °C/ min and a slow cooling rate of 0.3 °C/min. Figure 4. 5 depicts the temperature programs followed per cycle.

Samples in the vertical configuration (Figure 4. 6) were submitted to 80 cycles with fast cooling rate (2 °C/ min), and 33 cycles for the slow cooling rate (0.3 °C/min). Under each cooling rate 4 samples were tested. One of the samples included a T-type thermocouple (accuracy 0.5 °C) inside the PCM to monitor the temperature and to determine the melting and crystallization temperatures in each case. The thermocouple section outside the tube was insulated using 2 cm width EDPM foam in order to eliminate thermal bridges.

Samples on the horizontal configuration were tested solely under the slow cooling rate (0.3 °C/min) for 16 cycles, together with the corresponding vertical samples in the bath, at the same time.

Visual observation was used as the assessment method to determine solid phase segregation during the solidification process along the thermal cycles.

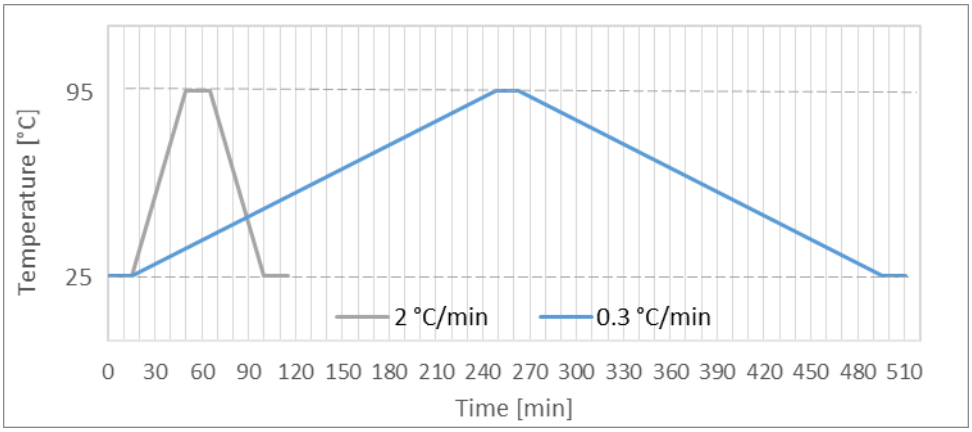

Figure 4. 5 Temperature programs for thermal cycling of U-SN eutectic: heating and cooling ramps (0.3 and 2 °C/min) with isothermal segments (15 min) in between

Figure 4. 6 U-SN eutectic samples for thermal cycling tests

X-ray diffraction XRD of the segregated material

X-Ray diffraction was carried out on the raw materials employed to prepare the eutectic mixture, the pure urea and the pure Sodium nitrate, on the fresh (non-cycled) eutectic mixture and on one of the previously thermally cycled samples. The sample selected for the X-ray diffraction had been submitted to 35 cycles at 0.3 °C/min. In this case, the sample was left to cool down into the tube until room temperature was reached, then the tube was broken down with care and, afterwards the solid sample was cut into three specimens, one from the bottom area, one from the upper part and the middle zone was the third specimen. All the specimens were manually grounded in an Agata mortar and were stored in a desiccator until the XRD tests took place. The methodology employed for the XRD measurements is fully described in [62].

4.2.3. NUCLEATION AND CRYSTAL GROWTH ASSESSMENT IN THE SUPERCOOLED LIQUID

An additional series of tests was carried out to determine the minimum temperature needed for the nucleation to take place, and how the subsequent crystal growth develops. For this, 2 samples (one in a horizontal tube and one in a vertical tube) were prepared following the same methodology as for the previous studies.

The experimental procedure consisted in melting the samples at 95 °C in the thermostatic bath, then the temperature of the thermostatic bath was lowered to a pre-defined temperature and held at that temperature for one hour to see whether crystallization occurred within this time by means of visual recognition. In the first experiment, the set-up temperature was the melting point of the eutectic mixture, 85 °C. The series of experiments consisted of repeating this procedure by decreasing the set-temperature in 1 degree each time, to 84 °C, 83 °C and 82 °C.

4.2.4. USE FEASIBILITY OF THE MATERIAL AFTER SEGREGATION

In order to evaluate the reversibility of the phase segregation one additional experiment was carried out. One sample that had been tested for 35 thermal cycles at 0.3°C/min, showing three segregated zones (all the samples tested under those conditions showed the same behavior) was heated up to 95 °C, then gently stirred (by hand) with the result of complete sample melting. The resulting liquid (after stirring and complete dissolution) was analyzed with the aim of determining if the material remained similar to the original mixture. X-ray diffraction and differential scanning calorimetry, DSC, were used to determine whether the composition and/or the thermal properties were different from those of the original eutectic mixture.

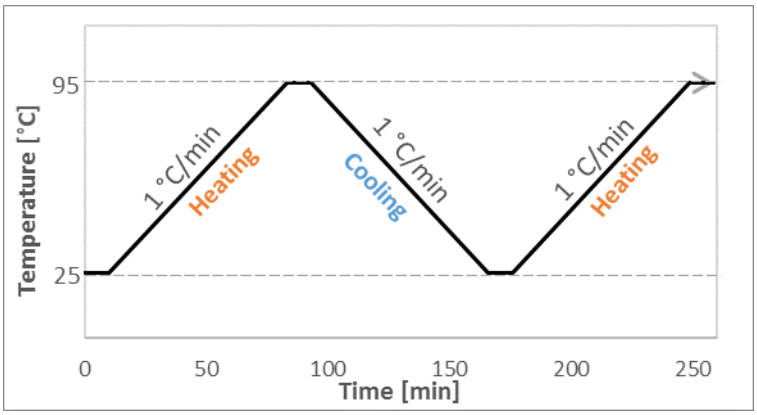

Figure 4. 7 DSC temperature program

The methodology employed for the XRD and DSC measurements are fully described in [62]. The temperature program used in DSC (Figure 4. 7) consisted on two heating ramps and one cooling ramp. The first heating segment serves to settle the sample on the bottom of the crucible to achieve a good contact. The thermal properties were evaluated from the cooling and second heating ramp. Both heating and cooling rates were of 1 °C/min, and isothermal segments of 10 minutes on either side of the dynamic segments.

4.2.5. MICROSTRUCTURAL AND MORPHOLOGICAL ANALYSIS

The material microstructure could be one of the causes for the phase segregation. In order to analyze it, the U-SN eutectic microstructures produced under different cooling conditions have been determined. Polarized light microscopy PLM, and scanning electron microscopy SEM, were used with this aim.

Generally, microstructural and morphological features are observed by light or electronic microscopy on samples that require a preparation, which includes sample cutting and polishing. In this case, however, due to the low meting point of the material and to its solubility into water, it was not possible to prepare metallographic or minerallurgy-inspection samples for the microstructural observation. As a result, an alternative method was devised.

Three samples were prepared by pouring the liquid material on top of glass sample holders. Two of them were produced by quenching the material from the molten temperature, 95 °C, to room temperature (samples 1 and 2), one sample was produced by slow cooling inside a heating cabinet at 80 °C (sample 3). In the samples 1 and 3 a coverslip glass was placed on top of the liquid, thus producing thin solid materials. In sample 2, after the liquid was poured, it was purposefully spreaded with a glass coverslip, but not covered with it.

A Panasonic DMC-FZ100 camera (resolution of 14 mega pixels) was used to take samples macrographs. A Leica DMLP polarizing light microscope with an attached camera was used to observe and take micrographs of different morphological features. A JEOL JSM-7000-F scanning electron microscope, equipped with an EDX spectrometer from Oxford Instruments INCA Energy 350, was used to observe and analyze the samples microstructure and to identify the compounds in each different feature.

The samples were coated with a Carbon layer of about 20 nm, by evaporation under vacuum using a Quorum Technologies Q150T ES, by passing an electric current through a bar of pure carbon in a high vacuum (4-10 mbar). The carbon temperature increases to over 3000 K, sublimates, and afterwards condense onto the sample.

The measurements were done under 10 kV using a beam current of the order of 0.1 nA. Secondary electrons and backscattered electrons imaging were employed, as well as EDX chemical identification. The observation of the microstructural features in the SEM, as well as the microanalysis, were limited by its low melting point.

4.3 RESULTS AND DISCUSSION

4.3.1. THERMAL CYCLING TESTS

During the thermal cycling, phase segregation was observed. Solids gradually appeared after each cycle, both on the top and on the bottom of the samples, without fully disappearing on heating above the eutectic temperature. Consequently, three zones can be distinguished in the samples: solid material on the top (translucent crystals), solid material in the bottom (very thin white crystals), and liquid in the middle zone.

4.3.2. INFLUENCE OF THE COOLING RATE

Segregation took place under both cooling rates employed in the study. Figure 4. 8 shows the evolution of the samples segregation after melting/solidification cycles with a cooling rate of 0.3 °C/min (images on the left) and 2 °C/min (images on the right). The distribution of the segregation on the bottom and onto the uppermost part of the sample is due to the density difference of the segregated materials and the liquid. The density of solid Sodium nitrate (2.26 g/cm^3) is higher than the liquid mixture density (1.42 g/cm^3 [62]), which is higher than solid pure urea density (1.32 g/cm^3). Then, the heavier Sodium nitrate falls down and the lighter urea rises up. The middle zone, liquid material (at 95°C), corresponds to the remaining molten eutectic mixture. This behavior is confirmed by XRD and explained in detail after the visual inspection analysis of the cycled samples.

During the tests, some bubbles formed, which evidence gaseous ammonia formation that comes from the urea thermal degradation. The formation of degradation products is studied in another chapter of the thesis.

The segregation is more significant in the samples exposed to 0.3 °C/min cooling rate than in the samples tested under 2 °C/min cooling rate. After only 8 cycles, the segregated solid in the samples tested under the slow cooling rate is visually 3 or 4 times larger than the solid segregated in the samples tested under the fast cooling rate. Indeed, the segregated amount produced after 14 cycles in the samples tested under the slow cooling rate is similar to that produced after 35 cycles under fast cooling rate.

The segregates obtained in the samples at the end of the test (33 cycles and 80 cycles for the slow cooling rate and high cooling rate respectively) show a similar amount of the material on the bottom of the tubes on both cases (visual inspection, not a quantitative measurement). The material segregated to the upper part of the tubes submitted to different cooling rates, on the contrary, presents a different appearance. Due to the material volume-change in the melting-solidification, the liquid lifted the lighter material upwards. The samples that cooled down at 2 °C/min, after several thermal cycles, presented a void between the upper segregated part and the rest of the material. The solid segregated on the upper part of the beakers remains in that place along the following thermal cycles. Due to the rapid cooling rate, the shrinkage that takes part upon liquid solidification creates a void between this segregated solid and the rest of the sample. This did not occur in the samples tested at 0.3 °C/min cooling rate (in the studied number of cycles) because the process was slow enough for the segregates to follow the liquid volume change.

The monitored temperature indicated that supercooling varies upon increasing number of thermal cycles. Figure 4. 9 shows the supercooling degree of the samples tested under both cooling rates. The supercooling degree slightly decreased with the number of cycles, which evidences that the pre-existence of crystals promotes the samples crystallization. The highest supercooling degree was registered in a sample tested under 2 °C/min cooling rate, which did not show the highest phase segregation. This provides evidence that a higher supercooling does not necessarily cause a higher segregation as might have been expected according to the literature [110], [115].

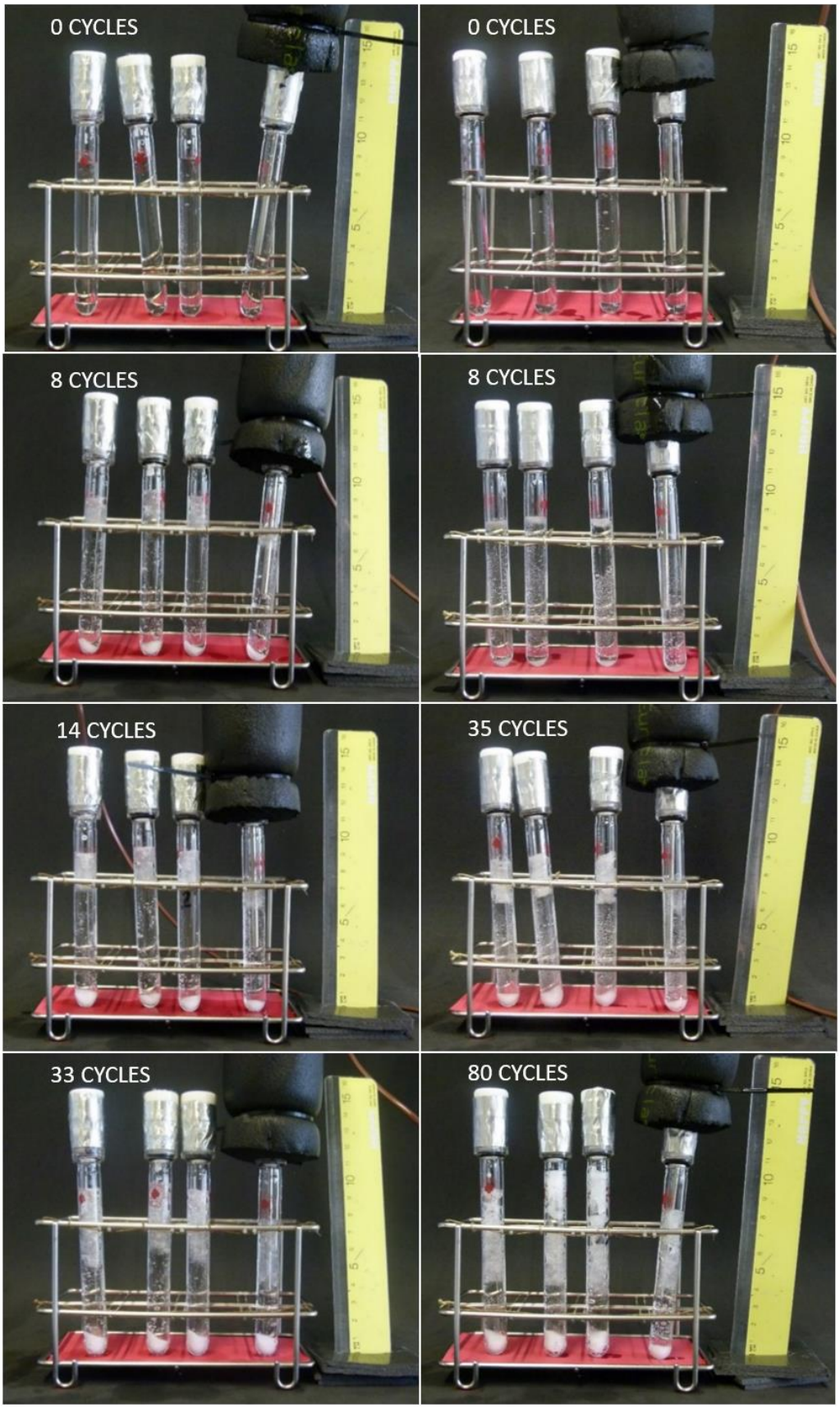

Figure 4. 8 Images of U-SN eutectic samples after selected number of thermal cycles at cooling rates of 0.3 °C/min (images on the left) and 2 °C/min (images on the right) where phase segregation is observed

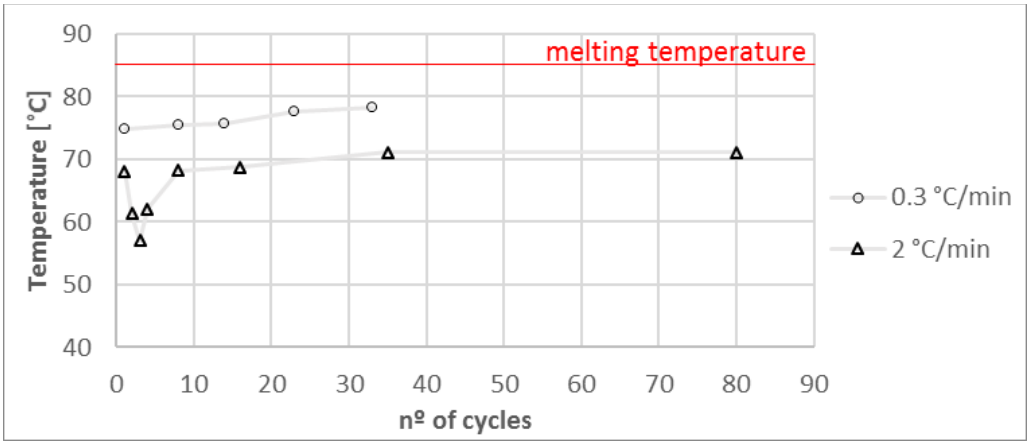

Figure 4. 9 Crystallization temperature of monitored samples during thermal cycling with cooling rates of 0.3 °C/min and 2°C/min

4.3.3. X-RAY DIFFRACTION XRD OF THE SEGREGATED MATERIAL

Figure 4. 10 shows the XRD patterns of the segregated solids placed on the top, middle, and bottom of the tubes after thermal cycling, as well as those of the pure urea, pure Sodium nitrate and the fresh eutectic mixture. It also includes the XRD pattern of a sample that was stirred to mix-up the segregated and liquid zones.

The peaks-position analysis showed that no new phase had formed in any of the studied cases. Only urea and Sodium nitrate were present in the cycled samples. As a result, it can be concluded that the mixture did not degrade or decompose to a significant amount.

The relative intensity of the peaks and their position serve to evaluate the compositional changes in a qualitative manner. At a first glance, the patterns corresponding to the segregated top and bottom zones are different from each other. The diffractogram of the upper portion show both urea and Sodium nitrate peaks, however the intensity of the peak placed at the 2Theta position of 22.42 degree corresponding to urea, has a much higher intensity compared to the intensity corresponding to Sodium nitrate peaks, this is that the proportion ratio between peaks is not the same. This indicates that it has a greater urea content than the eutectic mixture. On the other hand, the specimen from the bottom portion of the tube shows the opposite behavior. The diffractogram shows almost no urea, but Sodium nitrate appears in a greater proportion, which gives evidence that the solids in the bottom of the tube are Sodium nitrate crystals. It must be reminded that the specimens were extracted after full solidification took place, cutting them out from the selected zones in the sample, they were not extracted from the liquid material.

These results are in agreement with the physical characteristics of each compound: Sodium nitrate is denser (2.26 g/cm^3) than the eutectic liquid (1.42 g/cm^3) fall down to the bottom, while urea that is lighter (1.32 g/cm^3) than the liquid float onto it.

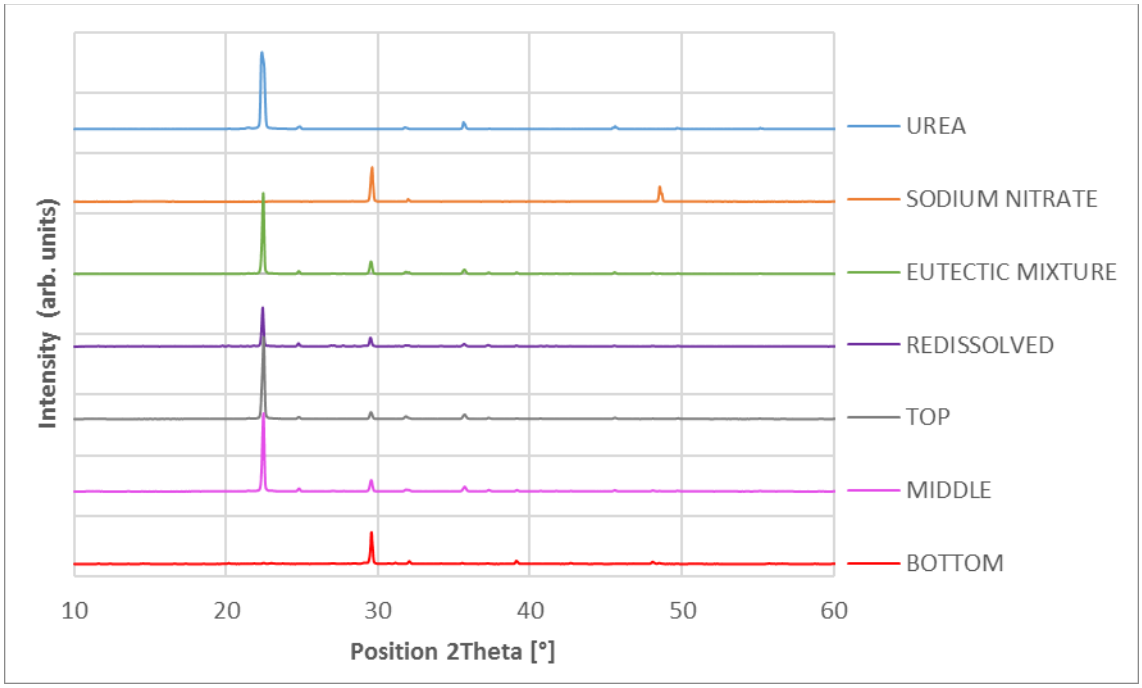

Figure 4. 10 Diffractograms of pure urea and Sodium nitrate, the non-segregated eutectic mixture, the liquid resulting from the redissolution of solid segregates, and the top, middle and bottom sections of a segregated sample

4.3.4. Influence of the container disposition: vertical and horizontal arrangements

No reliable conclusion could be drawn from the experiments carried out in vertical and horizontal position due to the circumstances that are explained onwards. However, several interesting observations can be pointed out. Figure 4. 11 shows the segregation in the samples after 16 cycles. It can be noticed that segregation occurs in both tubes and the horizontal tube has similar or slightly greater segregation. It is thought that it is due to undesired (unforeseen) different thermal conditions between the two samples: The horizontal tube was very short and therefore, its immersion in the thermostatic fluid was very shallow, close to the air-oil surface. As a result, the sample might have not followed the temperature program in an efficient and reliable way, being the heating and cooling conditions presumably different from those in the vertical tube. In addition, the curvature of the tube distorts the image observed, hindering a reliable comparison between the tubes.

In spite of the potential different cooling conditions of both samples, the experiments served to certify that the convection does not play an important role in the phase segregation taking place on the samples, because the horizontal arrangement showed the same or even more segregates than the vertical arrangement. If the convection was responsible for the segregation, then the horizontal tube should show no or lesser segregated solids than the vertical tube. However, its role may be more important in higher volumes.

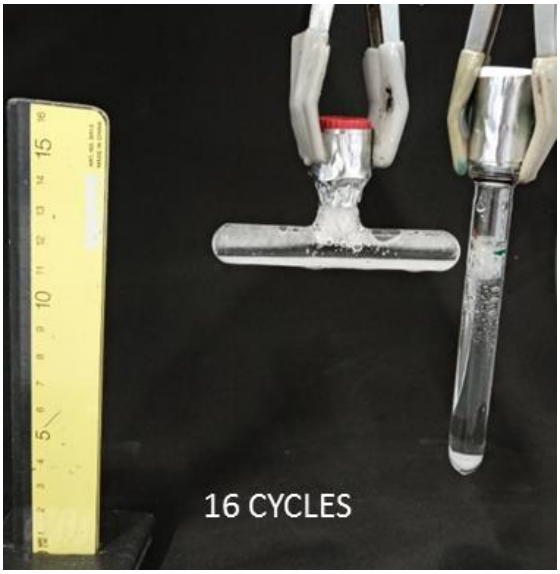

Figure 4. 11 Comparison of the phase segregation taking place in the U-SN eutectic when horizontal and vertical geometrical dispositions are used. Tests carried out for 16 melting/solidification cycles

4.3.5. NUCLEATION AND CRYSTAL GROWTH ASSESSMENT IN THE SUPERCOOLED LIQUID

The experiment consisted in submitting the U-SN eutectic to isothermal segments from 85 °C (melting temperature) to 82°C, decreasing the temperature 1 degree each time for 1 hour to determine if the crystallization happened at these temperatures. 82°C was the first temperature to promote crystallization.

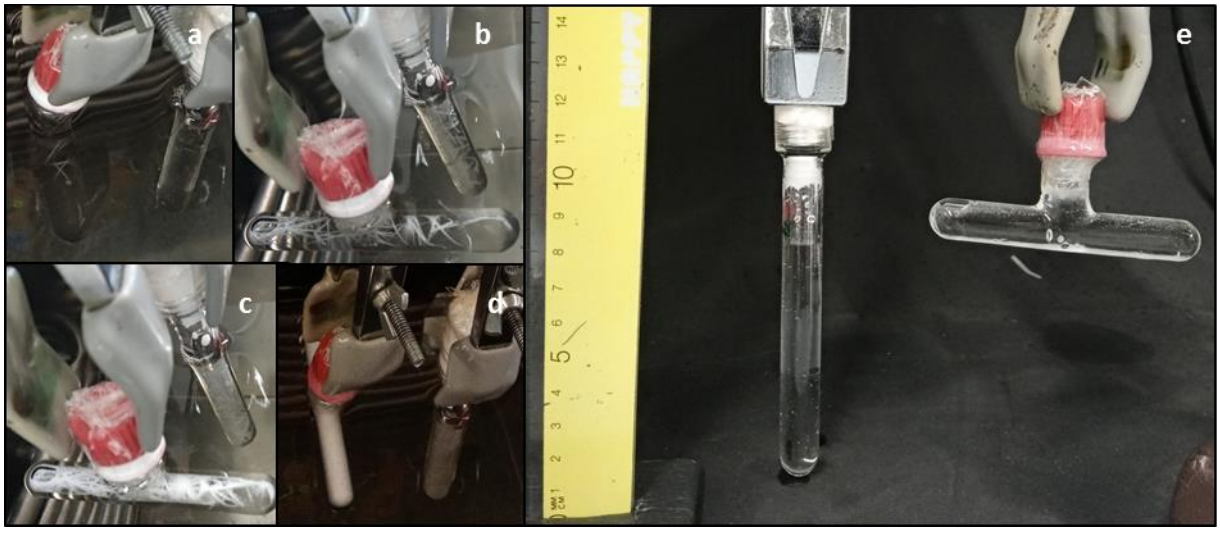

Figure 4. 12 Evolution of the primary crystal growth at 82 °C in horizontal and vertical arrangements (Images a, b, c and d) and the molten sample at 95 °C (image e)

Figure 4. 12 shows the first crystals formed at this temperature, which consist of needles that seem to appear from more than one initial nucleation point and grow to form acicular or fibrous radial structures. The round shape of the tubes distorts the image of the needles, which indeed are straight not curved. The first needle formation could be observed after approximately 4

minutes at 82°C. They grew up and the sample was fully solid after more than 30 minutes time at 82°C. It can be noticed that these primary crystals did grow long for a significant time without inducing the crystallization of the secondary phase, to grow coupled together (as it could be expected from a eutectic composition). On the contrary, non-reciprocal nucleation is observed, because the primary nucleating phase do not promote the crystallization of the secondary phase, thus being evidence of a divorced growth of both phases in this eutectic mixture in the experimental conditions. Figure 4. 12.e shows the presence of small crystals that did not melt after 1 cycle, thus enduring how phase segregation starts already in the first solidification cycle.

4.3.6. USE FEASIBILITY OF THE MATERIAL AFTER SEGREGATION

The fact that the produced solid phases dissolved into the molten liquid upon stirring, evidenced that the phenomenon was phase segregation.

The results from the XRD analysis indicated that the redissolved sample and the sample obtained from the middle of the tube (liquid portion with no segregates) show the same peaks of the eutectic mixture, i.e. the pure urea and Sodium nitrate peaks. Therefore, it can be said that there is no modification on the composition. The difference in the intensity of the peaks of the three diffractograms is due to the mass difference of the studied samples, however they render similar intensity proportion between peaks associated with urea and peaks associated with Sodium nitrate. It was therefore concluded that the phase-segregation does not have a direct relationship with other degradation processes that could occur in the samples.

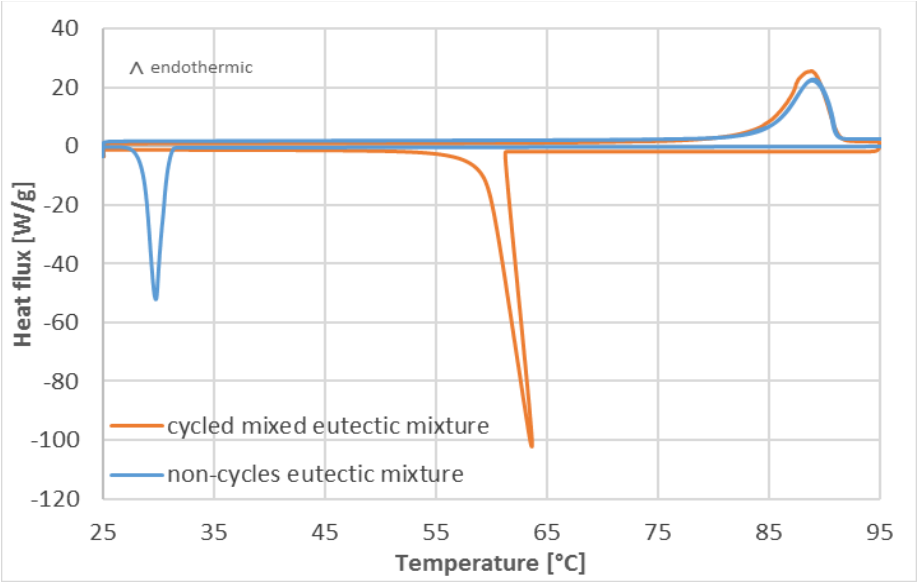

Figure 4. 13 Thermogram of a sample that has been redissolved by mechanical stirring after phase segregation and a fresh non-cycled U -SN eutectic sample. Thermal behavior on heating and cooling

The Differential scanning calorimetry measurements of the liquid obtained after the segregate redissolution indicate the following results: Figure 4. 13 corresponds to the thermograms of the cooling and second heating ramp of a sample after the redissolution of the segregates and fresh non-cycled U-SN eutectic sample. It shows an onset temperature of 83.69 °C and a latent enthalpy of 174.20 J/g during melting and an onset temperature of 61.39 °C and a latent

enthalpy of 160.3 J/g during crystallization. The fresh non-cycles eutectic sample showed an onset of 84.38 °C and a latent enthalpy of 168.8 J/g during melting and an onset temperature of 28.63 °C and a latent enthalpy of 153.4 J/g during crystallization.

Then, it was confirmed that the liquid obtained after redissolution of the solid segregates poses similar thermal properties as the non-cycled U-SN eutectic on melting. The stochastic nature of supercooling in small samples make that the crystallization onset was not alike. However, the supercooling characterization is studied and discussed in chapter 5.

The material potential-use after it experienced segregation is therefore feasible if a suitable stirring means is implemented in the system.

4.3.7. Microstructural and morphological analysis

The different sample preparation produced different morphological features even under simple visual inspection, without the need of a microscope. Samples 1 and 2 solidified by quenching at room temperature and therefore the rapid crystallization that gave smaller crystals. Sample 3 crystallized in conditions closer to equilibrium and large crystals formed.

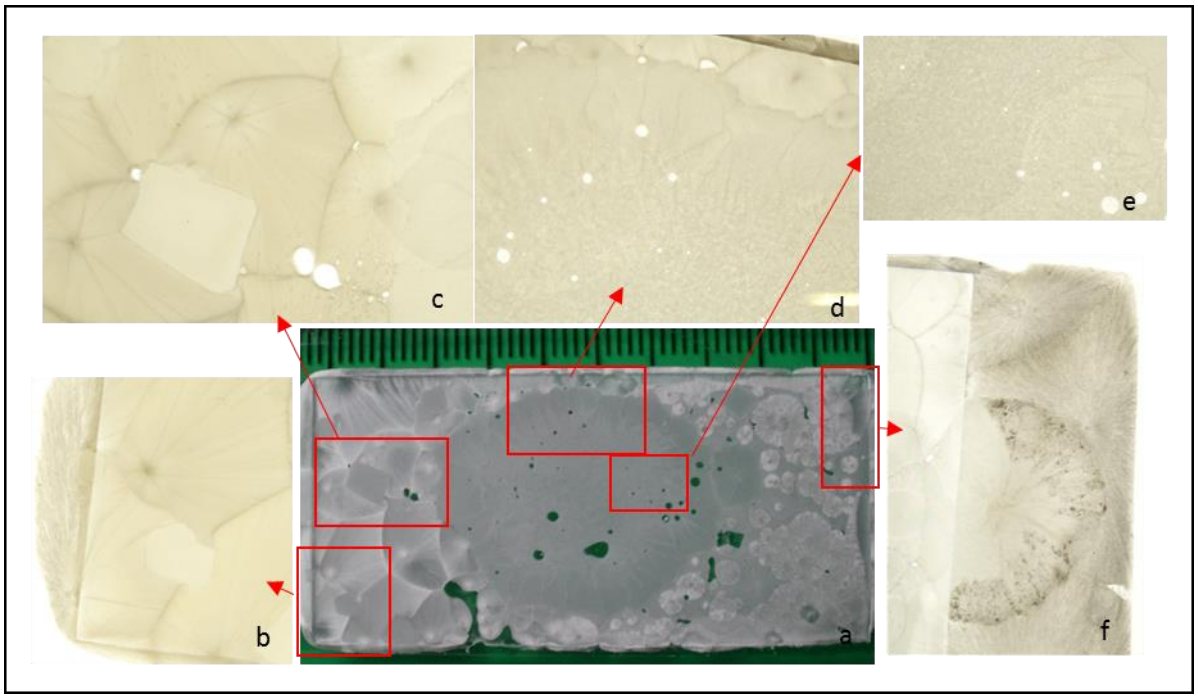

Figure 4. 14 Sample 1 produced by quenching at room temperature. Macrograph of the whole sample and micrographs showing the different zones that display details of the produced structures

Figure 4. 14, Figure 4. 15 and Figure 4. 16 gather macrographs and micrographs of samples 1, 2 and 3 respectively (macro pictures and PLM images). Figure 4. 14 (a) shows the sample 1 (upper marks represent millimeters); Figure 4. 14 (b) and Figure 4. 14 (c) show spherulites where the crystallization starting point can be clearly observed, together with prismatic-like grains. Figure 4. 14 (e) and Figure 4. 14 (d) correspond to the central part of sample 1. It presents a disordered mix of two phases. Figure 4. 14 (e) also shows a transition between the central (disordered) zone and spherulites produced in the border of the sample. Figure 4. 14 (f) corresponds to a zone

where spherulites grew out from the coverslip, thus looks less homogeneous because the crystal growth was not limited in the perpendicular direction to the sample holder direction.

Sample 2 is shown in Figure 4. 15. At first sight it seems that the whole sample has a similar acicular structure, which looks like small disordered needlelike crystals into a continuous matrix. On the visual inspection there is not any distinctive feature in the sample. Figure 4. 15 (b), Figure 4. 15 (c) and Figure 4. 15 (d) show that under the PLM the crystals can be observed at the edges because the layer of material is thinner there and the light transmits easier.

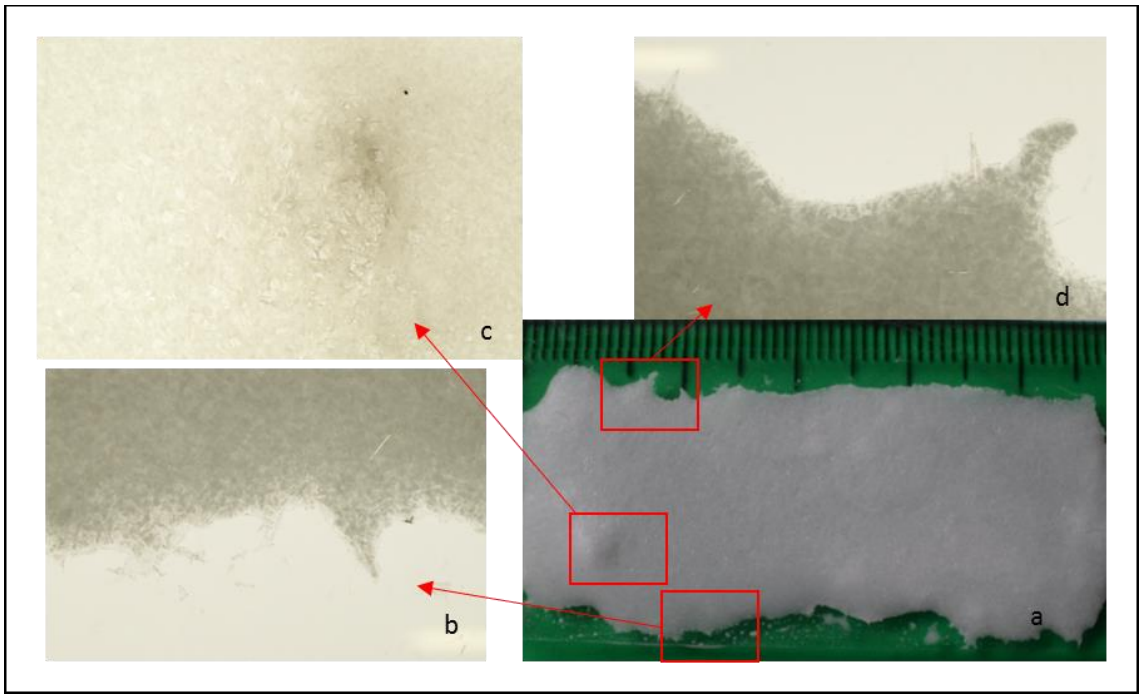

Figure 4. 15 Sample 2 produced by quenching at room temperature and induced nucleation. Macrograph of the whole sample and micrographs showing zones that display details of the produced structures

Figure 4. 16 shows sample 3. An extremely large grain grows from a bubble (Figure 4. 16 (a) and Figure 4. 16 (d)), with elongated crystals radially growing from it. At first sight, the crystals seem to have grown radially following a band or dendritic-like pattern. Figure 4. 16 € shows a zone where crystals have grown in a unique direction. Figure 4. 16 (b) and Figure 4. 16 (c) show details of zones where various crystals are confronted.

The PLM gives an idea of the different macro structures that are formed under the experimental conditions. However, it does not allow the identification of the microstructures that form the eutectic or the compositional differences in the structure. Therefore, scanning electron microscopy was used.

Even though secondary electrons were used to observe the microstructure, only the images from the backscattered electrons have been included in the general analysis. Backscattered electrons images serve to distinguish microstructural features with different composition. Microconstituents that contain heavier elements in their chemical composition have a high backscattered-electrons intensity and therefore, they are visualized as bright light-grey or white

colored features. The microconstituents composed of low atomic weight elements have a poor backscattered-electrons intensity and, as a result they render dark features, dark grey to black.

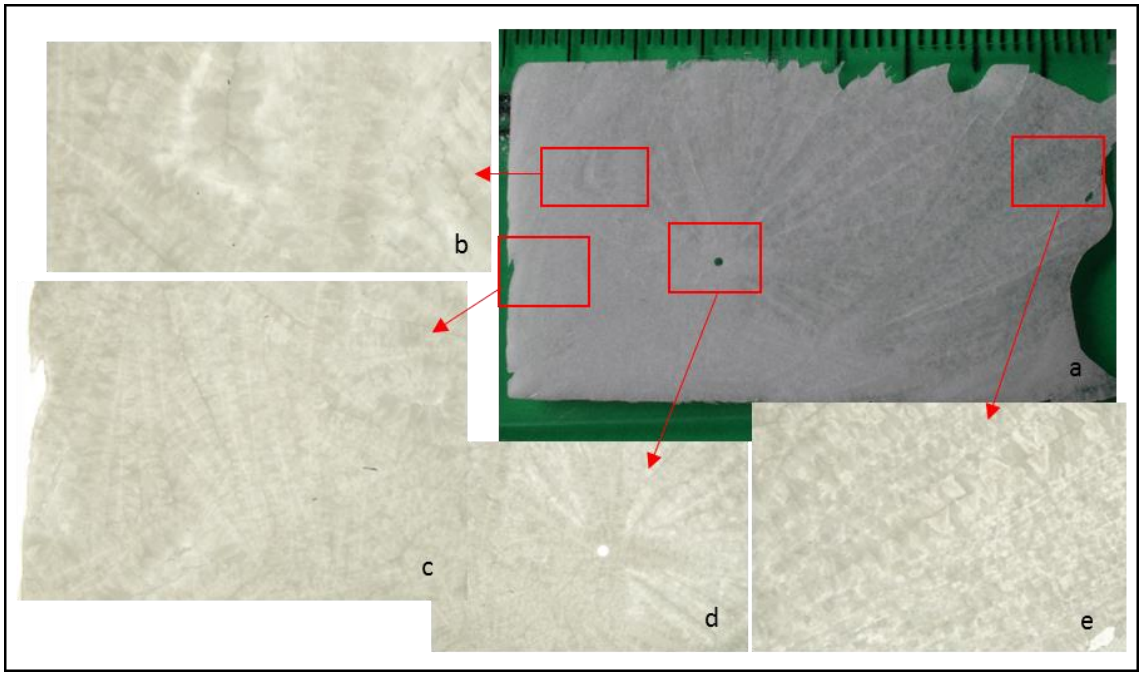

Figure 4. 16 Sample 3 produced by solidification taking place isothermally at 80 °C. Macrograph of the whole sample and micrographs showing the different zones that display details of the produced structures

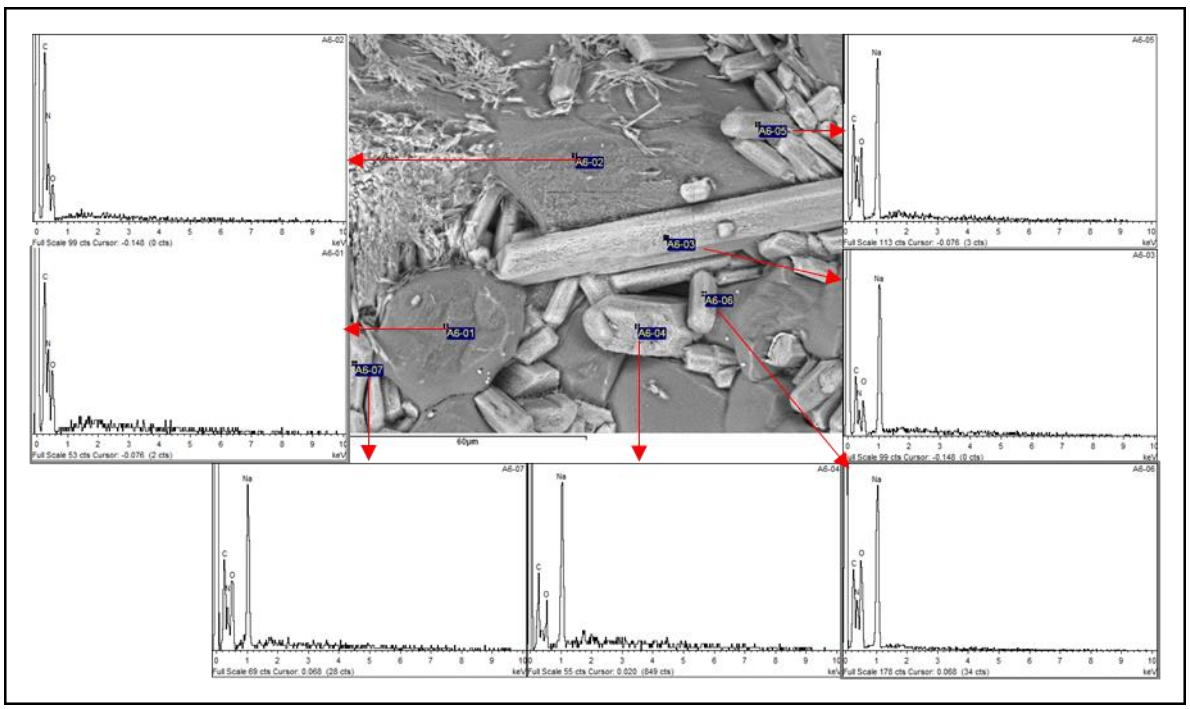

Figure 4. 17 EDX identification of elements present in different crystal formations

In the present case, Urea is formed by H, C, N and O while Sodium nitrate is composed of N, O and Na. The Sodium Nitrate grains render bright light-grey images while the Urea crystals correspond to the dark-grey features. In any case, for the aim of confidently identifying the

composition of the different microstructural features, EDX spectra of selected crystals were also carried out. Figure 4. 17 shows a micrograph of sample 3 together with the EDX spectrum of the different crystal formations observed in it. The EDX peaks corresponding to the darker crystals in the image indicate the presence of Carbon, Oxygen and Nitrogen which match with the urea ($CO(NH_2)_2$) elemental constituents. The EDX spectrum of the lighter crystals indicates Sodium, Carbon, Oxygen and Nitrogen peaks, which corresponds to Sodium nitrate ($NaNO_3$). However it also shows Carbon, which may be caused by the Carbon coating onto the samples.

Figure 4. 18 allows to take a closer look of the macrostructures previously identified in the PLM micrographs. Figure 4. 19 shows further magnifications of the images in Figure 4. 18. Four different microstructural features (habits) can be distinguished, which have been identified in Figure 4. 19 with the numbers 1 to 4: large columns, acicular/fibrous crystal clusters, prismatic crystals and drusy conglomerates.

Columnar crystals are stout long prisms with a column-like appearance. A single column might contain multiple parallel crystals. Acicular crystals have a needle-like shape that tapers to a point or a blunt termination. Their length is much greater than its width or diameter. Many acicular crystals can be clustered to produce fan-shaped or radially-shaped aggregates. Fibrous crystals are very fine sinew, string, or hair-like fibers. The habit also includes aggregates made up of a large number of parallel or radial fibers. Prismatic are well-developed elongated crystals with opposite faces normally parallel to one another. The crystals are often striated along their length or across their width. Then columnar, acicular, fibrous, and prismatic can resemble the same slender shape, however fibrous is the thinner, followed by acicular, then the prismatic and the thicker is columnar (also longer). Finally, the drusy habit describes an aggregate of minute crystals coating a surface or cavity.

Dark-grey large columns or prismatic crystals (identified in Figure 4. 19 with the number 1) of different sizes were observed in all the samples. They are made of Urea and can be considered the main crystallization habit for Urea. The fact that the samples were purposefully produced as a thin layer lead to observe long columnar crystals grown horizontally, and small prismatic crystals growing perpendicular to the sample holder direction. These great crystal columns are thought to be caused by the non-reciprocal nucleation behavior observed during the nucleation and crystal growth assessment test, were isothermal crystallization conditions at 82 °C were imposed. Large acicular crystals formed in the first place, and the remaining space was latter on filled in with smaller crystal formations that should be of the eutectic type. This behavior resembles hypoeutectic crystallization, and is a reported cause of semi-congruent melting, i.e. phase segregation [115], [123].

Then, the conglomerate crystals that grow in between of the urea columns should correspond to the eutectic structures. This is thought to be the clear-grey acicular/fibrous crystal clusters (identified in Figure 4. 19 as 2) can be seen in all the samples. The EDX tests confirmed they contain Sodium. However, this crystal clusters formations are different in samples 1, 2 and 3.

Figure 4. 20 gathers some images of the acicular/fibrous crystal clusters, taken in each sample. The clusters in sample 1 are composed of urea matrix and Sodium nitrate precipitated small crystals, which resemble a eutectic intimate mix. Samples 2 and 3 show fibers of different sizes.

It is thought that the fibers in sample 2 may be a metastable phase containing both urea and Sodium nitrate produced due to rapid solidification, and if they were able to diffuse the result would be precipitated Sodium nitrate in a urea matrix as in sample 1.

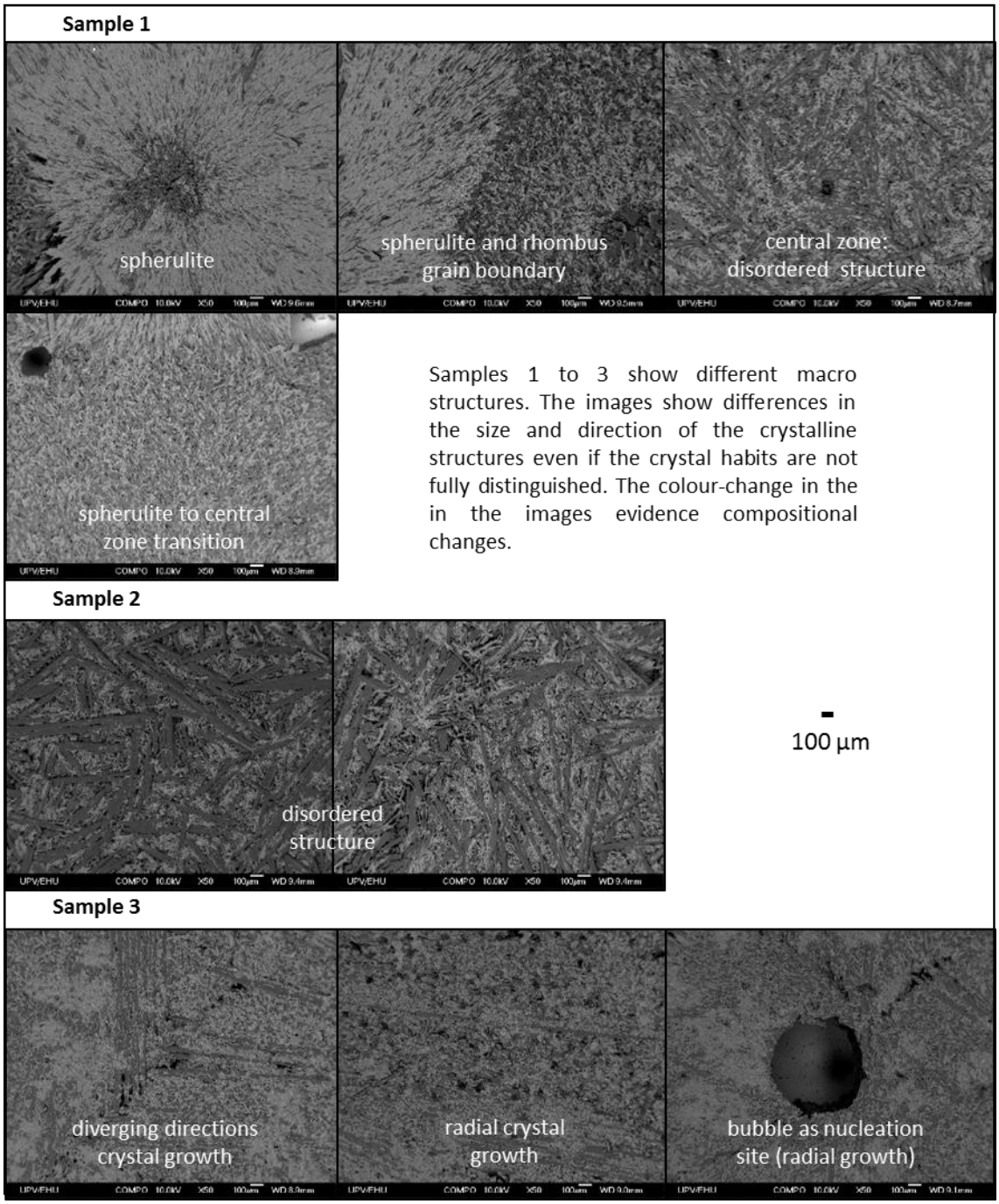

Figure 4. 18 Micrographs of the macrostructures previously identified in the PLM micrographs

Besides, it was observed during the SEM imaging that these formations where modified by the electron beam at high magnification, and it could be clearly seen that the lighter grey material (Sodium nitrate) precipitated into the urea matrix. Since the melting temperature of the material is very low, the electron beam energy, when focused on a tiny area, is high enough to produce diffusion and formation of the stable phases. Indeed, local melting was observed in some points.

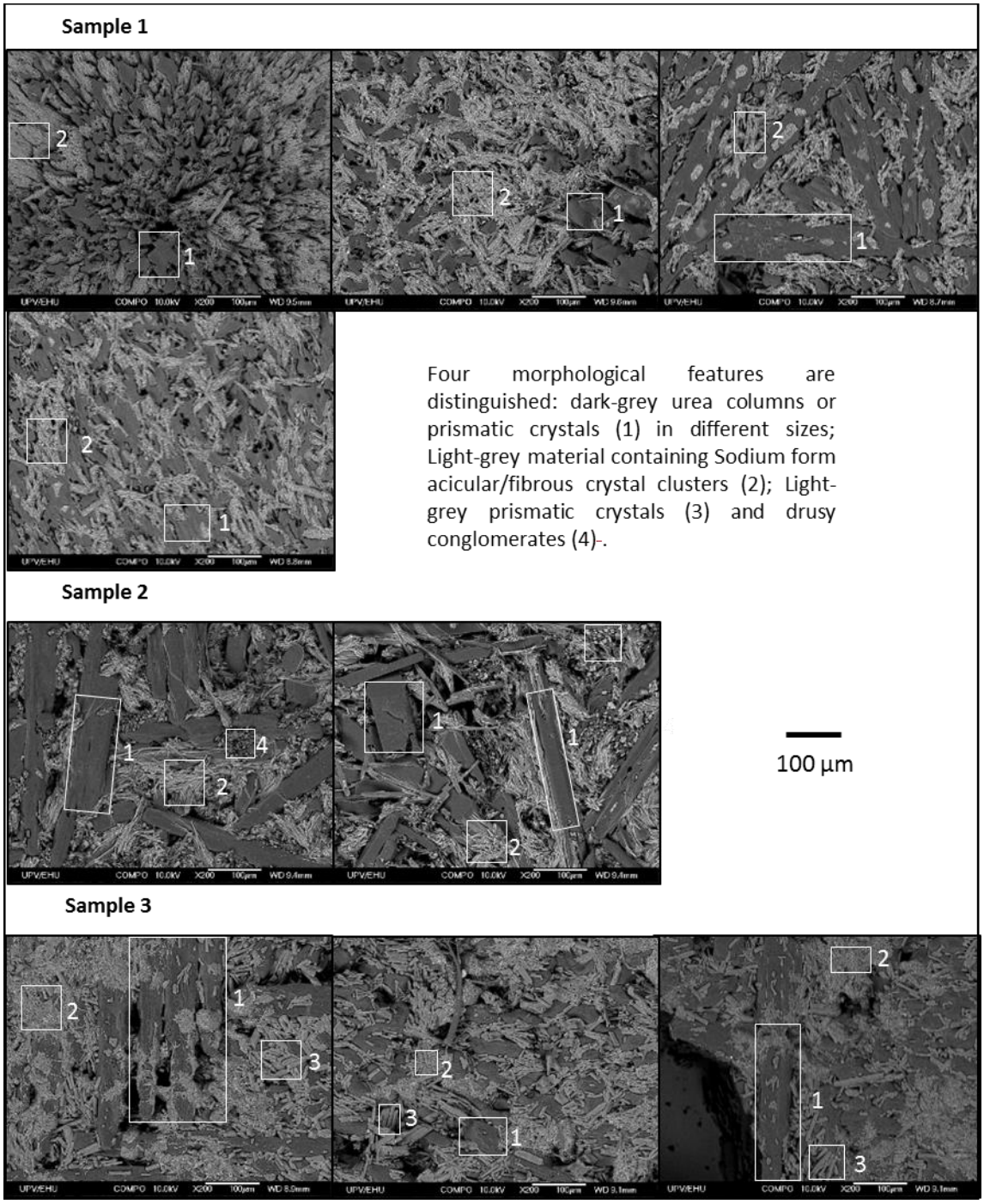

Figure 4. 19 Micrographs displaying the four identified morphological features in samples 1, 2 and 3

The metastable formation in rapid solidification is in agreement to Galenko et al [121] work, who determined that rapid solidification of eutectic systems can suppress the eutectic formation and instead produce a homogeneous metastable phase formed by the initial chemical composition (the composition of the liquid phase). Besides, Bevan Ott et al. [122] state that the cause of metastable solids formation in eutectic systems is the supercooling (that have been determined greater in faster cooling rates during the cycling tests). The appearance of this metastable phase in the U-SN eutectic mixture would be in agreement to the results of Chapter 3, in which the XRD results show the existence of one or more metastable phases that disappear by thermal treatment. However, the reason of the appearance of these phases was not apprehended in the study in Chapter 5, with the present study it can be concluded that it depends on the cooling conditions (which in previous studies were not completely controlled).

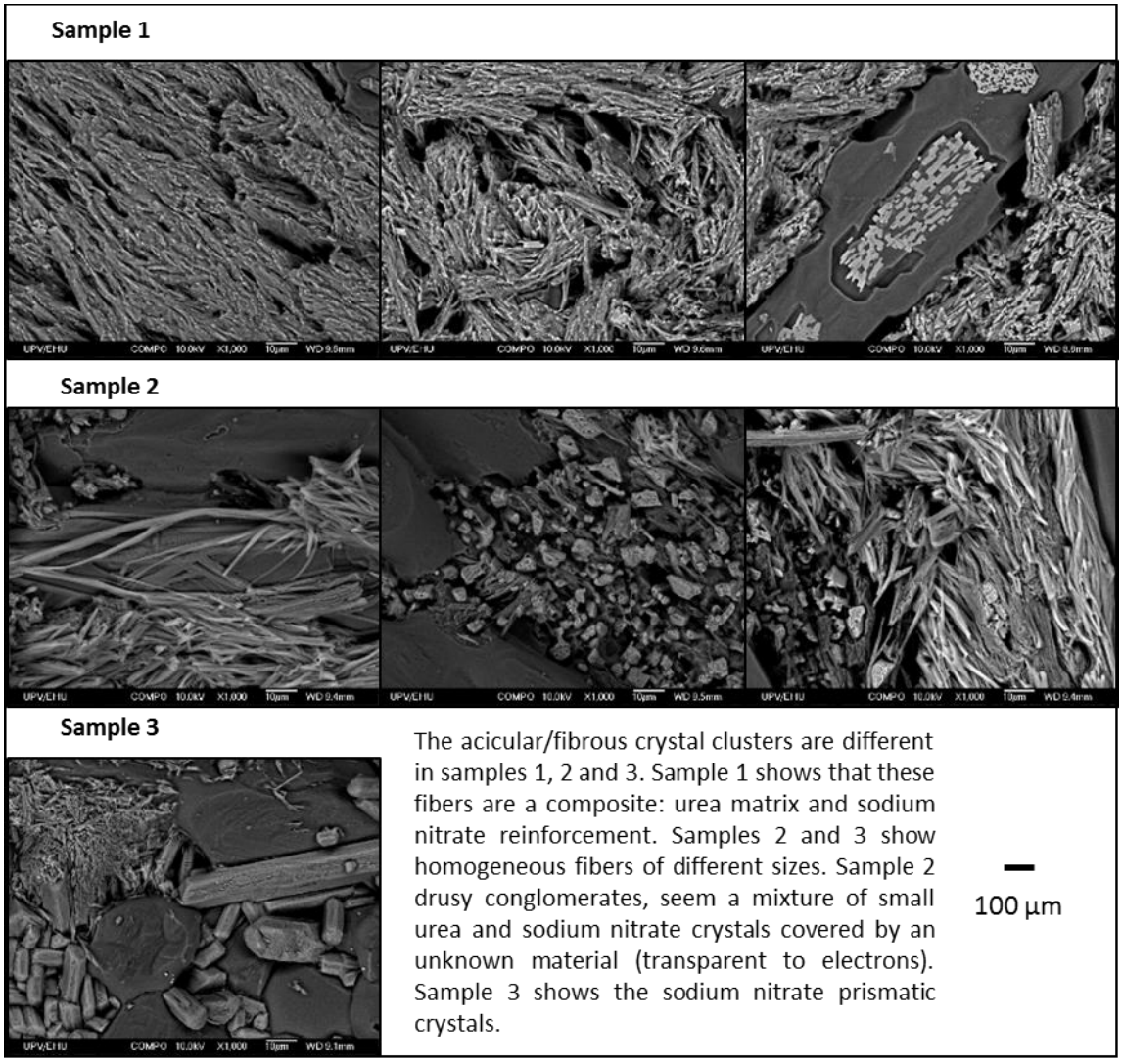

Figure 4. 20 Micrographs showing in detail the acicular/fibrous crystal clusters, drusy precipitates and prismatic crystals on sample 1, 2 and 3

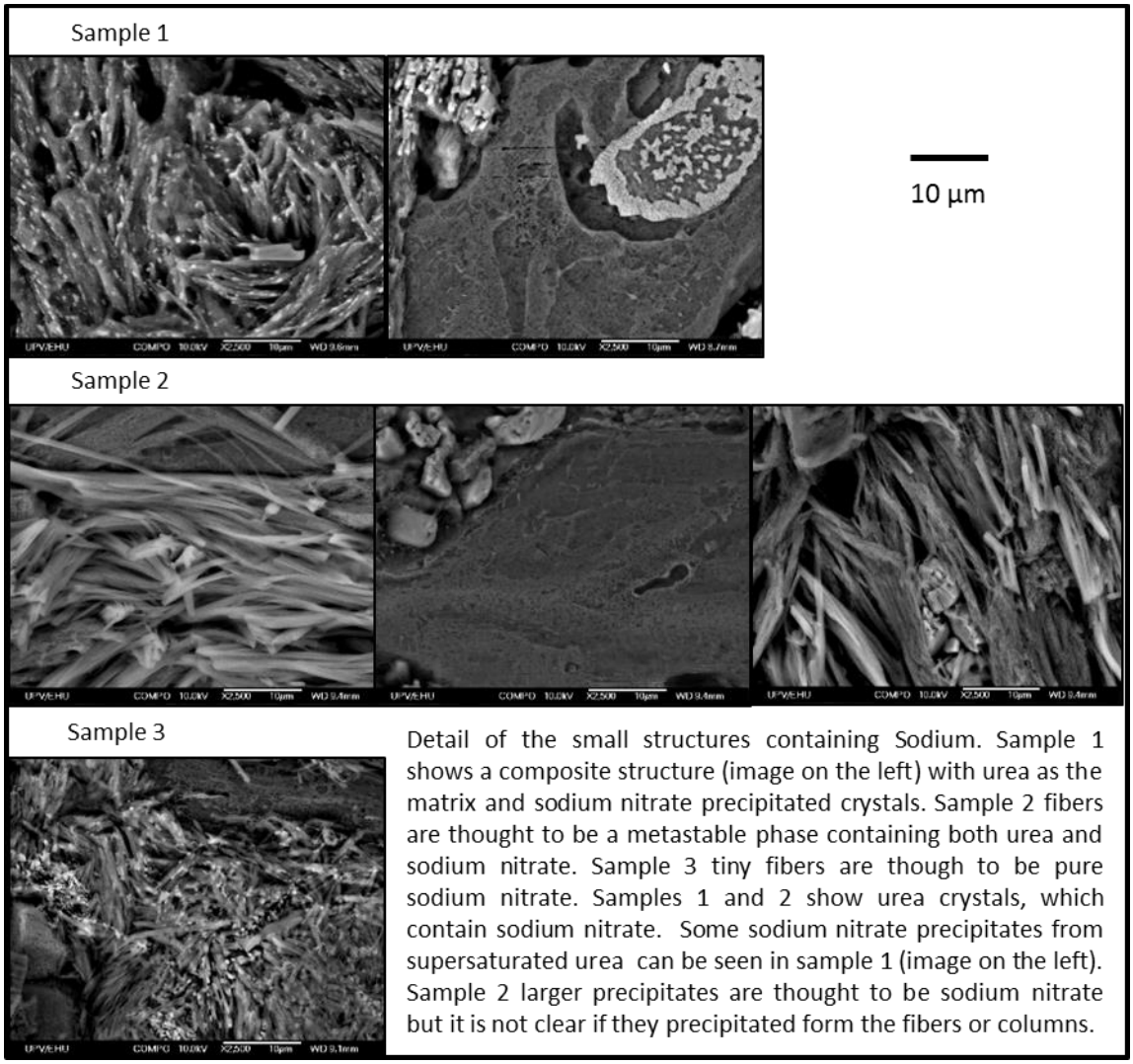

Figure 4. 21 Micrographs of the smaller crystals containing Sodium in samples 1, 2 and 3

The very small fibers containing Sodium in sample 3 pose the same morphology (not size) that those in sample 2, however, are not likely to correspond to a metastable phase, due the close to equilibrium conditions of the sample. They are more likely to be eutectic.

Light colored prismatic crystals (identified in Figure 4. 19 as 3) are only present in sample 3. They correspond to Sodium Nitrate. This sample was produced with extremely slow solidification rate, which is in agreement with the growth of large crystals, not obtained in normal cooling rates. A larger magnification of the crystals is included in Figure 4. 21. They appear most commonly in clusters between the huge urea columns. Moreover, due to the great size of the crystals the differentiated zones pose composition heterogeneity, and is assumable that during melting phase segregation is produced.

From the SEM images it can be derived that the mixture crystallizes in the form of single crystals that grow independent from each other, sometimes even voids exist between them. It implies that the crystallization of each phase is not coupled or cooperative, but divorced. According to the interface morphology classification [108] the two components in the eutectic mixtures have

non-dimensional entropies greater than 2 (equations 4.1 and 4.2), which correspond to f-f typology (which show irregular divorced eutectics).

$$\frac{\Delta S_{f.urea}}{R} = \frac{35.85 \frac{J}{mol.K}}{8.3 \frac{J}{mol.K}} = 4.32 > 2\ (faceted) \qquad (4.1)$$

$$\frac{\Delta S_{f.sodium\ nitrate}}{R} = \frac{26.87 \frac{J}{mol.K}}{8.3 \frac{J}{mol.K}} = 3.23 > 2\ (faceted) \qquad (4.2)$$

This type of crystal growth makes that the urea and Sodium nitrate crystals do not grow forming an intimate mixture any more. In addition to this, the distance between larger urea crystals formed because of the non-reciprocal nucleation and the microconstituents of Sodium nitrate makes that the melting does not completely occur as a eutectic. This causes the segregation to take place during fusion. The crystals that remain unmolten (because the mixture compounds are not in intimate contact) are subsequently segregated. Figure 4. 22 shows a picture of a sample during the melting at 95 °C, it can be seen that there are solid particles in suspension in the liquid, and segregates on the top and bottom of the liquid.

Figure 4. 22 U-SN sample after the melting process, showing solids in suspension, and segregated on top and bottom of the sample

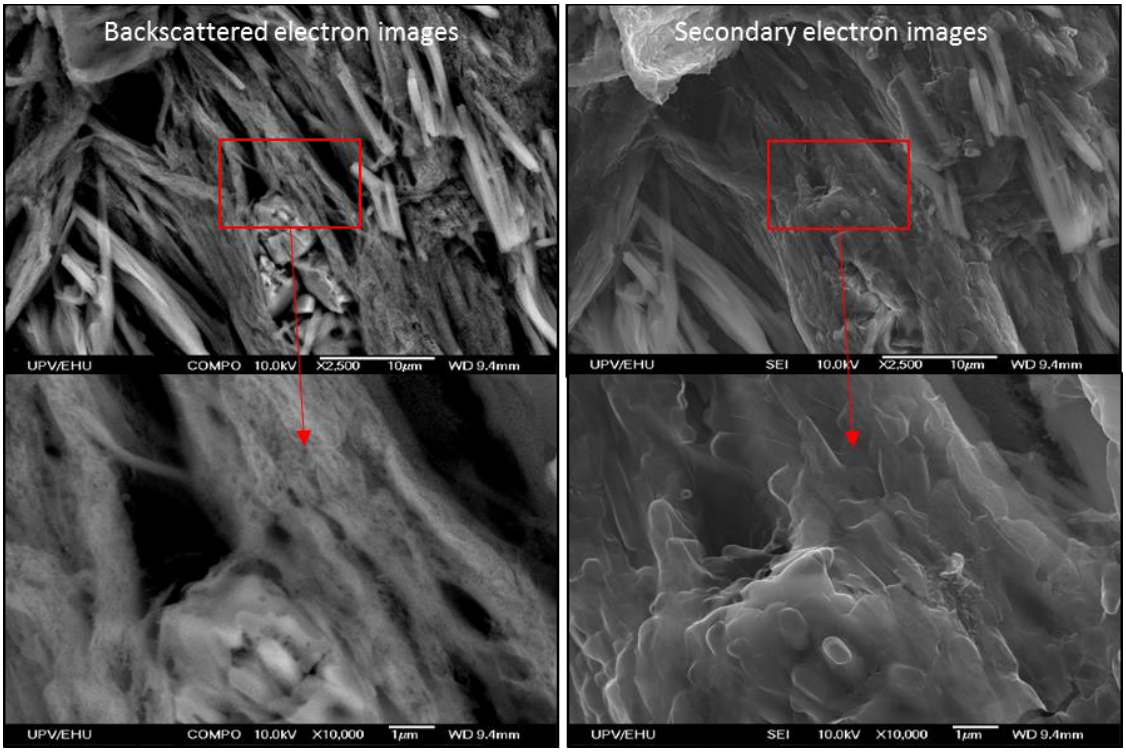

Figure 4. 23 Micrographs of sample 2 showing drusy conglomerate precipitates from the fibrous structures. The precipitates can be observed in the backscattered electron micrograph in the right, and the topography of the covering material (transparent to backscattered electrons) is shown in secondary electron image in the left

Figure 4. 23Figure 4. 21 shows some details of the Sodium nitrate precipitated into urea crystals, presumably from metastable phases or from supersaturated urea. Drusy crystal conglomerates (identified in Figure 4. 19 as 4) are only present in sample 2. They are formed by a mixture of small urea and Sodium nitrate crystals gathered and/or covered by a material which could not be identified by the backscattered electrons because it is transparent to them as shown in Figure 4. 23 (extremely light material, some polymers and hydrocarbons often present this behavior). Besides, it can not be discarded to be glassy material, that has not crystallized due to the fast cooling rate. The small Sodium Nitrate crystals observed in these images might have also been produced while the electron beam swept the sample at high magnification.

4.4 CONCLUSIONS

It was determined that the phase segregation of the U-SN eutectic varies depending on the microstructure, attained with different cooling rates during solidification upon cycling. Higher cooling rates showed less phase segregation than slower cooling rates. However, slower cooling rates are closer to the equilibrium and it might be assumed that in conditions closer to equilibrium the phase segregation would be diminished, however it is not the case. This behavior can be explained by the microstructure morphology.

The U-SN eutectic is faceted/faceted type, which implies that the urea and Sodium nitrate phases do not crystallize in a cooperative way, but separately. In addition, non-reciprocal nucleation was observed, the primary urea phase crystallization does not promote the

crystallization of the Sodium nitrate, resulting in coarser urea crystals and a crystallization similar to that foreseen in hypoeutectic compositions.

As a result of the non-reciprocal nucleation, the Sodium nitrate poses higher supercooling degree than urea. However, in the monitored samples only one peak was identified, in disagreement with Benicio et al. [115]. There is not a conclusive explanation to this finding, which could be due to a supercooling degree difference too small to be experimentally determined.

The hypothesis of a small difference on the supercooling degree between the two obtained phases can be backed with fact that, under normal cooling rates the microstructure forms in with large urea primary crystals and a homogeneous metastable phase, instead of forming the Sodium Nitrate eutectic microconstituent, as indicated by the SEM micrographs and EDX measurements. According to the observations carried out in the SEM, this metastable phase is deemed to be supersaturated urea, from which the Sodium nitrate crystals precipitated by diffusion when the temperature is high enough to promote it. In fact, the Sodium Nitrate precipitation took place during the SEM observation when the electrons-beam intensity was high. Even though the thermal properties of the metastable supersaturated urea could not be assessed, it can be foreseen a supercooling degree close to that of the U-SN mixture. On heating, previous to the melting the formation of Sodium nitrate will take place due to diffusion, which takes place at the eutectic temperature.

As a result of the crystallization habits in these eutectic types, segregation can be foreseen. In the case of the U-SN eutectic mixture, XRD assessment confirmed that urea crystals rose to the uppermost part of the thermally cycled samples due to its density being lighter than the liquid eutectic density, and the heavy Sodium nitrate crystals fell down to the bottom. Smaller crystals were obtained when samples were quenched, resulting in more homogeneous microstructures, opposite to the higher size crystals produced at slower cooling rates, which could be seen by visual recognition. Literature supports that higher crystal size results in higher phase segregation.

Natural convection is not likely to determine the phase segregation occurrence, however it serves as a mechanism by which the segregated mixture separates because of the density difference. The cycling tests with the sample in horizontal and vertical arrangements yielded similar results in terms of the amount segregated for both arrangements. Therefore, it served to certify that natural convection does not play an important role in the phase segregation taking place on the studied samples. However, it cannot be discarded that its role may be significant in higher volumes.

It was confirmed that the segregated samples can be recombined by melting and mixing aided with mechanical stirring or with other stirring means. The mixture thermal properties are similar to a fresh non-cycled eutectic mixture and, therefore the utilization as a PCM is feasible after the segregate is re-mixed. Furthermore, XRD diffraction confirmed that the phases present were urea and Sodium nitrate in the eutectic proportion.

It is concluded, the phase segregation of U-SN eutectic could be reduced by using fast cooling rates for the discharging process, although the possibilities for complete prevention seem unfeasible. However, the material potential-use after segregation is possible if a suitable stirring means is implemented in the system.

Chapter 5 : Supercooling characterization and modelling

5.1 INTRODUCTION

Supercooling is a feature posed by many PCM candidate materials [67]. The phenomenon occurs when the molten material is cooled down and does not crystallize at the melting temperature (liquid-solid equilibrium temperature), but at a lower temperature. The difference between the melting temperature and the actual crystallization temperature is called supercooling or undercooling. Supercooling occurs in most crystalline solids and especially, in highly crystalline solids. The supercooled solidification temperature is deemed to be stochastic, making actual crystallization temperature difficult to predict. In most TES systems, supercooling is an undesirable phenomenon, although some applications use it advantageously. In these cases, a triggering device which promotes nucleation on demand, is designed and implemented [125]–[127].

Organic PCM have been traditionally deemed as supercooling-free materials, while inorganic materials generally present important supercooling [4], [50], [128]–[130]. Inorganic materials, such as salt hydrates and salt mixtures, can exhibit supercooling degrees up to 100 °C [41], [42], [131]. In the case of organic materials, paraffins have little or no supercooling in bulk volumes, whilst fatty acids present a supercooling degree inferior to 5 °C [35], low enough to discard the need of any crystallization-triggering method in most potential thermal storage applications. However, supercooling is a significant problem in microencapsulated paraffins [132]–[134] and also in most sugar alcohols, which in addition to a large supercooling exhibit very slow crystal grow rates [37], [39]. These materials have very high viscosity which increases while the temperature decreases, leading in many cases to the formation of glassy solids instead of crystallization. It is worthwhile to mention that the existing literature on PCM supercooling is mostly devoted to determine and develop methods to avoid it, like the use of nucleating agents, cold finger devices, ultrasounds, stirring, mechanical shock, bubbling, electric and magnetic fields [135]–[138], with much less attention to the study of mechanisms and variables-related features.

Safari et al. [138] stated that the factors influencing the supercooling degree have not yet been clarified in the literature ,as a result there is not presently a standardized, or widely accepted, protocole to select a specific additive or a methodology to reduce the supercooling degree of a material. A material-supercooling degree depends on the experimental conditions, being the most important ones: the sample mass or volume, which is linked to the stochastic nature of the homogeneous nucleation mechanism (the higher volumes, the higher the probability to produce stable nuclei, the lower the supercooling); the presence of impurities and rough surfaces, which lead to the possibility of heterogeneous nucleation; and the cooling rate. These three factors are thought to influence the lag between the temperature for crystallization and the melting temperature. However, it is not known to what extent these parameters influence each material, and there are no set methodologies for the supercooling assessment or for the prediction of the supercooling degrees, which relate to technical parameters to be used in a defined application.

The main objective of the present study is to contribute to the clarification of the factors influencing supercooling from an application-related point of view. Thus, in addition to the above mentioned variables, mass (volume) and cooling rate, several application-related potential variables have also been taken into consideration, like the PCM container geometry, the heat transfer regime, and the material thermal properties. For that aim, a study comprising two different PCM has been carried out. The first PCM is the U-SN eutectic (71.25 wt% urea and 21.75 wt% Sodium nitrate) and the second PCM is polyethylene glycol 10000. The experiments included testing samples ranging from 7 mg to 0.45 kg, in containers of different geometries (cylinders, and boxes), submitted to different cooling rates, from very slow (0.3 °C/min) to very fast (up to 4600 °C/min), using different cooling media (air and thermal oil). A statistical analysis of the results was made to stablish which parameters are more relevant in the crystallization process and finally, propose linear regression models that include the most relevant parameters.

5.2 THEORETICAL BACKGROUND

The existing theories on homogenous and heterogeneous nucleation try to explain the supercooling phenomenon exhibited on crystallization on a physical basis, taking into account the thermodynamics of the crystal formation from the molten material according to the site at which nucleating events occur. In the homogeneous nucleation, the solid phase nuclei form uniformly throughout the liquid phase, whereas in the heterogeneous nucleation, nuclei form preferentially at structural heterogeneities, such as container surfaces, insoluble impurities, grain boundaries, dislocations, etc. These are microscopic or nanoscale considerations, since the crystallization starts from an initial nucleus or cluster that is formed by a small number of atoms or molecules. The distinction between both types of nucleation is explained in more detail in the following paragraphs according to the literature on the topic [56], [139]–[141].

5.2.1. HOMOGENEOUS NUCLEATION

Homogeneous nucleation refers to the primary nucleation that occurs spontaneously from a supercooled liquid in a system free of any crystalline nucleus. Thus, the new phase is formed when an embryo grows and reaches a certain critical size to become stable. Below this critical size the embryos are extremely unstable and redissolve. Even though the shape of these primal seeds is unknown, it is assumed that each nucleus is spherical and has a radius *r*. In addition, the molecules forming the new crystal have to become oriented into a fixed lattice contributing to the complexity of the process.

The solidification process can be analyzed through the Gibbs free energy (ΔG), which is made up of two terms. The first one corresponds to the free energy change due to the atomic aggregation to form a solid nucleus of a certain volume. When the temperature (at one point) is lower than the melting temperature, this free energy presents a negative value. The second term is associated to the liquid-solid boundary or surface free energy, which is always positive. The larger the surface, the larger the free energy. According to equation 5.1, due to the opposite increment of both terms in the equation, and to the fact that they depend differently on the radius, ΔG increases to reach a maximum and then decreases as shown in Figure 5. 1.

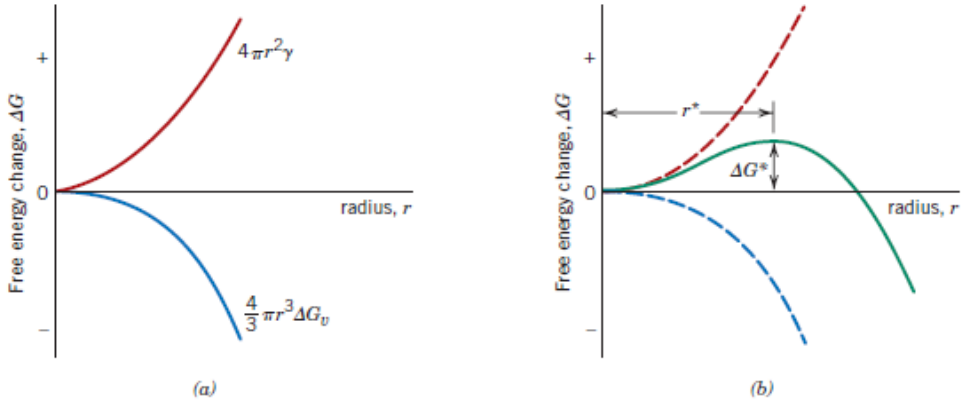

Figure 5. 1 a) Schematic curves for volume free energy and surface free energy contributions to the total free energy change attending to the formation of a spherical nucleus during solidification. b) Schematic plot of the free energy versus the nucleus radius, presenting the critical free energy change (ΔG) and the critical nucleus radius (r*)*[51]

As the ΔG value decreases the nuclei total surface increases. Only when the free energy change reaches a negative value the phase transformation will occur spontaneously. When the radius of the embryo increases up to *r**, a critical radius has been reached (equation 5.2), which corresponds to the maximum ΔG value (equation5. 3). Once the nucleus reaches *r**, any further increment will decrease the free energy change, and therefore radius grow will continue leading to a spontaneous decrease of the free energy. Those embryos with radius smaller than the *r** will strive to grow or to shrink and dissolve.

$$\Delta G = \frac{4}{3}\pi r^3 \Delta G_v + 4\pi r^2\gamma \qquad (5.1)$$

$$r^* = -\frac{2\gamma}{\Delta G_v} \qquad (5.2)$$

$$\Delta G^* = -\frac{16\pi\gamma^3}{3(\Delta G_v)^2} \qquad (5.3)$$

It is very difficult to achieve the formation of the critical nucleus in equilibrium conditions. Most embryos do not manage to reach the critical size but rather redissolve, thus not achieving crystallization at the melting temperature. In other words, the decrease of the first term on equation 1, more precisely the volume free energy ΔG_v corresponding to equation 4, is the driving force for the solidification process. The lower the temperature of the system below the melting temperature, T_m, the easier the nucleation will occur.

$$\Delta G_v = \frac{\Delta H_f (T_m - T)}{T_m} \qquad (5.4)$$

However, it has to be considered that in real systems embryos may not follow a spherical shape leading to a more complex behavior. Besides, on the macroscopic systems under real conditions, the energy level is not generally homogeneous all over the volume. In turn, there will be a statistical distribution of molecular kinetic energy within the system. In supersaturated regions, where the energy level temporarily rises to a high value, nucleation will be favored. For this reason, the homogenous nucleation is said to be a stochastic phenomenon, dependent of the volume/mass, because the smaller the volume the smaller the probability to have nucleation embryos that grow to be stable nucleus. Considering all this, the high volume involved in the real processes make the nucleation to be affected by other variables not conveniently considered by the classical thermodynamics, like those which influence the temperature distribution (thermal gradients) in the macro scale samples.

5.2.2. HETEROGENEOUS NUCLEATION

For a homogeneous nucleation to take place, the material should be free of any surface in contact with the liquid that may act as a nucleus. The presence of impurities, foreign bodies, pre-existing crystals within the system or even the container superficial roughness can affect the nucleation. As there is no general rule that explains this, each case (every material) should be analyzed independently.

The presence of suitable foreign bodies or "sympathetic" surface can induce nucleation at supercooling degrees lower than those required for the spontaneous nucleation. The overall free energy associated with the formation of a critical nucleus under heterogeneous conditions ΔG^*, is of an inferior value than the associated with homogeneous nucleation. The particle size and the interfacial tension are important factors for the heterogeneous nucleation process. It can occur by seeding from embryos retained in cavities, e.g. in foreign bodies or the walls of the retaining vessel, under conditions in which the embryos would normally be unstable on a flat surface. Therefore, for the supercooling characterization, the fact that there is an uncertainty regarding the existence of foreign bodies within the melt which are able to produce the material crystallization, hampers the assessment of the crystallization mechanism occurred in testing. In any case, the larger the volume the larger the probability for external nucleus to exist.

The heterogeneous nucleation is purposefully used in metallurgy to produce small grain size alloys by seeding the molten alloy with a large amount of exogenous nuclei. Seeding, using adequate nucleating agents, is also a method to reduce the supercooling degree of a material, to get crystallization temperatures closer to the melting temperatures. Thus, the published research about PCM supercooling is mostly devoted to developing methods to avoid or reduce it in different materials, instead of designing the studies to attain a deeper knowledge on the parameters that influence the phenomenon.

5.3 DESCRIPTION OF THE EXPERIMENTAL APPROACH

In spite of the apparently highly stochastic nucleation that might be initially foreseen on the PCM related applications, from the original premises it can be deduced that in real applications the sample volume will be large enough to conclude that some exogenous nucleus will be

present in most cases (a gas bubble, a rough surface, a trapped impurity or an entrapped crystal seed, etc). The exogenous nucleus undetermined-nature could be partly responsible for the unpredictable supercooling reported in PCM. However, the claimed unpredictability could be partly due to the system heterogeneous temperature distribution. The temperature distribution is highly dependent on the system geometry and the external cooling conditions. Besides, different PCM materials may have a different nucleation response because of their different characteristics. Studying the influence of these parameters in the supercooling degree lead to a practical/technical approach of the supercooling characterization. As a result, an experimental campaign was designed to assess the influence of several process-related parameters on the crystallization temperature with the aim to get knowledge about the extent they could have on the supercooling degree and to help in predicting the nucleation behavior of a material. Table 5. 1 gathers the parameters involved in the performed study.

Table 5. 1 Description of the parameters involved in the experimental study

Study parameters	Independent variables	Designation	Units
Volume	Mass	*m*	kg
	Characteristic length	*Lc*	m
Cooling media	Cooling rate	*v*	°C/min
	Heat transfer coefficient	*h*	W/K.m^2
PCM	Thermal conductivity	*k*	W/K.m
	Thermal diffusivity	*α*	m^2/s

The following independent variables where considered: The sample mass (*m*), which represents the sample volume, but remains unaffected by the temperature changes; The characteristic length (*Lc*) or volume/surface ratio, as a measurement of the geometry (linked with the volume, but includes information about the disposition); The cooling rate (*v*) or the velocity at which the cooling media lowers the PCM temperature; The heat transfer coefficient (*h*) which describes the external cooling flow regime; The PCM thermal conductivity (*k*) and thermal diffusivity (*α*), as the thermal properties of the material that govern the heat transfer through it.

In order to evaluate the influence of the described variables, the study comprised the use of five different container configurations (different mass and characteristic length), two heating/cooling media (different heat transfer coefficients), several different cooling rates, and two different PCM materials. All the experiments began heating up the PCM samples above the melting temperature to ensure the full melting. Then the samples were cooled-down upon different experimental conditions to reproduce different cooling rates.

5.3.1. Materials used: urea and Sodium nitrate eutectic mixture and polyethylene glycol 10000

Two materials were studied: the urea and Sodium nitrate eutectic mixture (71.25 wt% urea and 21.75 wt% Sodium nitrate) and Polyethylene glycol 10000. Pure urea, Sodium nitrate and polyethylene glycol (>99% purity) were purchased from Sigma-Aldrich.

The urea and Sodium nitrate eutectic mixture, hereinafter called by the name U-SN eutectic, shows a melting temperature of 85 °C and the melting enthalpy of 172 J/g. The phase diagram, the main thermophysical properties, and the characterization of the mixture main physical properties can be consulted in previously published articles [62], [63]. A preliminary supercooling assessment was also performed using differential scanning calorimetry, DSC, to evaluate supercooling dependency on the cooling rate using 10 mg samples. The study submitted samples to subsequent cooling ramps at 0.5, 2, 4 and 8 °C/min. The study concluded that there was not a clear correlation between the cooling rate and the supercooling. Only the measurements performed at 8 K/min showed a clear tendency towards higher supercooling, as expected because of the faster cooling rate. For lower cooling rates, it was only possible to state that all samples crystallized between 70 °C and 30 °C. The minimum supercooling degree observed was 15 °C.

Polyethylene glycol 10000, hereinafter called by the name PEG 10000, melts at 58 °C (though the manufacturer reports 62-65 °C) and has a latent enthalpy of 175 J/g (both experimentally determined by DSC). The selection for this material was prompted by the need to have a pure material, not a mixture, with a melting temperature on the application temperature-range. Mixtures could pose phase segregation and a complex two-phase crystallization behavior and since the U-SN eutectic was already such a complex material, a pure material was selected to ease the analysis. Most pure materials posing a melting temperature between 50-90 °C show very limited supercooling degree, , however, polyethylene glycol 10000 was selected because according to several authors [142]–[144] it exhibited a supercooling degree up to 20 °C.

5.3.2. CONTAINERS

5 container typologies were employed in the study, as it can be seen in Table 5. 2, which include: Mettler Toledo DSC crucibles, modified Ace Pressure tubes, self-manufactured Copper tubes and rectangular aluminum boxes. For the sake of brevity in the latter discussion, they are referenced as DSC, GD0, CuD1, CuD2, and RB respectively.

The DSC crucibles are 25 µl (very small) containers used to analyze samples in the DSC. They are closed by a lid which is sealed using a press. Ace pressure tubes are 8ml containers made of glass and closed by a threaded Teflon plug. The Copper tubes consist in two different diameters tubes. They were home-made by cutting a Copper tube to the desired length, welded to a Copper cap on the bottom and close at the upper end using a rubber plug. The rectangular aluminum boxes were home-made of commercial rectangular aluminum profiles, cut to the desired length, and the lids were welded to close the container. To carry out some of the experiments with very slow cooling rates, the containers were insulated using 2 cm width EPDM foam.

Table 5. 1Table 5. 2 summarizes the container characteristics and internal dimensions (to be filled in with the PCM). The last column, *Lc* [m] indicates the characteristic length parameter, which is the result of the volume divided by the surface of the sample geometry.

A thermocouple was placed inside all the containers (except the DSC crucibles), to be in contact with the contained PCM. Thermocouples were placed in the cylinder at 0.065 m from the bottom. In the case of the rectangular box, the thermocouple was introduced using stainless

steal fittings added to the openings on the upper lid at 0.03 m distance from lateral end and at 0.01 m distance from both large walls, to reach a depth of 0.06 m.

Table 5. 2 ***PCM container characteristics and dimensions***

Container ref.	Container Shape	Container Material	PCM Mass (kg)	PCM Dimensions [m]				*Lc* [m]
				Height	Radius	Width	Depth	
DSC	round box	Aluminum	$7\ 10^{-6}$	0.001	0.00125	-	-	0.001
GD0	cylinder D0	Glass	$4.5\ 10^{-3}$	0.04	0.002	-	-	0.0079
CuD1	cylinder D1	Copper	0.037	0.13	0.008	-	-	0.0038
CuD2	cylinder D2	Copper	0.178	0.13	0.0175	-	-	0.0082
RB	rectangular box	Aluminum	0.45	0.12	-	0.2	0.02	0.00097

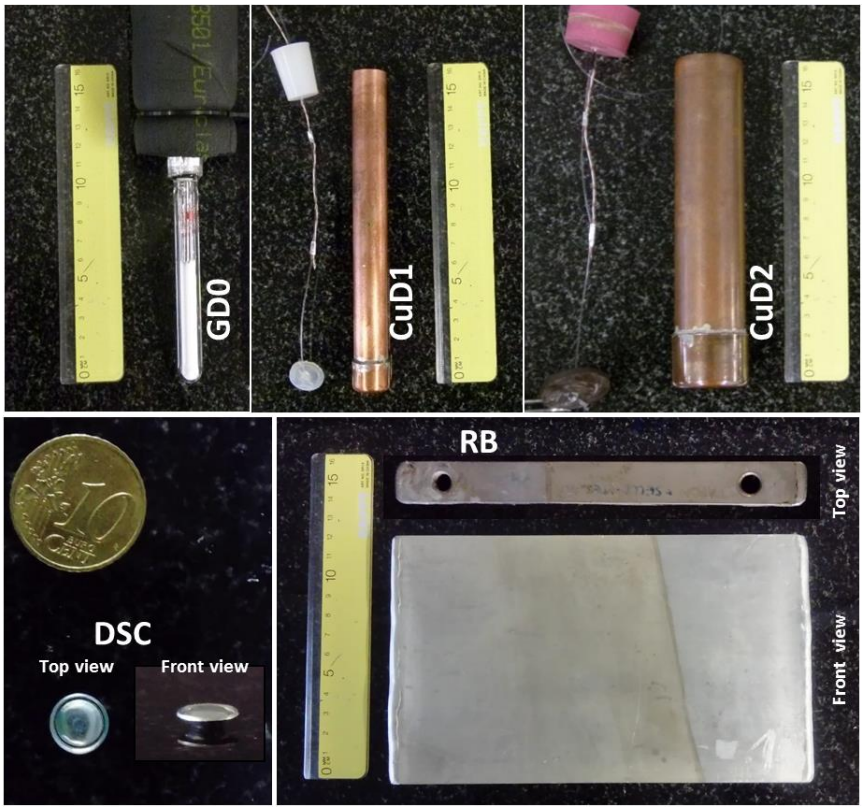

Figure 5. 2 PCM containers used in the supercooling characterization tests. The coin and the ruler (scale in cm) were placed beside each container to an idea of their size

5.3.3. COOLING CONDITIONS

Three different cooling conditions were defined, from now on called: quenching cooling, programmed cooling and insulated free cooling. For the sake of brevity in the latter exposition of the experiments performed, they are referred as Q, P and FC respectively. Experimental types induce different cooling rates and heat transfer coefficients. The cooling rates were

consequence of the experimental type. The heat transfer coefficients depend on the HTF itself and the stirring of the fluid, which was controlled by different intensities of the bomb in the thermostatic bath, and the use of fan inside the climatic chamber. Table 5. 3 describes the main characteristics of the equipment where the experiments were carried out. All experimental types were performed using the U-SN eutectic. However only programmed cooling experiments were performed with PEG 10000, with different stirring configurations one of the objectives of these experiments was to determine the relevance of the different heat transfer coefficients on the supercooling.

Quenching, Q, consisted on melting and heating the PCM to a predefined temperature (100 and 95 °C) and suddenly introducing it into a thermostatic bath or climatic chamber at a temperature close to room temperature (35 and 25 °C). One stirring level was used for the thermostatic bath and climatic chamber for this experiment. Thermally insulated and non-insulated samples were tested following this cooling sequence.

Programmed cooling, P, consisted in submitting the samples to a temperature program, where specific heating and cooling rates of the heat transfer fluid (from now on, HTF) were stablished. Experiments were carried out in the thermostatic bath and in the climatic chamber. The experiments with the U-SN were carried out with the lower stirrings levels (lower heat transfer coefficients for each apparatus). And in the case of the climatic chamber experiments, two experimental arrangements were tested: insulated and non-insulated tubes, which generate different cooling scenarios. The experiments with PEG 10000 carried out in the thermostatic bath, were performed on four different intensities of the bomb. Those carried out the climatic chamber used two stirring levels: the forced convection given by the equipment, and by additionally introducing a fan inside.

Insulated free cooling, FC, consisted in heating the samples inside a heating cabinet up to the desired temperature allowing soaking time to ensure fully melting. Once fully melted, the heating device was turned off while the samples remained inside the cabinet until room temperature was reached again, without forced ventilation. Two scenarios were tested: closed and opened door of the heating cabinet.

Table 5. 3 Description of the equipment used in the experimental campaigns

Equipment	Brand	Model	HTF
Thermostatic bath	Lauda	RP845	Bluesil 47V20 silicone thermal oil
Climatic chamber	Ineltec	PR-920	Air
Heating cabinet	Memmert	Oven U	Air
Hot plate	Heidolf	MR Hei End	Glycerin
DSC	Mettler Toledo	DSC1	N_2

The experiments continuously monitored and recorded the HTF temperature to determine the HTF imposed cooling rate. Besides, the PCM temperature was also continuously monitored to determine the PCM cooling rate, which depends not only on the HTF cooling rate, but also on the material and on the container geometry. The PCM temperature was measured inside the

sample in all cases except on the DSC samples. In those cases, due to the small mass in DSC crucibles, a negligible gradient is foreseen inside the PCM and the cooling rate is calculated according to the equipment.

It has to be reminded that each HTF, each stirring level of the HTF, and insulation condition have a different heat transfer coefficient *h* (or equivalent *h* in case of the insulated samples). The determination of *h* for each case is explained in the next section.

5.3.4. Determination of the heat transfer coefficient

The PCM cooling process occurs by the thermal contact of the container with a HTF. Thus, to analyze the influence of the cooling rate and cooling conditions on the supercooling it is necessary to determine the heat transfer coefficient, *h,* of each experiment.

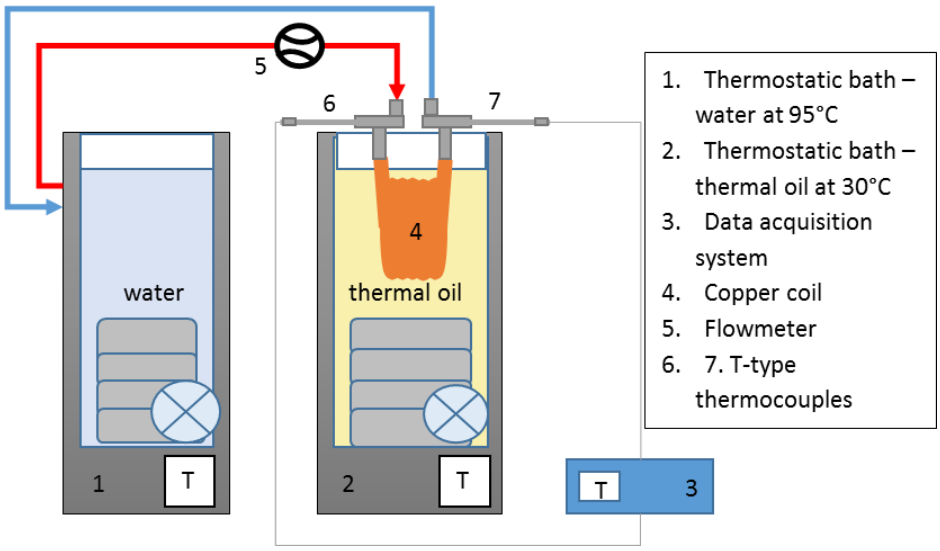

Figure 5. 3 Scheme of the experimental set up used for the determination of the convective heat transfer coefficient of the thermostatic bath

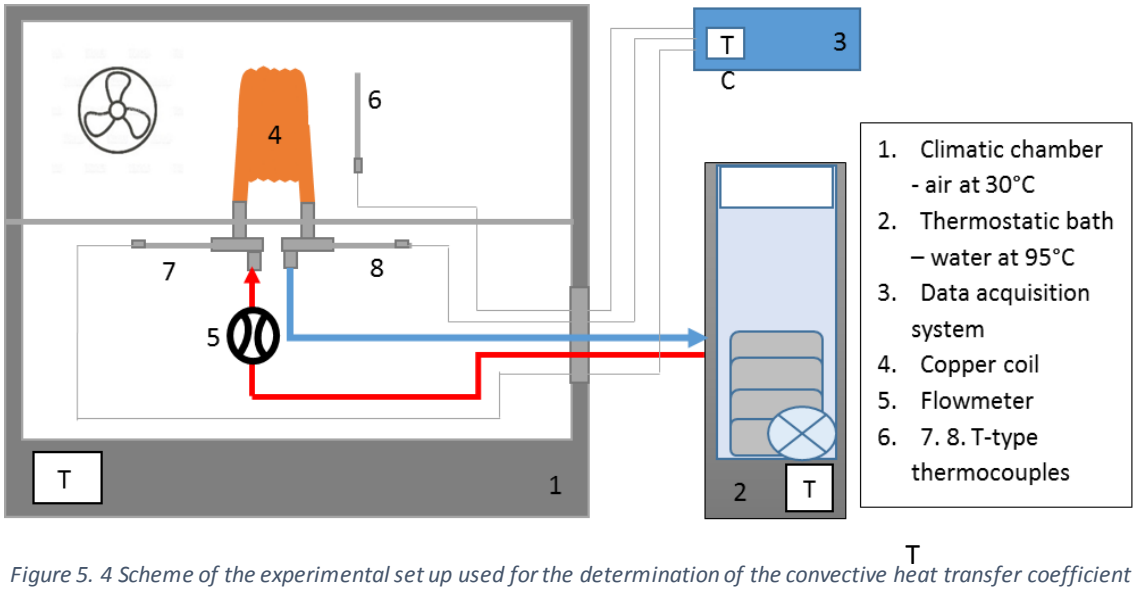

Figure 5. 4 Scheme of the experimental set up used for the determination of the convective heat transfer coefficient of the climatic chamber

For the case of the climatic chamber and thermostatic bath, the heat transfer coefficients were experimentally determined. To do so, a specific experiment was carried out, consisting in circulating water (flow rate of 3 L/min and 95 °C) through a copper coil (1.45 m long, 0.008 m inner diameter and 0.002 m thickness) immersed in the thermostatic bath with a HTFs at 30 °C. A similar experiment was carried out in the climatic chamber (different HTF). In both cases the mass flow rate, and the inlet and outlet temperatures of the water in the coil were continuously monitored, as well as the temperatures of the thermostatic bath and the climatic chamber. The experimental set-ups employed in each case are schematically depicted in Figure 5. 3 and Figure 5. 4.
Then the heat transfer coefficient was calculated (like in a heat exchanger) by the energy balance of the two fluids, using equation 5.5, where the overall heat transfer coefficient, $\bar{U}$, corresponds to equation 5.6.

$$\dot{m}C_p\Delta T = \bar{U}A\Delta T_m \tag{5.5}$$

$$\bar{U} = \frac{1}{\frac{1}{h} + \frac{L_{Cu}}{k_{Cu}} + \frac{1}{h_{int}}} \tag{5.6}$$

The heat transfer coefficient of the water inside the copper coil, h_{int}, is calculated from empirical correlations. Specifically, the Gnielinski's correlation for forced convection in pipes with upon turbulent flow is included to Contain the Nusselt number (equation 5.7 and equation 5.8), which depends on the Reynolds number (equation 5.9), the Prandt number (equation 5.10), and the friction factor. The thermophysical properties of the water (thermal conductivity, viscosities, and thermal diffusivity) are evaluated at the free temperature of the fluid, which are well known and taken from literature.

To calculate the friction factor for rough surfaces the Colebrook equation (equation 5.11) is used. The roughness of the surface ε is 0.0015 mm for the copper coil.

$$Nu = h_{int}\frac{D}{k} \tag{5.7}$$

$$Nu = \frac{\left(f/8\right)RePr}{1 + 12.7\left(f/8\right)^{0.5}\left(Pr^{2/3} - 1\right)} \tag{5.8}$$

$$Re = \frac{4\dot{m}}{\pi D\mu} \tag{5.9}$$

$$Pr = \frac{\nu}{\alpha} \tag{5.10}$$

$$\frac{1}{\sqrt{f}} = -2\ log\ (\frac{\varepsilon/_D}{3.7} + \frac{2.51}{Re\sqrt{f}}) \quad (5.11)$$

In the case of insulated samples in climatic chamber and heating cabinet, the overall heat transfer coefficient was calculated by introducing the thermal resistance of the insulation layer (equation 5.12). For the experiments performed in the heating cabinet (no forced convection, it was turned off for the tests) no experimental measurements were done. In order to calculate the equivalent heat transfer coefficient, typical heat transfer coefficient values for free convection of air were assumed for the air in the surroundings.

$$\bar{U} = h^* = \frac{1}{\frac{1}{h} + \frac{L_{cont.wall}}{k_{cont.wall}} + \frac{L_{insul}}{k_{insul}}} \quad (5.12)$$

In the DSC case, determining the heat transfer coefficient, or any equivalent parameter, is a complex problem. The heat transfer in the DSC takes place mainly by conduction between the bottom of the crucible and the ceramic plate where the crucibles are placed, which are in direct contact with the heating/cooling surface. The apparatus working procedure employs Nitrogen gas flow, which enters into the chamber at room temperature, but the configuration does not point towards a remarkable contribution of the heat-convection. For this reason, the heat transfer coefficient or equivalent for DSC samples was set out of the discussion.

5.3.5. Experimental campaign

Table 5. 4 gathers the summary of the experimental conditions employed in the studies performed with the U-SN eutectic; while Table 5. 5 gathers those employed with the PEG 10000. At least 2 repetitions were carried out for all experimental conditions.

Table 5. 4 Summary of the experiment types performed using U-SN eutectic.

		Equipment			
Test type	**Container type**	**Cooling**	**h (W/K.m²)**	**Experiment Designation**	**Repetitions**
Quenching	CuD1	Thermostatic bath	862.2	U-SN CuD1 Q1	3
		Climatic chamber	55.31	U-SN CuD1Q2	3
	CuD2	Thermostatic bath	862.2	U-SN CuD2 Q3	3
		Climatic chamber	55.31	U-SN CuD2 Q4	3
	Insulated CuD1	Climatic chamber	2.3*	U-SN CuD1 Q5	2
	Insulated CuD2	Climatic chamber	2.3*	U-SN CuD2 Q6	2
Program	GD0	Thermostatic bath	862.2	U-SN GD0 P1	3
	RB	Climatic chamber	55.31	U-SN RB P2	11
	DSC	Differential Scanning Calorimeter DSC	-	U-SN DSC P3	10
Free cooling	Insulated GD0	Heating cabinet turned off	0.00001*	U-SN GD0 FC1	4
	Insulated RB	Heating cabinet turned off	2.189*	U-SN RB FC2	3

*Calculated equivalent heat transfer coefficient

Table 5. 5 Description of the experimental types performed using PEG 10000. Different h within a same experiment type represent different stirring levels of the HTF

		Equipment				
Test type	Container type	Cooling	h (W/°C.m²)		Experiment Designation	Repetitions
Program (P)	CuD1	Thermostatic Bath	A1	862.2	PEG CuD1 A1P1	3
			A2	1056	PEG CuD1 A2P1	3
			A3	1182	PEG CuD1 A3P1	2
			A4	1250	PEG CuD1 A4P1	3
		Climatic Chamber	A5	55.31	PEG CuD1 A5 P2	3
			A6	103.9	PEG CuD1 A6 P2	3
	CuD2	Thermostatic Bath	A1	862.2	PEG CuD2 A1 P3	3
			A2	1056	PEG CuD2 A2P3	3
			A3	1182	PEG CuD2 A3 P3	2
			A4	1250	PEG CuD2 A4 P3	3
		Climatic Chamber	A5	55.31	PEG CuD2 A5 P4	3
			A6	103.9	PEG CuD2 A5 P4	3
	DSC	Differential scanning calorimeter DSC	-	-	PEG DSC P5	10

5.4 RESULTS AND DISCUSSION

The crystallization temperatures of both experimental campaigns were recorded and the results, together with its analysis are exposed below.A first observation of the results indicate that in the experimental conditions, the crystallization of U-SN eutectic never occurred at the melting temperature of ≈85°C. The measured supercooling degree ranges from 3.2 °C to 51 °C. The PEG 10000 crystallization temperature determined in the experiments was in all cases lower than the melting temperature ≈58 °C, with a supercooling degree ranging from 6.26 to 10.77 °C. Thus, the supercooling degree and its variation is rather lower than that of the U-SN eutectic.

Along the cooling process, the molten PCM and the HTF cool down at different rates, where the PCM follow the temperature variation of the HTF. The difference between these two cooling rates, and therefore their temperature profiles depends on both, the materials properties (PCM and HTF) and the geometry of the container.

Figure 5. 5 exposes the experimental crystallization temperatures of the U-SN eutectic depending on the HTF cooling rate (graph on top), PCM cooling rate (graph on the middle) and mass (bottom graph) respectively. The graph on the top shows that the crystallization temperatures are grouped around two zones depending on the HTF cooling rate, the experiments where low HTF cooling rates took place refer to the imposed temperature programs tests(P) in orange and free cooling tests (FC) in green pose lower supercooling degrees with a maximum of 13 °C (except for the DSC measurements which show supercooling degrees from 5 to 45 °C approximately), and the higher cooling rates refer to quenching (Q), in

purple/blue, which pose supercooling degrees from 7 to 43 °C. At a first glance, there is no indication that the degree of supercooling could be just related to the HTF cooling rate.

Figure 5. 5, middle, shows the evolution of the crystallization temperature with the PCM cooling rate. It follows a well defined decreasing trend as the cooling rate increases. It can be observed that the supercooling increases linearly with increasing PCM cooling rates except for the DSC experiments, which show a great dispersion of samples with the same cooling rate as previously indicated.

Figure 5. 5, bottom, shows the crystallization temperature versus the sample mass. No direct relationship between the sample mass and the crystallization temperature was found. However, there is a remarkable behavior that is assumed to happen because of the sample mass (volume). DSC samples (7-10 milligrams) present large supercooling degrees and a meaningful dispersion of the crystallization temperature. This is explained by the smaller probability of nucleation in small volumes. The data points towards the fact that above a certain sample-mass the stochastic nucleus formation in homogeneous nucleation is not a process defining-factor any more. This mass threshold has not been determined, but in any case it is lower than 4-5 grams (mass on the GD0 containers), which is the smallest mass employed in the study above the DSC. When the PCM mass is above that threshold, other parameters have significantly greater influence than the mass on the supercooling degree.

Figure 5. 6 includes the PEG crystallization temperature as a function of the HTF cooling rate (upper graph), the PCM cooling rate (middle graph) and the mass (bottom graph) respectively. At a first glance, there is no indication of crystallization temperature dependence on the HTF or PCM cooling rates with the CuD1 and CuD2 samples, however a linear trend is seen regarding the DSC samples. The crystallization temperature versus the mass show that, there is a correlation between the determined crystallization temperature and the sample mass in similar HTF cooling rates (assuming it is ore correct due to the fact that there was the temperature was not measured inside the container). DSC samples were tested in slower HTF cooling rates, showing lesser supercooling in those measurement, accounting for the temperatures that seem out of trend in the sample mass vs HTF cooling rate chart, where DSC samples show greater dispersion.

Both materials show very different supercooling behavior, both the supercooling degree and its scattering, when very small mass is employed (5-10 mg, DSC tests). U-SN eutectic has a higher tendency to supercool, being the nucleation a problem in small masses as the homogeneous nucleation theory indicates. In the case of the PEG 10000 nucleation does not seem to be related to the mass (volume) because the experiments carried out in the DSC crucibles show no significant dispersion within the same cooling rate, no stochastic behavior in such small sample mass. Instead, those experiments indicate a direct correlation to the cooling rate, which may imply a greater temperature lag between the sample and the container (in this tests the temperature is measured outside the container, not inside the PCM).

Test type	Container type	Cooling equipment	Experimental Designation	Simbols
Quenching (Q)	CuD1	Thermostatic bath	U-SN CuD1 Q1	
		Climatic chamber	U-SN CuD1 Q2	
	CuD2	Thermostatic bath	U-SN CuD2 Q3	
		Climatic chamber	U-SN CuD2 Q4	
	Insulated CuD1	Climatic chamber	U-SN CuD1 Q5	
	Insulated CuD2	Climatic chamber	U-SN CuD2 Q6	
Program (P)	GD0	Thermostatic bath	U-SN GD0 P1	
	RB	Climatic chamber	U-SN RB P2	
	DSC	Differential Scanning Calorimeter DSC	U-SN DSC P3	
Free cooling (FC)	Insulated GD0	Heating cabinet turned off	U-SN GD0 FC1	
	Indulates RB	Heating cabinet turned off	U-SN RB FC2	

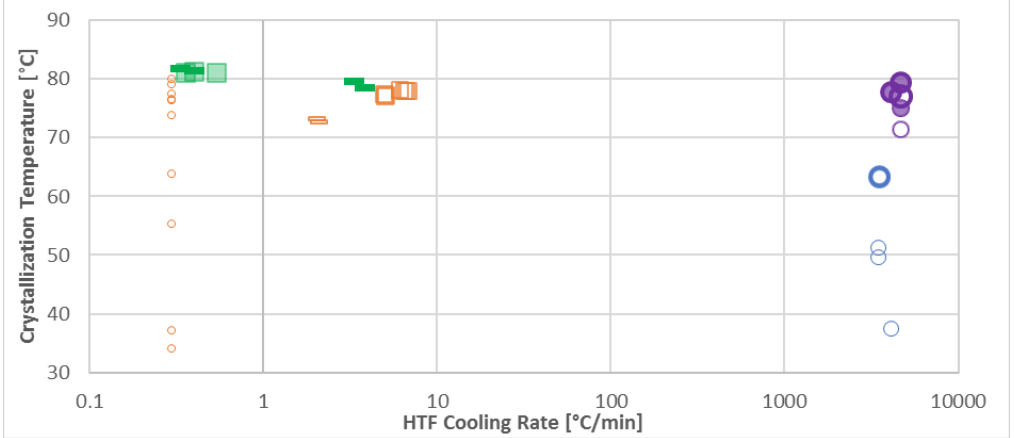

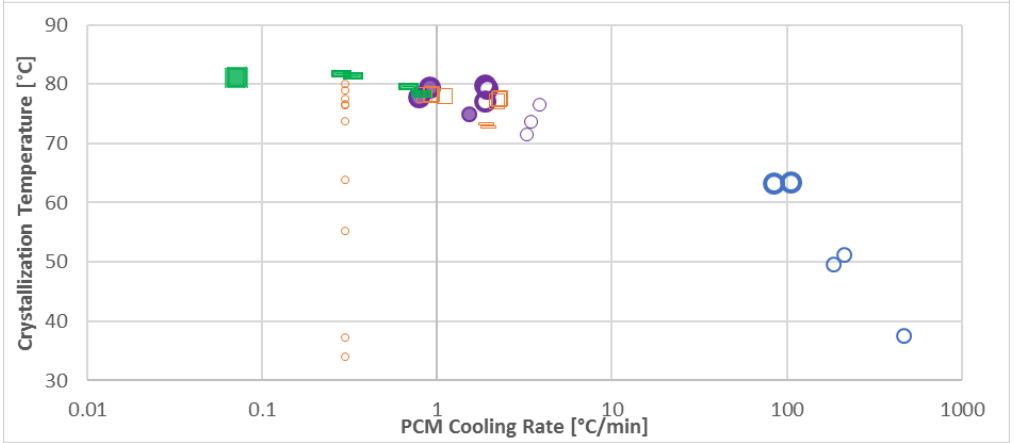

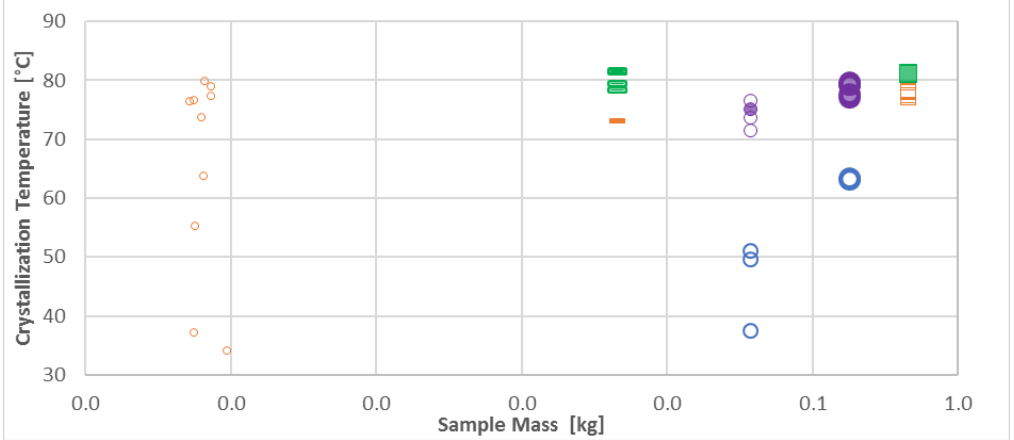

Figure 5. 5 Crystallization temperatures of U-SN eutectic depending on the HTF and PCM cooling rates, and mass

Test type	Container type	Cooling	Agitation Level	Designation	Simbols
Program (P)	CuD1	Thermostatic bath	A1	PEG CuD1 A1P1	
			A2	PEG CuD1 A2P1	
			A3	PEG CuD1 A3P1	
			A4	PEG CuD1 A4P1	
		Climatic chamber	A5	PEG CuD1 A5 P2	
			A6	PEG CuD1 A6 P2	
	CuD2	Thermostatic bath	A1	PEG CuD2 A1 P3	
			A2	PEG CuD2 A2P3	
			A3	PEG CuD2 A3 P3	
			A4	PEG CuD2 A4 P3	
		Climatic chamber	A5	PEG CuD2 A5 P4	
			A6	PEG CuD2 A6 P4	
	DSC crucible	DSC	-	PEG DSC P5	

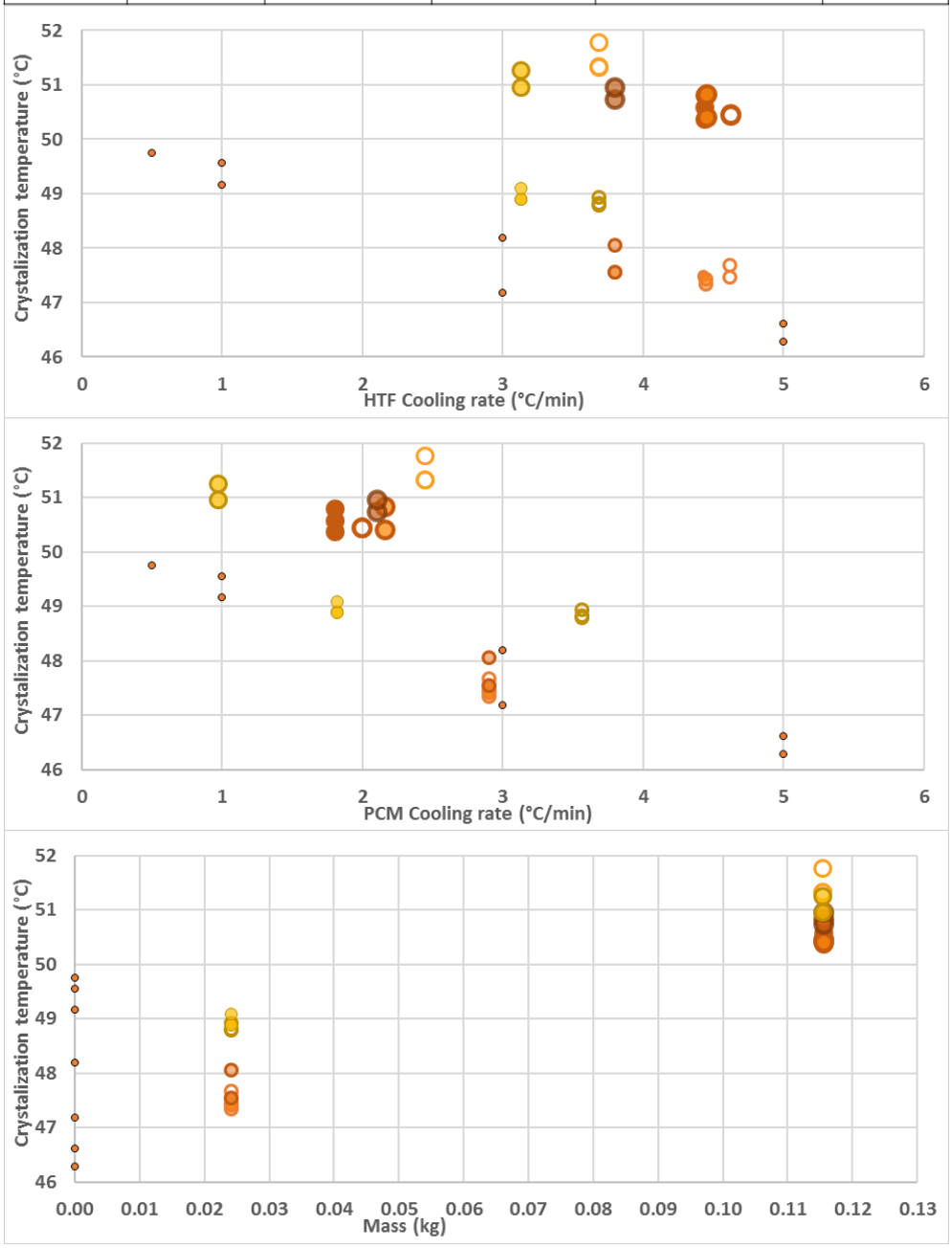

Figure 5. 6 Crystallization temperatures of PEG 10000 depending on the HTF and, PCM cooling rates and mass

5.5 DATA ANALYSIS

The experimental results (except DSC experiments) were analysed with the aim of determining if any of the selected parameters could explain the nucleation phenomenon. The DSC results were discarded from the statistical analysis due to the different nucleation process that seemed to take place in those experiments and the high complexity and unreliability of the *h* calculation of this case.

A statistical analysis was carried out using R-Commander [145]. The crystallization temperature, *Tc*, was set as the dependent variable or outcome variable, which is the variable to be explained by the model. The independent variables, also called predictor variables are the variables used to explain the dependent variable behavior and are those that can be modified or acted on. The independent variables set for the study were: the mass, *m*; the cooling rate inside the PCM, *v(PCM)*; the cooling rate of the heat transfer fluid, *v(HTF);* the heat transfer coefficient, *h*; the characteristic length, *Lc*; the thermal conductivity, *k*; the thermal diffusivity, *α*; and the Biot number, *Bi*.

The dimensionless Biot number (equation 5.13) was included in the study because it could be related to the supercooling phenomenon since it is an indirect indication of the existing thermal gradients when the body is heated or cooled from the surface. It gives the ratio of the heat transfer resistance inside of a body and the surrounding atmosphere.

$$Bi = \frac{h \cdot L_c}{k} \qquad (5.13)$$

The data set from the U-SN eutectic experimental campaign contains 30 values. The crystallization median temperature is 77.67 °C and the standard deviation is 10.53. Figure 5. 7 depicts the distribution of the obtained crystallization temperatures and the frequency. The frequency refers to the number of times a data value occurs on each temperature range. It can be observed that most of the values (21 values of 30) are in the 77.4 °C - 81.8 °C interval, which do not represent a very strong supercooling. The lower values from 37.55 to 67.05 °C with low frequencies correspond to the quenching experiments performed using the thermostatic bath (thermal oil as HTF), which showed PCM cooling rates ranging from 100 to 4600 °C/min. Then, the temperature ranges from 67.05 to 81.8 correspond to the remaining quenching tests (performed in the climatic chamber, thus air as HTF), program and free cooling tests.

The data set from the PEG 10000 experimental campaign contains 34 values. The crystallization median temperature is 49.72 °C and the standard deviation is 1.54. Figure 5. 8 depicts the distribution of the obtained crystallization temperatures and frequencies. It can be seen that data are distributed heterogeneously in the small range of crystallization temperatures. This is because of the sample size and cooling media influence. The higher crystallization temperature ranges (49.74 to 51.67 °C) represent the temperatures obtained with the larger size container CuD2, which ensured slower cooling rates. The lower temperature ranges (47.16 to 49.09 °C) result from the higher influence of the cooling media in the CuD1 smaller size samples.

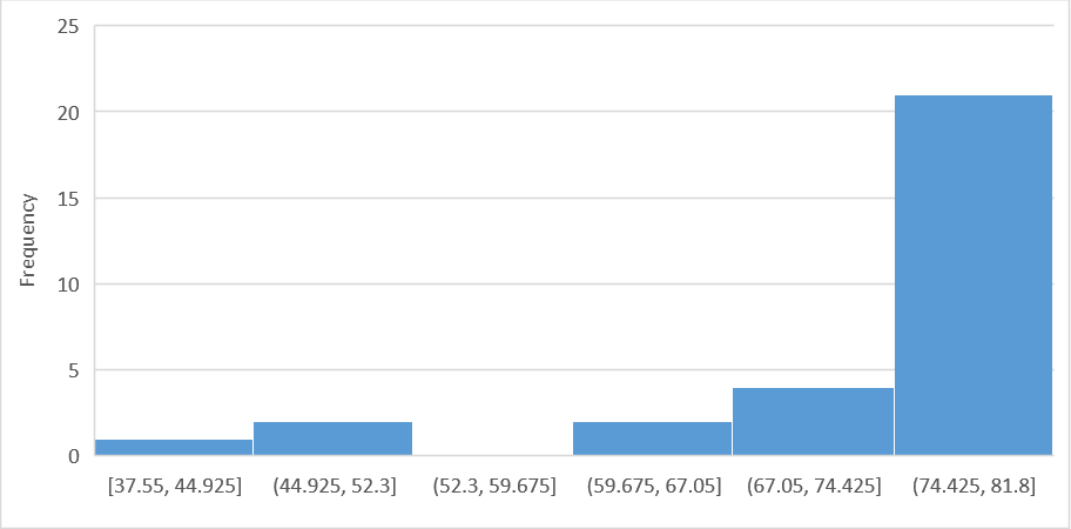

Figure 5. 7 Distribution of the U-SN eutectic experimental campaign crystallization temperatures

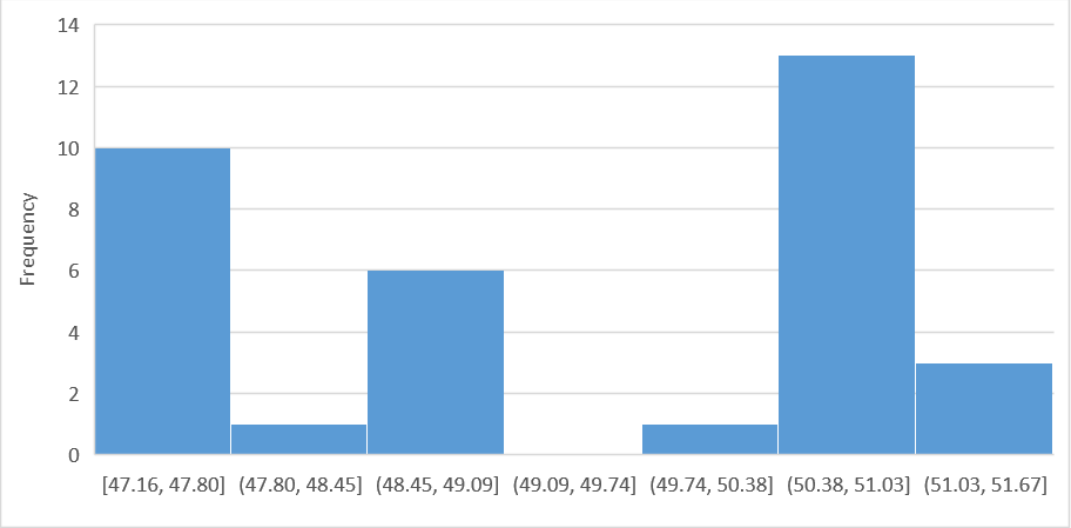

Figure 5. 8 Distribution of the PEG 10000 experimental crystallization temperatures

The crystallization temperature distribution depending on the experiment typology highlights that each type (quenching, program and free cooling) can introduce additional factors different from the defined variables that may affect the supercooling. Aspects, which have not been included in the studied variables, like for example the containers material, the temperature gradients of the HTF, the influence of the thermocouple, etc., might pose a significant effect on the supercoling. However, the different use of different equipment as cooling media, different containers, etc. make it possible to recreate a greater range of heat transfer coefficients, characteristic length/mass and cooling rates, which was the aim of the study. For that reason, the potential dependency of the test type and the supercooling is not taken into consideration in the present study. Besides, the use of temperature sensors is necessary to measure the crystallization temperature of the PCM, and can not be avoided.

5.5.1. Relevance of the independent variables in the crystallization temperatures. Correlation test

The first step in the evaluation of the dependent variable, *Tc*, with the independent variables was to check the linear correlation between them. Then a correlation test was performed using the Pearson correlation coefficient as a measure of each individual variable relevance on *Tc*. This coefficient shows the relevance in values between +1 and −1, where 1 is total positive linear correlation, 0 is no linear correlation, and −1 is total negative linear correlation.

Figure 5. 9 shows the Pearson coefficients for the crystallization temperature and the independent variables for U-SN. Thermal conductivity and thermal diffusivity are not shown as they are constant for all the experiments (of the same material). The results show that the greater individual relevance corresponds to *v(PCM), h* and the *Bi*. They are all negative, which means that they the higher the variable value, the lower the crystallization temperature, i.e. the larger the supercooling degree. The Pearson correlation coefficient for *v(PCM)* is 0.94, indicating that it has a very good linear relationship with *Tc*. For *h*, 0.8 also renders good linear relationship with *Tc*. The coefficient for *Bi* is <0.7, then discarded because it is considered too low to have a significant relevance compared to *v(PCM)* and *h*.

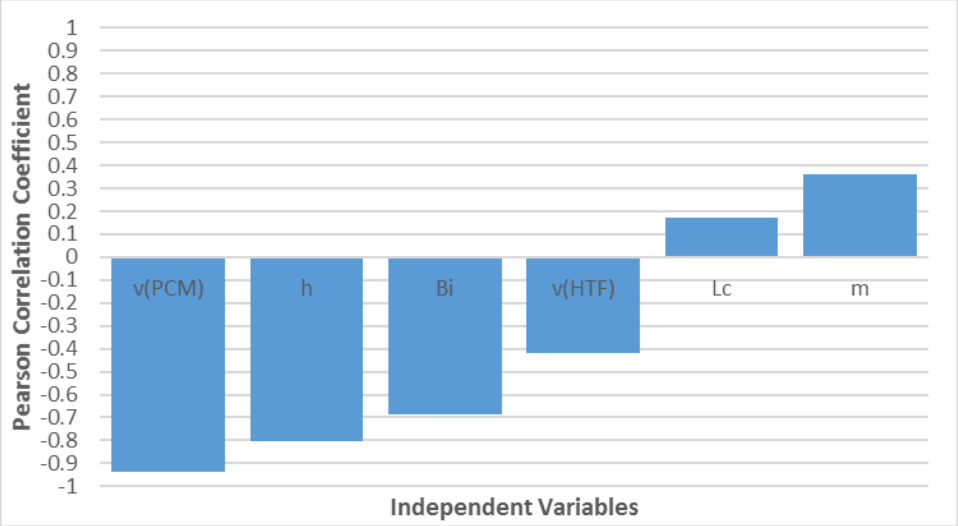

Figure 5. 9 Pearson correlation coefficients for the crystallization temperatures and the independent variables corresponding to the U-SN eutectic experimental campaign

Figure 5. 10 shows the Pearson coefficients for the crystallization temperature and the independent variables for PEG 10000. The results show that the greater individual relevance corresponds to the *Lc* and *m* (0.93 in both cases), which are measure of the sample volume, then correspond to the same study parameter. The following parameter in importance, is the *v(PCM)* however presents a smaller relevance, 0.64.

The linear correlation test yielded different relevance regarding the relationship of the dependent variable, *Tc*, with the independent variables. This is deemed to be mostly due to the different experimental ranges studied in both cases, very limited in the case of the PEG 10000 (as stated before), comprising fewer test configurations regarding the sample volume and

cooling rates, thus limiting the comparison of the results of both experimental campaigns. However, it is observed that the single *v(PCM)* variable is more relevant than the *v(HTF)* by itself, and can highly describe the phenomenon. There is no consensus for the other parameters, because the individual relevance seems to be highly dependent on the experimental.

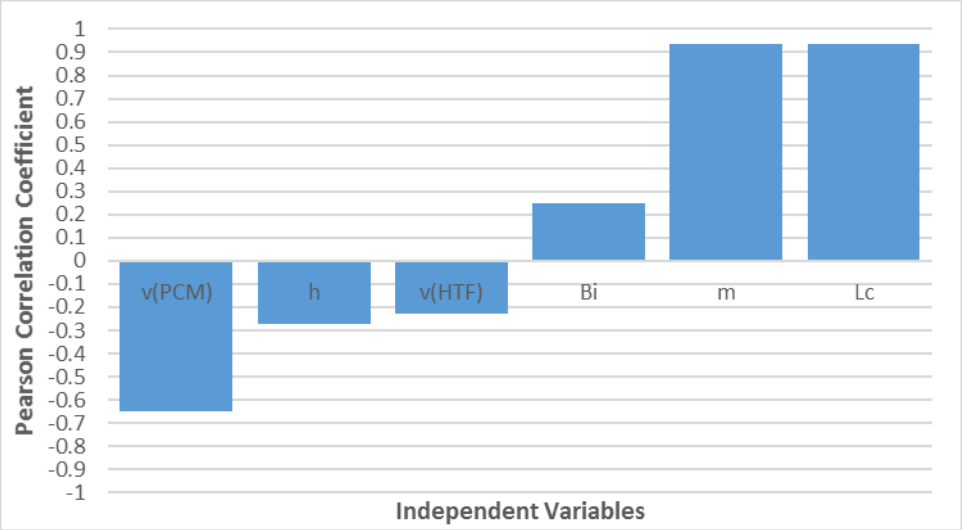

Figure 5. 10 Pearson correlation coefficients for the crystallization temperatures and independent variables corresponding to the PEG 10000 experimental campaign

Besides, the aggrupation of some variables may better describe the effects to be evaluated (temperature distribution behavior depending on the sample volume, cooling media characteristics and PCM properties) and pose a larger relevance in the supercooling phenomenon than single variables. For this reason, the first step in order to make associations was to multiply and divide each variable by the set of the remaining variables.

Figure 5. 11 depicts the Pearson correlation coefficients for the values resulting from multiplying the independent variables of the U-SN eutectic. The highest relevance comes from the multiplication of *v(PCM)* with other variables, and secondarily multiplication of the *h* with the other variables. However, the Pearson correlation coefficient in these cases was smaller than the one from single *v(PCM)* and *h*. The multiplication of *v(HTF)* times *h* surpasses the individual Pearson coefficient of both terms, but it does not overcome the *v(PCM).* Then it is concluded that the multiplication of the single variables do not report higher relevance to the one of the single parameters, and then all these parameters are discarded for further evaluation.

Figure 5. 12 depicts the Pearson correlation coefficients for the values resulting from multiplying the independent variables of PEG 10000. The same effect resulted from the multiplication of the

variables in both materials, no enhancement of the relevance was observed regarding the single variables.

Figure 5. 11 Pearson correlation coefficients of the dependent variable Tc *and the multiplication of independent variables of the U-SN eutectic experimental campaign*

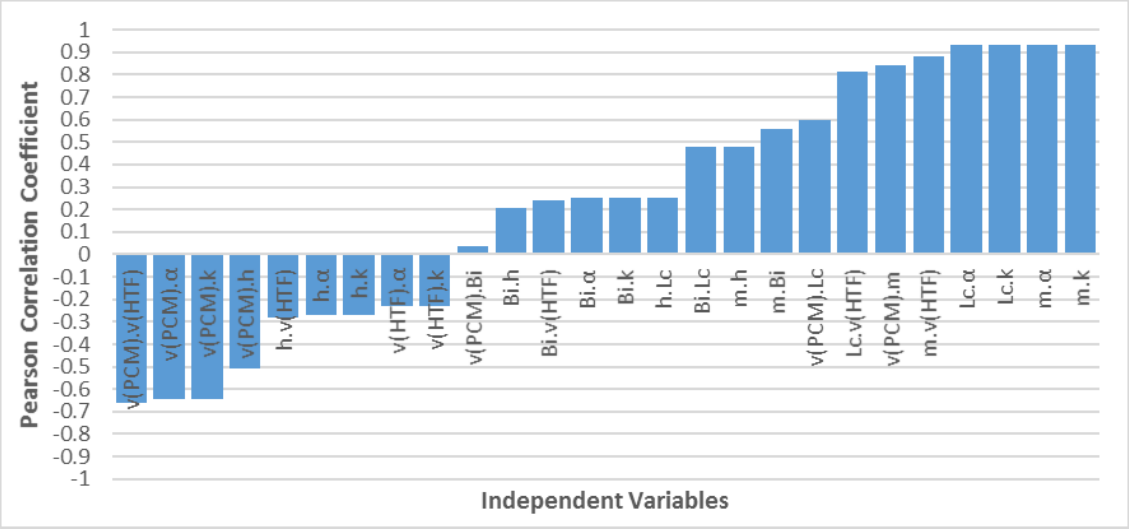

Figure 5. 12 Pearson correlation coefficients of the dependent variable Tc *and the multiplication of independent variables of the PEG 10000 experimental campaign*

Figure 5. 13 and Figure 5. 14 summarizes the interactions resulting from dividing the variables of U-SN eutectic and PEG 10000. The results for the U-SN points towards most of the high relevant variables to be related to *v(PCM)* and *h*. And in the case of PEG 10000, related to *m* and *Lc*. However, the highest Pearson correlation coefficients are -0.97 (very close to the total negative linear correlation), and in both cases comes from the division of the *v(HTF)* and the *Lc* of the PCM container. *v(HTF)/m* was showed the same relevance in the PEG 10000 analysis, however describes the same effect, and as the geometries in these experimental campaign were limited, then the *v(HTF)/Lc* parameter was preferred as in the U-SN results. This ratio was

encountered to be significantly relevant in both materials, regardless their experimental differences, and therefore is selected for further analysis.

It is physically meaningful that a significant relationship exist between the PCM crystallization temperature, *Tc*, and these variables because *v(PCM)*(which is the direct parameter acting on the supercooling determined previously) depend on both parameters. It is worthwhile to note that the *v(HTF)* and *Lc* are variables that can be controlled and modified in application, not the case of the *v(PCM)*, which need to be determined by means of experimental testing or modelling. The *v(PCM)* may serve to understand the phenomenon but can not be used in a practical approach to design an industrial process.

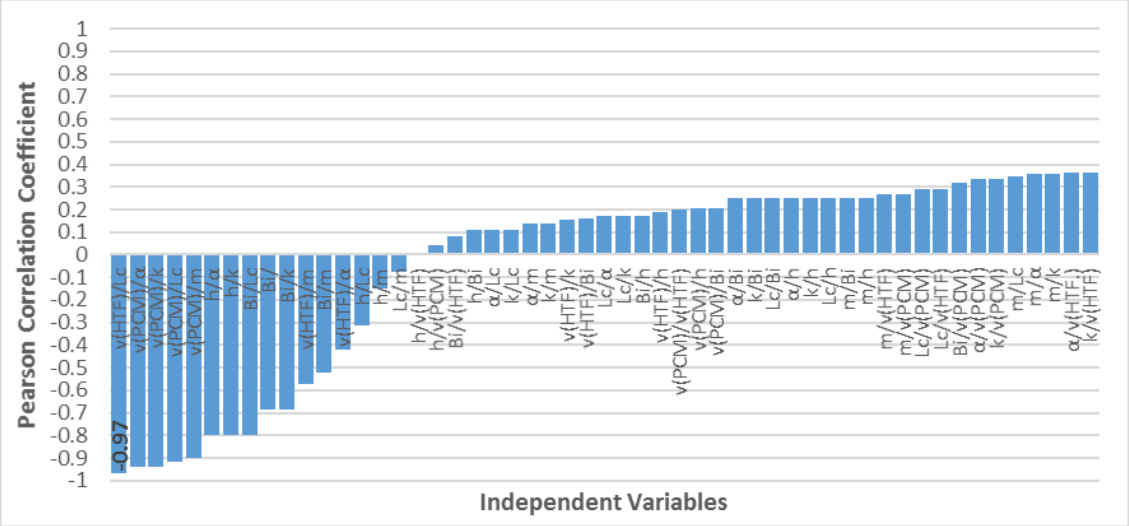

Figure 5. 13 Pearson correlation coefficients of the dependent variable Tc *and the division of independent variables of the U-SN eutectic experimental campaign*

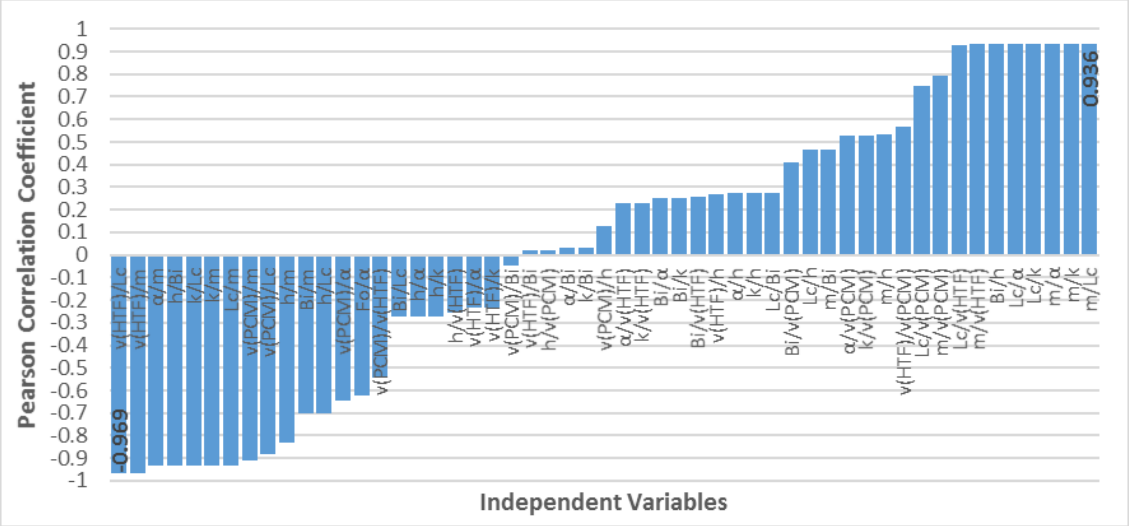

Figure 5. 14 Pearson correlation coefficients of the dependent variable Tc *and the division of independent variables of the PEG 10000 experimental campaign*

5.5.2. LINEAR REGRESSION MODELLING

In addition, according to the relevance obtained by the single independent variables and their aggrupation, linear regression models were determined. Regression modelling is a form of predictive modelling technique, which investigates the relationship between a dependent variable or the variable to be explained, and one or more independent variables, also called explanatory variables or predictors. It is a tool for finding the causal effect relationship between variables. In linear regression, the relationships are modeled using linear functions whose parameters are estimated from the data.

For the U-SN eutectic three models were compared involving the following independent parameters: the individual independent variable with highest relevance, *v(PCM);* the interaction with highest relevance, *v(HTF)/Lc* ratio and a model that included both *v(HTF)/Lc* ratio and *h*, which corresponded the second highest relevance of the individual parameter. Table 5. 6 presents the obtained models including R-squared and p-value parameters.Therefore, recalling the study parameters: volume, cooling media and PCM (in Table 5. 1), M1 represent the combined effect of the cooling media and PCM properties (cooling rate of the PCM is influenced directly by the HTF cooling rate and the PCM properties). M2 represents a combined effect of the sample volume and the cooling media, by the influence of the cooling rate but not the influence or of the HTF. M3 also represents the combined effect of the cooling media, but taking into account both cooling velocity and HTF considerations. The *m, k, α* and *Bi* independent variables are discarded as variables that describe the supercooling using a simple regression linear model methodology implemented.

In order to evaluate the models the p-value and R-squared parameters were used. These parameters are generally used in statistics for the evaluation of research data [146]. The p-value expresses the level of statistical significance between 0 and 1. The larger the p-value, the stronger evidence for having a relationship between the dependent and independent variables. R-squared is a statistical measure that represents the proportion of the variance (dispersion from the average value) for a dependent variable that is explained by the independent variables in a regression model. It provides a measure of how well the experimental outcomes are replicated by the model, where 1 is the better fitting.

According to the p-values, the three analyzed models support the hypothesis that the selected variables and interactions have great influence in the supercooling behavior. Besides, the obtained 3 equations have a good R-squared value, close to 1. The best fitting model is M3 U-SN, which includes *h* and *v(HTF)/Lc*, with a R-squared value of 0.95. Therefore, it has been selected as the most relevant model to describe the influence of the studied parameters on the supercooling degree of the U-SN eutectic.

Table 5. 6 Selected linear models for the U-SN eutectic

Model	Equation	Adjusted R-squared	p-value
U-SN M1	*Tc'=7.616329 +(0.1017.**v(PCM)***	0.875	2.234e-14
U-SN M2	*Tc'=6.702+(3.916e-8.**v(HTF)/Lc**)*	0.938	<2.2e-16
U-SN M3	*Tc'=6.151+(0.0052.**h**)+(03.385e-8.**v(HTF)/Lc**)*	0.951	<2.2e-16

Figure 5. 15 and Figure 5. 16 depict the results for the experimentally determined supercooling degree versus several variables HTF cooling rate and characteristic length ratio, and heat transfer coefficient respectively), and that predicted by the best fitting model, M3 U-SN model. Figure 5. 17 shows the fitting curve for the model where the experimental crystallization temperature values are represented in the x-axis and the modelled values in the y-axis.

It has to be remarked that, the determined models are valid only for the U-SN eutectic in the experimental intervals approached in this study. If the experimental conditions greatly differ from those herein employed (much larger or smaller cooling rates, heat transfer coefficients, etc.) or a different material is used, the models might not be valid.

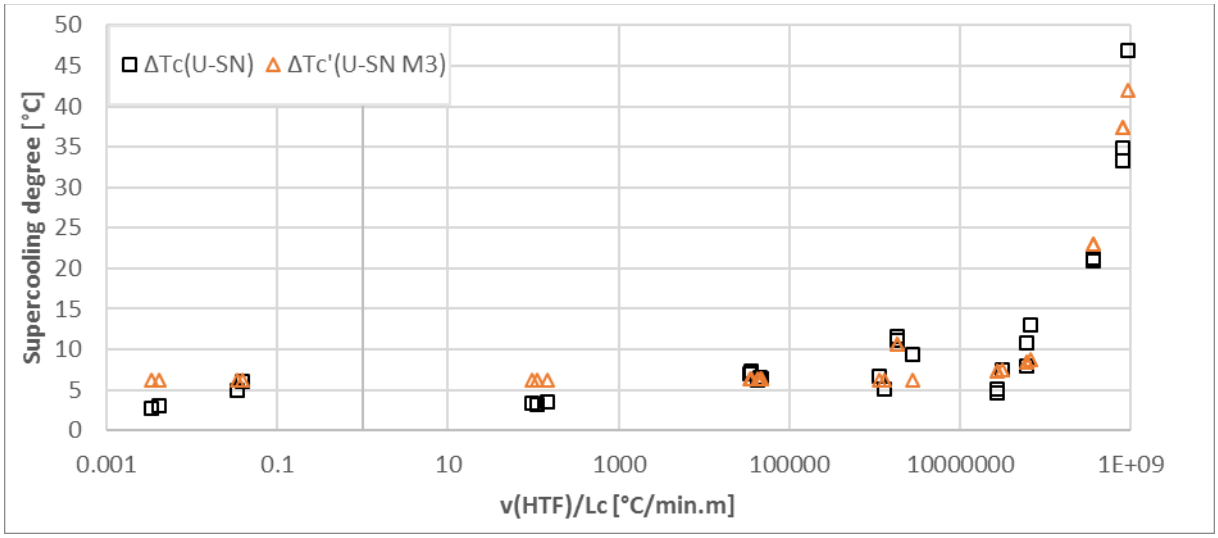

Figure 5. 15 Experimentally determined and modelled supercooling degree versus HTF cooling rate and characteristic length ratio values for U-SN eutectic

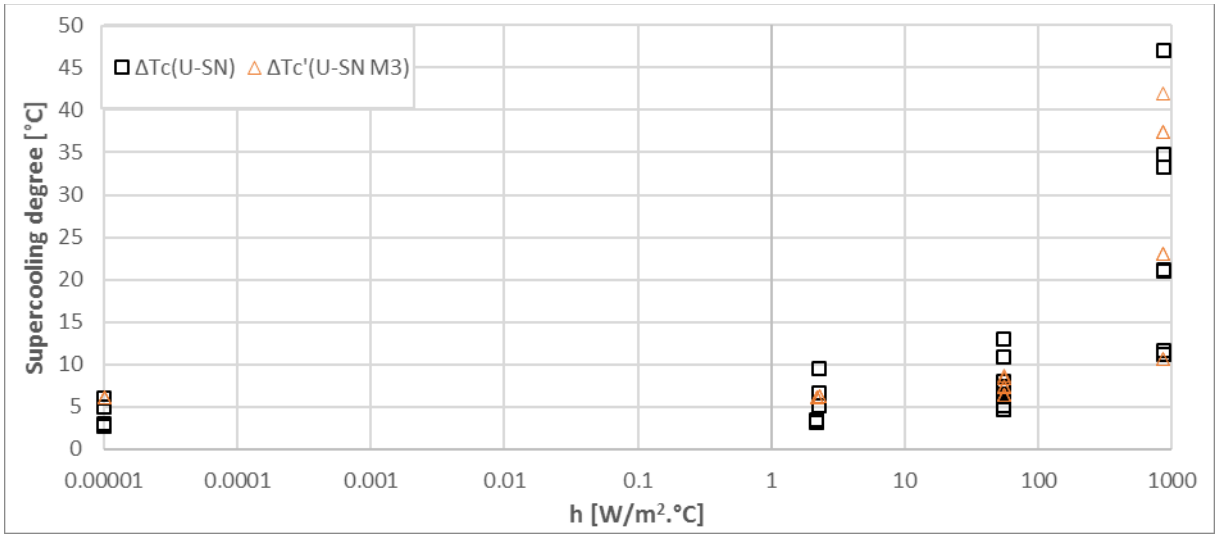

Figure 5. 16 Experimentally determined and modelled supercooling degree versus heat transfer coefficient values for U-SN eutectic

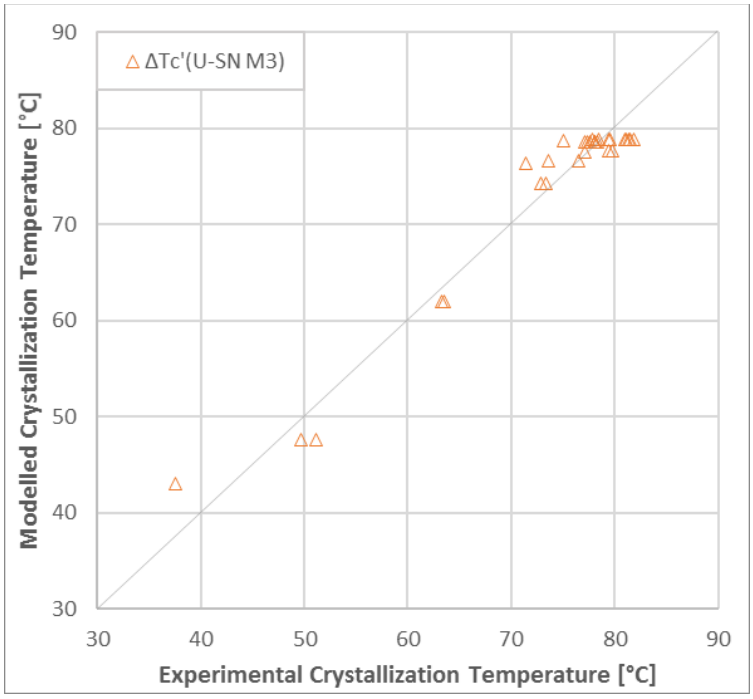

Figure 5. 17 U-SN M3 model fit with the experimental results

In order to analyze the potential validity of the use of the selected in dependent or explanatory variables to predict the supercooling in a different PCM, two models were determined for PEG 10000. Table 5. 7 presents the obtained models including R-squared and p-value parameters.

Table 5. 7 Selected linear models for the PEG 10000

Model	Equation	Adjusted R-squared	p-value
PEG M1	*ΔTc'=4.827+(5.067e-3.**v(HTF)/Lc**)*	0.9366	<2.2e-16
PEG M2	*ΔTc'=4.753+(1.668e-4.**h**)+(5.003e-3.**v(HTF)/Lc**)*	0.9375	<2.2e-16

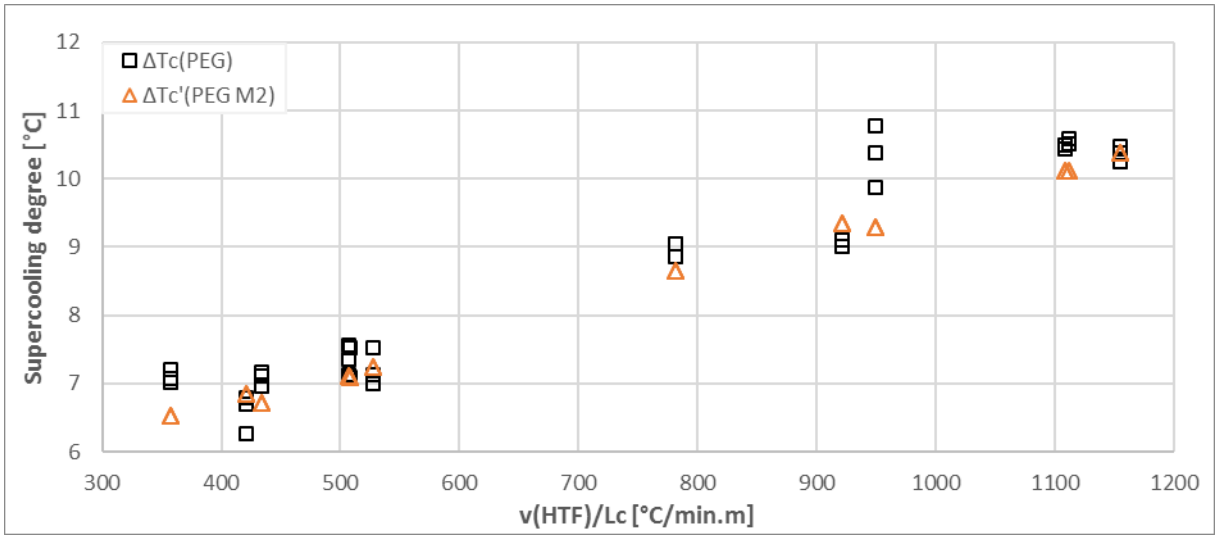

Figure 5. 18 Experimentally determined and modelled supercooling degree versus HTF cooling rate and characteristic length ratio values for PEG 10000

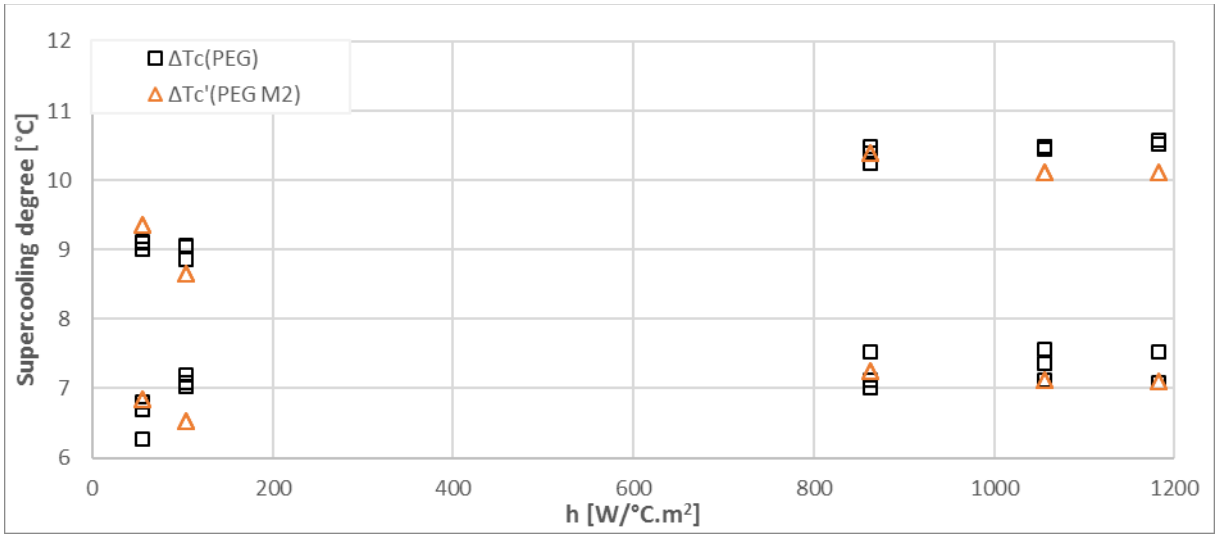

Figure 5. 19 Experimentally determined and modelled supercooling degree versus heat transfer coefficient values for PEG 10000

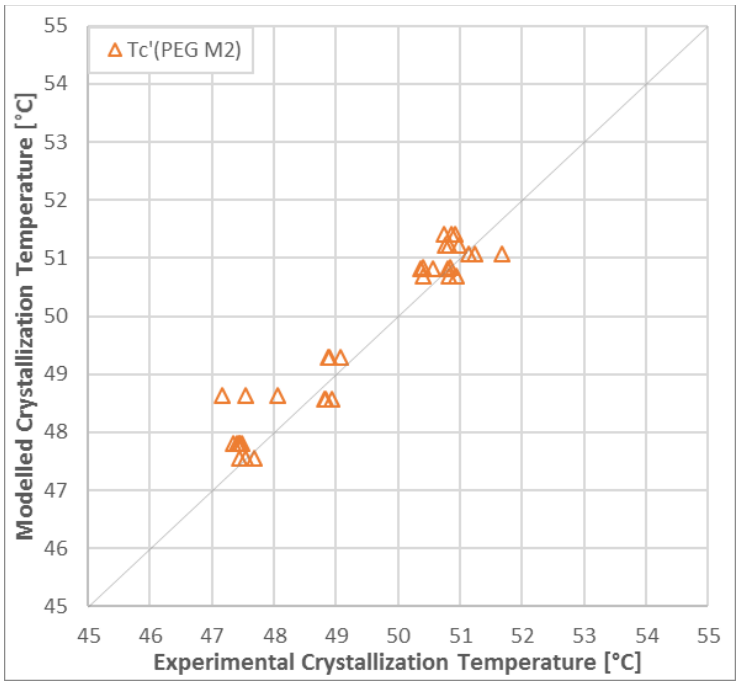

Figure 5. 20 PEG M2 model fit with the experimental results

The p-values for both models are very low, so there is a strong evidence that the supercooling degree depends on the defined characteristics (*h* and *v(HTF)/Lc* ratio). R-squared values are above 0.9, giving a good fitting of the models to the experimental results. Even if *h* did not show a high relevance as an individual variable in the PEG 10000 it was included to the model. This was done in order to evaluate the previous U-SN model parameters, which is based on the experimental results performed in a wider experimental range. Finally it was determined that including *h* increased the R-squared value. As a result, PEG M2 is selected as the best fitting model in this case. Figure 5. 18 and Figure 5. 19 show both, the experimental results and the

modelled supercooling according to PEG M2. Figure 5. 20 shows the PEG M2 model fit with the experimental results.

5.6 OVERALL ANALYSIS OF THE RESULTS

In spite of the experimental differences, both studies report that the highest relevance comes from the *v(HTF)/Lc*. This is an indirect indication of how the temperature varies inside the geometry. However, the *v(HTF)/Lc* is thought not to describe completely the supercooling phenomenon, because the cooling rate describe the velocity of the temperature change but not the effectivity of the heat exchange with the PCM container surface. The convective heat transfer coefficient introduces the effect produced by the use of different HTFs and/or the stirring. The results of the wider study (U-SN eutectic experimental) support this hypothesis. In fact, the ideal correlation should include all the study parameters (volume, cooling media and PCM parameters) then the PCM properties should be also included to fully describe the phenomenon in different materials. However, as the studied models only consider one material, no relevance comes from the PCM properties. Then if both materials parameters are evaluated jointly, a model that includes parameters regarding the PCM properties and the previously identified influencing parameter can be evaluated. Table 5. 8 shows the model following the crystallization temperatures for both U-SN eutectic and PEG 10000. The p-value for the MJ is very low, and R-squared value is 0.85, giving a good fitting but not as good as the obtained for models of the single materials.

Table 5. 8 Linear model for U-SN eutectic and PEG 10000

Model	Equation	Adjusted R-squared	p-value
MJ	*Tc'=79.54-(6.88e-3.**h**)-(1.169e-5.**v(HTF)/Lc**)-(6.18e4.**α**)*	0.8538	<2.2e-16

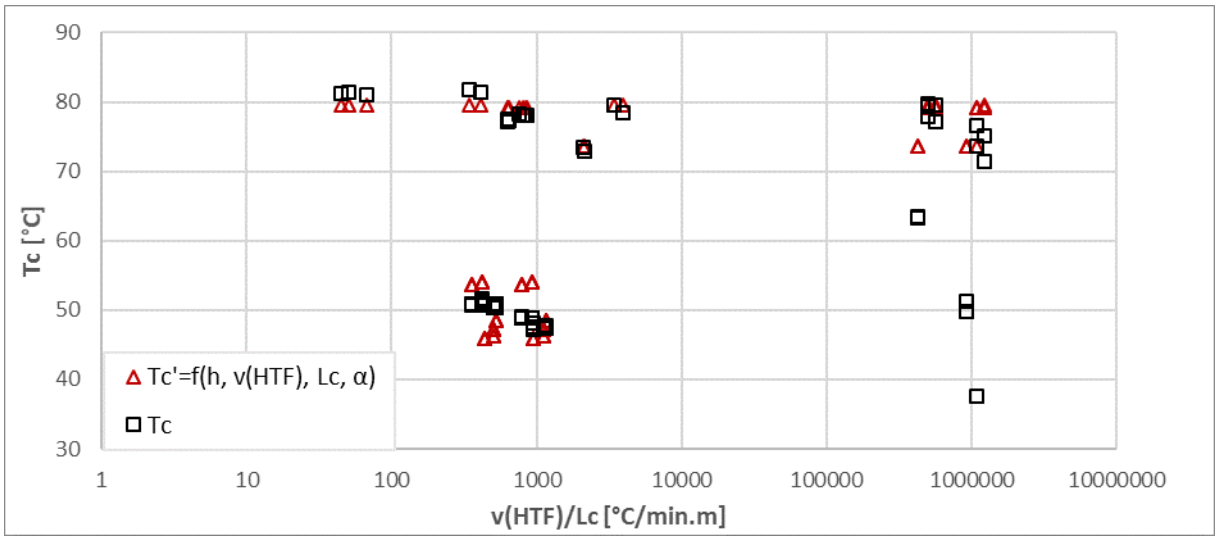

Figure 5. 21 Experimentally determined and modelled crystallization temperature versus HTF cooling rate and characteristic length ratio values for all experimental results (U-SN and PEG 10000)

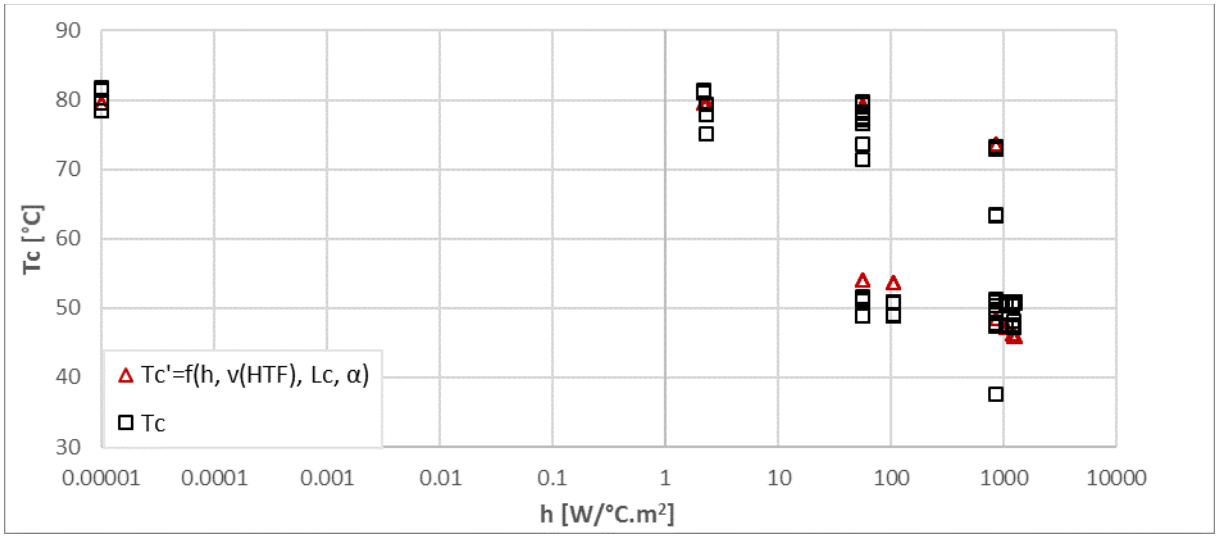

Figure 5. 22 Experimentally determined and modelled crystallization temperature versus heat transfer coefficient values for all the experimental results (U-SN and PEG 10000)

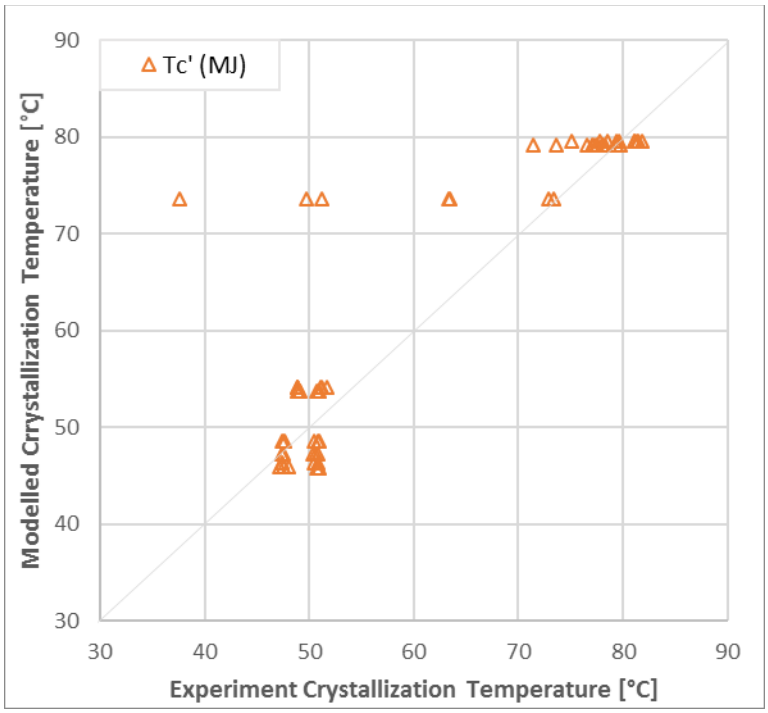

Figure 5. 23 MJ model fit with the experimental results

Figure 5. 21 and Figure 5. 22 depict the results for the experimentally determined crystallization temperature versus HTF cooling rate and characteristic length ratio and heat transfer coefficient respectively, and that predicted by MJ. Figure 5. 23 shows the MJ model fit with the experimental results of all the experiments performed (U-SN and PEG 10000). It can be observed that the model fits well in the zones corresponding to moderate *v(HTF)/Lc* ratio. It does not fit very well the quenching experiments where very fast cooling rates are achieved. This may point towards the nonlinearity of the supercooling if larger experimental ranges are taken into account. Further research should be done regarding different types of models which may describe better the phenomenon.

Besides, modelling each material separately APORTA more accurate results for the prediction. Further analysis should be done regarding models that include more PCM materials, so to confirm that these parameters can be used to model the supercooling of PCM in the temperature range studied. It is though that other PCM properties that have not been taken into account may also influence the supercooling behavior, so should be included in future studies. Furthermore, the use of a common model for more materials should be improved and validated.

In addition, it is believed that there are certain factors than can also influence the modellization of the supercooling behavior using experiments. For example, the accuracy of the independent variables used can be improved so the explanation/prediction of the supercooling may be also improved. Besides, in the quenching experiments the cooling rate of the HTF is calculated from the temperature difference of the heating media (glycerin bath) and the cooling media (thermal oil in the thermostatic bath) is assumed to happen in 1 second, because the immersion of the samples in the colder fluid was done very fast. However, this calculation may not follow the reality (time was not measured). Besides, the heat transfer coefficient, *h*, accuracy of the experimental and the calculations is uncertain, and calculated from experimental data with experimentally gathered correlations, which may introduce an important error.

5.7 CONCLUSIONS

From the present study it was determined that the supercooling degree of U-SN eutectic goes from 3.2 to 51 °C; and the supercooling degree of PEG 10000 goes from 6.26 to 10.77 °C, in the experimental conditions.

In addition, the variable analysis allowed the determination of the most relevant parameters to the supercooling of these materials. The studies show some discrepancies regarding the individual interaction of the independendent variables and the crystallization temperature variation, however is thought to be caused by the different experimental ranges of the studies. The PEG 10000 study has a very short *v(HTF)/Lc* range compared to the urea and Sodium nitrate mixture, then evaluates the supercooling in a more restricted dependency zone were the significance of some parameters may be reduced.

Despite, both studied materials give evidence for the HTF cooling rate and characteristic length ratio to be the most relevant parameter. In contrast to the PCM cooling rate or process time, the HTF cooling rate and characteristic length are variables that can be controlled or acted on in a direct way. There might be freedom in the variation of some of the parameters, but not in all of them. For example, the medium cooling rate may not be modified in some cases due to the process or application nature, thus being the geometry the parameter to take into account to reduce as possible the supercooling degree, because it can be freely modified. Therefore, the work main conclusion highlights the importance of the geometry or mass disposition regarding the supercooling degree more than the direct effect of the mass in representative samples. In addition, the contribution of the heat transfer coefficient as a measure of the medium characteristics, which influence the heat transfer with the PCM container surface. The correct combination of these parameters can be used for the design of the LHTES devices to reduce the

supercooling as much as possible, being otherwise impossible to be modified in the operation once installed.

A linear correlation describing the supercooling degree in the experimental conditions was determined for the U-SN eutectic and for PEG 10000. A final model was assessed for all the experimental results, including both materials. From the data analysis performed it was not possible to establish a law that can be used in different materials that predicts the supercooling phenomenon, but the methodology was able to assess the variables that can be used with this aim because show high dependency. Further research is needed to completely understand the interaction of the studied variables with the supercooling degree, in order to achieve a relationship that can be valid for different PCM in selected crystallization temperature ranges. A generalized model should be developed and validated to finally being able to use this kind of tools in application. However, a new characterization approach has been set from a practical and technical point of view. The knowledge gained can serve as a starting point to researchers willing to perform supercooling characterization of materials. Besides, can also work as a guide for the design of LHTES devices and their operation parameters, to be used with PCM materials that supercool.

Chapter 6 : LHTES system characterization and parametric study

6.1 INTRODUCTION

Remarkable aspects to take into account in the definition of a thermal storage device are scale (prototype, pilot unit), heat transfer fluid (HTF), geometry, construction materials, operational temperature range, thermal power, energy source or application, heat or cold storage . In a case of a latent heat thermal energy storage, the strategic choice of PCMs is added. Most researchers have centered their studies in the study of geometries, and thermal enhancement techniques [40], [67], [68]. In order to test the influence of geometry in the heat transfer, configurations such as shell and tubes, packed bed, plate, and others have been studied [32]. Despite the availability of several geometry types, shell and tube configuration has been commonly tested due to simplicity and compatibility with piping systems [17], [24], [32]. Shrivastava and Chakraborty [147], made a brief compilation of the available literature on the use of shell-and-tube heat exchangers for Latent Heat Thermal Energy Storage (experimental and numerical studies). They put into evidence that the configuration of a single tube in the shell is the most common type. Moreover, most of the studies consider laboratory prototypes of shell and tube heat exchangers.

In order to increase the thermal power of these systems, studies have been done to determine the influence of the operating parameters (inlet temperature, mass flow rate and direction of the HTF), the size of the tube and the shell, the use of multiple PCMs and the increase of the heat transfer surface with fins or matrixes [8], [71], [73], [148], [149]. Using multiple tubes inside the shell [150]–[154] instead of having a single tube, is also a good solution to improve the heat transfer but this configuration is not very often studied with industrial configurations.

Most studies mainly tested laboratory scale storage systems and center on obtaining the highest thermal performance. However, when it comes to higher scale devices the system feasibility of commercialization of the devices should be taken into account, to be sure that the technology could be used in the future at domestic, services or industrial sectors. Besides, the standardization of the performance parameters is also important to be able to compare the different solutions[147].

The international community working on the topic highlights this approach. The IEA Solar Heating & Cooling Programme, Task 42 " Compact Thermal Energy Storage" took place from 2009 to 2015 and dropped several conclusions [8].

- The need to couple the material properties to system performance for certain applications.
- To have a common basis for determining the performance of different storage technologies by means of more standardized and simplified system approaches and a set of Key Performance Indicators KPI's.
- The development of all components and system configurations should be more aimed at cost reduction of the final system

- Long term testing under real operating conditions.

Most recent task 58 "Material and Component Development for Thermal Energy Storage" which is active since 2017 has three main topics. One of them is the storage system implementation, focused on the performance of a storage within a heating or cooling system, including economic feasibility studies, case studies and system tests.

Therefore, the need of improving the LHTES economic feasibility has pushed the authors to think about alternatives to brand new design manufactured heat exchangers. The modification of commercially available heat exchangers is a potential solution. Researchers have previously adapted existing heat exchanger technologies to LHTES systems with different outcomes. Medrano et al. [73] compared three different commercial heat exchangers using PCM (paraffin) and water as HTF. Results were not very satisfactory. It raises the need of a correct design of systems for each application, so not simple modifications should be done, but understanding the thermal behavior and then taking that into account make big modifications as, modifying the number of tubes or its disposition in space. For it, the previous knowledge has to be gathered.

With the aim of providing further information about the adaptation of industrial heat exchangers into LHTES systems, the present chapter reports information of the thermal behavior of one commercial shell and tubes device adapted for the DHW and heating applications temperature range using commercially available paraffin as PCM. The originality of this study is to consider an industrial shell and (multi) tubes heat exchanger and to test the integration of PCM inside the shell to make it an efficient thermal storage system. The test plant, experimental campaign, analysis and results are described below.

6.2 EXPERIMENTAL METHODS AND DESCRIPTION

6.2.1. DESCRIPTION OF THE SYSTEM

The tests were carried out in the LaTEP facilities in the University of Pau and Pays de l'Adour, located in Pau, France. The pilot consists of a loop with a HTF thermal regulation device (Regloplas P180M/18), a modified shell and tubes heat exchanger (Ciat UDH 168 06C 2B F04), a coriolis flowmeter (Micro Motion – model ELITE CMF100, uncertainty < 1%), a volumetric flowmeter, valves and purge. The pilot scheme is shown in Figure 6. 1. The entire experimental device is separated from the rest of the room by a plexiglass enclosure for safety reasons.

The used HTF is liquid water. The water flows in the circuit connected to the HTF thermal regulation device in order to give the water the temperature, and pressure needed for the experiments. The pressure can be increased to maintain the water liquid in case of tests with high temperatures.

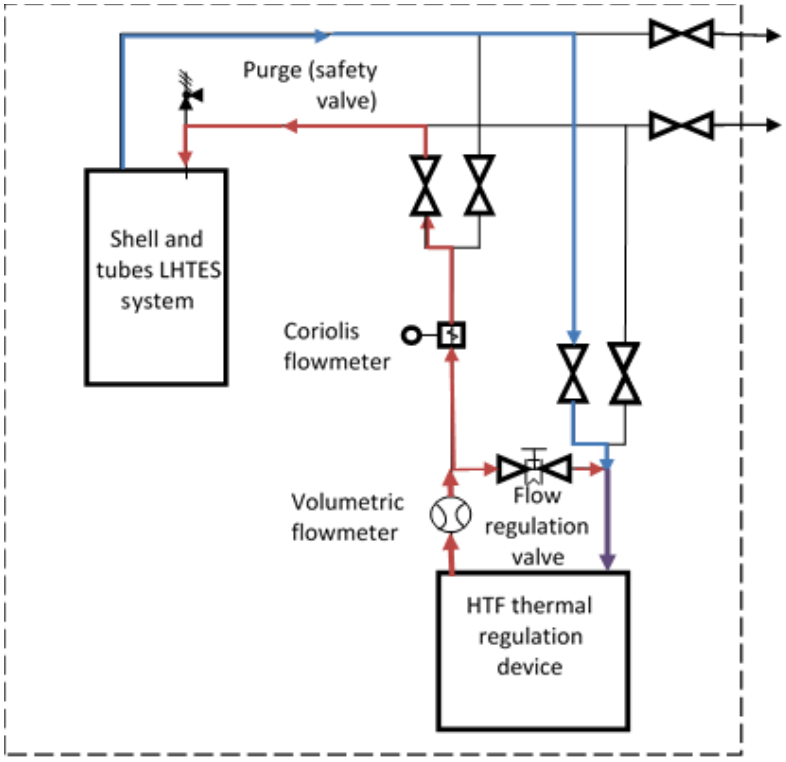

Figure 6. 1 Pilot scheme

Figure 6. 2 Modified LHTES system. a) outer shell without insulation b) tubes inside the shell c) insulated system

The shell and tubes LHTES system was adapted from a commercial heat exchanger (Figure 6. 2). It is configured by HTF inlet and outlet manifolds, 18 U-tubes where the HTF flows, and a shell filled with a PCM which covers the tubes. The tubes being bended in a Ushape, the HTF manifolds

are at the same side of the HEX. The construction material of the device is steel. The insulation materials are rock wool and aluminum foil cover. Table 6. 1 shows the dimensions of the LHTES.

Table 6. 1 Dimensions of the components of the LHTES system

Dimensions of LHTES		
Shell	Length	900 mm
	Diameter	168 mm
	Volume	8-10 L
U-Tubes	Inner Diameter	14 mm
	Outer Diameter	16 mm

With the purpose of analyzing the thermal behavior of the system, 19 T-type Thermocouples (accuracy ±0.1 °C) were used to monitor the temperature in certain points of the heat exchanger and surroundings. Thermocouples are placed at the inlet and outlet of the HEX to measure the HTF inlet and outlet temperatures, inside the shell (temperatures regarding the PCM), on the outer wall, and outside the HEX to measure room temperature. The thermocouples inside of the shell measure the PCM temperature and are in position using hose clamps fixed directly to the tubes. They are placed over three chosen sections in order to monitor the thermal behavior of the PCM. Each section (1, 2 and 3 in Figure 6. 3) had 5 thermocouples.

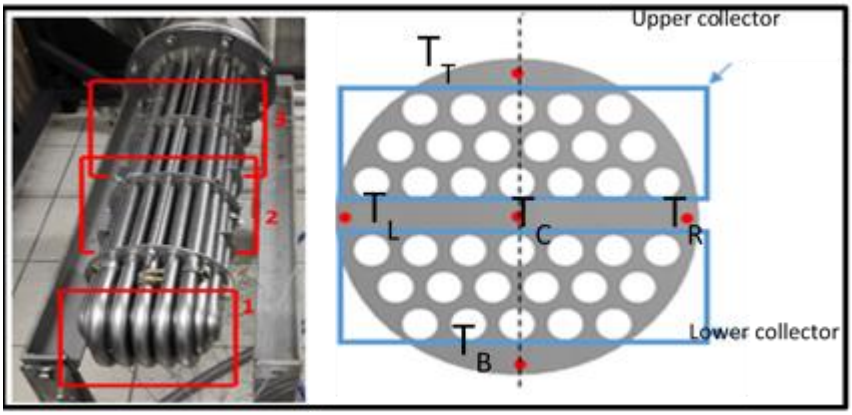

Figure 6. 3 Position of the thermocouples in the LHTES system

The installed measuring equipment is linked to an acquisition and interfacing system. The thermal regulation device is provided with a Profibus output allowing remote management of the test bench via a computer using the LabVIEW software. The temperature acquisition is carried out thanks to a CompactDAQ cDAQ-9188 chassis delivered by National Instruments and equipped with four NI-9213 sixteen-channel temperature acquisition modules.

The software interface makes it possible: the remote control of the installation to avoid the manual intervention by the operator in the secure enclosure when the experimental bench is in operation; personalized programs for temperature, pressure and mass flow rate changes; and finally, data recording during the experiments.

6.2.2. DESCRIPTION OF THE PCM

The present study focuses on the characterization of a storage system. Therefore, the PCM should be reliable and stable among time and cycling. Organic PCMs, such as paraffins are mainly used in the application temperature range due to their well-known thermal characteristics and reliability. Hence, a paraffin that meets the temperature parameter was used. The commercial name of the purchased wax is Rubitherm® RT-60 and corresponds to a melting point around 60°C, which is a suitable melting temperature for DHW and space heating application.

Table 6. 2 PCM properties

Rubitherm RT-60 properties	Typical Values
Temperature phase change range	53-60 °C
Latent heat	123.5 kJ/kg
Thermal conductivity	0.29 W/m.K
Density (solid)	880 kg/m^3
Density (liquid)	780 kg/m^3

The material thermal properties and density were experimentally determined in the UPV/EHU facilities in Bilbao, except for the density (value provided by Rubitherm®). A differential scanning calorimetry study was conducted to obtain the phase change temperature range, latent heat, specific heat and total enthalpy of the PCM at the study temperatures. A Mettler Toledo DSC1 was used for this purpose. Besides, the thermal conductivity was determined by the hot plate method using a THISYS conductivimeter from Hukseflux BV. The results are summarized in Table 6. 2 and Figure 6. 4.

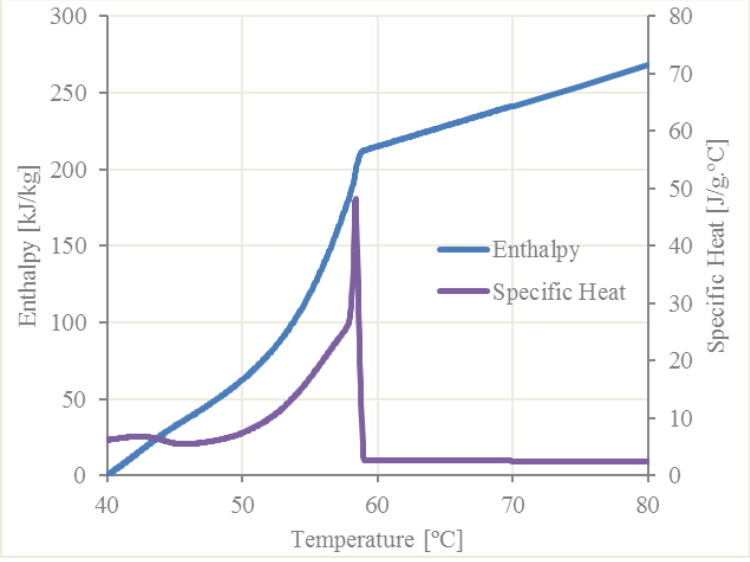

Figure 6. 4 Specific heat and total enthalpy of the PCM at the 40-80°C temperature range

6.2.3. LHTES SYSTEM SET-UP

The storage system described was previously modified, and preliminarily tested for a previous Ph. D. thesis [74]. The materials used was other PCM, concerning a different temperature range and potential application. The modifications done consisted on disabling the flow though the shell, by closing it to produce a closed container, installing the insulation and placing the thermocouples (inlet, outlet, and inside the shell).

Before starting the testing of the present study, some maintenance and refurbishment procedures were done in order to get the desired conditions.

In order to assure the optimal state of the water circuit the system was drained, and the water filter was cleaned. Besides, the by-pass valve that makes the control of the mass flow rate below the pump lower capacity (0.2 kg/min) possible was repaired.

Afterwards, the PCM used in the previous experimental campaign was removed by heating the material to a temperature higher than the melting temperature. Then, the liquid was emptied by the pipe located in the bottom of the shell. The remaining solidified material in the pipe was removed using a spatula (this zone was colder due to the direct contact with ambient). The mass of the removed PCM was weighted and the total amount previously introduced was confirmed to be retired from the HEX. Afterwards, the lower pipe was closed and solid grains of RT60 were introduced through a pipe located on the top of the shell. Water at 78 °C was circulating through the inner tubes, so that the paraffin could melt (liquid state occupies higher volume). A total of 7.11 kilograms of RT-60 paraffin were introduced in the shell and tubes HEX.

Next step was the calibration of the thermocouples that measure the inlet, outlet, wall and ambient temperatures. The calibration covered the temperature range from 0 to 200°C, particularly the calibration temperatures were: 0, 40, 60 80, 120, 160 and 200°C. For this purpose, a mixture of water and ice for 0 °C, and a block calibrator (Omega, model CL900A series) were used. Furthermore, a calibrated platinum RTD Pt100 sensor certified by UKAS (precision at 0 °C ±0.03 °C; precision at 100 °C ±0.08 °C) measured temperatures simultaneously. The accuracy of these thermocouples is confirmed to ±0.1 °C. The thermocouples placed inside the shell were not calibrated due to the difficulty to disassemble the HEX but because they are of the same type, the same accuracy is considered (±0.1 °C).

Insulation was improved during the first stages of the experimental campaign, when cold spots became evident. Some of the PCM temperatures in sections 1 and 3 of the HEX were up to 6 °C colder than the outlet temperature. The cold spots corresponded to the places where the supporting steel structure was in contact with the HEX as shown in Figure 6. 5. Rock wool was placed between the HEX and the structure. Even though the problem was reduced, temperatures on those cold spots never surpassed the outlet temperature. The structure material or structure configuration should be modified to avoid this problem.

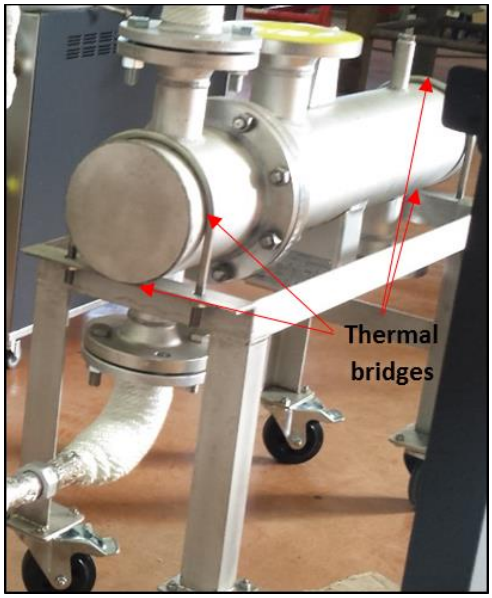

Figure 6. 5 Detail of the structure and HEX contact points causing thermal bridges

6.2.4. EXPERIMENTAL TESTING PROCEDURE

The experimental procedure consisted in monitoring complete charging and discharging processes. Each test started with the storage system being fully discharged (in the case of a charge test) or fully charged (in the case of discharge test). Water at the initial temperature and flow rate flowed through the internal u-shaped tubes until thermal equilibrium was reached. Then the experiment started by changing the temperature setpoint to the final temperature.

Different experimental conditions were tested to build a data-map of the performance variables such as charging/discharging time, power, and energy. These conditions are as follows:

- Flow rates:

  0.06 kg/s 0.09 kg/s 0.20 kg/s 0.40 kg/s 0.50 kg/s

- Initial and final temperatures:

  Charge:

  50-70 °C 50-8 °C 45-75 °C 40-70 °C 40-80 °C

  Discharge:

  70-50 °C 80-50 °C 75-45 °C 70-40 °C 80-40 °C

The LHTES system temperatures, HTF flow rate and ambient temperature were recorded every 10 seconds (Δt=10s).

6.3 THEORETICAL CONSIDERATIONS

One of the objectives of the analysis of the experimental charges/discharges is the determination of parameters regarding the energy being stored in the device, such as, the time needed to get a determined charge or discharge and the power at each moment.

For this purpose, the theoretical thermal energy that can be stored in the LHTES system is calculated, here on, *theoretical stored energy*. The value of the theoretical stored energy is needed to validate the results from the experiments, and to determine whether the system is charged or discharged by comparing the theoretical, with the actual stored energy values.

However, the fact that the insulation of the LHTES system is not perfect introduces another factor to take into account: thermal losses, which were determined for various temperatures of the LHTES system. Then, taking into consideration the energy that is transferred to the storage by the HTF, and the losses, an energy balance should be done to obtain the actual stored or released energy.

6.3.1. THEORETICAL STORED ENERGY

The total amount of energy that the LHTES system is capable to store is determined by the analysis of the different components that take part in the storage: PCM, HTF and LHTES system. Part of the energy is stored in form of latent heat, and a non-negligible amount of energy is stored in form of sensible heat. The stored latent heat is the energy from the PCM when the phase change occurs. The sensible heat is stored in the PCM (in the intervals before and after the phase change) and the HTF but also in the steel of the shell and tubes. The PCM stored energy is calculated using the specific enthalpy between the two ends of the selected temperature range, which is extracted from the results of the DCS (Figure 6. 4). Relevant information about the HTF and the HEX is given in Table 6. 3. Variations on the water and steel Cp values with temperature are very small, therefore considered constant.

Table 6. 3 Material properties for theoretical energy calculation

Material properties	*m [kg]*	*Cp [kJ/kg.K]*
HTF (water)	9.39	4.1862
HEX (steel)	52	0.47

The theoretical energy that the LHTES system is capable to store depends also on the temperature step/range of operation of the LHTES system, so that T_2 is the higher temperature and T_1 is the lower temperature during the charging or discharging processes. The equations 6.1 and 6.2 show the theoretical energy calculation.

$$Q_{Theoretical_{Stored}} = Q_{PCM} + Q_{HTF} + Q_{HEX} \quad (6.1)$$

$$Q_{Theoritical_{Stored}} = m_{PCM}\Delta h_{PCM} + m_{HTF} \cdot C_{p_{HTF}} \cdot (T_2 - T_1) + m_{HEX} \cdot C_{p_{HEX}} \cdot (T_2 - T_1) \quad (6.2)$$

For the studied temperature ranges, the stored theoretical energy is shown in Table 6. 4.

Table 6. 4 Theoretical energy of the temperature ranges tested

	50-70 °C	50-80 °C	45-75 °C	40-70 °C	40-80 °C
Theoretical energy [kJ]	2546	3178	3336	3628	4266

6.3.2. DETERMINATION OF THE SYSTEM ENERGY LOSSES

Theoretically, systems may be assumed as adiabatic systems. Nevertheless, real systems do have thermal losses to the ambient in some extent. In the study case, it was very difficult to get a well-insulated system because of the configuration of the structure holding the heat exchanger. These losses should be taken into account for the analysis of the experimental data.

For this purpose, the system energy losses were determined for the temperature range of 40 °C to 80 °C, every 5 degrees. These temperatures correspond to the lower temperature in the experimental campaign and the maximum operating temperature of the PCM as indicated by the manufacturer, respectively.

The procedure consisted in flowing water in the circuit at given temperatures for 12 hours (each step) to reach the steady state of the system. The tests performed had a mass flow rate of 0.06 kg/s, because at higher flow rate values the difference between the inlet and outlet temperatures of the HTF were smaller than the accuracy of the measurement at the steady state (±0.2 °C). Due to the high thermal resistance of the PCM and the insulation, it was considered that the HTF flow rate had a low influence in the losses. In addition, the losses were assumed similar in transient state than in steady state at the same temperatures.

Figure 6.6 shows the temperature profile of all thermocouple positions. Some temperatures show different behavior before and after the phase change (due to the change in the heat transfer main mechanism – convection or not inside the PCM). Most of PCM temperatures in steady state are noticeably lower than the outlet temperature, which implies great thermal losses.

Then, the losses were calculated using (equation 6.3), being the power at each temperature step in equilibrium.

$$\dot{Q}_{loss} = \dot{m} \cdot C_p \cdot (T_{in} - T_{out}) \qquad (6.3)$$

The power vs. temperature step data are shown in Figure 6. 6 (a) and (b). There are two tendencies. The orange points, corresponding to temperatures lower than the melting temperature, form a straight line, showing an increase of the losses with higher temperature up to the phase change temperature. Afterwards, the value becomes stable around 59 W. At a temperature higher than the melting temperature (60 °C), the heat transfers are not only by conduction but also by convection. Conduction is present in the solid phase and convection in the liquid one. It seems that the solid PCM is always present in the low insulated parts of the heat exchanger and change the tendency to a constant thermal loss value. The solid layer near

the wall of the HEX can play a role of insulation compensating for the increase in temperature of the HTF.

The ambient temperature also has an influence on the thermal losses. Thermal losses decrease when temperature steps match with higher temperature of the surrounding corresponding with daytime. Figure 6. 7. a shows the thermal losses values if all the steps are taken into account. Figure 6. 7. b shows the losses with ambient temperatures corresponding to night. Nevertheless, it is not possible to control or modify ambient temperature in the facilities. The worst scenario is assumed (lower ambient temperatures).

For the data analysis, the equation of a straight line corresponding to Figure 6. 7 a was used to describe the phenomenon when the mean storage system temperature was from 40 to 60 °C. Moreover, a constant value of 59 W was used with temperatures higher than 60 °C.

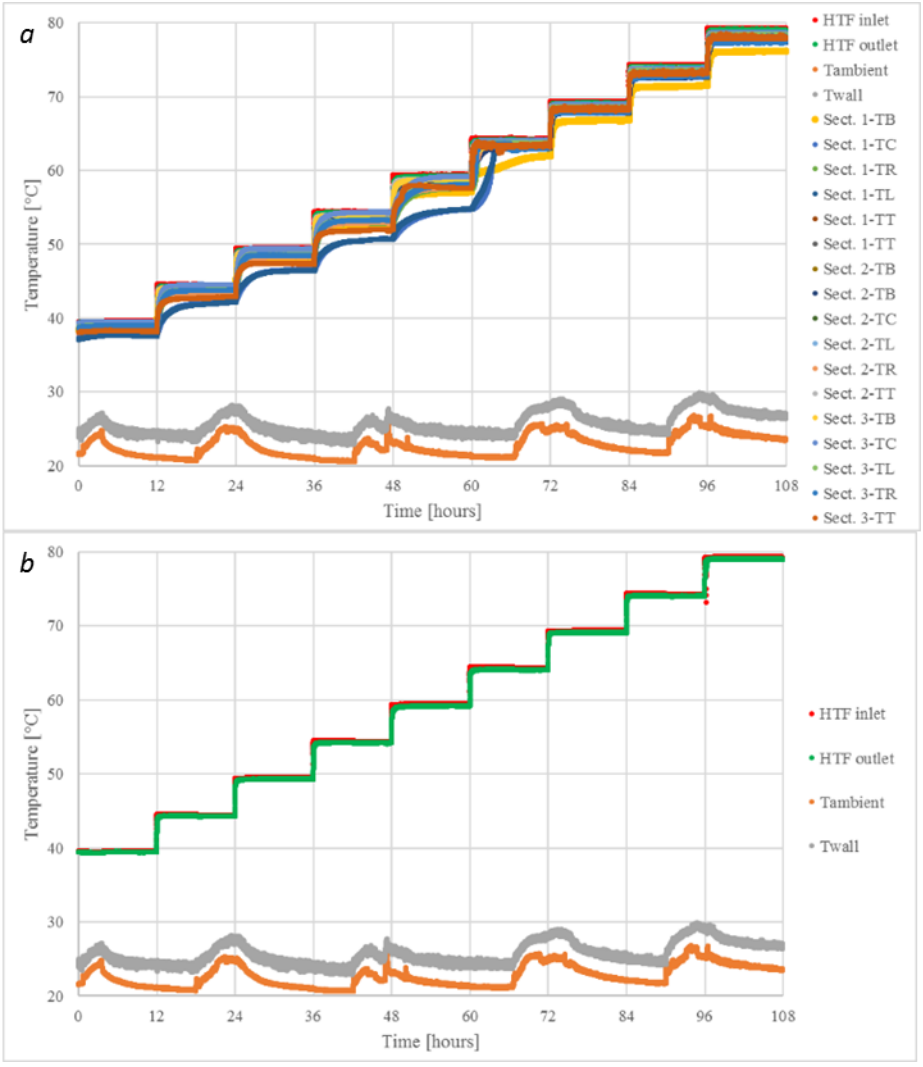

Figure 6. 6 Experimental temperatures a. All Measured temperatures b. Temperatures regarding HTF inlet, HTF outlet, ambient and insulation wall

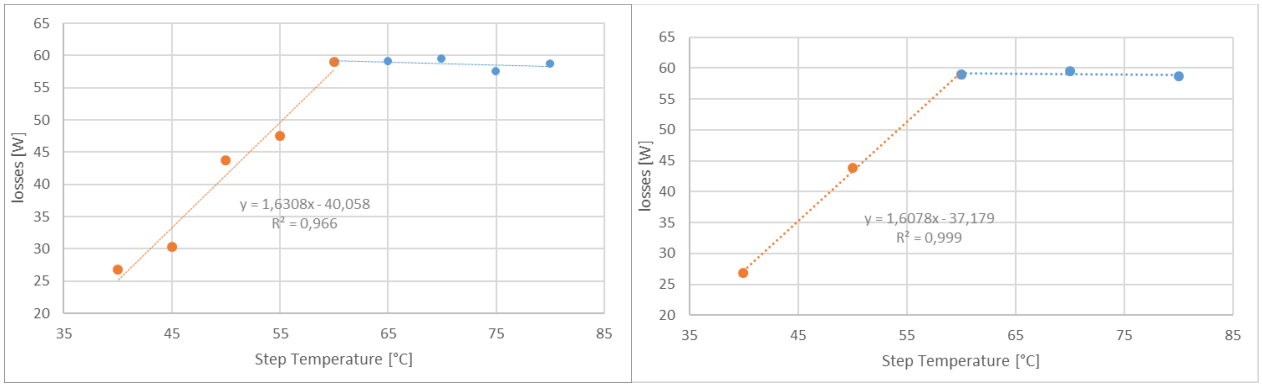

Figure 6. 7 System thermal losses vs. temperature a. Losses regarding all the studied points b. Values from losses obtained during night time

6.3.3. DETERMINATION OF THE REAL STORED ENERGY

Once the charging or discharging data is obtained the energy balance is used to determine the energy stored in each experiment. The transferred energy is the difference between the energy in the HTF at the inlet of the device, and the energy in the outlet (change in enthalpy between the inlet and the outlet of the HEX during the experiment). This energy transferred is not completely stored in the LHTES system as there are thermal losses with the ambient environment. The thermal energy losses were calculated from previous experiments (see paragraph 6.3.2). Finally, the way of calculating the real stored energy is indirect, by applying equation (6.4).

$$Q_{Stored} = Q_{Transferred} - Q_{Loss} \tag{6.4}$$

Where:

$$Q_{Transferred} = \int \dot{Q}_{transferred} \cdot dt = \Sigma\left[\dot{m} \cdot C_p \cdot (T_{in} - T_{out})\right] \cdot \Delta t \tag{6.5}$$

$$Q_{Loss} = \int \dot{Q}_{loss} \cdot dt \tag{6.6}$$

Afterwards, the real stored energy is compared to the theoretical stored energy to get a charging or discharging percentage at any time during the charge or discharge processes as shown in equation (6.7). In the discharge process, the values are negative.

$$Charge\% = \frac{Q_{Stored}}{Q_{Theoretical\,Stored}} \cdot 100 \tag{6.7}$$

6.4 RESULTS AND DISCUSSION

This section addresses the analysis and discussions of the data obtained from the experimental campaign. First, the charge and discharge modes are presented, and then the comparison of both.

The experimental results are valid when the difference between the HTF inlet and outlet temperatures remains above the accuracy limit of the set of thermocouples, which is ±0.2 K. Because of this, data obtained from flow rates 0.4 and 0.5 kg/s were discarded from the discussion. In these cases, the accuracy limit was reached when the charge/discharge percentage was too low to consider the charge/discharge completed in neither of the tests.

6.4.1. CHARGE MODE

In order to explain the phenomenon that takes place in the charge mode, one charging test is explained. The chosen experimental parameters were a 0.06 kg/s mass flow rate, and a 40-80 °C temperature range. Figure 6. 8 shows the typical temperature profile seen in all experimental charges, regarding the inlet and outlet temperatures. The HTF inlet temperature increases rapidly from the initial to the final value with time. However, the HTF outlet temperature follows a different evolution. It starts increasing, then it changes tendency during the phase change (starting from the melting temperature). Afterwards, it stabilizes at a temperature near to the final test temperature. It takes more time to reach the final temperature. The exchanged power is presented in the same figure. The power increases as the HTF inlet and outlet temperature difference increases, being maximum when the maximum temperature difference is attained. Then it decreases, as the temperature difference is decreased as well. It shows that high power is obtained in a very short period of time

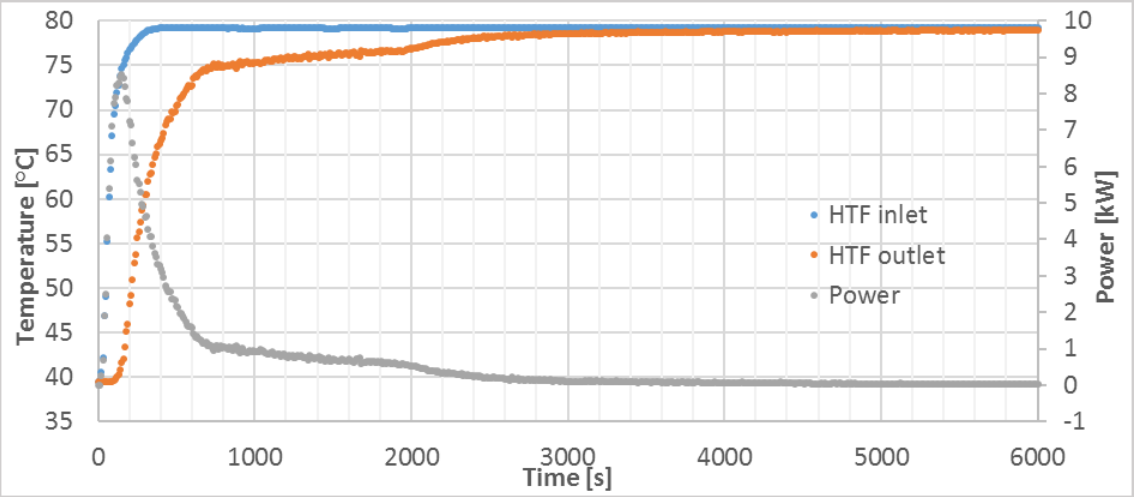

Figure 6. 8 Evolution of the HTF inlet and outlet temperatures and power with time, during charge mode (0.06 kg/s)

Figure 6. 9 shows the evolution of all the PCM temperatures inside the shell. The represented temperatures are from specific locations of the heat exchanger as shown in Figure 6. 3. The temperature trend with time is different for most thermocouples. Most of them take more time than the HTF to reach the final temperature. Furthermore, the final temperature is not reached in some cases, but a few degrees beneath (almost 5 degrees in the worst case). It is thought that this behavior is due to the situation of the measurement being near to the bad insulation spots (where the shell rests on the structure). So the melting/solidification processes are not finished in small problem areas when total charge is apparently achieved.

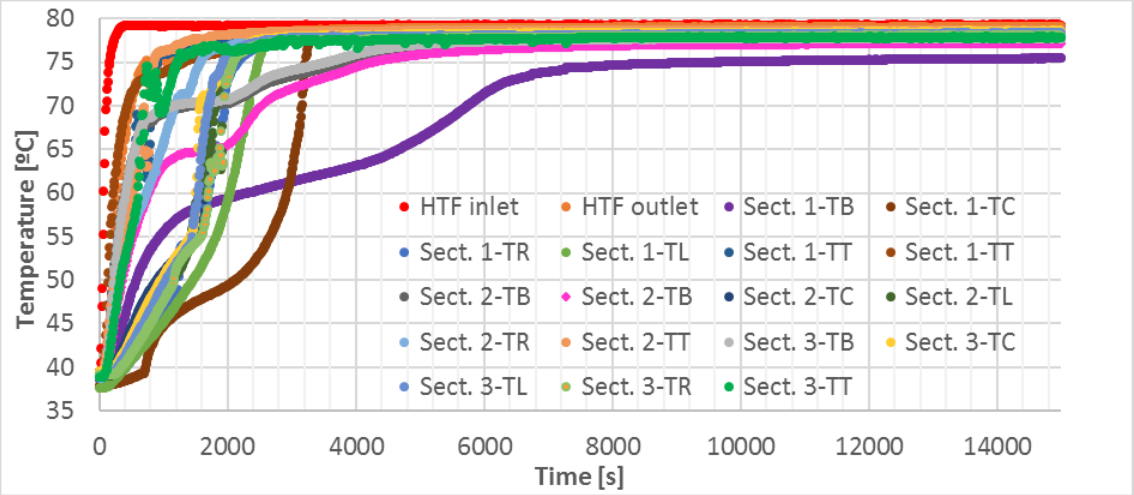

Figure 6. 9 Temperatures measured in the LHTES in charge mode (0.06 kg/s)

Figure 6. 10 shows the evolution of power and percentage of stored energy with time for the same experiment. Regarding the stored energy, the higher increase (steeper slope) matches the initial power sharp peak. After this peak the process achieved more than 60% charge. Then, the trend changes as the power decreases to get 90% of the charge, time needed to charge this final 10% increases threefold the time needed to charge the first 90%. Therefore, the total charge is not as efficient as a partial charge.

Figure 6. 11. shows the influence of the mass flow rate for the same temperature difference of the HTF. The duration of the charge mode decreases with the increase of the mass flow rate. Table 6. 5 summarizes the charging times needed for a 90% charge for several experimental tests.

The influence of the final temperature is highlighted. For the same flow rate, when this temperature increases, the charge mode is shorter. In fact, the temperature difference between this temperature and the melting temperature increases and it the same for the power.

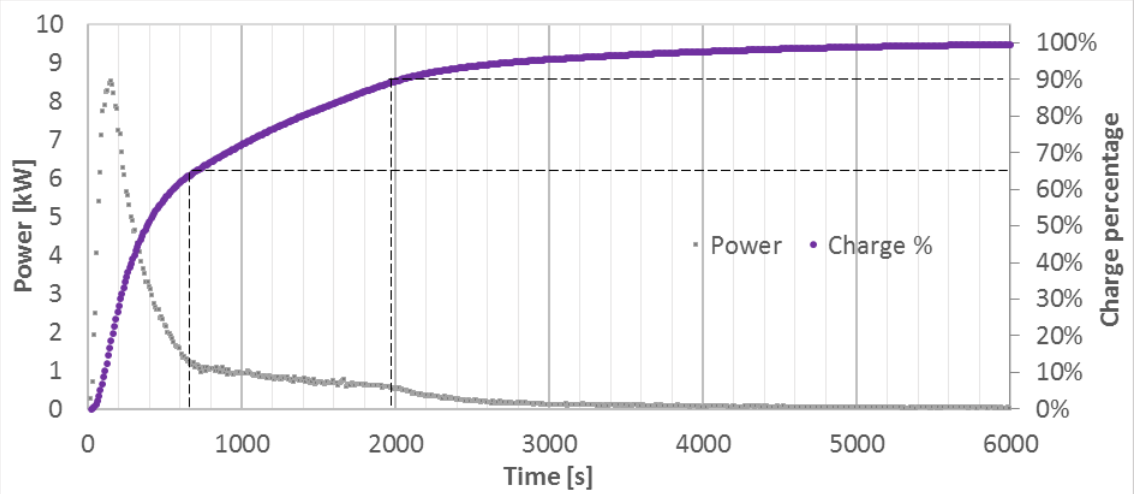

Figure 6. 10 Evolution of power and charging percentage with time (0.06 kg/s)

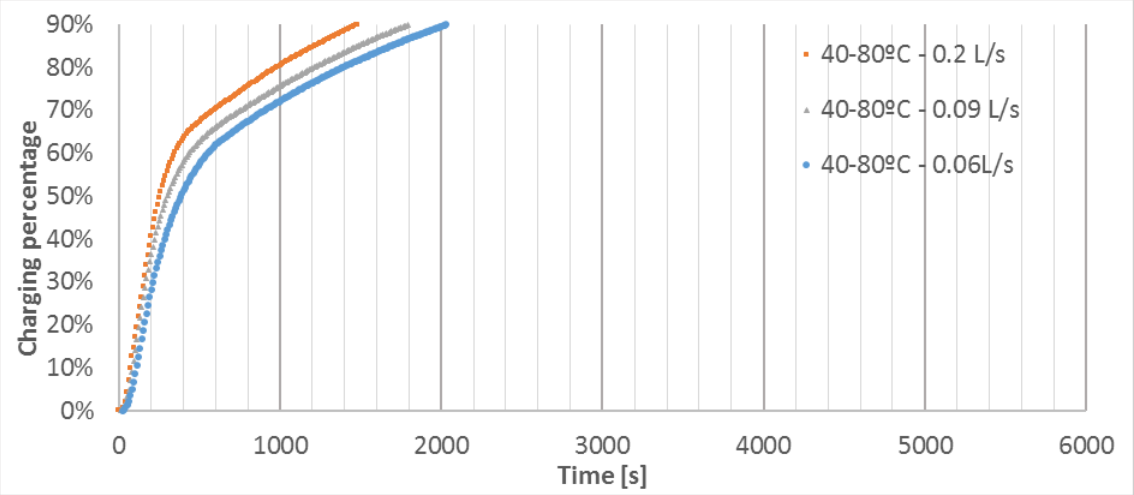

Figure 6. 11 Charging percentage of different flow rates with time

Table 6. 5 Time to reach 90% charge at different conditions

90% Charge time [s]		Temperature range			
		40-70 °C	***40-80 °C***	***50-70 °C***	***50-80 °C***
Flow rate	***0.06 [kg/s]***	2910	2000	3070	2020
	0.09 [kg/s]	2810	1770	2920	1890
	0.2 [kg/s]	2180	1460	1980	1490

Key performance indicators KPI values were gathered in order to get to know the device performance and to be able to compare it with other devices. The selected parameters were taken for values of 90% charge, which is the considered as a complete charge. The selected KPIs are: charging time, average power during the charge, and 5 minutes peak power which is the maximum value of the averaged power at time intervals of 5 min[152]. These parameters are shown in Figure 6. 12, Figure 6. 13 and Figure 6. 14.

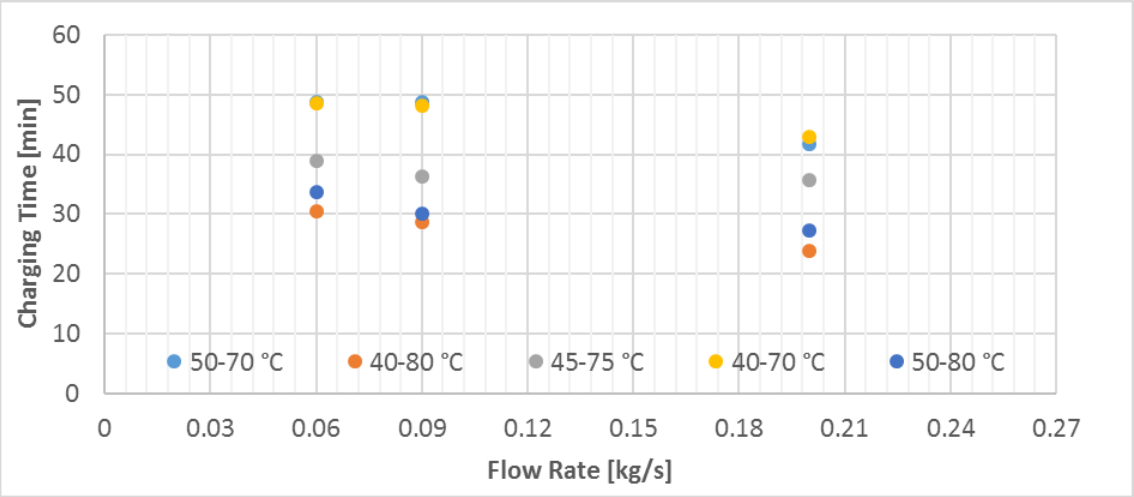

Figure 6. 12 Charging time versus flow rate

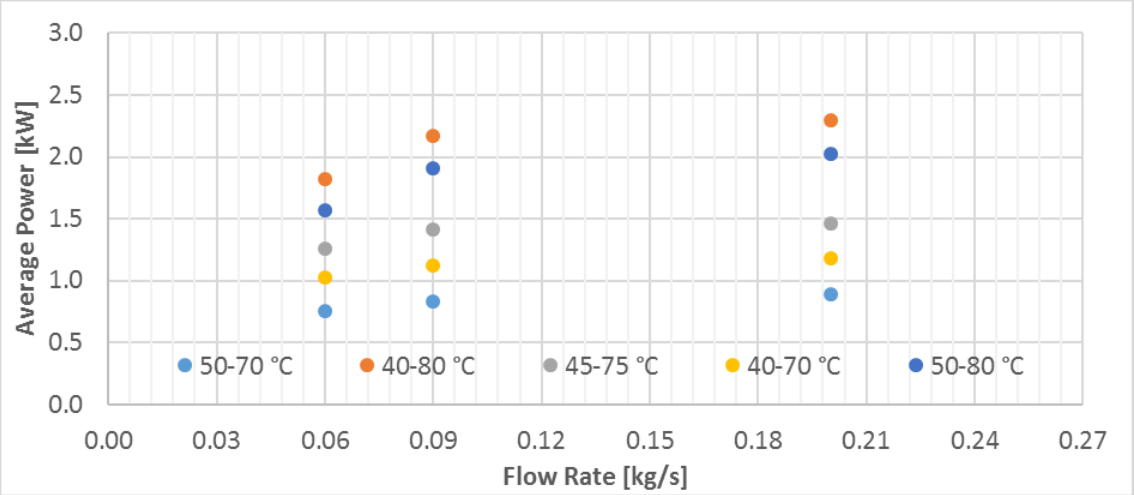

Figure 6. 13 Average power versus flow rate

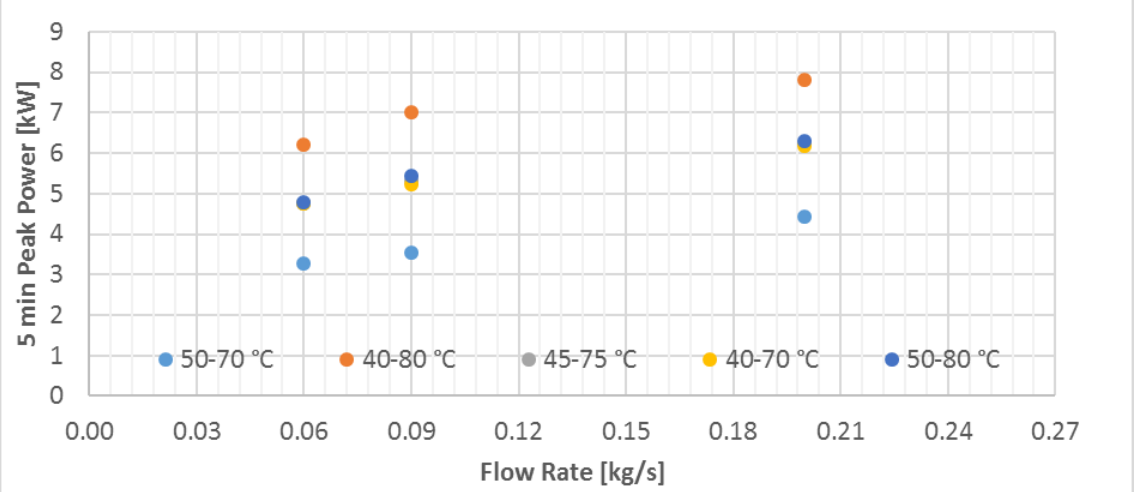

Figure 6. 14 5 minutes peak power versus flow rate

Taking into account all the performed experiments with different flow rates and initial/final temperature ranges, we can make the following remarks:

- The time needed to charge the device decreases when the flow rate increases, and so, the heat storage rate. The charging time is lower for the same flow rate when the power is increased with a higher temperature difference between the final temperature of the fluid and the melting temperature (60 °C). For the same temperature difference, the temperature interval with higher final temperature is faster.
- The heating power increases indeed due to a higher heat transfer coefficient inside the tubes with mass flow rate increase. For the same flow rate, average values increased with a higher temperature difference between the final temperature of the fluid and the melting temperature but being higher for those with lower final temperature interval. However, 5 minutes peak power values increased with higher temperature differences between starting and final temperature of the HTF. Values for 30°C temperature difference (40-70 °C, 45-75 °C, 50-80 °C) are very similar.

- The peak power to energy ratio, which provides a comparison between the 5-min peak power in relation to the energetic size of the energy store [152] also increases with mass flow rates. The higher the value is, the more efficient the heat exchanger is. However, in this case the storage capacity is low and the power distribution geometry is a sharp peak (great percentage of energy delivered very fast), which matches with the 5 minute peak power.

6.4.2. Discharge mode

Figure 6. 15 and Figure 6. 16, show the evolution of the inlet and outlet temperatures, power and discharged percentage with time of the discharge process concerning the 80-40°C and 0.06 kg/s experiment. In contrast to the charge mode, the discharge HTF inlet temperature evolution with time did not follow the initial and final set point temperatures. Due to a bad control of the HTF, temperature decreases more than the final programmed temperature and recovers afterwards. The HTF outlet temperature evolution follows the same tendency as the inlet. Because of the temperature disruption, it is not so easy to get clear information from these experiments. For this reason, full discharging percentages are not used to discuss the behavior of the device. Furthermore, the temperature difference between inlet and outlet reached the accuracy limit (± 0.2 K) for some experiments at 0.2 kg/s.

Figure 6.16 shows the PCM temperatures inside the shell. The descent of the temperature below the lower limit because of the regulation problem appears depending on the thermocouple situation/location. The PCM low thermal conductivity makes the cooling process slower, so thermocouples placed far from the tubes do not have time to perceive a punctual temperature variation. The heat transfer during the discharge mode inside the PCM is mainly conduction. The time needed by all the thermocouples to reach the final temperature is longer than in the charge mode.

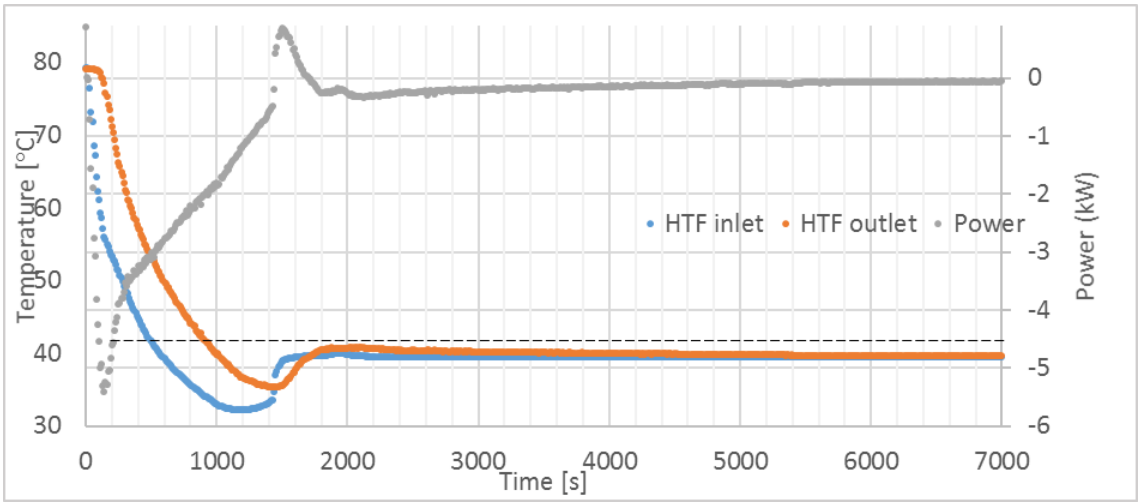

Figure 6. 15 HTF inlet and outlet temperatures and power with time for a flow rate of 0.06 kg/s for a discharge mode

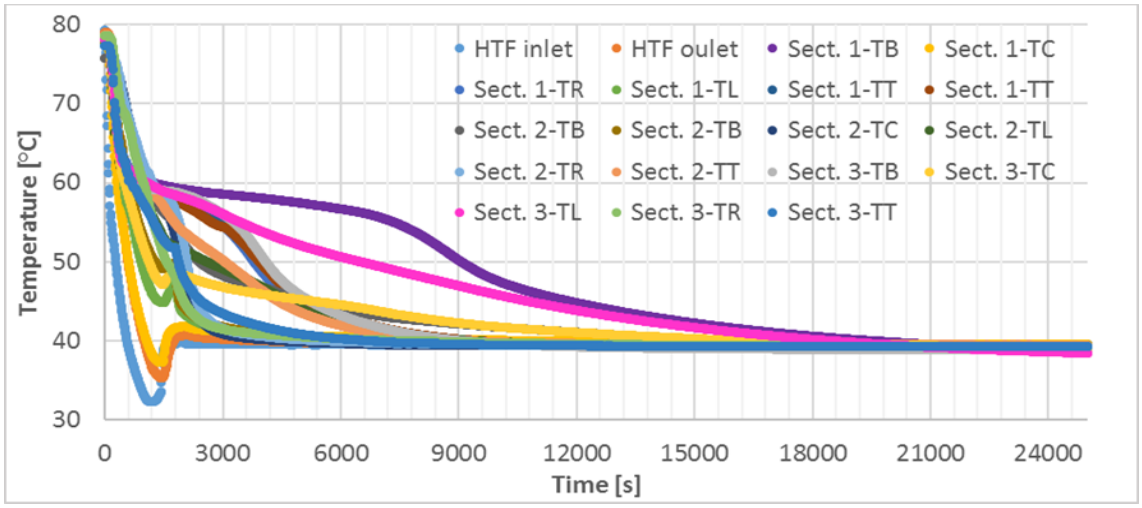

Figure 6. 16 Temperatures measured in the LHTES in discharge for a flow rate of 0.06 kg/s

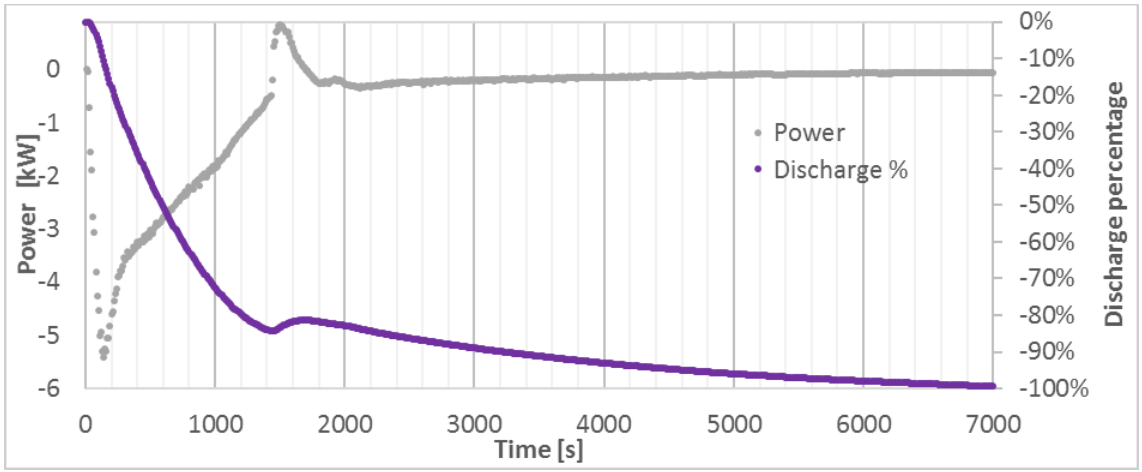

Figure 6. 17 Evolution of power and discharging percentage with time for a flow rate of 0.06 kg/s

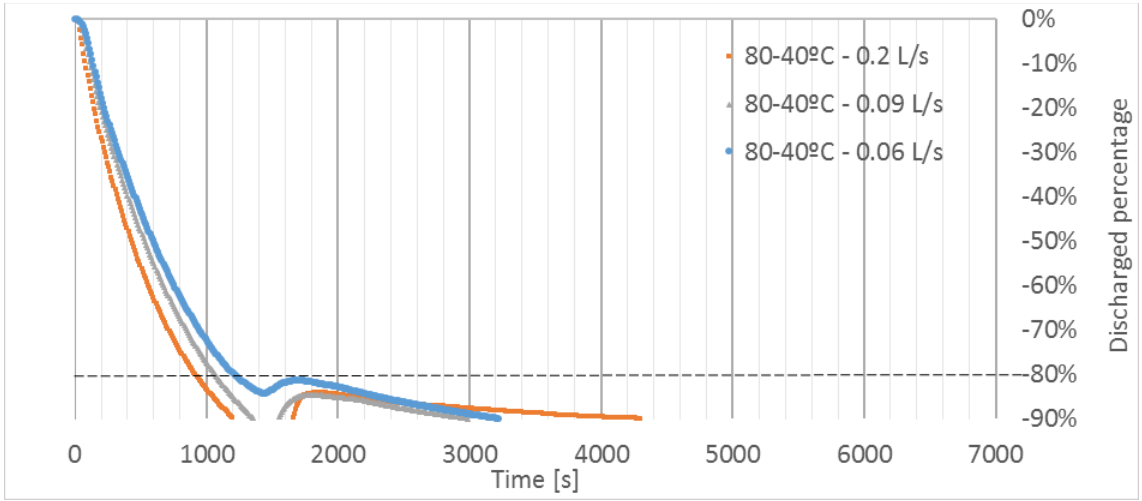

Figure 6. 18 Discharging percentage of different flow rates with time

Figure 6. 17 show the evolution of discharging power and percentage of energy released with time. The value of power is negative as it is the power that the system releases to the HTF. It

follows the same trend than the charge mode, coinciding the maximum power released with the maximum temperature difference reached. Therefore, as in the charging process, the higher discharging increase (steeper slope) matches the initial power sharp peak. Nevertheless, after the initial power peak, the regulation problem makes the temperature nor the power signals to be clean. In addition, the fact that the difference between inlet and outlet HTF temperatures rapidly reaches the accuracy limit (0.2 K) in the higher flow rates makes it difficult to extract results from the analysis of the obtained data. Then, the analysis of the discharging results should be assessed from the values before the disturbance and/or accuracy limit.

The experimental data from the discharges result in the following remarks:

- The time needed to have a determined percentage of discharged energy decreases when the flow rate increases. This trend can be seen in Figure 6.18, when 80 % of discharged energy is reached. (Example a discharge from the 80 °C as initial temperature and 40 C as final temperature with different flow rates).
- The charging time decreases for the same flow rate with higher temperature differences between the initial temperature of the fluid and the melting temperature (60 °C). Table 6. 1 shows the time needed for experiments in different conditions to get the 65% discharge.

Table 6. 6 Time to reach 65% discharge at different conditions

65% Discharge time [s]		**Temperature range**			
		80-40°C	***80-50°C***	***70-50°C***	***70-40°C***
Flow rate	***0.06 [kg/s]***	860	800	940	750
	0.09 [kg/s]	820	620	640	740
	0.2 [kg/s]	640	510	540	660

6.4.3. COMPARISON OF THE CHARGE AND DISCHARGE MODE

If the charge mode and discharge mode are compared for the same operational conditions some differences can be assessed:

- More time is needed for the discharge mode. During crystallization the heat is transferred by conduction within the layer of solid phase around the tube. The heat transfer is less effective than for the melting process, which is driven by both conduction and convection. The fact that it takes longer in time, results in the power signal being wider, and the maximum power is lower. Table 6. 7 shows the charging and discharging times for 50-80 °C at various flow rates.

Table 6. 7 Comparison of 80% charge and discharge times

80% Charge/ Discharge time [s]		**Temperature range**	
		50-80 °C	***80-50°C***
Flow rate	***0.06 [kg/s]***	1370	2500
	0.09 [kg/s]	1250	2130
	0.2 [kg/s]	1000	2200

6.5 CONCLUSIONS

A LHTES system modified from an industrial shell and tubes heat exchanger, containing RT60 as PCM, was tested in order to get to know the thermal behavior for the temperature ranges according to DHW and heating applications. A complete experimental campaign was performed with different flow rates and initial/final temperatures.

Data from the tests done at flow rates, 0.4 and 0.5 kg/s, were discarded because the inlet-outlet temperature difference reaches too soon the accuracy limit (0.2 K) which made the results non-reliable and made impossible to extract valid information from them. Data from the 0.06, 0.09 and 0.2 kg/s flow rates were analyzed. Taking into account the accuracy limit parameter, complete charges could be analyzed. But no complete discharges were achieved because of problems of regulation. Besides, 90% charges were considered more efficient because they take one third of the time it takes to get 100% charge.

In the both charge and discharge modes, the charging/discharging time decreases with higher flow rates. And, with the same flow rate, time decreases with the lowest or highest final temperatures. If charge and discharge processes from the same operational conditions are compared, it could be seen that the discharge process takes more time to finish. The difference in the charging and discharging behavior is given by the PCM melting being a process powered by mainly convection and conduction, and by the solidification process only driven by conduction. These results follow the expected tendency.

As a conclusion, the studied LHTES that was adapted from an industrial heat exchanger can be used to store latent thermal energy. However, the results are not ideal. The LHTES system volume for PCM is low compared to the HTF volume. So, the quantity of latent energy is low. Moreover, the small difference between the inlet and outlet temperatures of the HTF shows that the heat transfer between the PCM and the HTF is not very good. To improve the efficiency of this kind of devices, modifications improving the quantity of PCM and the heat transfer should be done. For this reason, a CFD modeling should be done to help the understanding of these results. Complementary studies should be done in order to determine the best parameters of modification that could be done in order to increase the energy quantity and the power. For example, one idea is to reduce the number of tubes, or the diameter of the tubes. For further studies, the insulation and control towards cooling should be improved.

Chapter 7 : Conclusions and future work

This project seeks the goal of contributing to the LHTES technology by working on both PCM materials and storage systems that are technically and economically viable for their integration in hot water and space heating applications in buildings, intending to increase the profitability of these type of plants and thus promoting their development. The vision includes an efficient storage system fitted with an economically feasible thermal storage device and a sustainable PCM. Both the PCM and the thermal storage devices had been identified from previous research works, i.e. the PCM is the urea-Sodium nitrate (U-SN) eutectic mixture, while the thermal storage device consists of a commercial shell and tubes heat exchanger. The original objectives included the analysis of the PCM behavior and its reliability under long term operational conditions and the definition of the optimum heat-management conditions in the selected LHTS system. The thesis research approach follows a path to reach the proposed objectives.

One of the main objectives is the study of the long-term behavior of the urea-Sodium nitrate (U-SN) eutectic mixture in the operating conditions encountered on a latent heat thermal storage system. This includes determining technical aspects regarding thermal degradation, supercooling and phase segregation. The material characterization serves to evaluate the use feasibility of the mixture as a PCM regarding its long-term use and the heat-extraction efficiency. Testing and analysis methodologies were developed to carry out a research approach based on operational representative conditions, rather than the traditionally employed fast laboratory tests used for PCM characterization.

The LHTES device consists of an industrial shell and tubes heat exchanger. The thermal behavior was characterized by a parametric campaign to provide a good knowledge of the operational behavior. The initially scheduled objectives included the development of a model to fit to the parametric campaign results. The model purpose was to serve for defining the required modifications to the commercial device, following a scientifically based approach. Unfortunately, time constrains hindered the achievement of this objective.

7.1 CONCLUSIONS REGARDING THE PCM STUDY

Hygroscopicity

The hygroscopicity behavior of the urea and Sodium nitrate eutectic mixture was assessed by measuring the moisture content of the samples under various storage conditions. Results indicate that the samples prepared in a closed container and solidified at environmental conditions have a low initial moisture content, low enough to show a negligible thermal properties change in comparison with fully dried samples.

When samples are stored in open atmosphere, exposed to humid air, they absorb water. As a result of the water absorption a change takes place on the original crystalline structure, as revealed by XRD analysis. One or several new phases form and coexist with the original phases. The new phase/s have not been identified because the analysis system did not identify any compound that could correspond to the obtained spectrum in the Powder Diffraction File (PDF) database. The unconfirmed hypothesis is that the unidentified species is a urea-water phase.

This leads to the fact that the original eutectic binary mixture become a ternary after water absorption, and the eutectic composition might presumably have changed accordingly. The hypothesis has not been confirmed, not being the objective of this thesis.
The thermal studies carried out in the samples stored in open atmosphere showed a decrease in the melting temperature, which reduced from the original melting temperature 85 °C to 45 °C. Similarly occurred with the latent melting enthalpy. These results agree with the presumption of a new eutectic ternary system, which is coherent with the present knowledge about the urea-water systems phase diagrams.

The PCM with a large humidity content can be easily dried. After drying, the original properties are recovered. The use of a traditional desiccating agent in a close container, for a short time, is a procedure good enough to recover the original properties.

The results indicated that the thermal properties of the U-SN eutectic mixture did not change if the water uptake was below 0.17 %. To attain a water content below this level the eutectic mixture can be prepared under normal environmental conditions without the need of any atmosphere control. To prevent water uptake after the mixture is ready, storage cabinets with desiccating agents or dry atmospheres should be used. Either, humid materials could be desiccated prior to their usage or final use preparation by a short time in contact with desiccating agents.

These results indicate that the LHTS device should assure closure tightness to prevent atmosphere-humidity to become in contact with the PCM. Finally, the recommendation to produce bulky pieces when the material requires to be stored for a long term before being introduced in the adequate LHTS device, because the water absorption rate depends on the surface-to-volume ratio.

Thermal Degradation

The study of the mixture thermal degradation was carried out from a perspective different from the most widely employed accelerated thermal cycling. The proposed methodology consisted of holding dry U-SN eutectic molten samples inside a heating cabinet at 100 °C for different periods, up to one year. Thermal and compositional analysis were performed to determine the degradation procedures and assess the reliability of the mixture long term use.

The results indicate that after one year the melting temperature decreased in 10 °C (from 85 °C to 75 °C), while the latent enthalpy decreased by 24% (from 165 J/g to 125 J/g). The energy storage density after 1 year at 100 °C is 177.5 KJ/dm^3. These degradation results would be discouraging if they were lineal. However, the obtained values-decrease occurred in the first 40 days. From that period onwards it remained unchanged for one year. In the assumption that this trend remains stable in longer time-periods, the studied material can be considered valid (regarding the thermal stability) for long term use. The thermal storage density in those conditions is 177.5 KJ/dm^3. More research is required to confirm the long term stability of the mixture.

The cause for the thermal properties decrease was the urea thermal decomposition to produce other compounds: biuret and cyanuric acid. The formation of these products was accompanied

of a certain mass loss, which in turn had a huge relevance in the material degradation. Despite the fact that the maximum mass loss after one year at 100 °C was only 2.2% of the initial mass, it accounts for nearly 25% of its thermal storage capacity. It was experimentally determined that when a gas-tight device is employed, the urea and Sodium nitrate eutectic mixture reaches the decomposition-reaction equilibrium and the process stops while, if the container is opened the equilibrium cannot be reached because some of the reaction products are gases. The long lifespan of the urea and Sodium nitrate eutectic mixture as a PCM is therefore determined by the use of a gas tight system where the product evolution stops when the ammonia equilibrium pressure is reached. Further studies should effectively determine the system equilibrium pressure, evaluate the feasibility of obtaining an effectively closed system and the compatibility of the PCM and ammonia with the potential containers.

The study highlights the importance of having a strict control of the handling and experimental parameters to prepare the system. Parameters such as the mass loss and the water-uptake have a great influence in the degradation and thermal behavior of this system.

Phase Segregation

When the U-SN eutectic mixture was employed in thermal cycling conditions (in samples greater than 4 g), phase segregation occurred. Three components formed when the material was above the melting temperature, a solid white material on the bottom of the containers, a solid white material on top of the container, and the liquid in between them. The occurrence and degree of the phase segregation depends on the microstructure attained, which in turn depends on the cooling rates during the solidification stage upon thermal cycling. Higher cooling rates showed less phase segregation than slower cooling rates. This behavior can be explained by the microstructure morphology.

The U-SN eutectic corresponds to a faceted/faceted type eutectic-microstructure, which implies that the urea and the Sodium nitrate phases do not crystallize in a cooperative manner, but separately. Non-reciprocal nucleation was observed. The primary urea phase crystallization does not promote the crystallization of the Sodium nitrate, resulting in coarser urea crystals and producing a microstructure similar to that of hypoeutectic compositions.

As a result of the non-reciprocal nucleation, the urea crystallizes in the first place. Then, Sodium nitrate poses a higher supercooling degree than urea. However, only one recalescence event was recorded in the experiments, in disagreement with the foreseen thermal behavior according to the consulted bibliography. There is not a conclusive explanation to this finding, which could be due to a supercooling degree difference too small to be experimentally determined. The hypothesis of a small supercooling-degree mismatch between the two obtained phases is bolstered by the fact that, under fast cooling rates the microstructure formed is composed of large urea primary crystals and a homogeneous metastable phase, instead of forming the Sodium nitrate eutectic microconstituent. According to the observations carried out in the SEM, this metastable phase is deemed to be supersaturated urea, from which the Sodium nitrate crystals precipitate by diffusion when the temperature is high enough to promote it.

Highly homogeneous microstructures formed when the liquid material was quenched under high cooling rates. Small crystals were obtained, forming a microstructure different to the microstructure formed under slow cooling rates, composed of large size crystals corresponding to the equilibrium phases, large enough to be observed by visual inspection. Literature supports that higher crystal size results in higher phase segregation and therefore, slower cooling rates respond to higher phase segregation.

Natural convection is not likely to determine the occurrence of phase segregation, but it could serve as a co-mechanism by which the segregated mixture separates because of the density difference. Thermal cycling tests carried out with the sample in horizontal and vertical arrangements yielded similar results in terms of segregation. Therefore, natural convection does not play an important role in the studied process phase segregation. However, it cannot be discarded that its role may be significant in higher volumes.

It was confirmed that the segregated samples recombine to form the original mixture by mixing the three segregated constituents, the two solids and the liquid, aided with mechanical stirring or with other stirring means. The regenerated mixture presented similar thermal properties to a fresh non-cycled eutectic mixture and, therefore the utilization as a PCM is feasible after the segregate is re-mixed. XRD diffraction confirmed that the phases present were urea and Sodium nitrate in the eutectic proportion.

It is concluded, the phase segregation of U-SN eutectic could be reduced by using fast cooling rates for the discharging process, although the possibilities for complete prevention seem unfeasible. However, the material potential-use after segregation is possible if a suitable stirring means is implemented in the system.

Supercooling

The U-SN eutectic mixture presents a supercooling degree ranging from 3.2 to 51 °C. A wide study including different container morphologies, cooling rates, heat transfer fluid (HTF) materials and PCM mass rendered results which were treated according to a variable-analysis to determine of the relevance of process parameters, other than the PCM characteristics, in the PCM supercooling. To carry out the study, in addition to the U-SN eutectic mixture, a different PCM was also used, PEG 10000. The supercooling degree of PEG 10000 ranged from 6.26 to 10.77 °C, in the experimental conditions.

The study gives evidence that the most relevant parameter to determine the supercooling degree is the HTF cooling rate and the characteristic length ratio of the container. In contrast to the PCM cooling rate or process time, the HTF cooling rate and the container characteristic length are process variables that can be controlled or acted on directly. There might be freedom in the variation of some of the parameters, but not in all of them. For example, the medium cooling rate may not be modified in some cases due to the process nature. In that case, the container geometry should be the parameter to take into account in order to reduce the supercooling degree.

The main conclusion highlights the importance of the container geometry, or the PCM mass disposition, regarding the supercooling degree on the contrary to the widely reported broad idea that the mass quantity determines the supercooling degree. Above a certain mass quantity level, the influence of the mass-quantity is negligible, but the influence on the geometrical distribution of the mass is very large. This level has not been determined, but the experiments carried out determined that any mass required for industrial or commercial purposes will stay above that level. Only the tiny mass employed on the DSC crucibles provided a different behavior.

The second large contributor to determine the supercooling degree is the HTF heat transfer coefficient, which is related to the heat transfer from/to the container surface.

The correct combination of the geometrical design and the HTF selection in the LHTES devices can assure the system to operate under a certain level of supercooling degree.

A linear correlation describes the supercooling degree in the experimental conditions for the U-SN eutectic and for the PEG 10000. A final model for all the experimental results, including both materials fitted with a 0.8538 R-squared value. It was not possible to establish a law to perfectly predict the supercooling phenomenon in different materials, but the methodology was able to assess which are the process variables that can be used with this aim, because of the high relevance and dependency encountered in the study. Further research is needed to completely understand the interaction of the studied variables with the supercooling degree, in order to achieve a relationship that can be valid for different PCM in different crystallization temperature ranges. The definition of a generalized model and its validation could provide a huge step forward to define proper design guidelines to LHTS systems.

The work carried out in this thesis has provided a new characterization approach to study the supercooling phenomenon in a macro-scale, for real applications, from a practical and technical point of view. The knowledge gained can serve as a starting point for researchers willing to perform supercooling characterization of materials. Besides, it can also work as a guide for the design of LHTES devices and their operation parameters, to be used with PCM materials exhibiting supercooling.

Summarizing remarks

Several considerations should be taken into account for the potential use of U-SN eutectic as a PCM:

The U-SN eutectic mixture should be prepared in controlled conditions for the mixture to have a water content below 0.17%.

The design of the LHTS device should take into consideration that the U-SN eutectic mixture must be contained under gas-tight conditions to avoid mass loss and to prevent thermal degradation.

The LHTS designed for the U-SN eutectic mixture should include a stirring or mixing system to prevent the phase segregation.

The LHTS design for each application should take into account the HTF cooling rate and characteristic length ratio in order to guarantee a low supercooling degree.

Further research should be done in order to design and build a prototype to be used with U-SN eutectic that meets these characteristics. The evaluation of the proposed solutions for the PCM use should be evaluated in order to finally confirm the material feasibility.

7.2 CONCLUSIONS REGARDING THE LHTES SYSTEM CHARACTERIZATION

An LHTES system modified from an industrial shell and tubes heat exchanger was tested containing a well known paraffinic PCM. This PCM was selected for its high reliability and well known characteristics, thus avoiding interferences from the material-related scattering that could occur if the U-SN eutectic mixture would have been used. The objective was to characterize the thermal behavior for the temperature ranges according to DHW and heating applications. A complete experimental campaign was performed with different flow rates and initial/final temperatures.

Data from the tests done at flow rates, 0.4 and 0.5 kg/s, were discarded because the inlet-outlet temperature difference reaches too soon the accuracy limit (0.2 K) which made the results non-reliable and made impossible to extract valid information from them. Data from the 0.06, 0.09 and 0.2 kg/s flow rates were analyzed. Taking into account the accuracy limit parameter, complete charges could be analyzed. But, no complete discharges were achieved because of problems of regulation. Besides, 90% charging percentage was considered more efficient because it takes one third of the time it takes to get a 100% charge.

In both charge and discharge modes, the charging/discharging time decreases with higher flow rates. And, with the same flow rate, time decreases with the lowest or highest final temperatures. If charge and discharge processes from the same operational conditions are compared, it could be seen that the discharge process takes more time to finish. The difference in the charging and discharging behavior is given by the PCM melting being a process powered by convection and conduction, and by the solidification process only driven by conduction. These results follow the expected tendency.

As a conclusion, the studied LHTES that was adapted from an industrial heat exchanger can be used to store latent thermal energy. However, the results are not ideal. The LHTES system volume for PCM is low compared to the HTF volume. Therefore, the quantity of latent energy is low. Moreover, the small difference between the inlet and outlet temperatures of the HTF shows that the heat transfer between the PCM and the HTF is not very good.

To improve the efficiency of this kind of device, modifications improving the proportion of PCM and the heat transfer should be done. For this reason, CFD modeling is needed to help the understanding of these results. Complementary studies should be done in order to determine the best parameters of modification that could be done in order to increase the energy quantity and power. For example, to reduce the number of tubes, or the diameter of the tubes. For further studies, the insulation and control towards cooling should be improved.

Chapter 8 : References

[1] IEA, 'IEA data and statistics', 2019. [Online]. Available: https://www.iea.org/data-and-statistics.

[2] I. Dincer, 'On thermal energy storage systems and applications in buildings', vol. 34, no. August 2001, pp. 377–388, 2002.

[3] I. Dincer, 'Thermal energy storage systems as a key technology in energy conservation', *Int. J. Energy Res.*, vol. 588, no. January 2001, pp. 567–588, 2002.

[4] L. F. Cabeza, a. Castell, C. Barreneche, a. de Gracia, and a. I. Fernández, 'Materials used as PCM in thermal energy storage in buildings: A review', *Renew. Sustain. Energy Rev.*, vol. 15, no. 3, pp. 1675–1695, Apr. 2011.

[5] H. Mehling and L. F. Cabeza, *Heat and cold storage with PCM*. 2008.

[6] G. A. Lane, *Solar Heat Storage: Latent Heat Material*. Boca Raton: CRC Press, 2017.

[7] H. Nazir *et al.*, 'Recent developments in phase change materials for energy storage applications: A review', *Int. J. Heat Mass Transf.*, vol. 129, pp. 491–523, 2019.

[8] A. Hauer *et al.*, 'IEA SHC Task 42 / ECES Annex 29 – A Simple Tool for the Economic Evaluation of Thermal Energy Storages', *Energy Procedia*, vol. 91, pp. 197–206, 2016.

[9] D. Aydin, S. P. Casey, and S. Riffat, 'The latest advancements on thermochemical heat storage systems', *Renew. Sustain. Energy Rev.*, vol. 41, pp. 356–367, 2015.

[10] V. Palomba and A. Frazzica, 'Comparative analysis of thermal energy storage technologies through the definition of suitable key performance indicators', *Energy Build.*, vol. 185, pp. 88–102, 2019.

[11] J. Lizana, R. Chacartegui, A. Barrios-Padura, and C. Ortiz, 'Advanced low-carbon energy measures based on thermal energy storage in buildings: A review', *Renew. Sustain. Energy Rev.*, vol. 82, no. November 2017, pp. 3705–3749, 2018.

[12] G. Krese, R. Koželj, V. Butala, and U. Stritih, 'Thermochemical seasonal solar energy storage for heating and cooling of buildings', *Energy Build.*, vol. 164, pp. 239–253, 2018.

[13] J. Sunku Prasad, P. Muthukumar, F. Desai, D. N. Basu, and M. M. Rahman, 'A critical review of high-temperature reversible thermochemical energy storage systems', *Appl. Energy*, vol. 254, no. October 2018, p. 113733, 2019.

[14] R. J. Clark, A. Mehrabadi, and M. Farid, 'State of the art on salt hydrate thermochemical energy storage systems for use in building applications', *J. Energy Storage*, vol. 27, no. November 2019, p. 101145, 2020.

[15] J. Lizana, R. Chacartegui, A. Barrios-padura, J. M. Valverde, and C. Ortiz, *Identification of best available thermal energy storage compounds for low-to-moderate temperature storage applications in buildings*, vol. 68, no. 331. 2018.

[16] M. E. Zayed *et al.*, 'Recent progress in phase change materials storage containers: Geometries, design considerations and heat transfer improvement methods', *J. Energy*

Storage, vol. 30, no. February, p. 101341, 2020.

[17] L. Kalapala and J. Krishna Devanuri, 'Influence of operational and design parameters on the performance of a PCM based heat exchanger for thermal energy storage - A review', *J. Energy Storage*, vol. 20, no. 1, pp. 497–519, 2018.

[18] Z. A. Qureshi, H. M. Ali, and S. Khushnood, 'Recent advances on thermal conductivity enhancement of phase change materials for energy storage system: A review', *Int. J. Heat Mass Transf.*, vol. 127, pp. 838–856, 2018.

[19] P. Larrinaga, G. Diarce, Á. Campos-Celador, and A. García-Romero, 'Parametric characterization of a full-scale plate-based latent heat thermal energy storage system', *Appl. Therm. Eng.*, vol. 178, no. March, p. 115441, 2020.

[20] L. Pu, S. Zhang, L. Xu, and Y. Li, 'Thermal performance optimization and evaluation of a radial finned shell-and-tube latent heat thermal energy storage unit', *Appl. Therm. Eng.*, vol. 166, no. November 2019, p. 114753, 2020.

[21] M. M. Joybari, S. Seddegh, X. Wang, and F. Haghighat, 'Experimental investigation of multiple tube heat transfer enhancement in a vertical cylindrical latent heat thermal energy storage system', *Renew. Energy*, vol. 140, pp. 234–244, 2019.

[22] Y. Liu, J. Duan, X. He, and Y. Wang, 'Experimental investigation on the heat transfer enhancement in a novel latent heat thermal storage equipment', *Appl. Therm. Eng.*, vol. 142, no. June, pp. 361–370, 2018.

[23] S. Seddegh, X. Wang, M. M. Joybari, and F. Haghighat, 'Investigation of the effect of geometric and operating parameters on thermal behavior of vertical shell-and-tube latent heat energy storage systems', *Energy*, vol. 137, pp. 69–82, 2017.

[24] J. Gasia, J. Diriken, M. Bourke, J. Van Bael, and L. F. Cabeza, 'Comparative study of the thermal performance of four different shell-and-tube heat exchangers used as latent heat thermal energy storage systems', *Renew. Energy*, vol. 114, pp. 934–944, 2017.

[25] M. K. A. Sharif *et al.*, 'Review of the application of phase change material for heating and domestic hot water systems', *Renew. Sustain. Energy Rev.*, vol. 42, pp. 557–568, 2015.

[26] I. PCM Thermal Solutions, 'PHASE CHANGE MATERIAL (PCM) HEAT EXCHANGERS', 2014. [Online]. Available: http://www.pcm-solutions.com/pcmheatex.html.

[27] Phase Change Energy Solutions, 'PhaseStor ™', *2020*. [Online]. Available: https://phasechange.com/products/phasestor/.

[28] Sunamp Ltd., 'Sunamp', 2020. [Online]. Available: https://www.sunamp.com/.

[29] R. T. GmbH, 'Phase Cube', 2020. [Online]. Available: rubitherm.eu/index.php/produktkategorie/phasecube.

[30] A. cooling Technologies, 'HVAC ENERGY RECOVERY', 2020. [Online]. Available: https://www.1-act.com/hvac/.

[31] J. Pereira da Cunha and P. Eames, 'Thermal energy storage for low and medium temperature applications using phase change materials – A review', *Appl. Energy*, vol. 177, pp. 227–238, 2016.

[32] S. D. Sharma and K. Sagara, 'LATENT HEAT STORAGE MATERIALS AND SYSTEMS: A REVIEW', *Int. J. Green Energy*, vol. 2, pp. 1–56, 2005.

[33] D. Rozanna, T. G. Chuah, a. Salmiah, T. S. Y. Choong, and M. Sa'ari, 'Fatty Acids as Phase Change Materials (PCMs) for Thermal Energy Storage: A Review', *Int. J. Green Energy*, vol. 1, no. 4, pp. 495–513, Jan. 2005.

[34] M. C. Costa *et al.*, 'The solid-liquid phase diagrams of binary mixtures of consecutive, even saturated fatty acids.', *Chem. Phys. Lipids*, vol. 160, no. 2, pp. 85–97, Aug. 2009.

[35] M. M. Kenisarin, 'Thermophysical properties of some organic phase change materials for latent heat storage. A review', *Sol. Energy*, vol. 107, pp. 553–575, 2014.

[36] A. Solé, H. Neumann, S. Niedermaier, L. F. Cabeza, and E. Palomo, 'Thermal stability test of sugar alcohols as phase change materials for medium temperature energy storage application', *Energy Procedia*, vol. 48, pp. 436–439, 2014.

[37] E. Palomo Del Barrio, R. Cadoret, J. Daranlot, and F. Achchaq, 'New sugar alcohols mixtures for long-term thermal energy storage applications at temperatures between 70 °C and 100 °C', *Sol. Energy Mater. Sol. Cells*, vol. 155, pp. 454–468, 2016.

[38] T. Nomura, C. Zhu, A. Sagara, N. Okinaka, and T. Akiyama, 'Estimation of thermal endurance of multicomponent sugar alcohols as phase change materials', *Appl. Therm. Eng.*, vol. 75, pp. 481–486, 2015.

[39] S. N. Gunasekara, R. Pan, J. N. Chiu, and V. Martin, 'Polyols as phase change materials for low-grade excess heat storage', *Energy Procedia*, vol. 61, pp. 664–669, 2014.

[40] G. Diarce, I. Gandarias, Á. Campos-Celador, a. García-Romero, and U. J. Griesser, 'Eutectic mixtures of sugar alcohols for thermal energy storage in the 50–90°C temperature range', *Sol. Energy Mater. Sol. Cells*, vol. 134, pp. 215–226, 2015.

[41] S. A. Mohamed *et al.*, 'A review on current status and challenges of inorganic phase change materials for thermal energy storage systems', *Renew. Sustain. Energy Rev.*, vol. 70, no. June 2015, pp. 1072–1089, 2017.

[42] M. Telkes, 'Thermal energy storage in salt hydrates', *Sol. Energy Mater.*, vol. 2, no. 4, pp. 381–393, Jul. 1980.

[43] A. Garcia-Romero, A. Delgado, A. Urresti, K. Martin, and J. M. Sala, 'Corrosion behaviour of several aluminium alloys in contact with a thermal storage phase change material based on Glauber's salt', *Corros. Sci.*, vol. 51, no. 6, pp. 1263–1272, 2009.

[44] G. Ferrer, A. Solé, C. Barreneche, I. Martorell, and L. F. Cabeza, 'Corrosion of metal containers for use in PCM energy storage', *Renew. Energy*, vol. 76, pp. 465–469, 2015.

[45] S. A. Mohamed *et al.*, 'A review on current status and challenges of inorganic phase change materials for thermal energy storage systems', *Renew. Sustain. Energy Rev.*, vol. 70, no. February 2016, pp. 1072–1089, 2017.

[46] S. N. Gunasekara, V. Martin, and J. N. Chiu, 'Phase equilibrium in the design of phase change materials for thermal energy storage : State-of-the-art', vol. 73, no. February 2016, pp. 558–581, 2017.

[47] H. Mehling and L. F. Cabeza, 'Phase change materials and their basic properties.', *Therm. Energy Storage Sustain. Energy Consum.*, 2007.

[48] E. Talmatsky and A. Kribus, 'PCM storage for solar DHW : An unfulfilled promise ?', vol. 82, pp. 861–869, 2008.

[49] Á. Á. Pardiñas, M. Justo Alonso, R. Diz, K. Husevag Kvalsvik, and J. Fernández-Seara, 'State-of-the-art for the use of phase-change materials in tanks coupled with heat pumps', *Energy Build.*, vol. 140, pp. 28–41, 2017.

[50] H. Nazir *et al.*, 'Recent developments in phase change materials for energy storage applications : A review', *Int. J. Heat Mass Transf.*, vol. 129, pp. 491–523, 2019.

[51] D. G. R. William D. Callister, Jr., *Materials Science and Engineering an Introduction*, vol. 1. 2010.

[52] R. Benages-Vilau, T. Calvet, and M. a. Cuevas-Diarte, 'Polymorphism, crystal growth, crystal morphology and solid-state miscibility of alkali nitrates', *Crystallogr. Rev.*, vol. 20, no. 1, pp. 25–55, 2014.

[53] P.- Edinburgh, 'Polymorphism in urea', pp. 34–35.

[54] M. K. Rathod and J. Banerjee, 'Thermal stability of phase change materials used in latent heat energy storage systems: A review', *Renew. Sustain. Energy Rev.*, vol. 18, pp. 246–258, 2013.

[55] H. Neumann, S. Niedermaier, S. Gschwander, and P. Schossig, 'Cycling stability of D-mannitol when used as phase change material for thermal storage applications', *Thermochim. Acta*, vol. 660, no. April 2016, pp. 134–143, 2018.

[56] J. W. Mullin, 'Crystallization', vol. Fourth edi, 2001.

[57] H. Fredriksson and U. Åkerlind, *Solidification and Crystallization Processing in Metals and Alloys*. 2012.

[58] D. Groulx, 'The rate problem in solid-liquid phase change heat transfer: Efforts and questions toward heat exchanger design rules', *Int. Heat Transf. Conf.*, vol. 2018-August, no. May, pp. 425–440, 2018.

[59] A. Paul, L. Shi, and C. W. Bielawski, 'A eutectic mixture of galactitol and mannitol as a phase change material for latent heat storage', *Energy Convers. Manag.*, vol. 103, pp. 139–146, 2015.

[60] K. Panchabikesan, M. V. Swami, V. Ramalingam, and F. Haghighat, 'Influence of PCM thermal conductivity and HTF velocity during solidification of PCM through the free cooling concept – A parametric study', *J. Energy Storage*, vol. 21, no. November 2018, pp. 48–57, 2019.

[61] S. Wu, T. Yan, Z. Kuai, and W. Pan, 'Thermal conductivity enhancement on phase change materials for thermal energy storage: A review', *Energy Storage Mater.*, vol. 25, no. April 2019, pp. 251–295, 2020.

[62] G. Diarce, E. Corro Martínez, L. Quant, Á. Campos-Celador, and A. García-Romero, 'The Sodium nitrate-urea eutectic binary mixture as a phase change material for medium

temperature thermal energy storage. Part I: Determination of the phase diagram and main thermal properties', *Sol. Energy Mater. Sol. Cells*, pp. 1–11, 2016.

[63] G. Diarce, E. Corro Martínez, Á. Campos-Celador, A. García-Romero, and J. M. Sala, 'The Sodium nitrate-urea eutectic binary mixture as a phase change material for medium temperature thermal energy storage. Part II: Accelerated thermal cycling test and water uptake behavior of the material.', *Sol. Energy Mater. Sol. Cells*, pp. 1–8, 2016.

[64] G. Diarce, L. Quant, Campos-Celador, J. M. Sala, and A. García-Romero, 'Determination of the phase diagram and main thermophysical properties of the erythritol–urea eutectic mixture for its use as a phase change material', *Sol. Energy Mater. Sol. Cells*, vol. 157, pp. 894–906, 2016.

[65] A. Sharma, S. D. Sharma, D. Buddhi, and R. L. Sawhney, 'Thermal cycle test of urea for latent heat storage applications', vol. 468, no. January 2000, pp. 465–468, 2001.

[66] M. Kamimoto, R. Sakamoto, Y. Takahashi, K. Kanari, and T. Ozawa, 'Investigation of latent heat-thermal energy storage materials. II. Thermoanalytical evaluation of urea', *Thermochim. Acta*, vol. 74, no. 1–3, pp. 281–290, 1984.

[67] M. Kenisarin and K. Mahkamov, 'Solar energy storage using phase change materials', *Renew. Sustain. Energy Rev.*, vol. 11, no. 9, pp. 1913–1965, 2007.

[68] F. Agyenim, N. Hewitt, P. Eames, and M. Smyth, 'A review of materials, heat transfer and phase change problem formulation for latent heat thermal energy storage systems (LHTESS)', *Renew. Sustain. Energy Rev.*, vol. 14, no. 2, pp. 615–628, 2010.

[69] A. Kasaeian, L. Bahrami, F. Pourfayaz, E. Khodabandeh, and W.-M. Yan, 'Experimental studies on the applications of PCMs and nano-PCMs in buildings: A critical review', *Energy Build.*, vol. 154, no. 1, pp. 96–112, 2017.

[70] M. A. Rosen and İ. Dinçer, *Thermal Energy Storage: Systems and Applications*. 2010.

[71] Z. Khan, Z. Khan, and A. Gafoor, 'A review of performance enhancement of PCM based latent heat storage system within the context of materials, thermal stability and compatibility', *Energy Convers. Manag.*, 2016.

[72] D. Aydin, Z. Utlu, and O. Kincay, 'Thermal performance analysis of a solar energy sourced latent heat storage', *Renew. Sustain. Energy Rev.*, vol. 50, pp. 1213–1225, 2015.

[73] M. Medrano, M. O. Yilmaz, M. Nogués, I. Martorell, J. Roca, and L. F. Cabeza, 'Experimental evaluation of commercial heat exchangers for use as PCM thermal storage systems', *Appl. Energy*, vol. 86, no. 10, pp. 2047–2055, 2009.

[74] S. Rigal, 'Stockage par matériaux à changement de phase de l'énergie thermique rejetée par l'industrie à basse température', Université de Pau et des Pays de l'Adour, 2017.

[75] A. G. Tereshchenko, 'Deliquescence: Hygroscopicity of Water-Soluble Crystalline Solids', *J. Pharm. Sci.*, vol. 104, no. 11, pp. 3639–3652, 2015.

[76] M.-J. Lee, H.-J. Jung, H.-J. Eom, S. Maskey, H. K. Kim, and C.-U. Ro, 'Hygroscopic behavior of individual NaNO particles', *Atmos. Chem. Phys. Discuss.*, vol. 11, no. 8, pp. 23203–23229, 2011.

[77] T. Bauer, D. Laing, U. Kröner, and R. Tamme, 'Sodium nitrate for high temperature latent heat storage', in *The 11th International Conference on Thermal Energy Storage – Effstock 14-17 June 2009 in Stockholm, Sweden*, 2009, no. June, pp. 1–8.

[78] E. A. Werner, 'Urea as a Hygroscopic Substance', *Nature*, p. 512, 1937.

[79] J. O. H. M. Eessen, 'Urea', 2012.

[80] A. L. Voskov, T. S. Babkina, A. V. Kuznetsov, and I. A. Uspenskaya, 'Phase equilibria in the urea-biuret-water system', *J. Chem. Eng. Data*, vol. 57, no. 11, pp. 3225–3232, 2012.

[81] A. M. Bernhard, D. Peitz, M. Elsener, A. Wokaun, and O. Kröcher, 'Hydrolysis and thermolysis of urea and its decomposition byproducts biuret, cyanuric acid and melamine over anatase TiO 2', *Appl. Catal. B Environ.*, vol. 115–116, pp. 129–137, 2012.

[82] H. L. Fang and H. F. M. DaCosta, 'Urea thermolysis and NOx reduction with and without SCR catalysts', *Appl. Catal. B Environ.*, vol. 46, no. 1, pp. 17–34, 2003.

[83] 'Compact Karl Fischer Moisture Meter KF-31'. [Online]. Available: https://www.mccat.co.jp/global/instrument/karl-fischer/entry-171.html.

[84] J.-H. Li, G.-E. Zhang, and J.-Y. Wang, 'Investigation of a eutectic mixture of Sodium acetate trihydrate and urea as latent heat storage', *Sol. Energy*, vol. 47, pp. 443–445, 1991.

[85] N. A. Pusci and M. Dezelie, 'Das Gleichgewicht in bin iren Systemen mit Erythrit als Komponente', 1932.

[86] M. Gambino and J. P. Bros, 'Capacite calorifique de l'uree et de quelques melanges eutectiques a base d'uree entre 30 et 140°C', *Thermochim. Acta*, vol. 127, pp. 223–236, 1988.

[87] R. Sakamoto, M. Kamimoto, Y. Takahashi, Y. Abe, K. Kanari, and T. Ozawa, 'Investigation of latent heat-thermal energy storage materials. III. Thermoanalytical evaluation of pentaerythritol', *Thermochim. Acta*, vol. 77, no. 1–3, pp. 241–249, 1984.

[88] S. Sebelius, T. T. Le, L. J. Pettersson, and H. Lind, 'Identification of urea decomposition from an SCR perspective ; A combination of experimental work and molecular modeling', *Chem. Eng. J.*, vol. 231, pp. 220–226, 2013.

[89] A. Lundström, B. Andersson, and L. Olsson, 'Urea thermolysis studied under flow reactor conditions using DSC and FT-IR', *Chem. Eng. J.*, vol. 150, no. 2–3, pp. 544–550, 2009.

[90] D. Wang, N. Dong, S. Hui, and Y. Niu, 'Analysis of urea pyrolysis products in 132.5-190 °C', *Energy Procedia*, vol. 158, pp. 2170–2175, 2019.

[91] M. Koebel and M. Elsener, 'Determination of urea and its thermal decomposition products by high-performance liquid chromatography', vol. 689, pp. 164–169, 1995.

[92] P. M. Schaber, J. Colson, S. Higgins, D. Thielen, B. Anspach, and J. Brauer, 'Thermal decomposition (pyrolysis) of urea in an open reaction vessel', *Thermochim. Acta*, vol. 424, no. 1–2, pp. 131–142, 2004.

[93] S. Tischer, M. Börnhorst, J. Amsler, G. Schoch, and O. Deutschmann, 'Thermodynamics and reaction mechanism of urea decomposition', *Phys. Chem. Chem. Phys.*, vol. 21, no.

30, pp. 16785–16797, 2019.

[94] S. Désilets *et al.*, 'Degradation mechanism and thermal stability of urea nitrate below the melting point', *Thermochim. Acta*, vol. 521, pp. 176–183, 2011.

[95] S. Désilets *et al.*, 'Analyses of the thermal decomposition of urea nitrate at high temperature', *Thermochim. Acta*, vol. 521, pp. 59–65, 2011.

[96] C. Villada, A. Bonk, T. Bauer, and F. Bolívar, 'High-temperature stability of nitrate / nitrite molten salt mixtures under di ff erent atmospheres', *Appl. Energy*, vol. 226, no. May, pp. 107–115, 2018.

[97] W. M. Jacobs *et al.*, 'The thermal decomposition of Sodium nitrate', *Inorf. Phys. Theor.*, 1959.

[98] M. K. Rathod and J. Banerjee, 'Thermal stability of phase change materials used in latent heat energy storage systems A review', *Renew. Sustain. Energy Rev.*, vol. 18, pp. 246–258, 2012.

[99] IEA SHC, 'Solar Heating & Cooling Programme IEA Task 58, Material & Components for Thermal Energy Storage', 2019. [Online]. Available: http://task58.iea-shc.org/subtasks.

[100] 'Hoke Gyrolok catalog'. [Online]. Available: http://catalog.hoke.com/Asset/GYROLOK-Tube-Fittings-Catalog----79002ENG.pdf.

[101] K. V. Oliver, A. Maréchal, and P. R. Rich, 'Effects of the hydration state on the mid-infrared spectra of urea and creatinine in relation to urine analyses', *Appl. Spectrosc.*, vol. 70, no. 6, pp. 983–994, 2016.

[102] G. Alva, L. Liu, X. Huang, and G. Fang, 'Thermal energy storage materials and systems for solar energy applications', *Renew. Sustain. Energy Rev.*, vol. 68, no. October 2016, pp. 693–706, 2017.

[103] H. Schmit, W. Pfeffer, C. Rathgeber, and S. Hiebler, 'Thermochimica Acta Calorimetric investigation of the concentration dependent enthalpy change around semicongruent melting CaCl 2 · 6H 2 O', *Thermochim. Acta*, vol. 635, pp. 26–33, 2016.

[104] H. Khadivinassab, D. M. Maijer, and S. L. Cockcroft, 'Characterization of macrosegregation in eutectic alloys', *Mater. Charact.*, vol. 129, no. May, pp. 319–322, 2017.

[105] B. Drevet, D. Camel, and M. Dupuy, 'Microstructure of the Sn-Cu6Sn5 fibrous eutectic and its modification by segregation', *Acta Mater.*, vol. 44, no. 10, pp. 4071–4084, 1996.

[106] R. Elliot, *Eutectic Solidification Processing: Crystalline and Glassy Alloys*. London, Boston: Butterworths, 1983.

[107] J. D. Hunt, 'Binary Eutectic Solidification', 1965.

[108] D. M. Stefanescu, *Science and Engineering of Casting Solidification, Chapter 9 Eutectic Solidification*, Second Edi. 2009.

[109] W. J. Boettinger and D. K. Banerjee, *Physical Metallurgy, Chapter 7 Solidification*, 5Th ed. 2015.

[110] M. N. Croker, R. S. Fidler, and R. W. Smith, 'The characterization of eutectic structures', *R. Soc. London*, vol. 335, no. 1600, pp. 15–37, 1973.

[111] K. A. Jackson, 'Interface Structure'. 1958.

[112] M. B. Djurdjevic, I. Vicario, and G. Huber, 'Revisión de las aplicaciones del análisis térmico en las plantas de fundición de aluminio ; Review of thermal analysis applications in aluminium casting plants', vol. 50, no. March, pp. 1–12, 2014.

[113] M. C. Flemings, 'Our Understanding of Macrosegregation : Past and Present', vol. 40, no. 9, pp. 833–841, 2000.

[114] H. C. De Groh III, 'Undercooling-Induced Macrosegregation in Directional Solidification', *Metall. Mater. Trans. A*, vol. 25, no. November, pp. 1–2, 1994.

[115] W. Benício, D. Castro, and M. De Lucena, 'Microstructure of Undercooled Pb-Sn Alloys', vol. 4, no. 2, pp. 83–86, 2001.

[116] B. . Allen and S. Isserow, 'Segregation at the eutectic temperature', *Acta Metall.*, vol. 5, no. 8, pp. 465–472, Aug. 1957.

[117] J. C. Heinrich, S. Felicelli, P. Nandapurkar, and D. R. Poirier, 'Thermosolutal Convection during Dendritic Solidification of Alloys: Part II. Nonlinear Convection', *Metall. Trans. B*, vol. 20B, 1989.

[118] J. Ribeiro, M. Strub, J. Bedecarrats, F. Strub, and J. Dumas, 'Thermal and dynamic study of water crystallization at the supercooling breakdown Thermal and dynamic study of water crystallization at the supercooling breakdown', no. January, 2006.

[119] K. R. Elder, J. D. Gunton, and M. Grant, 'Nonisothermal eutectic crystallization', vol. 54, no. 6, pp. 6476–6484, 1996.

[120] K. R. Elder, F. Drolet, J. M. Kosterlitz, and M. Grant, 'Stochastic eutectic growth', *Phys. Rev. Lett.*, vol. 72, no. 5, 1994.

[121] P. Galenko, 'Diffusionless Crystal Growth in Rapidly Solidifying Eutectic Systems', no. May 2006, pp. 2014–2016, 2016.

[122] J. Bevan Ott and J. Boerio-Goates, *Chemical Thermodynamics*. London, San Diego: Academic Press, 2000.

[123] K. Kobayashi, P. H. Shingu, H. Janbara, and R. Ozaki, 'The Role of the Primary Phase on Eutectic Solidification of Al-Si Alloys * By Kojiro Kobayashi **, Paul Hideo Shingu **, Hiroki Kanbara *** and Ryohei Ozaki ** silicon respectively , namely , to measure the undercoolings associated with the nucleation of', 1976.

[124] S. Chiba and J. A. Spittle, 'Variation of as-cast grain structure vvith composition in eutectic systems', *Mater. Sci. Technol.*, vol. 2, no. 2, pp. 165–168, Feb. 1986.

[125] S. Furbo, J. Fan, E. Andersen, Z. Chen, and B. Perers, 'Development of seasonal heat storage based on stable supercooling of a Sodium acetate water mixture', *Energy Procedia*, vol. 30, pp. 260–269, 2012.

[126] M. Dannemand, J. M. Schultz, J. B. Johansen, and S. Furbo, 'Long term thermal energy

storage with stable supercooled Sodium acetate trihydrate', *Appl. Therm. Eng.*, vol. 91, pp. 671–678, 2015.

[127] M. Dannemand, W. Kong, J. Fan, J. B. Johansen, and S. Furbo, 'Laboratory Test of a Prototype Heat Storage Module Based on Stable Supercooling of Sodium Acetate Trihydrate', *Energy Procedia*, vol. 70, pp. 172–181, 2015.

[128] B. Zalba, J. M. Marín, L. F. Cabeza, and H. Mehling, *Review on thermal energy storage with phase change: materials, heat transfer analysis and applications*, vol. 23, no. 3. 2003.

[129] M. M. Farid, A. M. Khudhair, S. A. K. Razack, and S. Al-Hallaj, 'A review on phase change energy storage: Materials and applications', *Energy Convers. Manag.*, vol. 45, no. 9–10, pp. 1597–1615, 2004.

[130] A. Sharma, V. V. Tyagi, C. R. Chen, and D. Buddhi, 'Review on thermal energy storage with phase change materials and applications', *Renew. Sustain. Energy Rev.*, vol. 13, no. 2, pp. 318–345, 2009.

[131] M. Kenisarin and K. Mahkamov, 'Salt hydrates as latent heat storage materials:Thermophysical properties and costs', *Sol. Energy Mater. Sol. Cells*, vol. 145, pp. 255–286, 2016.

[132] X. X. Zhang, Y. F. Fan, X. M. Tao, and K. L. Yick, 'Crystallization and prevention of supercooling of microencapsulated n-alkanes', *J. Colloid Interface Sci.*, vol. 281, no. 2, pp. 299–306, 2005.

[133] L. Huang, E. Günther, C. Doetsch, and H. Mehling, 'Subcooling in PCM emulsions-Part 1: Experimental', *Thermochim. Acta*, vol. 509, no. 1–2, pp. 93–99, 2010.

[134] E. Günther, L. Huang, H. Mehling, and C. D??tsch, 'Subcooling in PCM emulsions - Part 2: Interpretation in terms of nucleation theory', *Thermochim. Acta*, vol. 522, no. 1–2, pp. 199–204, 2011.

[135] Y. Zhao, X. Zhang, X. Xu, and S. Zhang, 'Research progress in nucleation and supercooling induced by phase change materials', *J. Energy Storage*, vol. 27, no. December 2019, p. 101156, 2020.

[136] H. Zahir, S. A. Mohamed, R. Saidur, and F. A. Al-sulaiman, 'Supercooling of phase-change materials and the techniques used to mitigate the phenomenon', *Appl. Energy*, vol. 240, no. July 2018, pp. 793–817, 2019.

[137] N. Beaupere, U. Soupremanien, and L. Zalewski, 'Nucleation triggering methods in supercooled phase change materials', *Thermochim. Acta*, vol. 670, pp. 1–18, 2019.

[138] A. Safari, R. Saidur, F. A. Sulaiman, Y. Xu, and J. Dong, 'A review on supercooling of Phase Change Materials in thermal energy storage systems', vol. 70, no. July 2016, pp. 905–919, 2017.

[139] D. V. Alexandrov, 'Nucleation and crystal growth kinetics during solidification: The role of crystallite withdrawal rate and external heat and mass sources', *Chem. Eng. Sci.*, vol. 117, pp. 156–160, 2014.

[140] V. Alexiades, A. D. Solomon, and D. G. Wilson, 'The formation of a solid nucleus in

supercooled liquid. i', *J. Non-Equilibrium Thermodyn.*, vol. 13, no. 3, pp. 281–300, 1988.

[141] H. Vehkamäki, *Classical Nucleation Theory in Multicomponent Systems*. Berlin: Springer, 2006.

[142] K. Pielichowski and K. Flejtuch, 'Differential scanning calorimetry studies on poly(ethylene glycol) with different molecular weights for thermal energy storage materials', *Polym. Adv. Technol.*, vol. 13, no. 10–12, pp. 690–696, 2002.

[143] Y. Kou *et al.*, 'Thermal analysis and heat capacity study of polyethylene glycol (PEG) phase change materials for thermal energy storage applications', *J. Chem. Thermodyn.*, vol. 128, pp. 259–274, 2019.

[144] L. Klimeš *et al.*, 'Computer modelling and experimental investigation of phase change hysteresis of PCMs: The state-of-the-art review', *Appl. Energy*, vol. 263, no. August 2019, p. 114572, 2020.

[145] 'Rcommander a graphical interface for R', 2013. [Online]. Available: https://www.rcommander.com/.

[146] A. Dean, D. Voss, and D. Draguljic, *Design and Analysis of Experiments*, Second Edi. Springer, 2017.

[147] S. A. and C. P.R., 'Shell-and-Tube Latent Heat Thermal Energy Storage (ST-LHTES).', in *Advances in Solar Energy Research. Energy, Environment, and Sustainability.*, T. H., A. A., C. P., and P. S., Eds. Singapore: Springer, 2019.

[148] S. Pakalka, V. Kęstutis, and G. Streckienė, 'Experimental Comparison of the Operation of PCM-Based Copper Heat Exchangers with Different Configurations', *Appl. Therm. Eng.*, vol. 172, 2020.

[149] M. Kabbara, D. Groulx, and A. Joseph, 'Experimental Investigations of a Latent Heat Energy Storage Unit Using Finned Tubes', *Appl. Therm. Eng.*, vol. 101, pp. 601–11, 2016.

[150] M. Osman, M. H. Abokersh, O. El-Baz, O. Sharaf, N. Mahmoud, and M. El-Morsi, 'Key Performance Indicators (KPIs): Assessing the Process Integration of a Shell-and-Tube Latent Heat Storage Unit', *J. Clean. Prod.*, vol. 256, 2020.

[151] G. Shen, X. Wang, and A. Chan, 'Experimental Investigation of Heat Transfer Characteristics in a Vertical Multi-Tube Latent Heat Thermal Energy Storage System', *Energy Procedia*, vol. 160, pp. 332–39, 2019.

[152] J. Gasia, J. Diriken, M. Bourke, J. Van Bael, and L. F. Cabeza, 'Comparative Study of the Thermal Performance of Four Different Shell-and-Tube Heat Exchangers Used as Latent Heat Thermal Energy Storage Systems', *Renew. Energy*, vol. 114, pp. 934–44, 2017.

[153] M. Esapour, M. J. Hosseini, A. A. Ranjbar, Y. Pahamli, and R. Bahrampoury, 'Phase Change in Multi-Tube Heat Exchangers', *Renew. Energy*, vol. 85, pp. 1017–25, 2016.

[154] F. Agyenim and N. Hewitt, 'The development of a finned phase change material (PCM) storage system to take advantage of off-peak electricity tariff for improvement in cost of heat pump operation', *Energy Build.*, vol. 42, no. 9, pp. 1552–1560, 2010.